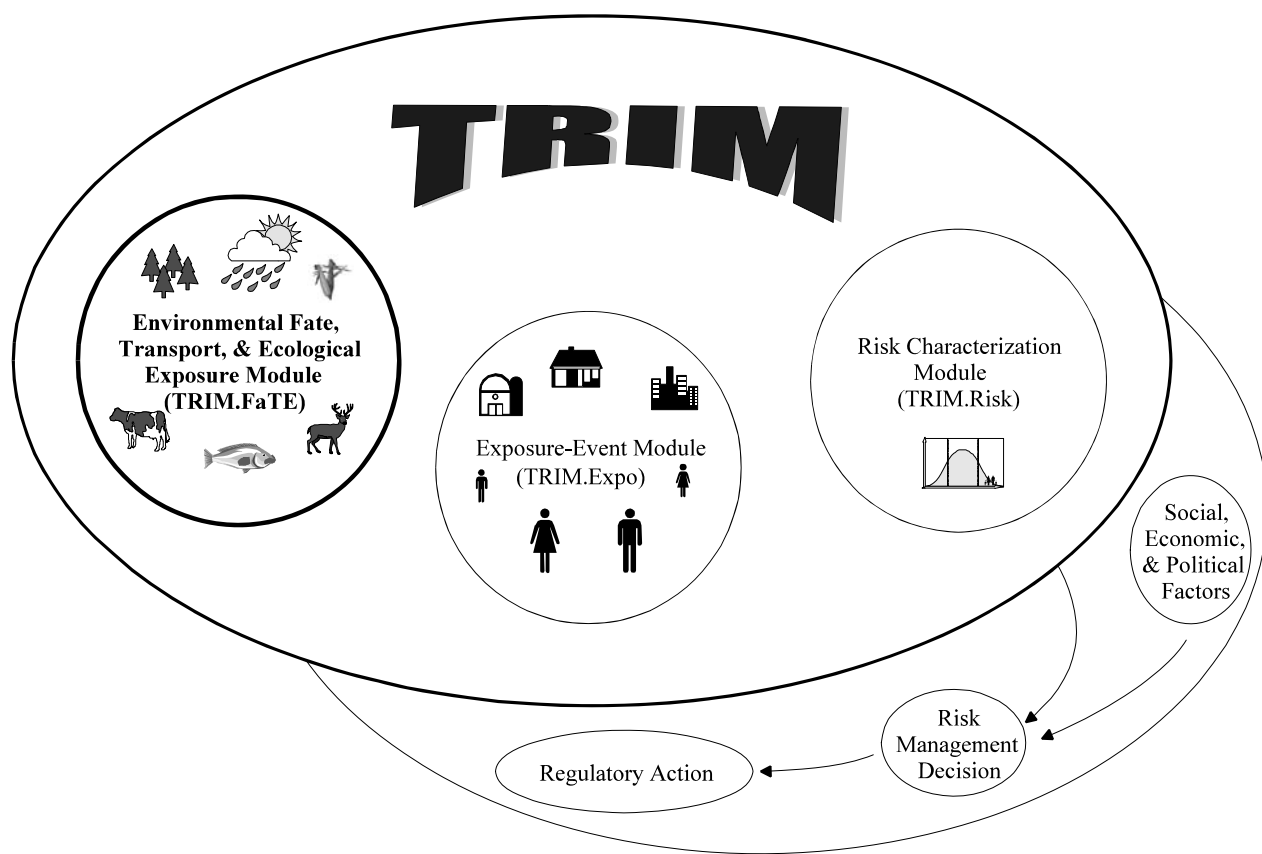




Evaluation of TRIM.FaTE

Volume II: Model Performance Focusing on Mercury Test Case



Evaluation of TRIM.FaTE

Volume II: Model Performance Focusing on Mercury Test Case

By:

Mark Lee, David Burch, Margaret E. McVey, Rebecca Murphy, and Baxter Jones
ICF Consulting, Research Triangle Park, North Carolina and Fairfax, Virginia
EPA Contract No. 68-D-01-052 (WA 3-06) and GSA Contract No. GS-10F-0124J (TO 1328)

Randy Maddalena, Deborah Hall Bennett, and Thomas E. McKone
Lawrence Berkeley National Laboratory, Berkeley, California
Interagency Agreement No. DW89786601

Rebecca A. Efroymsen, Bradford F. Lyon, and Daniel S. Jones
Oak Ridge National Laboratory, Oak Ridge, Tennessee
Interagency Agreement No. DW89876501

Alison Eyth
University of North Carolina-Center for Environmental Programs, Chapel Hill, North Carolina
EPA Contract No. 68-D-01-052 (WA 3-06) and GSA Contract No. GS-10F-0124J (TO 1328)

Prepared for:

Terri Hollingsworth, EPA Project Officer and Work Assignment Manager
Deirdre Murphy, Technical Lead
Emissions Standards Division

U.S. Environmental Protection Agency
Office of Air Quality Planning and Standards
Emissions Standards & Air Quality Strategies and Standards Divisions
Research Triangle Park, North Carolina

Disclaimer

This report is being furnished to the U.S. Environmental Protection Agency (EPA) by ICF Consulting in partial fulfillment of Work Assignment 3-06 under EPA contract 68-D-01-052 and Task Order 1328 under GSA contract GS-10F-0124J. The report has been reviewed and approved for publication by EPA. It does not constitute Agency policy. The opinions, findings, and conclusions expressed are those of the authors and are not necessarily those of EPA. Mention of trade names or commercial products is not intended to constitute endorsement or recommendation for use.

EPA has employed many models over the past decade for different applications and purposes associated with emissions of mercury to air. These have included models capable of long-range, large-scale modeling such as the Regional Lagrangian Model of Air Pollution (RELMAP), used for the *Mercury Study Report to Congress*, and more recently the Community Multi-scale Air Quality (CMAQ) modeling system, which includes simulation of atmospheric chemistry, as well as models capable of local-scale atmospheric transport such as the Industrial Source Complex (ISC) model. Mercury deposition estimated via those models has been used as input for watershed and aquatic ecosystem modeling, e.g., using the indirect exposure methodology for mercury (IEM-2M) or the Multimedia, Multi-pathway, Multi-receptor Exposure and Risk Assessment model (3MRA). Unlike many of those model applications, which informed regulatory decisions by the Agency, the analyses described in this document are solely for the purpose of model evaluation, as described herein.

Preface

This document, *Evaluation of TRIM.FaTE, Volume II: Model Performance Focusing on Mercury Test Case*, is part of a series of documentation for the Total Risk Integrated Methodology (TRIM). Additional evaluation analyses are presented elsewhere (EPA 2002a, EPA 2004, EPA 2005b) and will be augmented with future applications, while the detailed documentation of logic, assumptions, algorithms, and equations is provided in comprehensive Technical Support Documents (TSDs) and/or user's guides for each of the TRIM modules (see www.epa.gov/ttn/fera).

Primary U.S. EPA technical staff contributing to the planning, analysis, and interpretation of this TRIM.FaTE test case include Deirdre Murphy (overall technical lead), John Langstaff (sensitivity analysis and air modeling), Gerry Laniak (model comparison with 3MRA), and Robert Ambrose (model comparison with 3MRA). Craig Barber also contributed to analysis and interpretation (bioaccumulation comparison with 3MRA). Other EPA technical staff contributing to planning and early analyses for the mercury test case were TRIM team members Ted Palma, Robert Hetes, and Amy Vasu.

Reviewers for this document included: Gerry Laniak, Mike Cyterski, Ellen Cooter, and Donna Schwede of U.S. EPA's Office of Research and Development; Jeffrey Yurk of U.S. EPA Region 6; John Irwin of U.S. EPA and National Oceanic and Atmospheric Administration; and Stephen Kroner of U.S. EPA, Office of Solid Waste.

Inquiries should be directed to Dr. Deirdre Murphy, U.S. EPA, Office of Air Quality Planning and Standards, C404-01, Research Triangle Park, North Carolina, 27711; murphy.deirdre@epa.gov.

Table of Contents

	<u>Page</u>
Disclaimer	i
Preface	ii
Table of Contents	iii
EXECUTIVE SUMMARY	ES-1
1. INTRODUCTION AND OBJECTIVES	1-1
2. SPECIFICATIONS OF MODELED SCENARIOS	2-1
3. RESULTS AND DISCUSSION: DYNAMIC MODELING	3-1
3.1 Time Patterns of Mercury Mass Accumulation	3-3
3.2 Mercury Concentration Over Time in Various Compartment Types	3-12
3.2.1 Annual Average Concentrations (and Deposition)	3-12
3.2.2 Selected Instantaneous and Monthly Average Results	3-25
3.3 Speciation: How Do Concentrations of Hg ⁰ , Hg ²⁺ , and MHg Differ?	3-34
3.3.1 Speciation by Compartment Type	3-34
3.3.2 Spatial Variations in Speciation	3-40
3.3.3 Temporal Variations in Speciation	3-43
3.4 Spatial Variation of Total Mercury Concentration	3-49
3.4.1 Abiotic Compartments	3-49
3.4.2 Biotic Compartments	3-60
3.5 Comparison of Emission Cases	3-73
3.5.1 Emission Case A vs. Emission Case B	3-73
3.5.2 Emission Case B vs. Emission Case C	3-78
4. RESULTS AND DISCUSSION: STEADY-STATE MODELING	4-1
4.1 Configuring a TRIM.FaTE Scenario for Steady-state Mode	4-1
4.2 Steady-state Results	4-3
4.3 Comparison of Steady-state and Dynamic Results	4-5
5. SENSITIVITY ANALYSIS	5-1
5.1 Analysis Design/Methods	5-1
5.1.1 How Input Values Were Varied	5-2

5.1.2	Measures of Sensitivity	5-2
5.1.3	Limitations	5-4
5.1.4	Endpoints Analyzed	5-6
5.2	Influential Input Properties for Individual Compartment Types	5-7
5.2.1	Air	5-7
5.2.2	Surface Soil	5-11
5.2.3	Earthworm	5-14
5.2.4	Leaf	5-17
5.2.5	Surface Water	5-20
5.2.6	Aquatic Food Chain	5-27
5.2.7	Terrestrial Mammals	5-36
5.3	Broadly Influential Properties	5-42
5.3.1	Approach	5-42
5.3.2	Summary of Observations	5-42
5.3.3	Conclusions	5-47
5.4	Summary of Sensitivity Analysis	5-48
6.	COMPARISON OF TRIM.FaTE AND 3MRA MODELING RESULTS	6-1
6.1	Approach to Comparison of Modeling Results	6-4
6.1.1	Inherent Differences/Similarities in Spatial Resolution of Model Outputs	6-6
6.1.2	Model Set-up and Input Data	6-12
6.2	Air and Leaves	6-19
6.2.1	Divalent Mercury Concentrations in Air	6-19
6.2.2	Divalent Mercury Deposition	6-22
6.2.3	Divalent Mercury Concentrations in Leaves	6-26
6.2.4	Spatial Patterns for Air Concentrations and Deposition	6-28
6.3	Soil and Soil Biota	6-32
6.3.1	Divalent Mercury Concentrations in Surface Soil	6-32
6.3.2	Divalent Mercury Concentrations in Plant Roots	6-34
6.3.3	Divalent Mercury Concentrations in Earthworms	6-39
6.3.4	Spatial Patterns for Surface Soil	6-41
6.4	Surface Water, Sediment, and Fish	6-44
6.4.1	Mercury Concentrations and Speciation in Surface Water	6-44
6.4.2	Mercury Concentrations and Speciation in Sediment	6-48
6.4.3	Methyl Mercury Concentrations in Fish	6-52
6.5	Wildlife	6-58
6.5.1	Total Mercury Concentrations in Small Birds	6-60
6.5.2	Total Mercury Concentrations in Omniverts	6-62
6.5.3	Total Mercury Concentrations in Small Mammals	6-64

6.6	Summary of 3MRA-TRIM.FaTE Comparison	6-66
6.6.1	Overview of Results and Model Differences	6-66
6.6.2	Possible Future Areas for Model Comparison	6-68
7.	COMPARISONS WITH MEASUREMENT DATA	7-1
7.1	Description of Measurement Data and Relationship to TRIM.FaTE Model Results ..	7-1
7.2	Comparison with Air Measurement Data	7-6
7.3	Comparison with Soil and Soil Biota Measurement Data	7-7
7.4	Comparison with Sediment and Aquatic Biota Measurement Data	7-9
7.5	Summary of Measurement Data Comparisons	7-11
8.	REFERENCES	8-1
APPENDIX A: DOCUMENTATION OF INPUT PROPERTIES FOR TRIM.FaTE		
MERCURY TEST CASE		
		A-1
APPENDIX B: DETAILED RESULTS FOR EMISSION CASE B		
		B-1
B.1	Mass Accumulation Tables	B-1
B.2	Concentration Tables and Charts	B-5
APPENDIX C: STEADY-STATE: INPUTS AND DETAILED RESULTS		
		C-1
C.1	Estimation of Steady-State Inputs for Mercury Test Case	C-1
C.1.1	Estimating Constant Values for Time-varying Inputs	C-1
C.1.2	Meteorological Inputs	C-4
C.1.3	Plant Inputs	C-7
C.1.4	Water Body Flow Inputs	C-10
C.2	Compartment-specific Steady-state Results	C-11
C.3	Detailed Comparison of Steady-state and Dynamic Simulation Results	C-21
APPENDIX D: DETAILED RESULTS FOR SENSITIVITY ANALYSIS		
		D-1
D.1	Input Properties Assessed in the Mercury Test Case Sensitivity Analysis	D-1
D.2	Sensitivity of Predicted Concentration to TRIM.FaTE Input Properties	D-23
D.3	Properties with Absolute Elasticities > 0.5	D-71
D.4	Properties with Absolute Sensitivity Scores > 0.5	D-75
APPENDIX E: SUPPLEMENTAL MATERIALS FOR 3MRA-TRIM.FaTE		
COMPARISON		
		E-1
E.1	Description of 3MRA Processes	E-1
E.2	Detailed Results for 3MRA-TRIM.FaTE Comparison	E-4

APPENDIX F: SUMMARY OF AVAILABLE OFF-SITE MONITORING DATA F-1

F.1 Off-site Air Monitoring Data F-1
F.2 Off-site Soil Monitoring Data F-5
F.3 Off-site Sediment Monitoring Data F-6
F.4 Off-site Biota Monitoring Data F-7

EXECUTIVE SUMMARY

The United States Environmental Protection Agency (EPA) recently has developed and begun applying TRIM.FaTE, a comprehensive multimedia chemical fate and transport model based on mass transfer and mass balance concepts. This report documents a series of model evaluation activities for TRIM.FaTE based on its application to mercury air emissions from a mercury cell chlor-alkali facility (now-closed) in the northeastern United States.¹ The mass balance approach used in TRIM.FaTE, including mercury transformations in various environmental media and types of biota, ensures that the predicted distribution of mercury in the environment reflects the total mercury available – mercury is neither created nor destroyed during the modeling. TRIM.FaTE's mass balance approach incorporates fugacity principles, deriving from and building on the CALTOX model and the earlier modeling concepts and formulations of Mackay (Level 1, 2, and 3 partitioning models) and Thibodeaux (chemodynamics concepts).

As discussed at length in Volume I of this report and highlighted in recent EPA Science Advisory Board reviews of TRIM.FaTE and 3MRA (another EPA model with a complex multimedia fate and transport component), model evaluation for a multimedia model such as TRIM.FaTE is a particularly challenging undertaking. “Validation” of such models, in the classic sense (e.g., proving the model produces accurate results across a range of input conditions), is not generally possible, in part because there are no comprehensive data sets of measured chemical concentrations (and associated contributing pollutant sources) for use in such comprehensive studies, nor are there other fully validated multimedia models against which TRIM.FaTE can be benchmarked. Thus, evaluation of TRIM.FaTE is not a yes/no exercise but a continuing accumulation of evidence leading to model refinement and eventually to increasing levels of confidence in the model results.

The overall objective for TRIM.FaTE evaluation, as discussed in Volume I of this report, is to refine and build confidence in the model by conducting and publicly reporting on a wide-ranging suite of model evaluation activities, of which the mercury performance evaluation study reported here is an important example. Other examples include recent and in-progress evaluation studies focusing on organic chemicals, including dioxins/furans and polycyclic aromatic hydrocarbons. The ongoing TRIM.FaTE model evaluation has been designed to be consistent with the Agency's peer review policy for models and its evolving regulatory environmental modeling guidance.

TRIM.FaTE

TRIM.FaTE is a spatially explicit, compartmental mass balance model that describes the movement and transformation of pollutants over time, through a user-defined, bounded system that includes both biotic and abiotic components (compartments). TRIM.FaTE predicts pollutant concentrations in multiple environmental media and pollutant concentrations and intakes for biota, all of which provide both temporal and spatial exposure estimates for ecological receptors (i.e., plants and animals). The output concentrations from TRIM.FaTE also can be used as inputs to a human ingestion exposure model.

¹ This evaluation does not draw conclusions regarding the facility. Rather, it is intended to facilitate conclusions regarding the performance of TRIM.FaTE.

TRIM.FaTE is Different

TRIM.FaTE is a transparent computer framework, accompanied by an initial library of algorithms and values, into which a user loads selected algorithms and input values, along with the design (e.g., spatial, temporal, and ecosystem details) of the scenario to be modeled. With its two-way linkages among the various environmental media and biota types being modeled, its continuous mass-balancing, its scalable complexity, and its transparency to the user, TRIM.FaTE is significantly different from many other multimedia or single-medium chemical fate and transport models in common use. As demonstrated through the broad range of analyses described in this report, TRIM.FaTE allows a user to perform dynamic, mass-balanced studies of the multimedia fate and transport of mercury in abiotic and biotic media. It also models two-way transformations of chemicals and keeps track of the reaction products within the mass balance system – for example, transformations back and forth between methyl mercury and inorganic divalent mercury, and between the latter and elemental mercury. In another distinguishing feature, the TRIM.FaTE framework accommodates the simulation of mercury transfers within terrestrial and aquatic trophic webs using bioenergetic algorithms, which allow uptake of mercury via food, water, air, and soil and which allow individual species to ingest more than one type of food. TRIM.FaTE allows modeling scenarios to be set up with as much, or as little, complexity as desired.

TRIM.FaTE not only estimates chemical concentrations, but allows a full accounting of chemical mass flows, accumulation, and distribution throughout the modeling system. The media and biota being modeled are connected to each other, as appropriate, and chemical mass can flow both ways across the linkages as specified by various transfer processes (e.g., deposition, diffusion, volatilization, bio-uptake, excretion), allowing for physical and biological feedback mechanisms to be accounted for explicitly (e.g., re-emission from surfaces such as soil, vegetation, and surface water). Plants and animals exchange chemical mass continuously with environmental media, which in the case of plants can have a noticeable effect on the overall distribution of mercury mass in soils, surface water, and air. The distribution of chemical mass within the modeled system changes over time according to the dynamic transfers and processes modeled. As an example of the kind of mass balance/distribution problems that can be addressed, TRIM.FaTE can be used to examine temporal questions related to chemical mass distribution (e.g., time that might be required for different environmental components to approach steady-state, changes in chemical distribution after a source stops emitting mercury). One also can readily examine the impact of including or varying the configuration of a particular environmental medium or biota type (e.g., terrestrial plants, aquatic macrophytes) on chemical mass distributions and concentrations in the modeled system.

TRIM.FaTE is Flexible

TRIM.FaTE is designed to be highly flexible in its set-up and adaptable to user-specified input data and algorithms. Therefore, it can be applied to a variety of problems and questions related to chemical fate and exposure and risk assessment, such as the multimedia assessment of risks associated with hazardous and criteria air pollutants. A user can set up a wide range of study designs in TRIM.FaTE at varying levels of complexity, specifying the time resolution, spatial scale and resolution, environmental media and biota types to be included, kinds and format of outputs, and other study characteristics. This report demonstrates this flexibility,

illustrating time and spatial resolution of modeling inputs and results, generation of chemical mass outputs along with predicted concentrations, modeling of mercury speciation and transformation, modeling in both dynamic and steady-state modes, and adaptability of TRIM.FaTE to sensitivity analyses and to comparisons with other models and monitoring data.

Sensitivity of TRIM.FaTE Results Makes Sense

TRIM.FaTE is working as intended, with the modeling results reflecting the algorithms and inputs used. The modeling results in most cases also appear to be sensitive to input parameters known to be important in determining chemical fate and transport. Chapter 5 describes an initial, local sensitivity analysis covering nearly all of the input properties of the model. As discussed in that chapter, the modeling results are explainable based on the methods and input values used; this study shows that TRIM.FaTE produces results based on what the user gives it. Broadly influential properties – those that exert relatively high influence on chemical concentrations for a range of media types – include mercury emission rates from the source, air deposition-related properties, mercury transformation rates and K_d (phase partitioning) values, and water and air temperature. Several parameters also are noted that influence methyl mercury concentrations in fish through the food chain dynamics simulated in this application of TRIM.FaTE, including characteristics of the algal and benthic invertebrate communities and water-column and benthic fish that comprise the aquatic food web. The sensitivity analysis reported here begins the process of demonstrating that the influence of model inputs on outputs is consistent with the expectations based on the algorithms employed, which were derived from what is currently known about mercury fate and transport.

TRIM.FaTE Compares Well

In large measure, the TRIM.FaTE test case results are consistent with results of comparison simulations performed using EPA's 3MRA model, the limited available mercury measurement data for the test case site, and measurement and modeling data from the literature. Even given some significant differences in model structure, set-up, and inputs, the long-term (annual average) mercury concentrations predicted in various environmental media and biota by TRIM.FaTE and 3MRA (discussed in detail in Chapter 6) are usually within an order of magnitude, and in most cases closer. Predicted mercury speciations (i.e., fractions in elemental, divalent, and methyl mercury form) generally agree as well. Simulations using both models predicted divalent and elemental mercury as the predominant forms of mercury in surface water and sediment, although due to different transformation factors and processes, 3MRA predicted a higher percentage of elemental mercury in these media than TRIM.FaTE. For several reasons related to uncertainty in the literature and in the corresponding modeling methods and inputs, comparisons of the mercury concentration and speciation results for terrestrial animals are more uncertain than for the other media. Where results from the two models do not agree closely, such as for mercury concentrations in the root zone soil and the benthic sediment, the differences are explainable based on differing model algorithms and/or inputs. The results of this model comparison have already been used to refine inputs or algorithms for both model applications, and to raise questions for further examination.

TRIM.FaTE modeling results are placed in the context of the available mercury measurement data for the test case site in Chapter 7. Measurement data such as these are

especially hard to compare with multimedia modeling results, given major uncertainty about historical releases from the emission source and from other nearby and distant sources (including non-air sources) that may have contributed to the measured levels. In addition, measurements are available for very few locations, media, and points in time (especially compared with the TRIM.FaTE outputs), and most measures are of total mercury, with very limited data on speciation. Overall, for the limited measurement data that are available, TRIM.FaTE results are generally consistent with measured values, with most predictions falling within about an order of magnitude of the measured concentrations. Exceptions are noted for some biota, with modeled concentrations in a few animal types lower than measured concentrations by more than an order of magnitude. However, more information about the historical mercury sources and additional measurement data would be required to make a more conclusive statement regarding model performance.

Throughout the report, literature data on mercury measurements and modeling results are cited and compared with the TRIM.FaTE results. The comparison with 3MRA modeling results, comparison with available measurement data for the test case site, and comparison with literature reports have continued to increase confidence in TRIM.FaTE and the current set of algorithms.

TRIM.FaTE's Steady-state and Dynamic Modes Are Complementary

As an example of the ability to work at different levels of complexity within the TRIM.FaTE framework, the model can be applied in either a dynamic or steady-state mode. The dynamic mode, demonstrated in detail in Chapter 3, allows time resolution in the inputs and produces time-varying results as appropriate at a user-set level of resolution, but it also requires substantially more computer resources. The steady-state mode, described in detail in Chapter 4, provides no time resolution of results and does not accept time-varying inputs (thus requiring user designation of representative constant values), but yields overall mass distributions and concentration results in much shorter computer simulation times. Thus, the steady-state mode has practical advantages for in-depth sensitivity analyses and Monte Carlo analyses of uncertainty. As shown in Chapter 4, the steady-state mode compares favorably with the dynamic mode, with generally consistent mercury mass distribution, concentration, and speciation patterns. As part of the analyses described, the differences in results between the two modes are disaggregated into differences attributable to input differences (i.e., converting time-varying inputs for the dynamic mode into constants for the steady-state mode) and differences attributable to how well the steady-state solution approximates the dynamic results at the end of a 30-year modeling period.

Dynamic Modeling Results Demonstrate TRIM.FaTE's Capabilities

Both the steady-state and dynamic modes produce results that appear reasonable – internally consistent, logical in direction and trend, logical in relationships between media, and logical based on the algorithms and inputs used. Chapter 3 provides a sampling of TRIM.FaTE's capabilities in the dynamic mode. Two time trends dominate in mercury mass accumulation from a continuous air source, either: (1) a gradual increase which slows (flattens out) as time progresses (e.g., in soils, sediment, animals closely linked to soil such as earthworms, soil arthropods, and the animals that feed on them), or (2) a repeated five-year spiking pattern that corresponds to variations in the five years of meteorological data inputs used (e.g., in air, leaves,

herbivores and most other terrestrial animals, and to a lesser extent surface water and fish). The latter pattern illustrates the influence of the meteorological inputs, especially the wind and precipitation data, directly on air, then on leaves, and then moving through the terrestrial herbivore food chains. At the end of the 30-year dynamic modeling period, most of the mercury mass remaining in the modeling region is in the soil and benthic sediment compartments.

Mercury concentrations follow time trends similar to those observed for chemical mass accumulation. The concentration results, which indicate where the intensity of the mercury is highest and lowest (e.g., which media, locations, times have highest concentrations), are complementary to the mass results, which indicate where the highest and lowest total amounts of mercury are (factoring in the overall volume/mass of the various system components). Within the food chains modeled for both water-column and benthic fish, mercury concentrations follow expected patterns and are consistent with model inputs (e.g, highest concentrations in carnivores, then omnivores, then herbivores). For all the animals, both aquatic and terrestrial, it is clearly evident that the modeled diet affects the temporal pattern and total accumulation of mercury estimated by TRIM.FaTE. Among atmospheric deposition processes, the wet vapor deposition of divalent mercury is dominant, followed by dry vapor deposition of divalent mercury. The time trend for atmospheric deposition differs from that for air concentration because of the elevated influence of precipitation events on deposition.

The modeled speciation of mercury is generally as expected. Elemental mercury, the primary emitted form, is dominant in air and, because of its much higher soil mobility than other forms, in deeper soil layers. Divalent mercury is dominant in most other media except for fish and piscivorous wildlife, such as the common loon, where methyl mercury dominates.

One interesting finding is the difference between the spatial pattern in the air concentration and atmospheric deposition results, which is shown to be attributable to the difference in wind direction patterns when it is raining versus when it is not. As would be expected, the spatial pattern of surface soil concentrations (and biota closely linked to surface soil) follows the deposition pattern more closely than the air concentration pattern. Based on comparative analysis of the different emission cases, the mass and concentration results for nearly all media and biota other than air and the deeper soils are almost entirely attributable to the divalent mercury component of the emission. Even when the elemental mercury level is almost 20 times higher in the emissions, as in this test case, its local multimedia impact is small relative to the concurrently emitted divalent mercury.

Conclusions

TRIM.FaTE can provide time-series and spatially resolved predictions of mercury mass and concentration in environmental media and biota that are logical and appear consistent with expectations based on the algorithms used, which were derived from what is currently known about mercury fate and transport. Predicted TRIM.FaTE mercury concentrations and speciation results compare reasonably well with 3MRA modeling results, limited measurement data for the test case site, and reports from the literature (note that there are not much available data with which to compare the mass results). TRIM.FaTE simulation in the steady-state mode has some limitations common to all steady-state modeling formulations, especially related to treatment of time-varying meteorological input data, but the results are generally reflective of simulation in

the dynamic modeling mode, at least under the conditions tested. Thus, sensitivity analysis based on steady-state simulations, as presented in this report, appears to be informative about results from simulations in both steady-state and dynamic modes.

Specific observations with regard to results from the application of TRIM.FaTE in this test case, given the algorithms and inputs used, include the following.

- (1) Elemental mercury emitted to air in a model ecosystem yields relatively little local (within ~ 10 km) deposition and multimedia impact, with emitted divalent mercury accounting for most of the localized deposition and multimedia impact and most emitted elemental mercury traveling beyond the local area and potentially depositing over a much larger area.
- (2) Divalent mercury was the dominant mercury species deposited in the test case, and wet vapor deposition was the dominant process, followed by dry vapor deposition (together, wet and dry vapor deposition of divalent mercury accounted for approximately 95 percent of total deposition, with all other processes/species less than five percent combined), and the amount and spatial pattern of atmospheric deposition was highly dependent on both precipitation and wind direction.
- (3) Surface soil, and then benthic sediments and root zone soils, were the largest reservoirs for locally deposited mercury mass over the 30-year time frame of the dynamic modeling, and also in the steady-state modeling (where sediment and root zone soil accumulations were higher than the 30-year results and much closer to surface soil accumulation).
- (4) For the modeled surface water bodies, higher trophic level fish and wildlife reached higher mercury concentrations in 30 years than the lower trophic level animals that were components of their diets.
- (5) In the steady-state modeling, carnivorous fish and piscivorous wildlife reached the highest mercury concentrations among all animals modeled.
- (6) Weather-related temporal (seasonal and annual) patterns are reflected in the dynamic predictions of mercury mass accumulation and concentration for various environmental media and biota, such as surface water and terrestrial herbivores.
- (7) Specific configuration of and input properties used for aquatic food chains, including diet components (e.g., proportion benthic invertebrates), ingestion rates, biomass at various trophic levels (including algae), and predation pressure by piscivorous birds or mammals, can greatly affect methyl mercury concentrations in fish.
- (8) The modeled diets of animals simulated in TRIM.FaTE affect the temporal pattern and magnitude of their mercury accumulation.
- (9) Modeled plant uptake of mercury via roots is low compared with mercury that accumulates in and on leaves directly from the atmosphere.

The application and analyses described within this report significantly expand our knowledge, familiarity, and confidence in the TRIM.FaTE model and the library of algorithms and inputs used here. That said, as with any model there are areas of relatively greater confidence and areas of relatively greater uncertainty, the latter of which often reflect scientific uncertainties about environmental processes. Such areas of greater modeling uncertainty may provide focus for the attention of future TRIM.FaTE users, and for future evaluation and potential refinement of inputs and algorithms. In general, the level of confidence in TRIM.FaTE results is greatest at the scale of annual (or longer-term) concentration and mass results for a modeling region within 10 to 20 km of a source. Examples of areas of relatively greater uncertainty and potential focus for future attention include speciation of mercury in wildlife and sediments, as well as mercury mass accumulation in benthic sediments. The findings of this study and other test case applications of TRIM.FaTE involving mercury, dioxins/furans, and polycyclic aromatic hydrocarbons, including previously reported evaluation activities and model documentation, have all contributed to improved understanding of TRIM.FaTE performance and confidence in its application as a multimedia modeling approach for local-scale multimedia fate and transport of air pollutant emissions. The features offered by TRIM.FaTE that distinguish it from other commonly used multimedia modeling approaches provide incentives for its application. In future applications, users are encouraged to design appropriate scenarios, paying close attention to algorithms and inputs, and to critically evaluate results, contributing their findings to the longer-term knowledge base on TRIM.FaTE and similar models.

1. INTRODUCTION AND OBJECTIVES

Volume I of this evaluation report (EPA 2002a) describes in detail a wide range of model evaluation activities for TRIM.FaTE, which were undertaken to implement EPA's overall evaluation plan for the model as presented in the *TRIM Status Report* (EPA 1999a) and reviewed by EPA's Science Advisory Board (EPA 2000a). This document, Volume II of the evaluation report, describes the mercury test case, a detailed performance evaluation of TRIM.FaTE based on mercury emitted to air from a specific industrial source. Unlike the other types of model evaluation discussed in Volume I of this evaluation report, which focus on specific aspects of the model (e.g., inputs, individual process models), *performance evaluation* focuses on the performance of the model as a whole.

Mercury Test Case Goal

Since its beginnings in 1999, the primary goal for the TRIM.FaTE mercury test case has been to contribute to model development, testing, evaluation, and refinement.

Background on Performance Evaluation

Performance evaluation compares modeling results to some type of benchmark, such as monitoring data, other modeling results, and expert judgment. Generally, the optimized model, as modified based on all prior evaluations, is used for performance evaluation. Matching model output to monitoring data is often considered the most desirable form of performance evaluation. Although comparing model output to measured values provides useful information on the model, history "matching" experiments provide only part of the overall picture of a model's quality, reliability, and relevance (Beck et al. 1997). Several other forms of performance evaluation also are used. In addition to monitoring data, or in the absence of such data, outputs from other models and expert opinion about how outputs should look can be used as comparison benchmarks in performance evaluation. Examples of performance evaluation activities include:

- Model-to-model comparison;
- Comparison of model output to measurement data (e.g., measured concentrations in environmental media and biota);
- Round-robin experiments (where several different users independently set up either the same model or similar models and generate output using the same data for a particular case study); and
- Some forms of regional sensitivity analysis (where output is tested against expert judgment about a plausible bound).

To date, TRIM.FaTE performance evaluation activities have focused on model-to-model comparisons and the comparison of model outputs to measurement data, along with detailed review and assessment of the patterns and trends (and underlying reasons for them) observed in the model outputs, as described in this report.

The ongoing TRIM.FaTE model evaluation has been designed to be consistent with the Agency's peer review policy for models (EPA 2005a) and its evolving regulatory environmental modeling guidance (Habicht 1992, EPA 1994, EPA 1998c, EPA 1999d, and EPA 2003a). Each successive performance evaluation provides an opportunity to use the model and learn more about how it works. Beyond the ultimate findings of the performance evaluation itself, the experience gained through such exercises contributes to an overall understanding of the model, which ultimately enables both model developers and users to better judge the quality of the model. In addition to the mercury test case described here, other examples of TRIM.FaTE model evaluation include recent and in-progress studies focusing on organic chemicals, including dioxins/furans (EPA 2004, EPA 2005b) and polycyclic aromatic hydrocarbons.

Objectives and Limitations of the TRIM.FaTE Mercury Test Case

The primary objectives of the mercury test case are to evaluate the:

- Performance of TRIM.FaTE in dynamic and steady-state simulations of real world conditions; and
- Utility of the steady-state solution for performing sensitivity and uncertainty analyses.

The primary means for evaluating model performance for the mercury test case is through consideration of the compatibility of the TRIM.FaTE results with literature findings of mercury distribution throughout the multiple components of ecosystems, as well as comparison of TRIM.FaTE results to results generated by alternative models (including one other multimedia model), and consideration of the compatibility of the sensitivity analysis conclusions with the conceptual models that were the basis for the TRIM.FaTE library algorithms and properties.

With regard to the sensitivity analysis, TRIM.FaTE's steady-state mode has been employed at a substantial savings in model run time. Inherent in using this mode rather than the dynamic mode is the presumption that sensitivity of steady-state results reflects or is representative of the sensitivity of results at time points of interest during a dynamic simulation.

As noted at the beginning of this chapter, the main goal of the TRIM.FaTE

Modeling of Mercury Emissions to Air

EPA has employed many models over the past decade for different applications and purposes associated with emissions of mercury to air. These have included models capable of long-range, large-scale modeling such as the Regional Lagrangian Model of Air Pollution (RELMAP), used for the *Mercury Study Report to Congress*, and more recently the Community Multi-scale Air Quality (CMAQ) modeling system, which includes simulation of atmospheric chemistry, as well as models capable of local-scale atmospheric transport such as the Industrial Source Complex (ISC) model. Mercury deposition estimated via those models has been used as input for watershed and aquatic ecosystem modeling, e.g., using the indirect exposure methodology for mercury (IEM-2M) or the Multimedia, Multi-pathway, Multi-receptor Exposure and Risk Assessment model (3MRA). Unlike many of those model applications, which informed regulatory decisions by the Agency, the analyses described in this document are solely for the purpose of model evaluation.

mercury test case has been to support model development, testing, evaluation, and refinement. It is primarily an evaluation exercise, and the focus of this report is on the simulations performed for model performance evaluation. Thus, the absolute results of this test case exercise (e.g., the exact media concentrations estimated by the model) may be of less interest and relevance than whether the patterns, trends, and general magnitudes observed in the model outputs are consistent with the expected multimedia behavior of mercury released to air. The values of specific results can be affected by changes in the values of various input properties (as informed by the sensitivity analysis), whereas the overall model performance is dependent on the integration of all algorithms, formulas, and input properties, which have been supplied particular parameter values for purposes of the test case. Consequently, the primary focus of the material presented in this document is on the patterns, trends, and general magnitudes of the model outputs rather than the specific or absolute results.

Background on the Mercury Test Case

Preliminary, limited evaluations of TRIM.FaTE focused primarily on organic chemicals. An earlier prototype of TRIM.FaTE was compared with two similar models, CalTOX (McKone 1993a, McKone 1993b, McKone 1993c) and SimpleBox (van de Meent 1993, Brandes et al. 1997). The pollutants modeled for that comparison were polycyclic aromatic hydrocarbons (PAHs) (EPA 1998a). The mercury test case described in this report addresses the need to evaluate the performance of the current version of TRIM.FaTE with an inorganic chemical release scenario, particularly one that includes a persistent and mobile form of inorganic pollutant that can undergo reversible environmental transformations between different chemical species in different media. As noted above, separate evaluations of TRIM.FaTE based on organic chemical release scenarios, including PAHs and dioxins/furans, are recently completed or in progress (EPA 2004, EPA 2005b, other documentation in preparation).

Mercury is one of the 187 HAPs listed under section 112(b) of the CAA, is a Great Waters pollutant of concern (EPA 2000b), is identified as a pollutant of concern under the Urban Air Toxics Strategy (EPA 1999b), and is one of the seven specific pollutants listed for source identification under section 112(c)(6). In addition, the findings of the *Mercury Study Report to Congress* (EPA 1997) indicate that mercury air emissions may be deposited or transported to water bodies, resulting in mercury uptake by fish. Ingestion of mercury-containing fish is the dominant pathway of concern for health effects in humans, particularly developmental effects in children.

TRIM.FaTE

TRIM.FaTE is a spatially explicit, compartmental mass balance model that describes the movement and transformation of pollutants over time, through a user-defined, bounded system that includes both biotic and abiotic components (compartments). TRIM.FaTE predicts pollutant concentrations in multiple environmental media and in biota and pollutant intakes for biota, all of which provide both temporal and spatial exposure estimates for ecological receptors (i.e., plants and animals). The output concentrations from TRIM.FaTE can also be used as inputs to a human ingestion exposure model.

Mercury can take on multiple forms in the environment and each form has a different set of physical/chemical property values that influence fate and transport of the pollutant. The three main forms of mercury include elemental mercury, which is a liquid at room temperature and

volatilizes into the gas phase; inorganic mercury, which exists as a number of different compounds in both the particulate phase and gas phase; and organic mercury, which exists as a number of different compounds and is the most bioavailable form. TRIM.FaTE was specifically designed to consider reversible transformation and to simultaneously track major chemical species of a pollutant in multiple environmental media, and it includes appropriate algorithms and input data for modeling transformation of mercury among its elemental (Hg^0), inorganic (represented as divalent mercury, Hg^{2+}), and organic (represented as methyl mercury, MHg) forms. Additional background on mercury in the environment is provided in EPA's *Mercury Study Report to Congress* (EPA 1997).

Of the four types of stationary sources identified in the 1997 *Mercury Study Report to Congress* as having the highest total national emissions of mercury at that time, the chlor-alkali facility release scenario was selected for the TRIM.FaTE evaluation test case, in part because of its relatively lower release height for emitted mercury and the potential for local environmental and human health impacts. One of the primary reasons for selecting the particular facility to model was that there are relevant monitoring data for mercury in the area. The site is generally representative of a rural location with a large number of nearby lakes and rivers. The name of the facility, which is now closed, and its exact location are not identified in this report. ***This evaluation does not draw conclusions regarding the facility. Rather, it is intended to facilitate conclusions regarding the performance of TRIM.FaTE.***

In addition to the performance evaluation reported here, the mercury test case site, set-up, and data have been used by EPA for several years for a variety of TRIM.FaTE model development and testing purposes. Numerous smaller-scale and reduced complexity analyses have been performed, including many of the assessments reported in Volume I of this evaluation report (EPA 2002a), to assist in understanding, troubleshooting, and refining the model during its developmental phase.

Role of Environmental Measurements in TRIM.FaTE Performance Evaluation

An extensive review of the literature was undertaken following the Science Advisory Board's initial comments on the importance of model evaluation for the TRIM project (EPA 1998b). The review focused on identifying multimedia data sets for use in evaluating the performance of TRIM.FaTE. Several studies were identified that report chemical measurements in multiple environmental media. The majority of these studies focus on measuring current chemical concentrations in the environment with little emphasis on temporal variability or trends. Several of the studies were designed to assess multimedia partitioning (e.g., atmospheric partitioning among gas, aerosol, and water phases) or to investigate specific environmental processes such as the transfer rate across an environmental interface. The usefulness of some of the reported environmental measurements was limited because in many cases the source of the chemical contamination was not well characterized. Although historical emission patterns can potentially be reconstructed for certain chemicals using sediment chronology (Cowan et al. 1995), little effort has gone into matching historical emissions to multimedia environmental concentrations.

None of the studies identified during EPA's literature review provides complete and concurrent information on chemical concentrations in the five major environmental media (i.e., air, water, sediment, soil, biota) along with the associated source term(s) and historical environmental characteristics (e.g., meteorology, hydrology, landscape properties). Although some of these studies can be used to evaluate certain aspects of the model, it is important not to overvalue these results when judging the overall quality of the model (see EPA 1999a for details about the studies identified).

Comparisons of TRIM.FaTE outputs to monitoring data are difficult because complete multimedia data sets from well-characterized systems (e.g., known source, meteorology, and landscape) to use in a performance evaluation are not currently available. However, limited data sets are becoming available through the literature and through unpublished sources (e.g., multimedia monitoring by state or local agencies). These smaller data sets, including those collected by EPA for the mercury test case site, have contributed to this performance evaluation of TRIM.FaTE.

2. SPECIFICATIONS OF MODELED SCENARIOS

This chapter summarizes the specifications of the scenarios modeled for the TRIM.FaTE mercury test case. It is supplemented by Appendix A, which provides detailed documentation of the values and references for all of the input properties (e.g., chemical transformation rates and partition coefficients, soil and surface water parameters) used in the modeling. Three forms of mercury – elemental (Hg^0), divalent (Hg^{2+}), and methyl (MHg) – were included in the modeling, with transformation among forms modeled where supported by the available data. More details about specifications used for the steady-state modeling and the sensitivity analysis are provided in Chapters 4 and 5, respectively.

TRIM.FaTE is a multimedia, mass balancing, compartment model that simulates the transport and fate of pollutants emitted to air through time and space. It is extremely flexible in set-up and application, and it can produce a wide variety of results (e.g., mass and concentration of various chemicals over time and space for dozens of different environmental media and biota). The modeling concepts, approaches, algorithms, equations, and assumptions used in TRIM.FaTE are documented in detail in a two-volume *TRIM.FaTE Technical Support Document* (EPA 2002b and c, available with other TRIM.FaTE documentation at www.epa.gov/ttn/fera) and are not discussed at length here. All TRIM.FaTE model runs discussed in this report were performed in November and December 2003, except for the sensitivity analysis results reported in Chapter 5 and Appendix D. Those model runs were performed in June 2003 (see Chapter 5 for differences between these sets of model runs).

Overview

The modeling scenarios for this test case are based on a former manufacturing facility in the northeastern U.S. (now closed) that used a mercury cell chlor-alkali process in the production of chlorine and consequently was a source of mercury emissions to the atmosphere. Information available about this facility was used in configuring the source in the TRIM.FaTE mercury test case scenarios, as described in the next section. Information available for the facility location was used in the selection of values for environmental setting parameters, as documented in Appendix A.

To facilitate TRIM.FaTE evaluation using several different types of information, three different dynamic modeling emission cases (i.e., scenarios) and one steady-state scenario were modeled. The various TRIM.FaTE scenarios are outlined below.

- **Scenario A** – source emissions only (no boundary contributions or initial concentrations), with emission of only divalent mercury. Modeling duration is 30 years, with source emissions for entire duration. This case is used in the model comparison, which focused exclusively on divalent mercury emissions (Chapter 6).
- **Scenario B** – source emissions only (no boundary contributions or initial concentrations), with emission of both elemental and divalent mercury. Modeling duration is 30 years, with source emissions for entire duration. This case is used for much of the general results presentation and analysis (Chapter 3).

- **Scenario C** – source emissions *plus* air boundary contributions and initial concentrations in environmental media and biota, with emission (and boundary contributions) of both elemental and divalent mercury. Modeling duration is 40 years, with source emissions for the first 30 years only. This case incorporates some “background” contamination and is used in the consideration of available measurement data (Chapter 7).
- **Steady-state Scenario** – same emissions as Scenario B, but with time-varying input properties set to constants. This case is used for the sensitivity analysis (Chapter 5), and the steady-state results are also discussed in the context of the dynamic results for Scenario B (Chapter 4).

Regardless of which mercury species were emitted from the source in a given scenario, TRIM.FaTE always modeled the fate of three forms of mercury (including transformations among the different forms): elemental (Hg^0), divalent (Hg^{2+}), and methyl (MHg) mercury.

Source Specifications

The values used for source emissions of mercury to air are based on summarized data provided by a state agency in 1999. Fugitive emissions make up the bulk of air emissions for the modeled facility. In the modeling, all source emissions are released directly into one air compartment (referred to as the source compartment) that is centered (in the x-y plane) on the location of the source area – no modeling distinction is made between stack and fugitive emissions. Given that the modeled source height is very low (0.01 m), and that the atmospheric mixing height is used as the top boundary of the source compartment (and other air compartments), all modeled air emissions enter the system below the mixing height (i.e., no tall stacks modeled). Source emission rates are modeled as constant and continuous for an assumed 30-year source operating period. Re-emission of mercury compounds (e.g., from surface soil or surface water to air) is simulated by TRIM.FaTE throughout the modeling duration according to the various particle resuspension, volatilization, diffusion, and other process algorithms, as applicable (see EPA 2002c for algorithm details).

Speciated mercury emissions data were not available for the test case facility. For Scenarios B and C and the Steady-state Scenario, the total mercury emissions, which were provided by the state agency, were assumed to be 95 percent elemental mercury and five percent divalent mercury, which is believed to be within a realistic range of values for a chlor-alkali facility. For example, Landis et al. (2004) reported that roughly two percent of gaseous mercury emitted from the cell building roof vent (thought to be the largest source) over a nine-day period at a chlor-alkali plant in Georgia was inorganic divalent reactive gaseous mercury. Scenario A included only the divalent mercury emissions. The modeled emission rates are shown in the text box below. Note that the phase distribution (e.g., particle, gas) of the emitted compounds is not set as an input in TRIM.FaTE; rather, the model calculates the phase distribution at each time step based on chemical properties such as Henry’s Law constant and other input properties (see EPA 2002b,c for details).

Scenario	Modeled Emission Rate (g/day)	
	Elemental Mercury (Hg ⁰)	Divalent Mercury (Hg ²⁺)
A	0	17.663
B, C, Steady-state	335.6	17.663

Spatial Specifications of the Scenarios

The overall extent of the area for which chemical transport and fate are modeled (i.e., the modeling region) was set based on the location of the emissions source, expected mobility of the chemical of primary interest with respect to deposition (i.e., divalent mercury, which deposits at much higher rates than elemental mercury), locations of receptors of interest (e.g., water bodies supporting robust fish populations), and watershed boundaries for the water bodies of interest (see EPA 2003b for discussion of considerations in setting TRIM.FaTE spatial boundaries and spatial layouts). This test case was intended to be a local analysis focused on nearby water bodies; therefore, the modeling region boundaries were set to encompass the water bodies and watersheds of main interest, and not necessarily to capture the deposition of a large fraction of the emitted mercury mass.

The modeling layouts used for the mercury test case (i.e., the number, size, shape, and location of all volume elements, which are the spatial entities in which compartments are located) are shown on the same scale in Exhibits 2-1 and 2-2 for the air and surface parcels, respectively (see text box for basic spatial terminology; for further discussion of TRIM.FaTE spatial concepts and definitions, see EPA 2002b). As evident from these layouts, the internal and outer boundaries of the air parcels (Exhibit 2-1) do not line up exactly with those for the surface parcels (Exhibit 2-2), which is typical for TRIM.FaTE applications to date. These differences result from the differing considerations for modeling the movement of chemicals in different types of media (air versus soil and water). The air layout extends beyond the surface layout in all directions because of the desire to account for at least some of the “blow-back” of airborne chemical into the area of primary

Basic TRIM.FaTE Spatial Terminology

Parcel – A planar (i.e., two-dimensional), horizontal geographical area used to subdivide the modeling region. Parcels, which are polygons of virtually any size or shape, are the basis for defining volume elements (by adding a vertical dimension) and do not change for a given scenario.

Volume element – A bounded three-dimensional space that defines the location of one or more compartments.

Compartment – The TRIM.FaTE modeling unit that contains chemical mass; chemical mass is transported between and transformed within compartments. A specific compartment is characterized by its physical and spatial composition and its relationship to other compartments. Within a compartment it is assumed that all chemical mass is homogeneously distributed and is in phase equilibrium.

Exhibit 2-1 Layout of Air Parcels

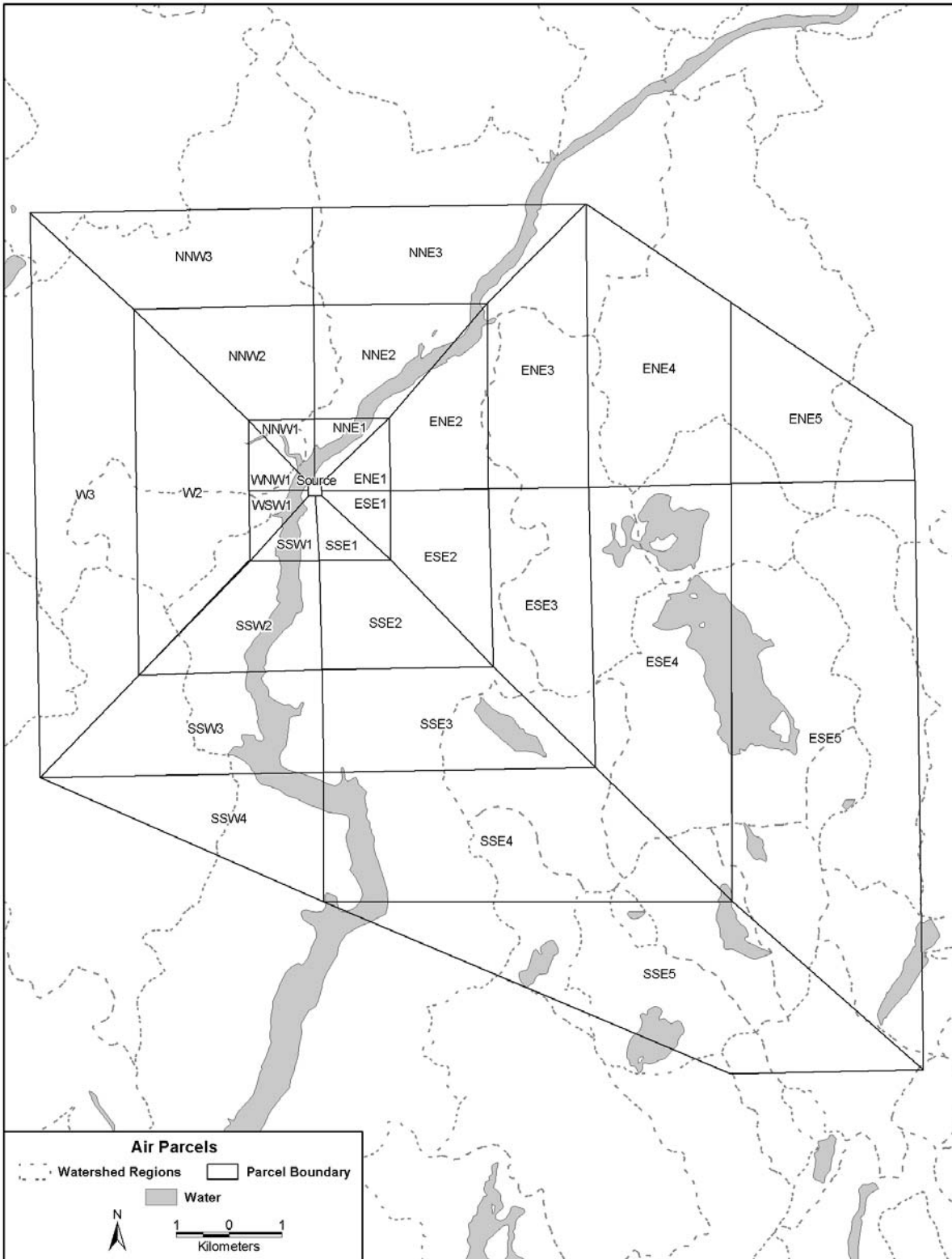
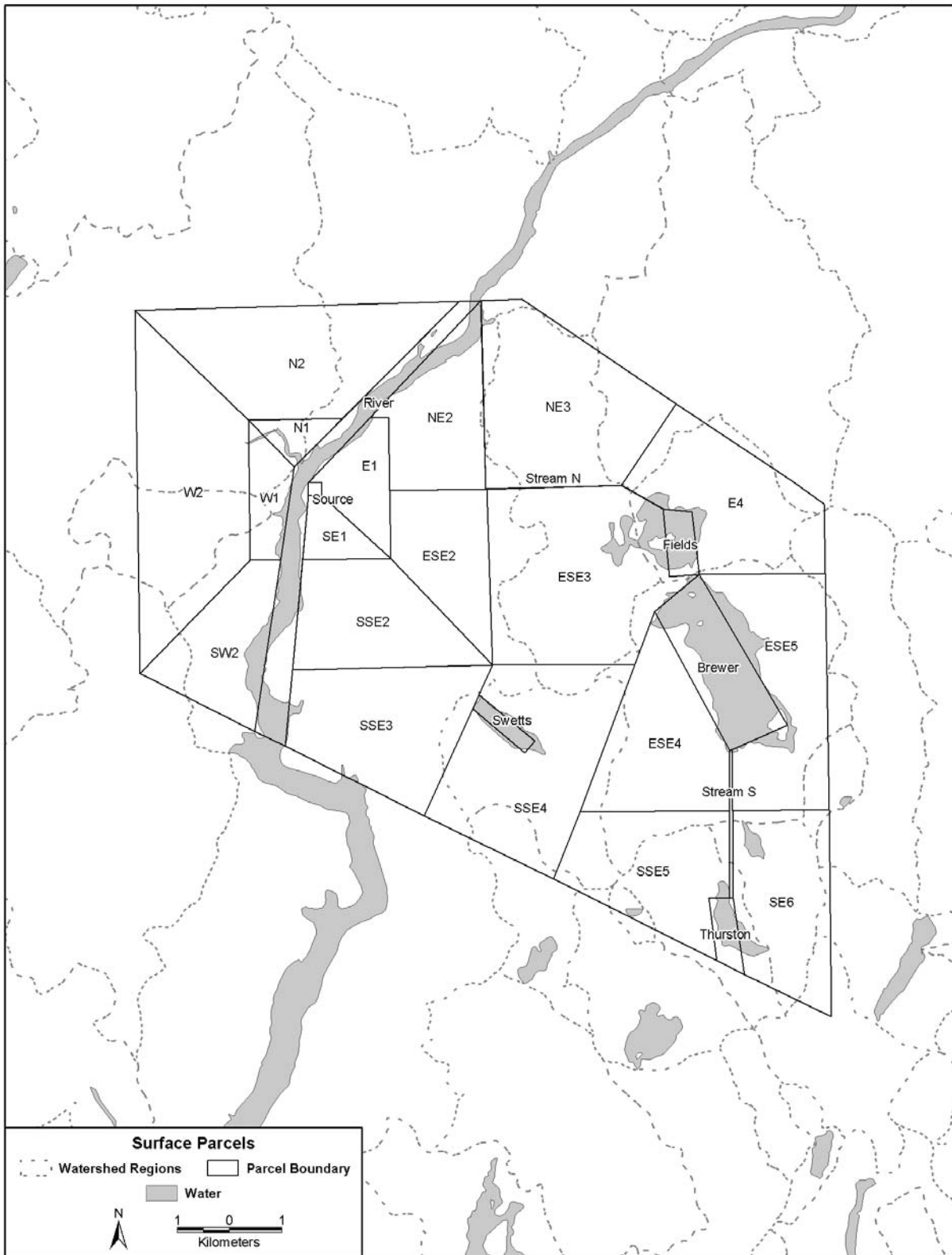


Exhibit 2-2
Layout of Surface Parcels (same scale as Exhibit 2-1)



interest (represented, in this case, by the surface layout) that results from changes in wind direction.¹

The surface parcel layout consists of 20 soil parcels (including a small source parcel centered on the emission source), four lake parcels, one large river parcel, and two small stream parcels (total of 27 surface parcels). The air configuration includes 30 parcels arranged in an approximate radial grid originating from the source parcel, which is centered on the emission source (for the mercury test case scenarios, the source air parcel lines up exactly with the source surface parcel) (see EPA 2002a for evaluation of different air parcel layouts, including the approximate radial grid design used here). Similar to the surface parcel layout, the air grid extends farther to the east and southeast so that it covers the water bodies of interest, and their watersheds, in that direction. The air grid was scaled so that the inner air parcels line up at least in part with the surface parcels, and with at least one air parcel extending beyond the boundary of the surface parcel layout on all sides (i.e., the air parcel grid is larger than the surface parcel grid). The total size of the air grid is approximately 227 km², and the total area encompassed by the surface parcel layout is approximately 126 km².

Soil parcel boundaries were located to minimize overland flow between adjacent terrestrial parcels (including the external boundary of region), with some attention also given to maintaining homogeneity of land use and plant type patterns. Some of the initial soil parcels were then subdivided to provide additional spatial resolution. Availability of monitoring data, intended to be used in comparisons with model outputs, was also considered in developing the soil parcel layout. Water bodies were selected for inclusion as parcels in the modeling scenarios primarily based on their size and proximity to the emission source and the availability of monitoring data. Six of the seven water bodies are part of the same system of lakes and streams feeding into the river.²

Compartments Modeled in the Scenarios

Consistent with the concepts employed in TRIM.FaTE (see TRIM.FaTE TSD Volume 1, Chapters 3 and 5 for more detail), volume elements were created with the same horizontal dimensions of the parcels. For example, a volume element was configured for each air parcel with the same x and y dimensions. The vertical dimension (i.e., the height) of all the air volume elements was set to vary with the mixing height, which varied over time according to the meteorological input data. A single layer of air volume elements was used for all scenarios.

¹ In TRIM.FaTE, chemical mass in air that crosses the external air boundary enters an air sink and cannot re-enter the modeling region. Therefore, if the external boundaries of the air and surface layouts line up exactly, transport of chemical mass to air beyond the boundaries of the surface parcels makes that mass unavailable to the surface parcels for the entire modeling period (i.e., there can be no modeled “blow-back” of this mass).

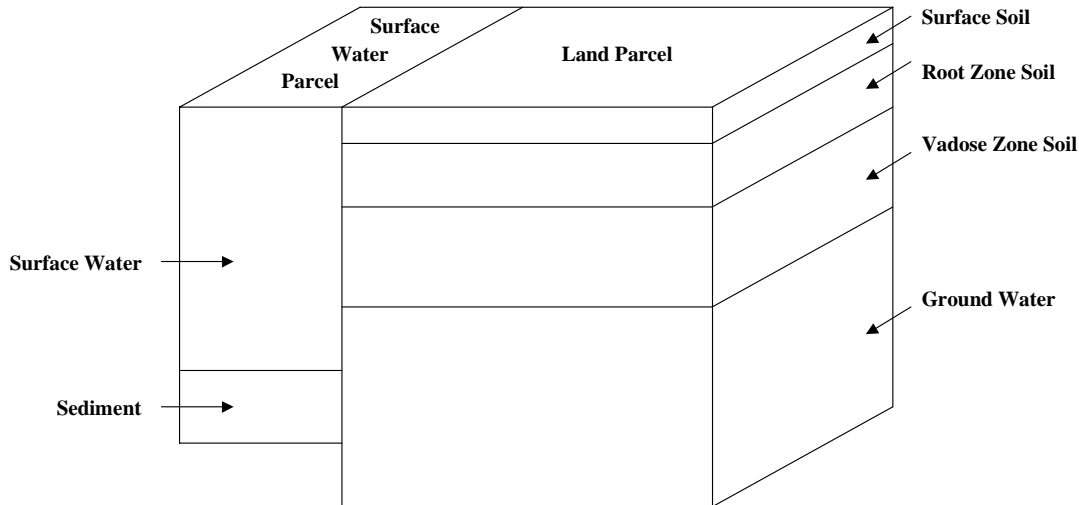
² Although the river near the facility on which the scenarios are based is tidal, it was modeled for test case purposes as a non-tidal river because the TRIM.FaTE library did not include algorithms to accommodate tidal influence on pollutant movement. Additionally, because the river was not a primary focus for the evaluation, the entire extent of the river within the modeling region was designated as a single parcel. For these reasons, results for the river compartment are not emphasized in this report and are not used in consideration of the measurement data.

For each surface parcel, one of the following was created:

- Set of soil volume elements (surface soil, root zone soil, and vadose zone soil) and a ground water volume element; or
- Pair of surface water and sediment volume elements.

As illustrated in Exhibit 2-3, the soil and ground water volume elements are aligned exactly with the x-y dimensions of the land parcels, and situated vertically in series just below the layer of air volume elements (i.e., the land surface serves as the bottom of the air volume elements and the top of the surface soil volume elements). Similarly, the surface water and sediment volume elements are aligned exactly with the x-y dimensions of the surface water parcels, and situated vertically with the surface water volume element just below the layer of air volume elements and the sediment volume element just below its corresponding surface water volume element. The vertical dimension (i.e., depth) of all abiotic volume elements other than air was set as a constant (non-time-varying) value.

Exhibit 2-3
Schematic of Volume Element Layering: Two Hypothetical Surface Parcels



Abiotic compartments are associated with each of the volume elements as follows:

- 30 air compartments (corresponding to the 30 air volume elements);
- 20 each of surface soil, root zone soil, vadose zone soil, and ground water compartments (corresponding to the 20 each surface soil, root zone soil, vadose zone soil, and ground water volume elements, respectively); and
- Seven each of surface water and sediment compartments (corresponding to the seven surface water and seven sediment volume elements, respectively).

Biotic compartments (representing biological populations within the ecosystem) are associated with the various abiotic volume elements. The biota included in the test case were selected based on the availability of monitoring data, the need for model comparisons, the need to adequately account for mass distribution of mercury, and/or the need to represent particular trophic levels. The different biotic compartment types, representing plants and animals in both aquatic and terrestrial ecosystems, that are included in the test case scenarios are shown in Exhibit 2-4. Exhibits 2-5 and 2-6 provide further detail on the relationship between volume elements and biotic compartment types, and on the modeled spatial distribution of the various biota. Additional details about the biotic aspects of the model set-up, including the modeled population densities for each compartment, are provided in Appendix A.

Input property values were set with a consideration of site or region-specific information, where appropriate. Additional details on the model setup and documentation for input property values are reported in Appendix A.

Temporal Aspects of the Dynamic Scenarios

Given the history of the facility being modeled and the timing of the available monitoring data, the modeling period was set at 30 years for emission cases A and B, and 40 years for emission case C (the source emission duration remained at 30 years for case C). Thus, the emission source started emitting at the beginning of the modeling period (roughly considered to be late 1960s) and continued for 30 years (most of the monitoring data are from the late 1990s). The output time step for the three dynamic scenarios was set to two hours; that is, the model provided outputs in terms of moles, mass, and concentration of elemental, divalent, and methyl mercury for each of the 417 compartments at two-hour intervals throughout the 30-year modeling period. Two hours was selected as the output time step to strike a balance between volume of model outputs and adequate time resolution to capture anticipated time-varying results. These outputs are instantaneous values (“snapshots”) every two hours, not some type of time-averaged values. Thus, the raw output was voluminous for each emission case, with more than 100 million calculated values each for moles, mass, and concentration. Most of the subsequent data review and analysis was performed on annual (and in some cases monthly) averages of the two-hour instantaneous output data.

The vast majority of numeric property values set for the test case scenarios are modeled as constant over time (see Appendix A for input values), but a few inputs – notably

Exhibit 2-4
Biotic Compartment Types Modeled for the Mercury Test Case

Biotic Compartment Type	Representative Subgroup or Species
<i>Terrestrial Plants</i>	
Leaf Particle on leaf Stem Root	Of three vegetation types – deciduous forest, coniferous forest, grasses/herbs (stems and roots not currently modeled in TRIM.FaTE for deciduous and coniferous forest vegetation types)
<i>Terrestrial Animals</i>	
Soil detritivore	Soil arthropod, Earthworm
Ground-invertebrate feeder	Short-tailed shrew
Herbivore	Meadow vole, White-tailed deer
Insectivore	Black-capped chickadee
Omnivore	Mouse
Carnivore	Long-tailed weasel, Red-tailed hawk
<i>Semi-aquatic Animals</i> ^a	
Insectivore	Tree swallow
Omnivore	Mallard, Raccoon
Piscivore	Common loon
Carnivore	Mink, Bald eagle
<i>Aquatic Plants</i>	
Macrophyte	Submerged aquatic vegetation generalized from <i>Elodea sp.</i>
<i>Aquatic Animals</i>	
Benthic invertebrate Benthic omnivore Benthic carnivore Water-column herbivore Water-column omnivore Water-column carnivore	These compartment types represent trophic niches arising either from a benthic or water-column source. ^b

^a The term “semi-aquatic” is used in TRIM.FaTE documentation to refer to birds and mammals that reside and/or nest on land but that include at least some aquatic biota in their diets.

^b These compartment types were not parameterized using the concept of a single representative species that might feed on organisms from more than one trophic level or from both benthic and water-column environments. Rather, the total biomass for a single representative fish species that feeds from both benthic and water-column sources has been divided into two compartments for that species: one that feeds from benthic sources and one that feeds from water-column sources, respectively.

Exhibit 2-5
Volume Element Relationships and Spatial Distribution of Biotic Compartments

Volume Element	Associated Biotic Compartment Types	Notes on Spatial Distribution of Biotic Compartments ^a
Air	None	–
Surface soil	<i>Terrestrial plant</i> : leaf, particle on leaf, stem, root	All surface soil volume elements (VEs) except source; vegetation types vary across VE (see Exhibit 2-6); stem and root only included for grasses/herbs vegetation type
	<i>Terrestrial animal</i> : soil detritivore (soil arthropod), ground-invertebrate feeder (short-tailed shrew), herbivore (meadow vole, white-tailed deer), insectivore (black-capped chickadee), omnivore (mouse), carnivore (long-tailed weasel, red-tailed hawk)	All surface soil VEs except source, N1, and W1, except that meadow vole only included for grasses/herbs vegetation type (SW2, NE2)
	<i>Semi-aquatic animal</i> : insectivore (tree swallow), omnivore (raccoon), carnivore (mink, bald eagle)	All surface soil VEs except source, N1, and W1, except that raccoon and mink also not included for three VEs that do not border modeled lakes or river (ESE2, W2, NE3)
Root zone soil	<i>Terrestrial animal</i> : soil detritivore (earthworm)	All root zone soil VEs except source
Vadose zone soil	None	–
Ground water	None	–
Surface water	<i>Aquatic plant</i> : macrophyte	All surface water VEs except the two small streams
	<i>Semi-aquatic animal</i> : omnivore (mallard), piscivore (common loon)	All surface water VEs except the two small streams
	<i>Aquatic animal</i> : water-column herbivore, omnivore, carnivore	All surface water VEs except the two small streams
Sediment	<i>Aquatic animal</i> : benthic invertebrate, omnivore, carnivore	All sediment VEs except the two small streams

^a No biotic compartment types modeled for source volume elements because they are considered too industrial/contaminated. No animal compartment types modeled for surface soil volume elements N1 and W1 because they are considered too developed/urban (note that earthworm is modeled for root zone soil volume elements N1 and W1).

Exhibit 2-6
Spatial Variation of Vegetation Types and Terrestrial/Semi-aquatic Animal Compartment Types^a



^a As modeled, the source parcel has no associated animals, and soil parcels N1 and W1 have earthworm only. Except where footnoted, all other soil parcels have the following associated animal compartment types: bald eagle, black-capped chickadee, earthworm, long-tailed weasel, mink, mouse, raccoon, red-tailed hawk, short-tailed shrew, soil arthropod, tree swallow, and white-tailed deer.

^b These parcels have all the species listed in footnote a, plus the meadow vole.

^c These parcels have all the species listed in footnote a, except for the raccoon and mink.

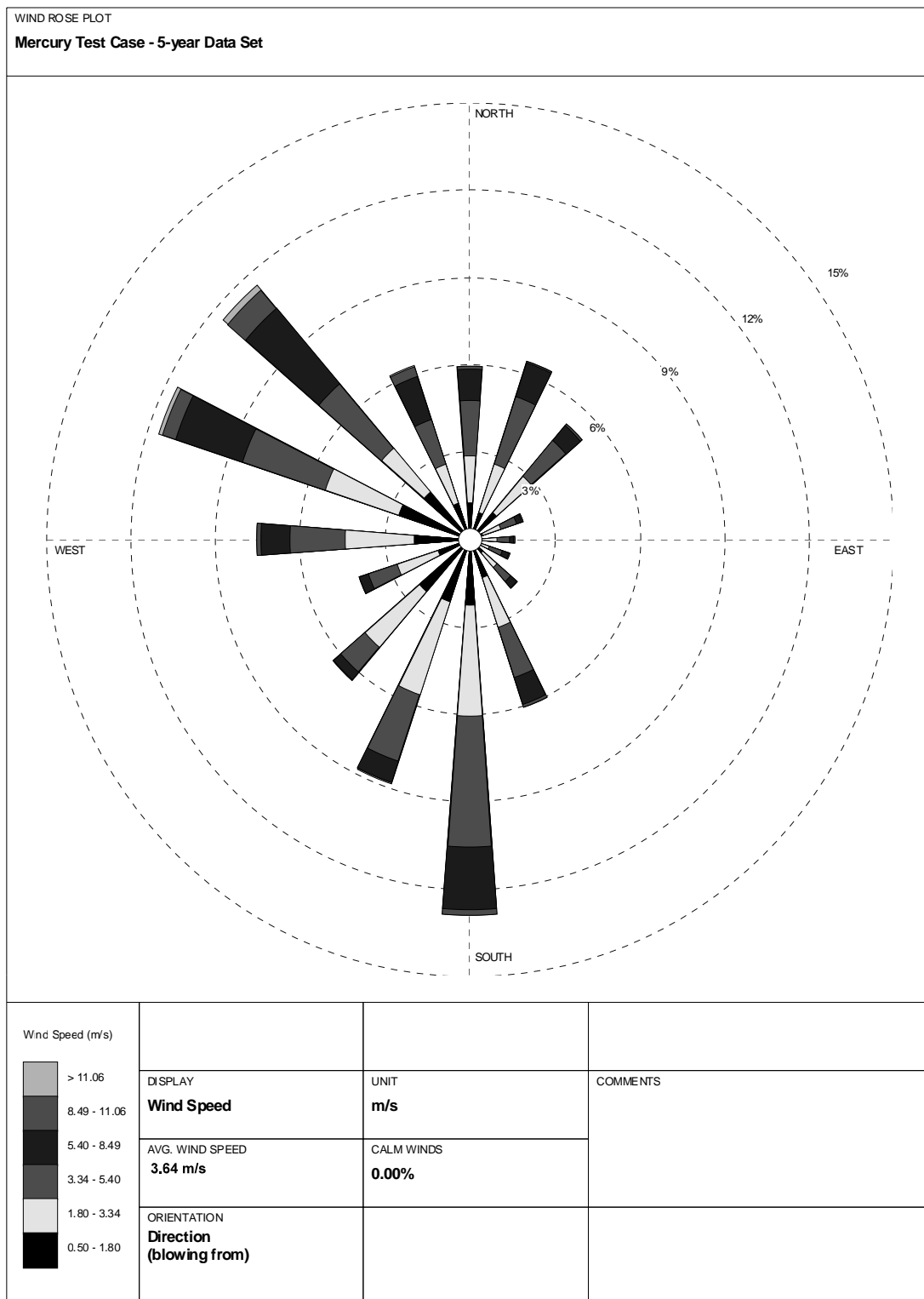
meteorological and seasonal parameters – are time-varying (see list in Section 4.1). The seasonally varying properties included in these scenarios are those affecting plants (i.e., hours of daylight, length of growing season) and meteorological properties such as air temperature. These scenarios did not include simulation of certain winter weather-related conditions (e.g., frozen precipitation, snow or ice covered surfaces).

In the case of the meteorological properties, the best and most complete data available for the vicinity of the facility were used to construct a five-year hourly data set for 1987 to 1991 of all TRIM.FaTE meteorological data inputs. The data set is a composite from three meteorological data measurement stations – wind speed and direction and air temperature from a nearby station (within 10 km), precipitation rate from a different nearby station with more complete records (within 20 km), and the upper air data needed to estimate mixing height from a station roughly 150 km to the southwest. The five-year meteorological input data set is repeated as needed to provide values for the full analysis (e.g., six times for a 30-year modeling period). Pre-processing of the raw meteorological data (e.g., units conversions, setting minimum values) to facilitate use in TRIM.FaTE followed the approach outlined in the *TRIM.FaTE User's Guide* (EPA 2003b). A wind rose representing the entire five-year composite wind data set (roughly 43,800 data points for both wind direction and speed) is provided in Exhibit 2-7. Winds are predominantly from the northwest and south, and very rarely from the east (similar to on-site meteorological data for 1998-99; see wind rose in Appendix F). Wind speeds reported in the original data source as zero (roughly 20 percent of all hourly values) were set to a minimum value of 0.75 m/sec for TRIM.FaTE modeling, which explains the absence of calm winds in the wind rose. Note that the lowest reported non-zero value in the original data source is 1.03 m/sec.³

As noted earlier, Scenario C included initial concentrations in each compartment in the system (intended to correspond to the point in time when the facility being modeled began operation). These initial concentrations were developed using a separate preliminary TRIM.FaTE simulation. The purpose of this preliminary simulation was to represent historical mercury contamination unrelated to the industrial facility source included in scenarios. In setting the duration of this preliminary model run, the time needed for the slowest responding compartments (e.g., sediment, vadose zone soil) to reach steady-state was considered. A 30-year dynamic simulation was performed in which boundary contributions of mercury in air set at “background” levels were the *only* source of mercury introduced to the modeling region (i.e., no emissions source within the region’s boundaries was modeled, nor were any boundary contributions other than via air). Background concentrations of mercury in the air that flows across the boundary and into the test case modeling region – 1.6E-09 g/m³ for elemental mercury and 1.6E-11 g/m³ for divalent mercury – were typical concentrations for the eastern U.S. atmosphere as reported in the *Mercury Study Report to Congress* (EPA 1997). The resulting environmental media and biota concentrations for each compartment at the end of 30 years (i.e., the final two-hour snapshots) were used as initial concentrations. Although mercury concentrations did not reach steady-state for most compartment types by 30 years (and some

³ Early testing with TRIM.FaTE’s air component showed that inputting wind speeds of zero causes mass buildups in the source compartment that can produce artifactual results. A minimum value of 0.75 m/sec (an approximation for a lower reporting limit) was adopted for initial test cases and is suggested in the *TRIM.FaTE User's Guide* (EPA 2003b).

Exhibit 2-7 Wind Rose Representing TRIM.FaTE Five-year Input Data Set



likely would take hundreds of years to get there), in most cases the rate of increase was tapering off by year 30. Thus, given model run time considerations along with the significant uncertainties about the timing and magnitude of air background in the site vicinity, a 30-year dynamic run was considered sufficient for the purposes of establishing initial concentrations.⁴

To place the modeled Scenario C initial concentrations in the context of measurement data, they were compared with measured values reported in the *Mercury Study Report to Congress* (EPA 1997). In general, the ranges (across compartment locations) of initial concentrations of total mercury calculated by TRIM.FaTE in the 30-year model run described above are roughly comparable to the measurement data presented for most media, with TRIM.FaTE concentrations generally lower than measured data (see text box below). For surface soil, Scenario C initial concentrations fall within the lower end of the range of typical measured concentrations for U.S. soils reported. Initial concentrations for surface water are also within the relatively broad range of measurement data reported for freshwater lakes, though at the low end of that range. For sediment, Scenario C initial concentrations are lower than the range of measured data but still within an order of magnitude of most reported concentrations. Differences are greater for fish. Scenario C initial concentrations for higher trophic level fish (e.g., water-column carnivore) are lower than reported measured values by one to two orders of

Medium	Case C Initial Conc (total Hg)	Measurement Data Reported in <i>Mercury Study Report to Congress</i>
Surface soil	21-47 ng/g DW, ~100% Hg ²⁺	<ul style="list-style-type: none"> • Reported values range from 8 to 406 ng/g dry wt • “Typical” US soils reported by NJDEPE to range from 8 to 117 ng/g dry wt • Most Hg reported to be Hg²⁺, with some MHg as well (0.3% to >10%)
Surface water	0.34 -0.63 ng/L, 89% Hg ²⁺ , 10% Hg ⁰ , 1% MHg	<ul style="list-style-type: none"> • Reported values for freshwater lakes range widely; from <0.1 to 74 ng/L total mercury; most values between 1 to 10 ng/L • Concentrations vary widely; seasonality may be one factor in variability
Sediment	12-18 ng/g DW, >99% Hg ²⁺	<ul style="list-style-type: none"> • Means for U.S. lake sediment samples range from 70 to 310 ng/g dry wt • Other lakes (WI, MN) range from 34 to 753 ng/g • RTC reports “concentrations exceeding 200 ng/g are not unusual”
Fish-WCC ^a	9.1-13 ng/g WW, >99% MHg	<ul style="list-style-type: none"> • Mean Hg concentrations reported for two nationwide studies were 110 and 260 ng/g fresh wt across all species • Means from these two studies were higher for bass and trout, lower for catfish • Measured Hg concentrations in sportfish species from various other studies were generally similar to data from the above two nationwide studies • Most values were between 100 and 1,000 ng/g, with some outliers on both low and high ends <ul style="list-style-type: none"> • bass: <100 to 600 or higher, some >1,000 ng/g • panfish: <50 to 700, some around 1,000 ng/g • “bottom feeders”: 50 to ~500 ng/g, but lower than most other fish types
Fish-WCO	2-2.9 ng/g WW, 88% MHg	
Fish-BC	1.4-2 ng/g WW, 95% MHg	
Fish-BO	0.45-0.66 ng/g WW, 57% MHg	

^a WCC = water-column carnivore, WCO = water-column omnivore, BC = benthic carnivore, BO = benthic omnivore.

⁴ Steady-state model runs were not used to develop initial concentrations because boundary contributions of a chemical cannot currently be modeled by TRIM.FaTE’s steady-state mode.

magnitude. Differences are even greater for water-column omnivores, with Scenario C initial concentrations lower by two to three orders of magnitude and for benthic fish, with initial concentrations lower than reported measured values by up to three orders of magnitude.

It is expected that some of the reported measurement locations were selected to include sites of interest, including sites subject to contamination from nearby sources of mercury (i.e., the measured values being compared may not be fully comparable “background” values). Moreover, as noted above, initial concentrations based on a 30-year TRIM.FaTE model run have not reached steady-state for some compartment types. In fact, of the compartment types compared, the ones farthest from reaching steady-state after 30 years – surface water, sediment, and fish, all at least an order of magnitude below expected steady-state levels – are lowest in relation to the reported ranges of measurement data (see Chapter 4 for comparisons of steady-state to dynamic modeling results for TRIM.FaTE). Therefore, it seems reasonable that the Scenario C initial concentrations estimated by TRIM.FaTE are toward the lower end of, or in some cases below, the ranges of reported measured values.

3. RESULTS AND DISCUSSION: DYNAMIC MODELING

This chapter presents the TRIM.FaTE dynamic modeling results for the mercury test case. The main purpose of this chapter is to provide a broad cross-section of the extensive modeling results and give a sense of the overall patterns and trends in the data, rather than to focus in-depth on any particular parts of the data. Steady-state modeling results, sensitivity analysis results, comparisons with another multimedia model, and evaluations against monitoring data are presented in subsequent chapters of this report. A few steady-state modeling results related to mercury speciation are included in Section 3.3 for comparison with the dynamic modeling results.

As described in Chapter 2, TRIM.FaTE produced voluminous results for this test case – detailed time-series data for three species of mercury for various abiotic media and numerous biota at varying locations – and only selected results are highlighted here. Appendix B contains additional summary tables and charts to supplement the results presented in this chapter. TRIM.FaTE modeling processes and algorithms are noted in some of the results discussions, but detailed descriptions are not provided here (see EPA 2002b,c for more information; also, the series of process tables in Chapter 6 provides a summary of the processes modeled for certain compartment types).

The presentation of results starts with a summary of the distribution of total mercury mass over time among the different compartment types (Section 3.1). Then, Section 3.2 presents the total mercury concentration results over time for various compartment groupings. Section 3.3 addresses differences in the results for the three different species of mercury modeled. Spatial variations in the total mercury concentration results are presented in Section 3.4, and comparisons among the three dynamic emission cases are presented in Section 3.5.

Except for Section 3.5, all of the results discussed in this chapter are for emission case B (both elemental mercury and divalent mercury emitted from the source, no boundary contributions or initial concentrations included). In general, the mass and concentration results presented are *annual averages*, which are calculated by averaging the bi-hourly instantaneous output data over each year of the modeling period.¹ With the exception of one section devoted to analysis of the mercury speciation results, most of the data are presented as *total mercury* (i.e., sum of elemental mercury, divalent mercury, and mercury portion of methyl mercury).

Because interpretation of all the results for animals is so strongly dependent on what they eat, a summary of the modeled animal diets and soil ingestion rates is provided for reference here at the beginning of the results chapter (Exhibit 3-1; see Appendix A for full referencing of the values). Also, referral back to the site layout maps in Exhibits 2-1 and 2-2 is helpful for interpreting the compartment-specific results.

¹ For leaf and particle-on-leaf compartments of the deciduous forest and grasses/herbs vegetation types, annual averages usually are estimated from the bi-hourly output data only for the days when leaves were present (i.e., they represent a growing season average for the given year).

Exhibit 3-1
Diets for Animal Compartment Types Modeled for Mercury Test Case

Animal Species (Trophic Level/Niche)	Land- or Water- based^a	Terrestrial, Aquatic, or Mixed Diet	Modeled Diet Fractions	Modeled Soil Ingestion Rate (kg/kg-day)
White-tailed deer (terrestrial herbivore)	L	T	100% terrestrial plant	0.00013
Meadow vole (terrestrial herbivore)	L	T	100% terrestrial plant	0.0006
Mouse (terrestrial omnivore)	L	T	50% terrestrial plant 50% soil arthropod	0.001
Black-capped chickadee (terrestrial insectivore)	L	T	70% soil arthropod 30% terrestrial plant	0
Short-tailed shrew (terrestrial ground- invertebrate feeder)	L	T	58.5% earthworm 41.5% soil arthropod	0.0611
Weasel (terrestrial carnivore)	L	T	50% mouse 25% short-tailed shrew 25% meadow vole	0
Red-tailed hawk (terrestrial carnivore)	L	T	30.3% mouse 25.7% black-capped chickadee 20% short-tailed shrew 20% meadow vole 4% soil arthropod	0
Mink (semi-aquatic carnivore) ^b	L	M	23% mouse 23% meadow vole 17% benthic invertebrate 15% benthic omnivore 10.3% water-column herbivore 8% black-capped chickadee 3.7% water-column omnivore	0
Bald eagle (semi-aquatic carnivore)	L	M	23% mouse 17% benthic carnivore 17% benthic omnivore 11% water-column carnivore 11% water-column herbivore 11% water-column omnivore 10% black-capped chickadee	0

Animal Species (Trophic Level/Niche)	Land- or Water- based ^a	Terrestrial, Aquatic, or Mixed Diet	Modeled Diet Fractions	Modeled Soil Ingestion Rate (kg/kg-day)
Raccoon (semi-aquatic omnivore)	L	M	69% benthic invertebrate 21% earthworm 4.6% benthic omnivore 4% water-column herbivore 1.4% water-column omnivore	0.0029
Tree swallow (semi-aquatic insectivore)	L	A	100% benthic invertebrate (represents aquatic insects)	0
Mallard (semi-aquatic omnivore)	W	M	66.5% terrestrial plant 33.5% benthic invertebrate	0.00085
Common loon (semi-aquatic piscivore)	W	A	50% benthic omnivore 50% water-column omnivore	0
Water-column herbivore ^c	W	A	100% algae	n/a
Water-column omnivore ^c	W	A	100% water-column herbivore	n/a
Water-column carnivore ^c	W	A	100% water-column omnivore	n/a
Benthic omnivore ^c	W	A	100% benthic invertebrate	n/a
Benthic carnivore ^c	W	A	100% benthic omnivore	n/a

^a Refers to the volume element with which the animal compartment is associated in TRIM.FaTE. “W” means the compartment is associated with a surface water or sediment volume element, and “L” means the compartment is associated with a surface soil volume element.

^b In TRIM.FaTE documentation, “semi-aquatic” refers to animals that reside and/or nest on land but that are modeled as having aquatic biota in their diet.

^c Not modeled as individual species; see footnote to Exhibit 2-4.

3.1 Time Patterns of Mercury Mass Accumulation

This section presents a series of charts showing the accumulation of total mercury mass over time within various parts of the modeling system. As noted above, the data presented are for emission case B. Corresponding data are presented in tabular form in Appendix B.1.

In emission case B, mercury mass was input to the modeling system only via emissions to air from a single industrial source. Source emissions were modeled at the following rates, which were assumed to be continuous and constant over the entire 30-year modeling period.

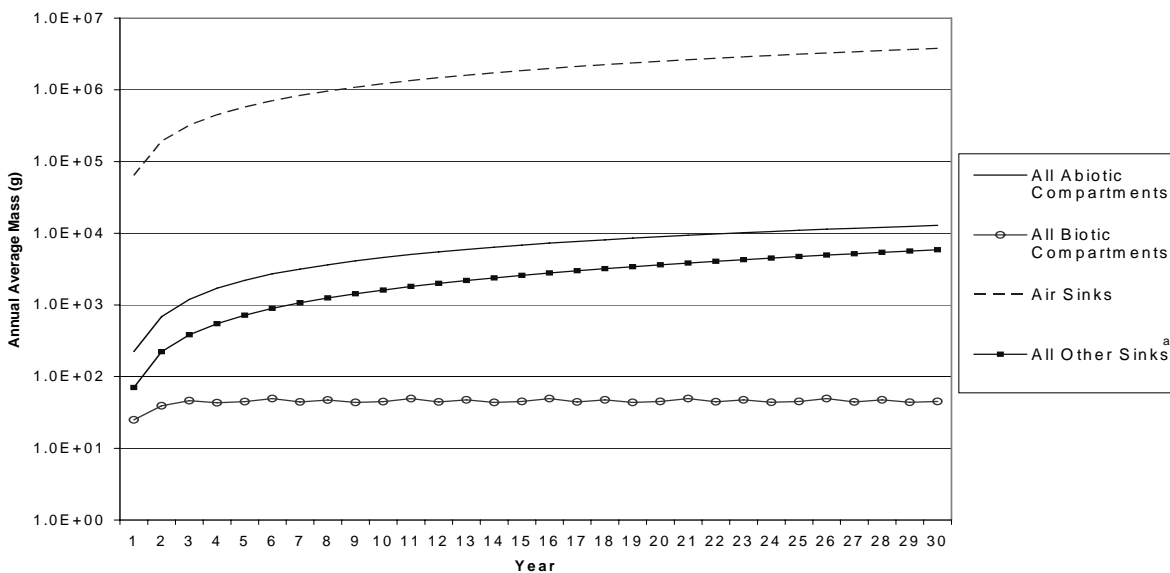
- Elemental mercury (Hg⁰) – 335.6 g/day (~ 123,000 g/yr, or 3.68 million grams over 30 years)
- Divalent mercury (Hg²⁺) – 17.663 g/day (~ 6,450 g/yr, or 0.19 million grams over 30 years)

Therefore, approximately 353 g/day of total mercury were input to the modeling system (~ 129,000 g/yr, or 3.87 million grams over 30 years), and the modeling results confirm that all of the input mass was accounted for by TRIM.FaTE throughout the modeling period. The speciation of air emissions for the test case was based on an assumption that 95 percent of the total mercury emitted was in the form of elemental mercury.

Overall Mass Distribution

Exhibit 3-2 shows a very broad picture of where the emitted mass accumulates for the mercury test case scenario. By far, most of the total mercury mass (>99 percent) ends up in the air sinks (i.e., transported via wind advection beyond the modeling region boundaries), not a surprising result given that all emissions are to air and nearly all are in a gaseous/vapor form (based on the speciation assumption and the phase distribution algorithms/input data used), and that the size of the air modeling region is relatively small (maximum source-to-boundary distance is 16 km, minimum is 5.2 km). Thus, the wind quickly blows most of the emitted mercury mass beyond the modeling region boundaries, where it is tracked by TRIM.FaTE for mass balance accounting purposes but its transport and fate are no longer modeled. For divalent mercury, which deposits at a more rapid rate than elemental mercury, a lesser amount (92 percent) of the emitted mass is in the air sinks at the end of 30 years.²

**Exhibit 3-2 – Log Scale
Total Mercury Mass: Overall Distribution in Compartments and Sinks**



^a Includes soil advection and surface water advection sinks (i.e., transported outside the modeling region via soil runoff/erosion and surface water outflow).

² The other eight percent of the emitted divalent mercury, roughly 15 kg, remains in the compartments of the modeling region or is in the other (non-air) sinks at the end of 30 years. The modeled total amount of divalent mercury deposited from air to the surface (soil, surface water, and plants) over 30 years is roughly 40 kg (21 percent of the 193 kg emitted). The difference, about 25 kg of divalent mercury, is believed to be primarily a result of re-emission to air from soil, surface water, and plant leaves, in most cases following transformation to elemental mercury. A small amount of the deposited divalent mercury is transformed to methyl mercury (net of less than 1 kg).

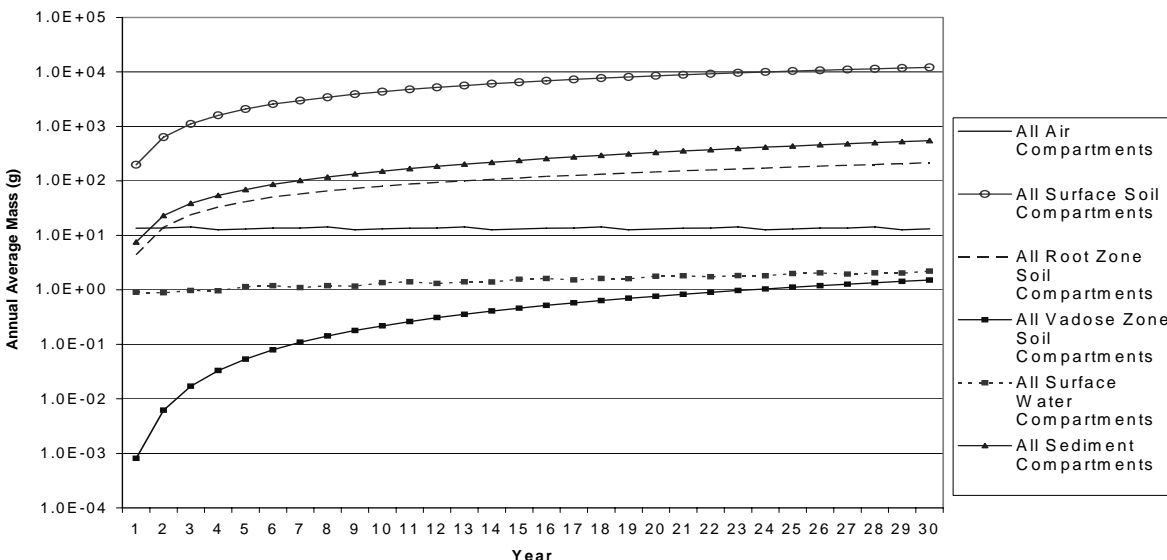
Compared with the air sinks, a much smaller (roughly 1,000-fold) amount of the total mercury mass accumulates in the surface soil advection and surface water advection sinks. This mass leaves the modeling region via soil runoff and erosion across the boundaries or surface water outflows. These results show that the relatively small size of the modeling region would not allow tracking of the *overall* impact of mercury air emissions from the facility on ecological or human health. The initial design of the test case (including sizing of the modeling region), however, was focused on the area in the immediate facility vicinity, especially the local ponds and lakes and their watersheds.

As shown in Exhibit 3-2 (and Appendix Table B-1), most (>99 percent) of the total mercury mass remaining within the modeling region (i.e., not in the sinks) at any time is in the abiotic compartments. The abiotic mass increases steadily over time, following a similar time pattern as air sink accumulation (i.e., accumulation appears to be roughly proportional to emissions). The abiotic mass as a percentage of total mercury mass in the system is fairly constant over the 30-year period, in the range of 0.3 to 0.4 percent and declining slightly over time. The amount of mercury mass in biota is much lower than in the abiotic media, which is in part a result of the lower relative volume (and mass) of the biotic compartments. After the first two years the mercury mass in biota does not appear to be increasing over the modeling period, but it actually is very slowly increasing over time. At 30 years, approximately 0.001 percent of the total mass in the system is in biotic compartments.

Mass Distribution in Abiotic Compartments

The patterns of total mercury mass accumulation in abiotic compartment types are shown in Exhibit 3-3. All soil compartment types and sediment accumulate mass steadily over time, and at 30 years all appear to be increasing at roughly similar rates (mercury in vadose zone soil, which has by far the lowest mass of any soil compartment type throughout the modeling period,

**Exhibit 3-3 – Log Scale
Total Mercury Mass: Abiotic Compartment Types^a**



^a Ground water not included (2.4E-06 g at year 30).

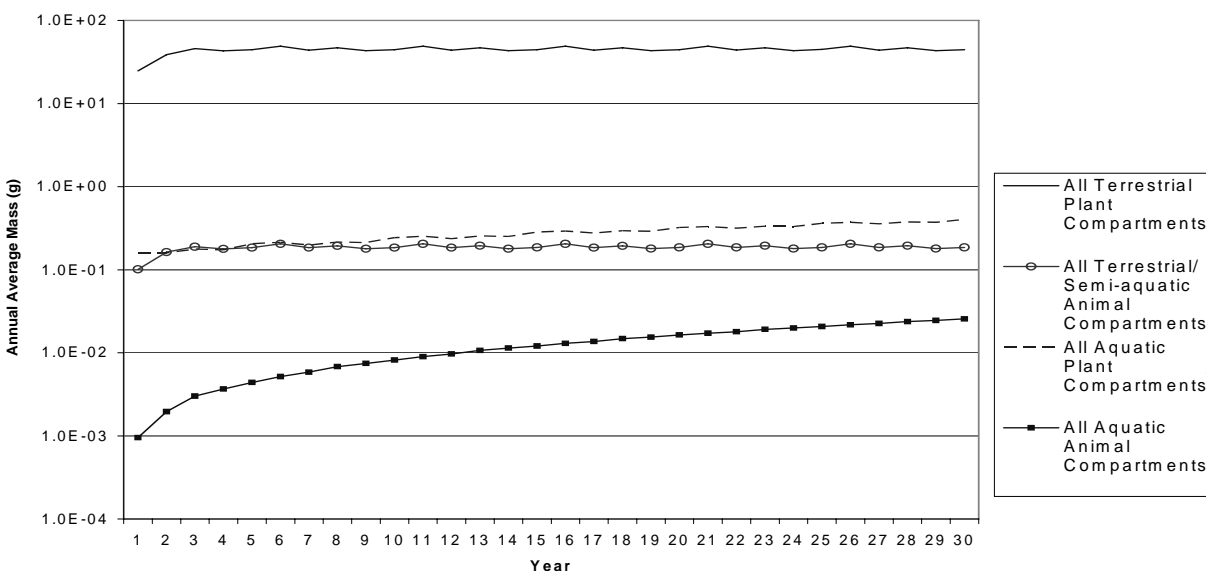
increases fastest during the 30-year period and is still increasing at a somewhat higher rate at 30 years). Among abiotic media, surface soil has by far the most mercury at 30 years, roughly 12,000 grams, sediment has approximately 550 grams, and root zone soil has roughly 210 grams.³ Mass in air follows a five-year repeating pattern and does not increase over time. The five-year repeating pattern of results, which shows up for air and several other compartment types, corresponds to the five-year repeating meteorological input data used in the modeling and indicates a strong relationship between the results for a given compartment type and the meteorological data inputs. Mass accumulation in surface water increases slowly over time, probably as a result of continuing inputs from air (and as an indirect result of mass build-up in sediment and surface soils), and follows a less pronounced (i.e., smaller peaks and valleys) five-year repeating pattern. Total mercury mass accumulation in ground water is very low, more than five orders of magnitude lower than in the vadose zone soil at 30 years.

Mass Distribution in Biotic Compartments

Mercury mass accumulation in four broad groupings of biota is presented in Exhibit 3-4. During the 30-year period, mass accumulation ranks as follows:

terrestrial plants >> aquatic plants > terrestrial/semi-aquatic animals > aquatic animals

**Exhibit 3-4 – Log Scale
Total Mercury Mass: Terrestrial Plants, Terrestrial/Semi-aquatic Animals,
Aquatic Plants, and Aquatic Animals**



^a Macrophyte compartments only; algae not included in this grouping because they are modeled as a phase of surface water (not as a distinct compartment type).

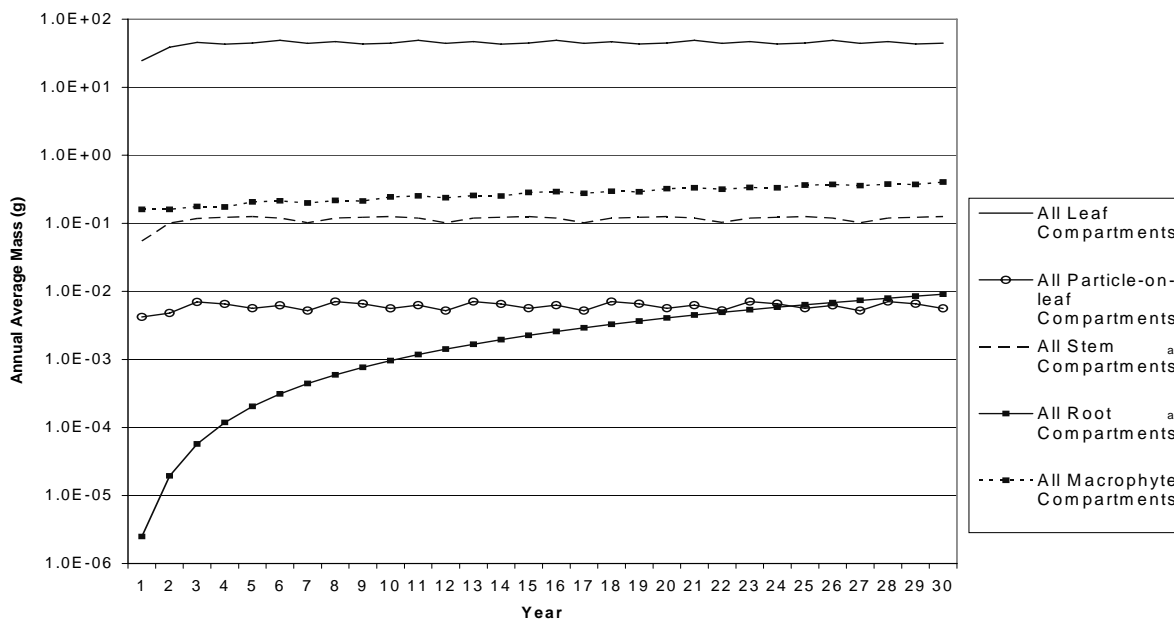
³ Note that in the mercury test case model runs, the sediment compartment was allowed to continually accumulate chemical mass, with no mass removal to a sediment burial sink. A TRIM.FaTE user could modify this approach to modeling chemical mass accumulation in sediment by changing the algorithms used in the library.

After the first couple of years, the annual average mass of mercury in terrestrial plant compartments follows a non-increasing, five-year repeating pattern, reflecting a relationship with air and with the meteorological input data. Mass in terrestrial/semi-aquatic animal compartments follows a similar non-increasing, five-year repeating pattern, albeit at a much lower level of mass (>100-fold lower). As shown in Appendix B.1 tables, the mercury mass in terrestrial/semi-aquatic animal compartments is dominated by mercury mass in the white-tailed deer, which has the highest total biomass density of the animal species included in the modeled scenario. This dominance of the white-tailed deer, combined with the fact that the species is 100 percent herbivorous, explains the high degree of similarity in time patterns of mass accumulation for terrestrial plants and animals. Mass in aquatic plant (macrophyte) compartments is increasing slowly and follows a slight five-year repeating pattern, similar to surface water, which seems consistent with the partitioning approach used to model transfers between surface water and macrophytes. Mass in aquatic animal compartments increases steadily during the modeling period but is still relatively low at 30 years. Other than terrestrial plant compartments, which have accumulated roughly 45 grams of total mercury at 30 years, the biotic compartments have a very small amount of mercury mass (<1 gram for terrestrial/semi-aquatic animals, macrophytes, and aquatic animals combined at 30 years). As noted previously, this is in part a result of the lower relative volume (and mass) of the biotic compartments. As shown in Section 3.2, total mercury concentrations for some of the biotic compartment types span similar ranges as concentrations for some of the abiotic compartment types.⁴

Exhibit 3-5 shows total mercury mass accumulation patterns in the four terrestrial plant compartment types, along with macrophytes for comparison. By far, the largest mass accumulation is in the leaves, followed by the stem (due to method limitations, stems and roots were only modeled in the four grasses/herbs volume elements, but this relative ranking would likely hold true regardless). The time trend of mass accumulation for leaves, particles on leaves, and stems is very similar – a non-increasing, five-year repeating pattern. All three compartment types are strongly affected, directly and/or indirectly, by the meteorological data inputs. In contrast, the root compartment type starts at very low mercury mass and accumulates over time in a smooth pattern – it surpasses the mass in particles on leaves around year 25 and is continuing upward at year 30. The root is less directly affected by weather patterns and is more affected by exchanges of mass with root zone soil, which has a similarly shaped smooth upward time trend.

⁴ In the context of an exposure or risk assessment, the accumulated total mercury mass results for biota discussed in this section would be more relevant to chemical body burden estimates than to chemical intake estimates (for which the mercury concentration results discussed in Section 3.2 would be more relevant).

Exhibit 3-5 – Log Scale Total Mercury Mass: Plant Compartment Types

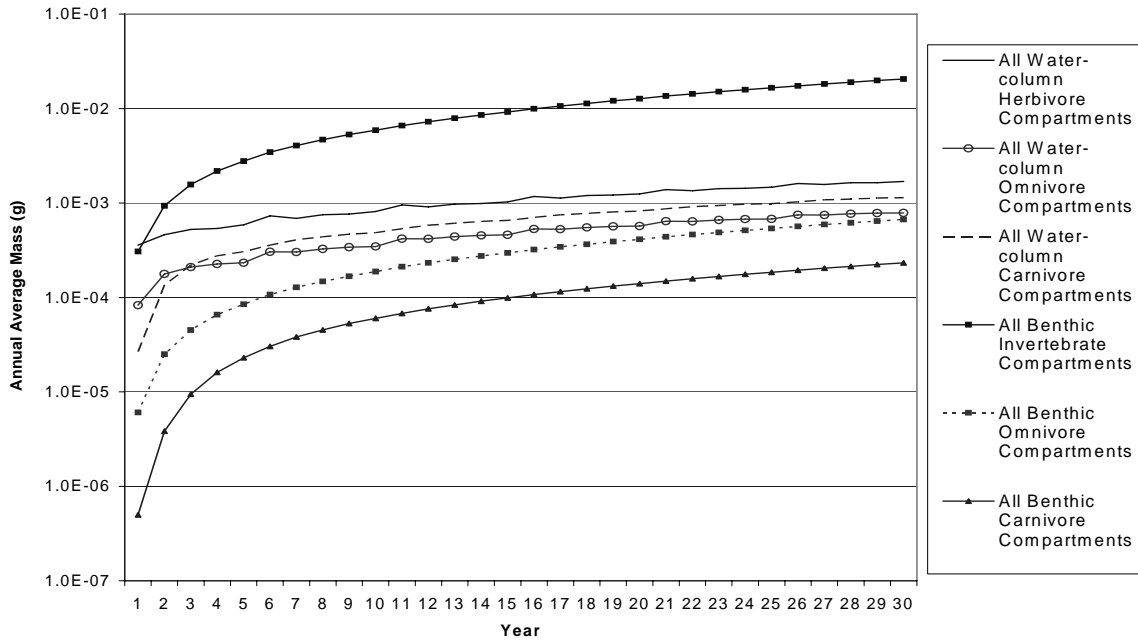


^a Stem and root only modeled in the four grasses/herbs volume elements (vs.19 volume elements for leaf and particles on leaf).

Patterns of total mercury mass accumulation in fish and benthic invertebrates, which were modeled for four ponds and one river, are shown in Exhibit 3-6. The three benthic animal compartment types follow an accumulation pattern that increases smoothly and is very similar to the pattern for sediment, as would be expected because partitioning of mercury between sediment and biota is what drives the benthic invertebrate mass accumulation. Benthic omnivores, in turn, eat benthic invertebrates in this test case scenario, and benthic carnivores eat benthic omnivores. Although their mercury mass accumulation is small relative to most abiotic and plant compartment types, benthic invertebrates dominate mass accumulation among aquatic animals (as noted in footnote 3, chemical mass in sediment was not transferred to a sediment burial sink in this test case). Mercury mass accumulation in the three benthic animal compartment types spans two orders of magnitude at year 30, primarily because of the much higher value for benthic invertebrates.

The mercury mass in the three water-column fish compartment types at year 30 is close (roughly within a factor of two, with herbivores highest), with mass increasing over time and following a slight five-year repeating pattern. The pattern, which is most apparent for herbivores and least apparent for carnivores, is similar to the pattern for surface water, which is directly affected by meteorological data inputs. Surface water partitions mercury mass to algae, which is the food source for water-column herbivores in this test case scenario, which are eaten by water-column omnivores, which are eaten by water-column carnivores.

**Exhibit 3-6 – Log Scale
Total Mercury Mass: Fish and Benthic Invertebrate Compartment Types**



Mass accumulation in terrestrial and semi-aquatic animal compartment types is presented in Appendix Table B-6. It is not shown in a chart here because of complexities in making comparisons as a result of variations in the number of volume elements in which each species is present (e.g., some species, such as the meadow vole, are only present in a subset of land-based volume elements, and others, such as the common loon, are only present in surface water volume elements). However, it is clear that terrestrial and semi-aquatic animal compartments accumulate only a very small proportion of the total mercury mass emitted over 30 years. Within the modeled ecosystem for this test case, the white-tailed deer accumulates by far the most total mercury of any terrestrial/semi-aquatic animal (approximately 95 percent of total mercury mass present in terrestrial/semi-aquatic animals), largely because of its relatively high biomass in the ecosystem; the mouse is next highest, accumulating roughly 2.5 percent of total mercury mass. The temporal mass accumulation patterns for terrestrial/semi-aquatic animals, as with aquatic animals, are typically similar to those of their sources of food (or to other sources of mercury uptake, as in the cases of soil arthropods, earthworms, and benthic invertebrates).

Summary of Mass Accumulation Over Time

For the test case modeling scenario, greater than 99 percent of the total mercury emitted (92 percent of divalent mercury) to air ends up in the air sinks (i.e., passes out of the modeling region via wind advection). As noted earlier, this modeling result is not inconsistent with the test case focus on local impacts. Within the modeling region, the compartment types can be grouped according to mass accumulation at the end of the 30-year modeling period, as shown in Exhibit 3-7. By far most of the remaining mercury mass ends up in the abiotic compartments and terrestrial plant leaves, with surface soil accumulating the highest amount (22 times sediment and 57 times root zone soil, the next highest compartment types at 30 years). The mercury mass distribution results reported here are dependent not only on the physical/chemical

Exhibit 3-7
Summary of Accumulation of Total Mercury Mass within Modeling Region^a

Accumulated Mass of Total Mercury at Year 30 (g)	Compartment Type ^b	Trend at Year 30 ^c	Dominant Form ^d
>10,000	Surface soil	Up (16%)	Hg ²⁺
>1,000 - 10,000	No compartment types	n/a	n/a
>100 - 1,000	Sediment Root zone soil	Up (26%) Up (20%)	Hg ²⁺ Hg ⁰ (67%), Hg ²⁺ (33%)
>10 - 100	Leaf Air	Flat Flat	Hg ²⁺ Hg ⁰
> 1 - 10	Surface water Vadose zone soil	Up (11%) Up (35%)	Hg ²⁺ (76%), Hg ⁰ (23%) Hg ⁰
>0.01 - 1	Macrophyte White-tailed deer Stem Benthic invertebrate	Up (10%) Flat Flat Up (23%)	Hg ²⁺ Hg ²⁺ Hg ²⁺ Hg ²⁺ (88%), MHg (11%)
>10 ⁻⁴ - 10 ⁻²	Root Mouse Short-tailed shrew Meadow vole Mallard Earthworm Raccoon Water-column herbivore Water-column carnivore Water-column omnivore Particle on leaf Benthic omnivore Benthic carnivore	Up (43%) Flat Up (17%) Flat Flat Up (19%) Up (20%) Up (15%) Up (16%) Up (16%) Flat Up (25%) Up (25%)	Hg ²⁺ Hg ²⁺ Hg ²⁺ Hg ²⁺ Hg ²⁺ Hg ⁰ (68%), Hg ²⁺ (32%) Hg ²⁺ (88%), MHg (12%) MHg (52%), Hg ²⁺ (48%) MHg MHg (89%), Hg ²⁺ (11%) Hg ²⁺ MHg (57%), Hg ²⁺ (43%) MHg
>10 ⁻⁶ - 10 ⁻⁴	Black-capped chickadee Tree swallow Red-tailed hawk Long-tailed weasel Soil arthropod Mink Ground water Bald eagle	Flat Up (23%) Up (1%) Up (2%) Up (42%) Up (2%) Up (65%) Up (8%)	Hg ²⁺ Hg ²⁺ (75%), MHg (23%) Hg ²⁺ Hg ²⁺ Hg ²⁺ Hg ²⁺ Hg ⁰ Hg ²⁺ (60%), MHg (39%)
≤10 ⁻⁶	Common loon	Up (17%)	MHg (79%), Hg ²⁺ (21%)

^a Does not include mercury mass transferred to sinks.

^b See Exhibit 2-4 or 3-1 for trophic level/niche descriptors for animal compartment types.

^c Percent increase from year 25 to year 30 shown in parentheses.

^d Hg⁰ = elemental mercury, Hg²⁺ = divalent mercury, MHg = methyl mercury. Listed form comprises at least 90 percent of total mercury, except where noted.

properties of mercury but on the model set-up and other inputs for the test case. Items such as the overall size, shape, and orientation of the modeling region (with respect to wind direction), depth/height of the various abiotic compartments, number and kind of biotic compartments included, and biomass density used for each biotic compartment could have an impact on the mercury mass distribution.

With respect to the pattern of mass accumulation over time (as represented by the annual average mass), the compartment types can be classified as either displaying a smooth trend or a “spiking” that repeats in a five-year pattern, corresponding to the five-year repeating meteorological input data. The following text box summarizes how the compartment types break out, along with whether they are increasing in mass at 30 years or flat.

Mass Accumulation Patterns of Compartment Types		
	Smooth Time Trend	Repeating Five-year Spiking
Flat^a	no compartment types	Air Leaf, particle on leaf, stem White-tailed deer Black-capped chickadee Mallard Mouse Meadow vole
Mass Increasing Slowly (< 5% over years 25 to 30)	no compartment types	Red-tailed hawk Long-tailed weasel Mink
Mass Increasing More Rapidly (≥ 5% over years 25 to 30)	All three soils, ground water Root Soil arthropod, earthworm Short-tailed shrew Raccoon Sediment Benthic invertebrate, both benthic fish Tree swallow	Surface water ^b Macrophyte ^b All three water-column fish ^b Bald eagle ^b Common loon ^b

^a Not perceptibly increasing over 30 years, but very small increases may be occurring for some compartment types.

^b Spiking is generally less pronounced than other noted compartment types.

3.2 Mercury Concentration Over Time in Various Compartment Types

This section presents a series of charts comparing the concentration of total mercury over time among selected compartment types for emission case B. Atmospheric deposition data are also presented, immediately after the air concentration modeling results. Only a subset of the compartment types modeled are covered in this section; additional tables and charts of mercury concentration over time are presented in Appendix B.2. In both this section and Appendix B.2, the focus is on the following locations. (Appendix B.2 contains a complete set of full-page charts for all compartment types, both soil locations, and both surface water locations.)

- Compartments SW2 and SSE4 for all soil, ground water, and associated biotic compartment types (a few results also are presented for compartment W2); and
- Swetts Pond and Brewer Lake compartments for all surface water, sediment, and associated biotic compartment types

Swetts Pond, a relatively small water body near the emission source, was selected for presentation of surface water and related results, in part because it has been a focus of monitoring data collection. Brewer Lake was selected because it is the largest lake modeled and is farther from the source than Swetts Pond. Compartments SW2 and SSE4 were selected because they provide locations at different distances and directions from the source; moreover, SSE4 almost entirely surrounds Swetts Pond, and SW2 is the location of some relevant monitoring data collection. The site layout maps in Exhibits 2-1 and 2-2 show the location of these and other specific compartments discussed.

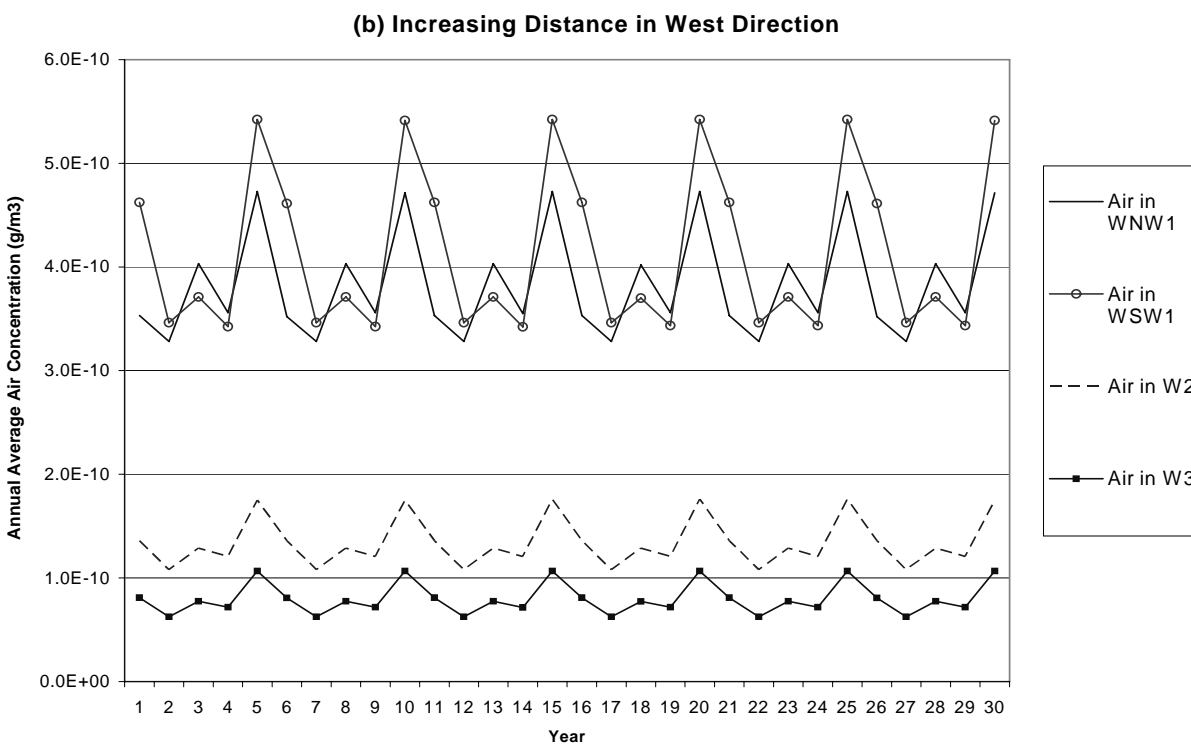
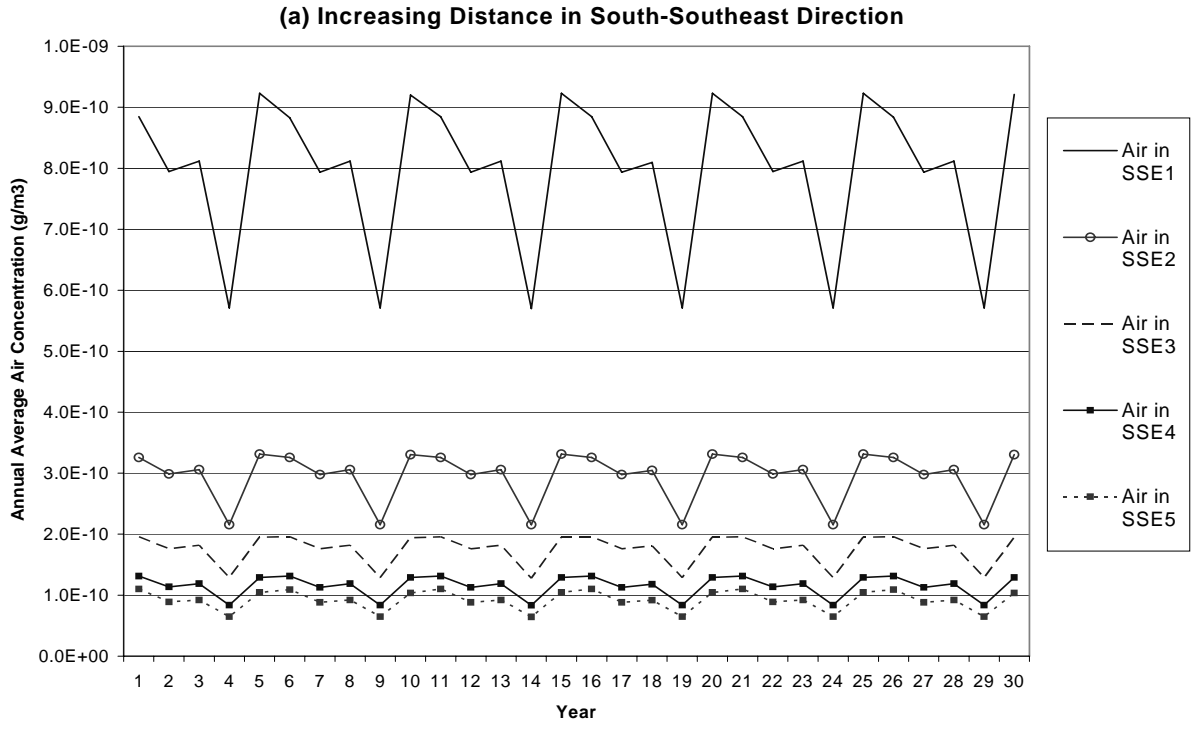
3.2.1 Annual Average Concentrations (and Deposition)

Air Compartments

TRIM.FaTE is a multimedia model focused primarily on impacts to media other than air. It is not intended to be used as an air dispersion model for human inhalation exposure and risk assessments, largely because it does not provide the spatially detailed results (especially near the emission source) that are preferable for such assessments. Deposition and partitioning from air, however, provide the initial inputs of chemical mass to the other media being modeled.⁵ Thus, evaluation of the air results is important. Exhibit 3-8 presents examples of the pattern of concentration of total mercury in air over time and distance for compartments oriented in two directions – south-southeast and west – from the source (see Exhibit 2-1 for location and relative distance from source of specific air compartments). For all directions and distances, the air concentrations of mercury immediately begin a five-year repeating pattern that remains steady over time (i.e., does not increase or decrease, simply spikes up and down in a repeating pattern). This reflects the strong influence of the meteorological input data, which follows a five-year

⁵ The current version of TRIM.FaTE produces essentially a vertical average concentration over the full volume element height. Most deposition processes are driven by the vertical distribution of a chemical in air, not just the concentration at ground-level, so this approach seems reasonable for most types of deposition. However, vapor dry deposition is driven by ground-level concentrations, and therefore may be underestimated by TRIM.FaTE.

Exhibit 3-8
Total Mercury Concentration in Air vs. Time at Increasing Distance from the Source



repeating pattern, on mercury concentration in air. The time pattern is similar at the various distances in a given direction, and the peak-to-valley ratio is similar at various distances also (i.e., similar level of fluctuation). However, the time pattern differs for the two different directions shown, presumably due to the effects of wind direction and speed. As expected, air concentration decreases with distance, with larger rates of decrease close to the source. The TRIM.FaTE-modeled annual average concentrations across all air compartments (except source), roughly 0.1 to 1 ng/m³ elemental mercury, are similar to the short-term median modeled air concentration within 10 km of a chlor-alkali plant emitting elemental and divalent mercury at rates within a factor of two of the rates used in the simulation discussed here, 0.58 ng/m³ elemental mercury (Landis et al. 2004).⁶

Atmospheric Deposition Flux

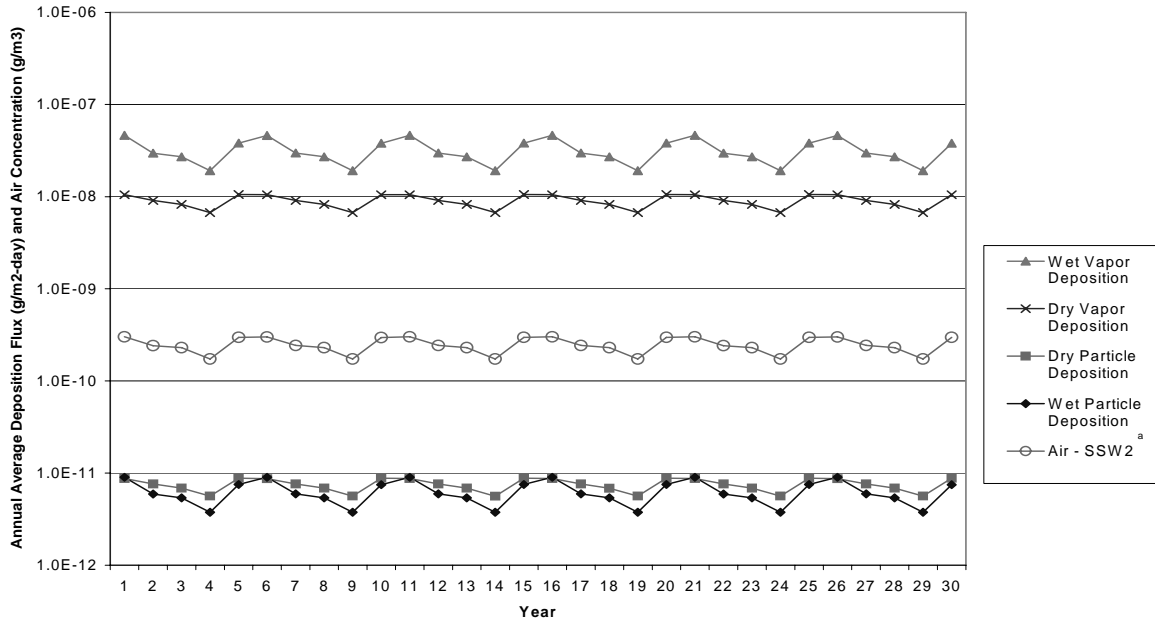
Deposition is the major process by which mercury mass is transferred from the air to the surface in TRIM.FaTE. Four types of deposition are modeled by TRIM.FaTE – wet particle, dry particle, wet vapor, and dry vapor. As an example of the time pattern of deposition, the total mercury deposition fluxes to surface soil in parcel SW2 are displayed in Exhibit 3-9. The air concentrations for the corresponding air parcel (SSW2) are also plotted. Of the four types of deposition, wet vapor and dry vapor deposition are the predominant forms for total mercury (30-year average of 78% and 22% of the total mercury deposition flux, respectively, for SW2). Wet particle and dry particle deposition are much smaller (on average 0.02% of the total deposition flux each, for SW2), consistent with information reported in the *Mercury Study Report to Congress* (EPA 1997).

Similar to the air concentrations, all four deposition fluxes follow five-year repeating patterns that remain steady over time. The repeating patterns of the dry particle and dry vapor deposition fluxes are very similar to the SSW2 air concentration pattern. However, the wet particle and wet vapor deposition patterns are slightly different (the amplitude is larger and the time-series peak on different years, reflecting the impact of rain). Wet deposition only occurs when there is precipitation, and the wet deposition flux patterns are highly influenced by precipitation frequency and amount and other meteorological conditions (such as wind direction) when it is raining. The differences in these precipitation-related input data from year to year affect the wet deposition more than the dry deposition or air concentration.

The levels of dry vapor deposition for divalent mercury modeled by TRIM.FaTE in this test case are similar to the levels modeled by Landis et al. (2004) for the area within a 10 km radius of a chlor-alkali plant in Georgia emitting elemental and divalent mercury at rates within a factor of two of the rates used in the simulation discussed here; levels of elemental mercury dry vapor deposition modeled by TRIM.FaTE are somewhat lower. Those authors report an annualized average dry vapor deposition flux of 2.8 ug/m²-yr (maximum of 320 ug/m²-yr near the emission source) for reactive gaseous mercury within the 10 km radius (and 4.6 ug/m²-yr

⁶ The estimated mercury emission rates used in this test case are within a factor of two of the values reported for elemental mercury (measured at 518 g/day, Kinsey et al. 2004, versus 336 g/day here) and divalent mercury (estimated at 10.4 g/day, Landis et al. 2004, versus 17.7 g/day here) emissions over a nine-day period at a chlor-alkali plant in Georgia.

**Exhibit 3-9 - Log Scale
Total Mercury Deposition Flux to Soil Surface vs. Time: SW2**



^a Because of the differences in the air and surface parcel layouts, the boundaries of the SSW2 air parcel do not match those of the SW2 surface parcel (see Exhibits 2-1 and 2-2), but this air parcel does have substantial overlap with the surface parcel (among air parcels, SSW2 has the most overlap with surface parcel SW2).

(maximum of 500 ug/m²-yr) for total mercury, including elemental). Comparable TRIM.FaTE values for average divalent mercury dry vapor deposition flux to soil range from approximately 1.3 to 15 ug/m²-yr (approximately 1.5 to 17 ug/m²-yr for total mercury dry vapor deposition) across the modeling region (i.e., within 4.7 km to 14 km of the source depending on direction, given the asymmetric soil parcel layout), with soil parcel SW2 roughly 3.0 ug/m²-yr (roughly 3.3 ug/m²-yr for total mercury) (see Section 3.4 for more details about deposition flux of mercury to surface soil across the modeling region). The TRIM.FaTE source parcel, which is most comparable to the maximum deposition locations reported in Landis et al. (2004), has an average divalent mercury dry vapor deposition flux of 330 ug/m²-yr (360 ug/m²-yr for total mercury). Elemental mercury comprises almost 40 percent of the total mercury dry vapor deposition modeled by Landis et al. (2004), compared with roughly 10 percent as modeled by TRIM.FaTE in this test case.

The following text box shows, for deposition to all soil parcels over the entire modeling period in the case B scenario, the percent that each mercury species contributes to the total mercury deposition flux and to each of the four types of deposition. The predominant species that deposits is divalent, consistent with information summarized in the *Mercury Study Report to Congress* (EPA 1997). There is some elemental mercury deposition, and only trace amounts of methyl mercury deposition. Both elemental and divalent mercury are emitted from the source in this scenario, explaining in part why they make up almost all of the total deposition flux.

Elemental mercury emissions are 19 times higher than divalent for case B, as noted in Chapter 2. However, divalent mercury is the predominant species that deposits, due to its relatively high vapor washout ratio (i.e., ratio of concentration in rain to concentration in vapor) and vapor dry deposition velocity. The methyl mercury concentration in air is much smaller than either of the other two species because it only exists in air due to emissions from the surface following transformation of mercury deposited in other forms.

Mercury Species	Percent of Deposition Flux – All Soil Parcels/Entire Modeling Period ^a				
	Total Deposition	Wet Particle	Dry Particle	Wet Vapor	Dry Vapor
Hg ²⁺	95% (100%)	~ 100% (~ 0%)	~ 100% (~ 0%)	97.6% (68.7%)	89.8% (31.3%)
Hg ⁰	5.0% (100%)	~ 0% (~ 0%)	~ 0% (~ 0%)	2.4% (32.6%)	10.2% (67.4%)
MHg	~ 0% (100%)	~ 0% (64%)	~ 0% (36%)	0% (0%)	~ 0% (~ 0%)
Total Hg	100% (100%)	100% (~ 0%)	100% (~ 0%)	100% (66.9%)	100% (33.1%)

^a Percent of total Hg deposition flux by Hg species for each deposition type and for total deposition (columns sum to 100%). Values in parentheses are percent of an individual Hg species deposition flux by deposition type (rows sum to 100%).

Divalent mercury accounts for almost 100 percent of the modeled wet particle and dry particle deposition fluxes, nearly 98 percent of the wet vapor deposition flux, and roughly 90 percent of the dry vapor deposition flux. Elemental mercury accounts for a small amount of the wet vapor deposition flux and approximately 10 percent of the dry vapor deposition flux, which is the dominant process for elemental mercury deposition in this test case.

The modeled fraction of total mercury deposition flux that is wet deposition, roughly 67 percent, is consistent with limited data summarized in the *Mercury Study Report to Congress* (EPA 1997), which indicates wet deposition fractions (for rain) of 45 percent and 63 percent for two different locations in Wisconsin. It also is consistent with data reported in Landis et al. (2004) for locations near a chlor-alkali plant in Georgia, which yields a wet deposition fraction for total mercury of roughly 70 percent (based on measured total wet deposition and modeled dry vapor deposition for locations roughly 30 km apart).

In addition to deposition of mercury from air to the surface, TRIM.FaTE also estimates mercury re-emission (after being first deposited from air) from surface soil, surface water, and leaves to air. A comparison was made between TRIM.FaTE modeled emission fluxes of elemental mercury from surface soil to air and the measured soil-to-air fluxes in the vicinity of a chlor-alkali plant reported in Southworth et al. (2004). TRIM.FaTE fluxes at three different points in time over the 30-year modeling duration vary from 4.2 to 17 ng/m²-hr for the source compartment (increasing over time as soil concentration increases), which has the highest soil concentrations of mercury, to 0.07 to 0.18 ng/m²-hr for soil compartment ESE2 and 0.019 to 0.08 ng/m²-hr for soil compartment W2 (and are lower at the edge of the modeling region where soil concentrations are lower). Note that TRIM.FaTE modeled soil emission fluxes of divalent and methyl mercury are negligible. Measured levels reported in Southworth et al. for five locations very near the emission source (e.g., 50 m away; data most comparable to TRIM.FaTE source

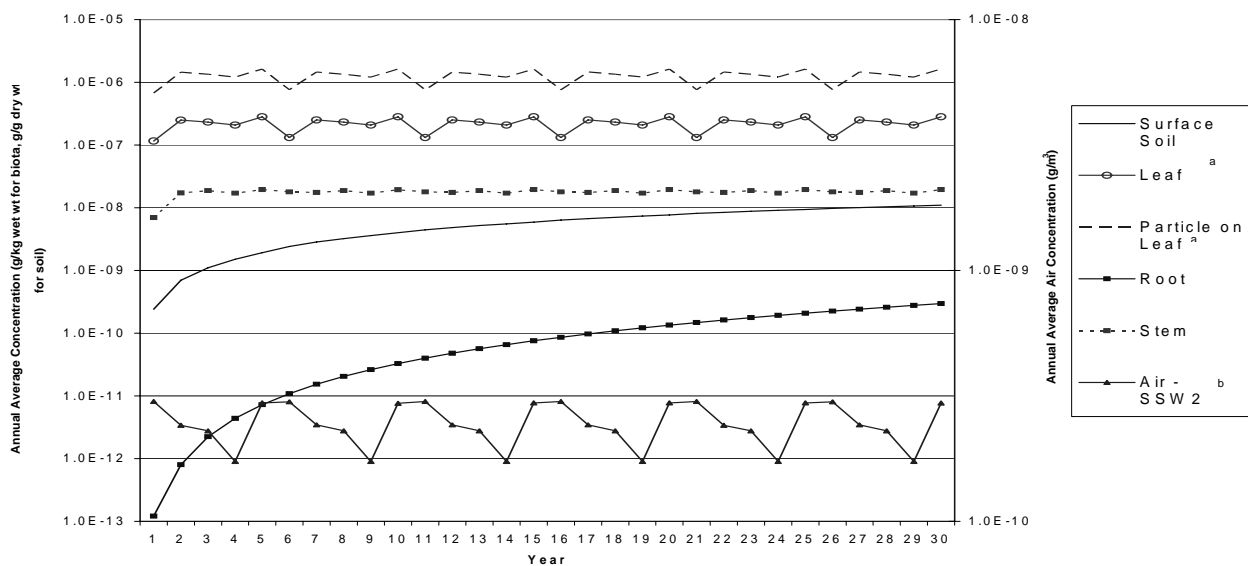
compartment) range from 2 to 13 ng/m²-hr for elemental mercury, with a background level of 1 ng/m²-hr 5 km away from the source; the authors report these fluxes to be lower bounds.

Thus, the TRIM.FaTE source compartment flux is similar to the measured flux range in Southworth et al. (and TRIM.FaTE surface soil concentration of total mercury is also comparable, 1 to 2 ug/g versus an average of roughly 5 ug/g for Southworth et al.). The other TRIM.FaTE compartment fluxes are considerably lower than the measured background level in Southworth et al. (TRIM.FaTE surface soil concentrations of total mercury also are considerably lower, 0.005 to 0.01 ug/g versus 0.3 ug/g for Southworth et al.). Moreover, the TRIM.FaTE modeling results are consistent with the finding reported in Southworth et al. that soil emission flux of elemental mercury is linearly correlated with total mercury concentration in surface soil (see Figure 10 in that paper). Analysis of 19 surface soil compartments (source compartment omitted) in year 14 shows a strong linear correlation ($R^2 = 0.88$, $y = 17x + 0.01$) between instantaneous elemental mercury emission flux and annual average total mercury surface soil concentration for that year. On an equal soil concentration basis, the TRIM.FaTE emission fluxes are higher, which is consistent with the measured values being reported as lower bounds.

Plant Compartments

Exhibit 3-10 illustrates the dynamics of total mercury concentration for the plant compartment types in SW2 (modeled as grasses/herbs), along with the corresponding surface soil and air compartments for reference. The leaf, particle-on-leaf, and stem concentrations quickly

**Exhibit 3-10 - Log Scale
Total Mercury Concentration in Air, Soil, and Plants vs. Time: SW2 (grasses/herbs)**



^a Each annual average data point shown for leaf and particle on leaf is the average of values during the days (May 13 - September 29 each year) for which leaves were modeled as present during the entire day (i.e., represents a growing season average).

^b Because of the differences in the air and surface parcel layouts, the boundaries of the SSW2 air parcel do not match those of the SW2 surface parcel (see Exhibits 2-1 and 2-2), but this air parcel does have substantial overlap with the surface parcel (among air parcels, SSW2 has the most overlap with surface parcel SW2).

reach five-year repeating patterns that remain steady over time, as does the overlying air sorbed to particles that can blow off or be washed off the leaf.) The stem pattern is smoother (only minor spiking) than those for leaf and particle on leaf (which, as expected given the modeling methods, track very closely with each other). In contrast, the root concentration follows a smooth upward track and is still increasing relatively rapidly at year 30, similar to the surface (and root zone) soil concentration, although the rate of increase for both root and soil has decreased by year 30 compared with earlier years (note that, as modeled in the test case scenarios, the root receives mercury inputs only from the root zone soil). The magnitude of total mercury concentration in the plant compartments at year 30 ranks as follows (note that root is the only one in which mercury concentration is perceptibly increasing):

particle on leaf > leaf > stem >> root

However, even though the particle-on-leaf concentrations of total mercury are consistently higher than the leaf and stem compartments, much less mass of total mercury accumulates in the particle-on-leaf compartments, in part because the volume of those compartments is small relative to the leaf and stem compartments (see Section 3.1). For the three compartment locations chosen for analysis, the ratio of particle-on-leaf concentration to leaf concentration for total mercury is 5.7 (SW2, grasses/herbs), 22 (SSE4, coniferous), and 22 (W2, coniferous) (see Appendix B.2 for data on compartments SSE4 and W2). The leaf-to-stem concentration ratio for total mercury is 15 for SW2 at year 30, and the stem-to-root concentration ratio is 63. These latter two ratios cannot be derived for SSE4 or W2 because stems and roots were not modeled for coniferous plants.⁷

Examining the results for all three compartment locations selected for analysis (see Appendix B.2) indicates that regardless of direction from the emission source, leaf and particle-on-leaf compartments quickly reach a non-increasing, five-year repeating pattern of total mercury concentration. As observed for the air results, the time patterns (i.e., patterns of peaks and valleys) vary for different directions from the source, presumably due to directional differences in air concentration and deposition that result from variations in the meteorological data.

We are unaware of reported patterns of plant accumulation of mercury in the literature for comparison with these results. In general, the results in Exhibit 3-10 show that mercury concentrations in soil increase over time as mercury deposition from the source (through air)

⁷ In TRIM.FaTE, individual birth, growth, and death of plants (or animals) are not modeled explicitly. For plants, however, the seasonal events that are modeled address some issues associated with individual growth. The leaf litter that falls to the ground in the fall contains all of the chemical accumulated in and on the leaves during the growing season. With litter fall at the end of each growing season, however, accumulation of contaminant in the leaves (see EPA 2002c for description of process algorithms) begins anew at the beginning of the next growing season. Therefore, the concentration of mercury in the plant leaves, particles on leaves, and stems (which receive mass input from leaves) does not show an increase between years 1 and 30. For trees, the current TRIM.FaTE library does not model woody stems or roots (lack of appropriate data to develop algorithms and parameter values for mercury). Thus, the trunk and roots cannot accumulate the chemical. For deciduous trees, the leaf fall at the end of the growing season is the same as for the herbs and grasses; in this application, TRIM.FaTE resets the leaf compartment concentrations to zero for the beginning of the next growing season. For coniferous trees, there is a continuous loss of a portion of the needles throughout the year. In the mercury test case modeled scenarios, achievement of equilibrium concentrations of mercury in the leaves appears to occur within a year.

continues, but more slowly in later years as the entire terrestrial system approaches an equilibrium. The plant roots reflect the soil concentration, but also indicate accumulation of mercury in the roots over time compared with soil concentrations, which is consistent with the limited data available on mercury accumulation by plant roots (see additional discussion of root uptake in Section 6.3.2). The mercury concentrations in plant stems, leaves, and particles on leaves for the grasses/herbs does not continue to increase after the first year. This pattern reflects litter fall at the end of the growing season, when the mercury in the leaves and particles on leaves is deposited to soil.

Surface Water, Sediment, and Associated Biotic Compartments

Exhibit 3-11 shows *total mercury* concentrations over time for surface water and related compartments for Swetts Pond. TRIM.FaTE models quite a few mass transfer and transformation processes for mercury in surface water and sediment (see process tables in Section 6.4 for a summary, or EPA 2002c for details), making it sometimes challenging to interpret results.

The top chart in Exhibit 3-11 shows surface water and water-column biota (plus common loon, which has a diet of 50 percent water-column omnivores and 50 percent benthic omnivores), and the bottom chart shows sediment and sediment biota (plus tree swallow and raccoon, which have diets containing 100 percent and 69 percent benthic invertebrates, respectively). Surface water and macrophytes have a similar slowly increasing, five-year repeating pattern of total mercury concentration, reflecting the continuing input of mercury to surface water from air, the impact of meteorological input data on surface water, and the partitioning of mercury between surface water and macrophytes. Total mercury concentrations in the macrophytes, however, are much higher than surface water concentrations (close to 1,000 times higher throughout the 30 years; note that macrophyte density was modeled as 1 kg/L).

Mercury concentrations in the three water-column fish compartments and the common loon follow gradually increasing trend lines, with concentrations in the herbivore and omnivore showing a slightly more pronounced five-year repeating pattern, probably reflecting the algal diet of the herbivore.⁸ The time patterns appear generally smoother (i.e., showing less of the variable pattern of the surface water compartment) at successively higher levels in the food chain – the water-column carnivore and common loon have smoother total mercury concentration time lines than the water-column herbivore and omnivore. (The spiking in the time pattern is more apparent for Brewer Lake, shown in Appendix Chart B-4b.)

The five-year repeating pattern originates with the pattern of atmospheric deposition in this case study that resulted from use of five years of meteorologic data for the site, then repeating the five years of data six times to provide 30 years of data for the total simulation. That repeating pattern is reflected in mercury deposition to soil and surface water and is reflected in everything that depends on mercury deposition. The algae in surface water are in “instantaneous” equilibrium with surface water mercury concentrations, and so directly reflect

⁸ Although total mercury concentration data were not examined in detail for algae, concentrations in algae would be expected to follow a pattern similar to surface water, based on the modeling methods.

the five-year repeating pattern of the meteorologic data. The herbivorous fish, not surprisingly, closely track the concentrations of mercury in their food, the algae.

In terms of relative magnitude of total mercury concentration, the water-column fish compartments follow the expected order:

carnivore > omnivore (4.5:1 at year 30)

omnivore > herbivore (1.2:1 at year 30)

Although herbivores have the lowest concentration, their relatively high total biomass causes them to accumulate the most total mercury mass among the water-column fish (see Section 3.1). The total mercury concentration in the common loon tracks very closely with (and slightly lower than) the water-column omnivore, which comprises half of its modeled diet.

Total mercury concentrations in sediment, all benthic biota, and tree swallows and raccoons feeding out of Swetts Pond follow a smooth upward time trend, reflecting the steady accumulation of mercury in sediment, the partitioning between sediment and benthic invertebrates, and the diets of the upper trophic level benthic fish and the two semi-aquatic animals. Total mercury concentrations in benthic fish and invertebrates are somewhat lower but generally within an order of magnitude of water-column fish. The total mercury concentrations for the benthic invertebrate and two benthic fish compartments are fairly close (all within roughly a factor of three at year 30 for both water bodies). After a few years, SSE4 tree swallow concentrations of total mercury mirror closely the benthic omnivore time pattern, reflecting that both have a diet of 100 percent benthic invertebrates. Total mercury concentrations in SSE4 raccoons are increasing a little more slowly than concentrations in the other benthic and related compartments shown, possibly because their diet has a sizable (21 percent) non-aquatic component consisting of animals (earthworms) having much lower mercury concentrations than benthic invertebrates for this location.

Exhibit 3-12 shows modeled concentrations of *methyl mercury* over time for fish and selected other animals in Swetts Pond. Given the significance of organic mercury compounds, including methyl mercury, in fish, these data are presented here in addition to the total mercury data in Exhibit 3-11 (see also Exhibit 3-24 for comparative data in table form). The top chart in Exhibit 3-12 shows surface water and water-column biota (plus common loon), and the bottom chart shows sediment and sediment biota (plus tree swallow and raccoon). As expected, the concentrations of methyl mercury in fish and fish-eating wildlife increase over time and are higher in the higher trophic levels, as are the percentages of total mercury that is methyl mercury. Also, as expected, methyl mercury concentrations in fish consistently increase up through the food chain (carnivore > omnivore > herbivore). The ratios of methyl mercury concentrations for the fish and benthic invertebrate compartments are:

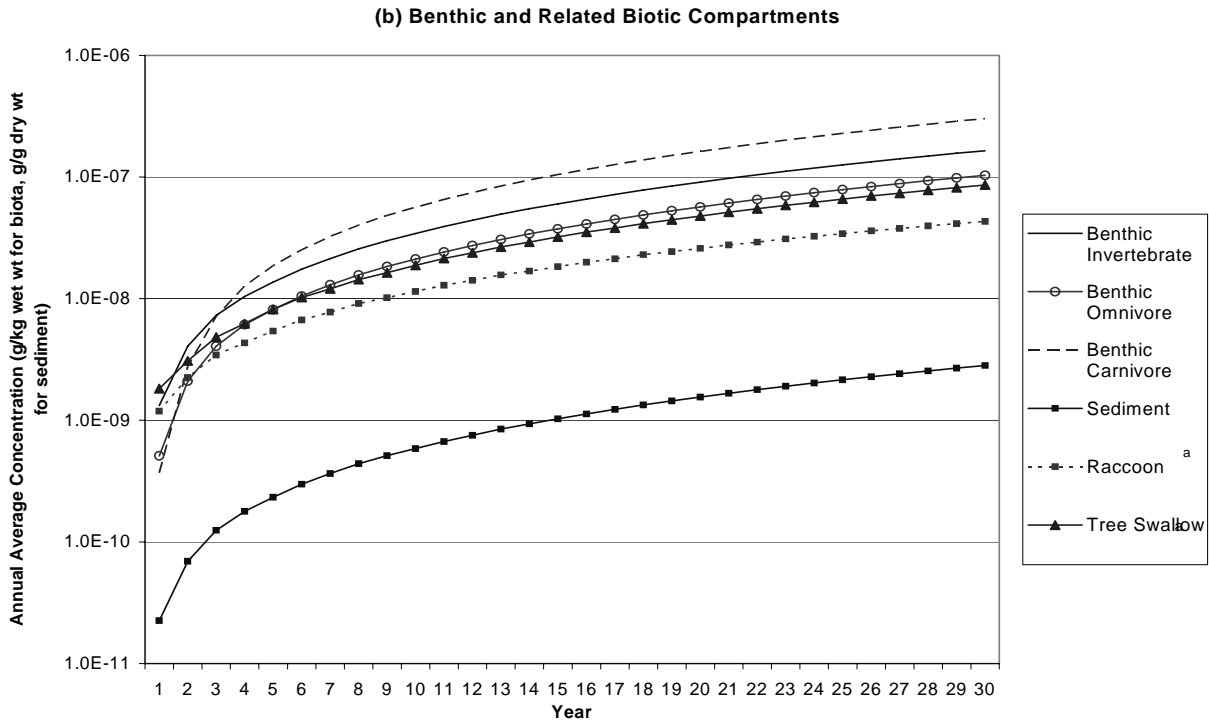
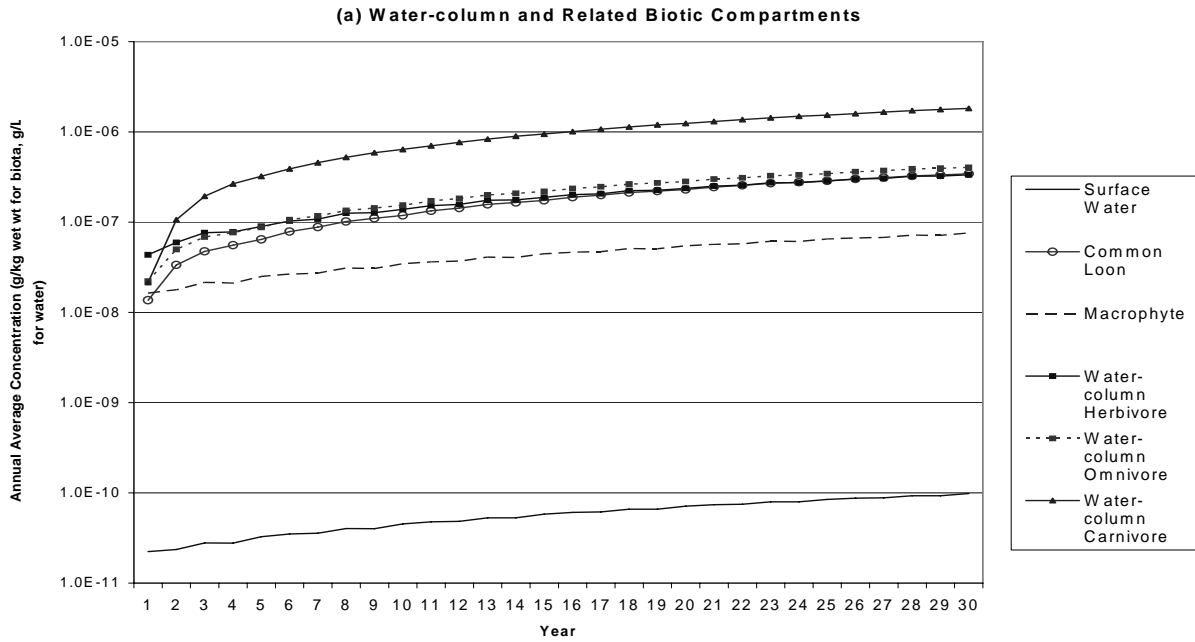
water-column carnivore > water-column omnivore (5.1:1 at year 30)

water-column omnivore > water-column herbivore (2.2:1 at year 30)

benthic carnivore > benthic omnivore (4.9:1 at year 30)

benthic omnivore > benthic invertebrate (3.2:1 at year 30)

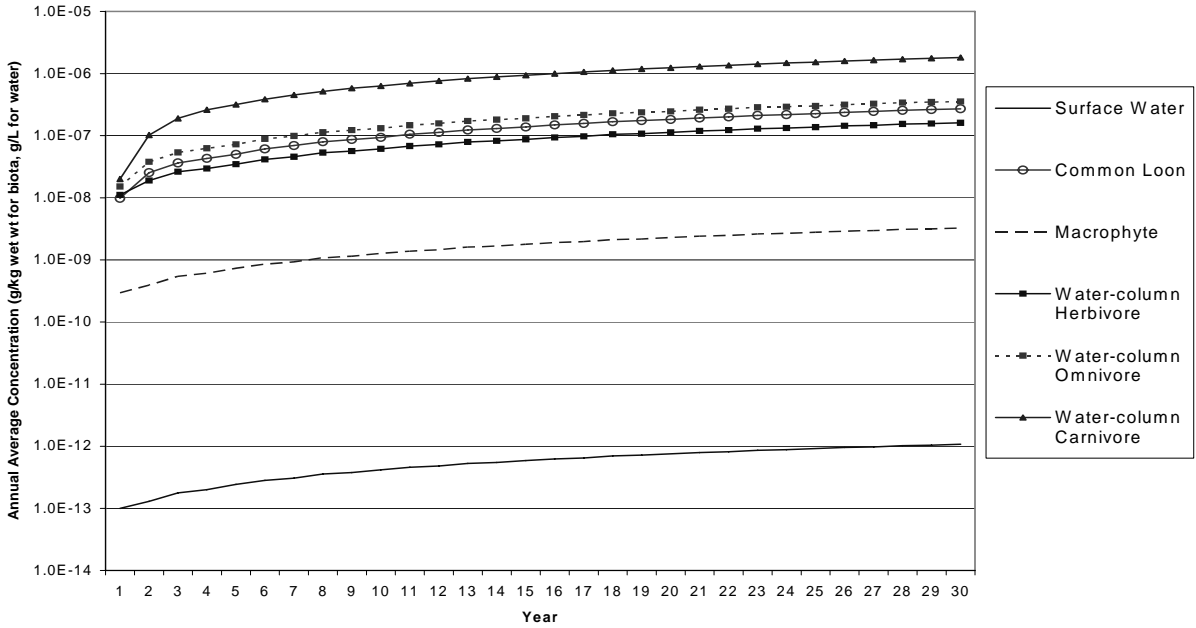
Exhibit 3-11 - Log Scale Total Mercury Concentration in Surface Water and Related Biota vs. Time: Swetts Pond



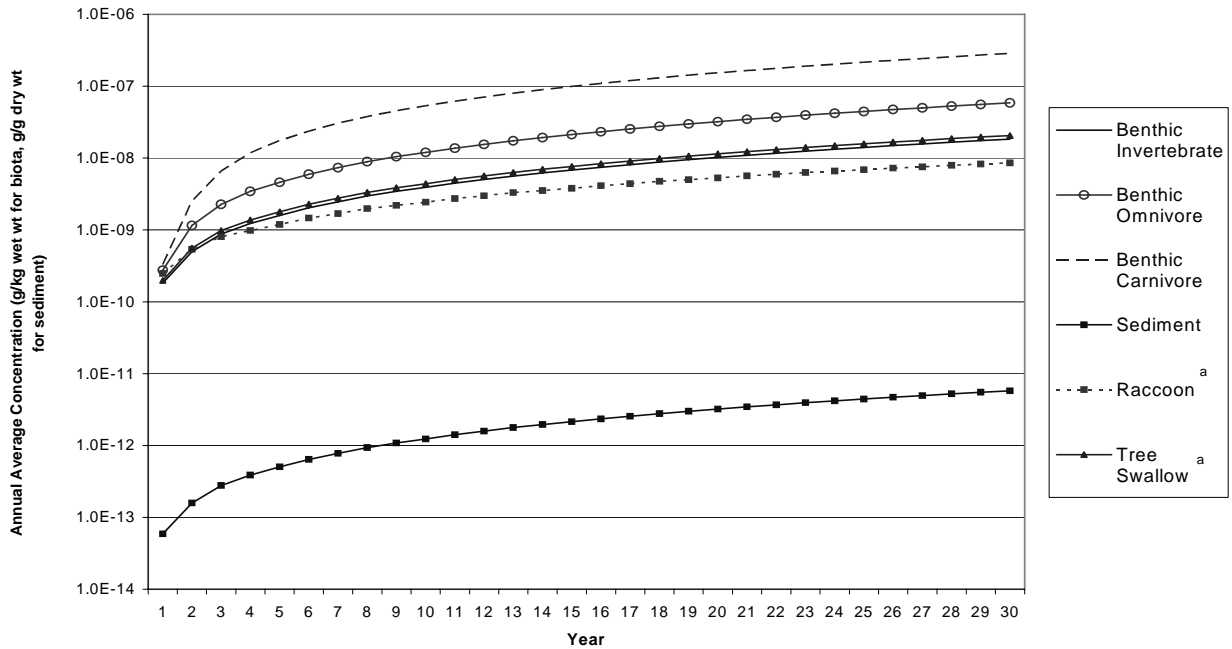
^a Results shown for compartment SSE4, where semi-aquatic animals feed from Swetts Pond.

Exhibit 3-12 - Log Scale Methyl Mercury (as Hg) Concentration in Surface Water and Related Biota vs. Time: Swetts Pond

(a) Water-column and Related Biotic Compartments



(b) Benthic and Related Biotic Compartments



^a Results shown for compartment SSE4, where semi-aquatic animals feed from Swetts Pond.

Methyl mercury concentrations in the raccoon and tree swallow track closely with their aquatic diet component, benthic invertebrates, in which (like the macrophyte) the mercury is primarily in the divalent form (see Section 3.3 for more discussion of mercury speciation).

Terrestrial Animal Compartments

Nine terrestrial animal compartment types (including soil arthropod and earthworm) were included in the TRIM.FaTE mercury test case. Exhibit 3-13 shows examples of total mercury concentrations over time for several of these animals in two trophic groupings: (a) terrestrial herbivores and omnivores, whose diets include vegetation, and (b) terrestrial carnivores, whose diets include various herbivores and omnivores.

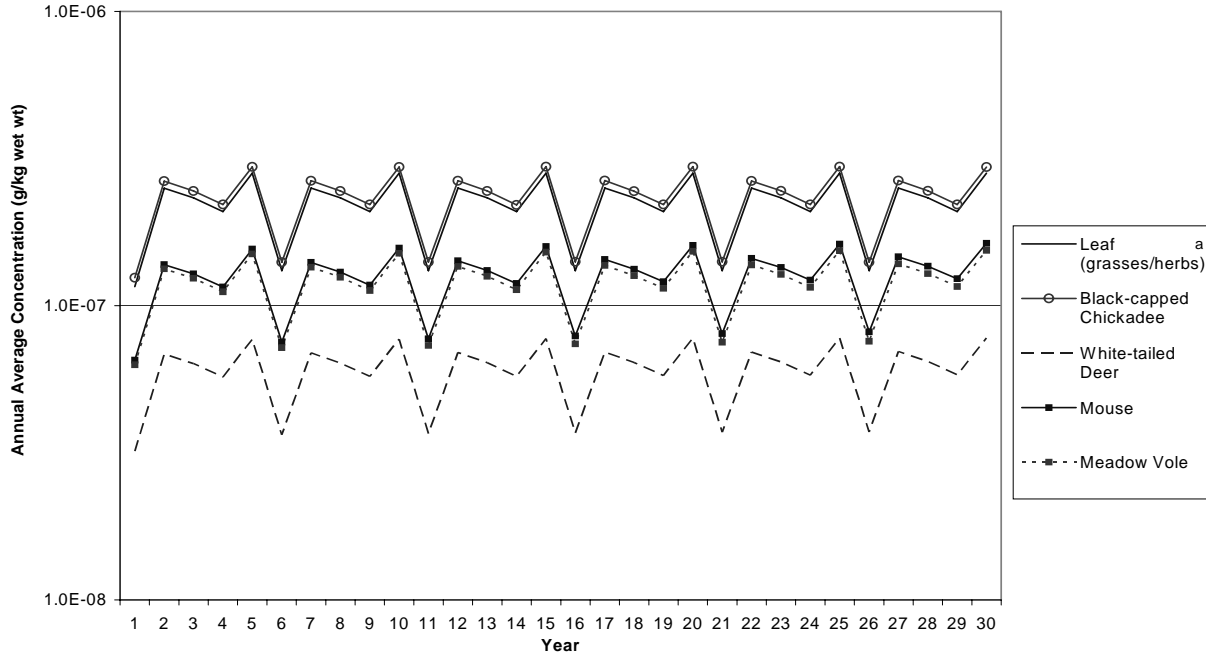
In the top chart of Exhibit 3-13, total mercury concentrations in the four terrestrial animal compartment types for which terrestrial plants (only leaf and particles on leaf are modeled as ingested) comprise a major portion of their diet are shown, along with leaf compartment concentrations for reference: white-tailed deer (diet = 100 percent terrestrial plants), meadow vole (100 percent), mouse (50 percent, with remainder soil arthropod), and black-capped chickadee (30 percent, with remainder soil arthropod).⁹ In this chart, the five-year repeating time patterns of concentration for leaf and all four animals are strikingly similar. Because the mercury concentrations in soil arthropods are so low, the arthropod portion of the mouse and chickadee diets likely has negligible impact on mercury mass accumulation in these animals. This is illustrated by the temporal concentration pattern for mercury in the chickadee, which was modeled as having zero soil ingestion. If soil arthropods were having a substantial impact, the chickadee pattern – similar to the leaf, not to soil or soil arthropods – would be smoother and increasing and would look less like the leaf pattern. The total mercury concentrations among the four animals are all similar in magnitude – roughly a four-fold range – with white-tailed deer having the lowest concentration, although their greater biomass in the test case scenario leads deer to accumulate by far the most mercury mass among the animals (see Appendix Table B-6).

The bottom chart in Exhibit 3-13 shows results for two terrestrial carnivores (along with their major diet components in this application): long-tailed weasel (diet = 25 percent shrew, balance is mouse and vole) and red-tailed hawk (20 percent shrew, balance is mouse, vole, chickadee, and very small amount of soil arthropod). Total mercury concentrations in the shrew follow a smooth upward time trend line, similar to the patterns for surface soil (which it ingests at a relatively high rate) and for its biotic diet components, soil arthropods and earthworms. All the other animals on the chart have strikingly similar five-year repeating time patterns. Total mercury concentrations in the mouse, vole, and chickadee, as shown on the top chart, follow the pattern of the leaf. Total mercury concentrations in the weasel and hawk, which have similar diets, have very similar increasing, five-year repeating patterns. The basic five-year repeating pattern for the two carnivores reflects the herbivores in their diet, while the damping of amplitude

⁹ Seeds and berries, which are a component of the diet of chickadees, were not modeled explicitly (i.e., as separate compartments) in this TRIM.FaTE application. Rather, leaves and particles on leaves were used to represent plant material in the chickadee diet. It is recognized, however, that mercury accumulation and the adherence of dust particles may differ among various types of plant material.

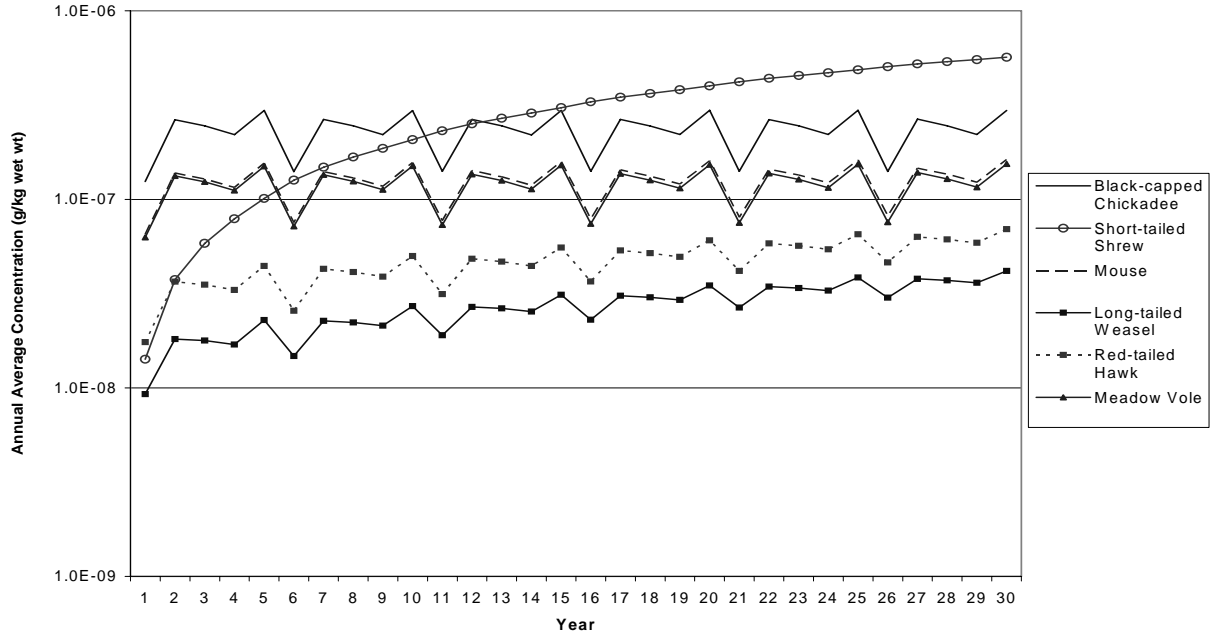
**Exhibit 3-13 - Log Scale
Total Mercury Concentration in Terrestrial Animals vs. Time: SW2 (grasses/herbs)**

(a) Terrestrial Herbivore and Omnivore Compartments



^a Each annual average data point shown for leaf and particle on leaf is the average of values during the days (May 13 to September 29 each year) for which leaves were modeled as present (i.e., represents a growing season average).

(b) Terrestrial Carnivore (Weasel and Hawk) Compartments



(compared to the herbivores) and the increase over time probably reflect the shrew (increasing smoothly over time) portion of their diet.¹⁰

3.2.2 Selected Instantaneous and Monthly Average Results

This section presents instantaneous and monthly average concentration results for a subset of compartments to show patterns not apparent from the annual average results discussed elsewhere and to illustrate the types of temporal results that are available from TRIM.FaTE.

The presentation here includes bi-hourly instantaneous estimates and monthly averages for examples of air, surface soil, surface water, and water-column herbivore and carnivore compartments. The instantaneous results are “snapshots” of model predictions, not averages of some smaller time step (see “Temporal Aspects of the Dynamic Scenarios” subsection in Chapter 2), while the monthly averages (as well as the annual averages presented elsewhere in the report) are simply arithmetic averages of the instantaneous results, which were output at a two-hour frequency during the simulation. The bi-hourly results are presented for the last year of the simulation, and the monthly results are presented for the last five years.¹¹

The overall trends in total mercury concentration estimates and the magnitude of their variation within the time period presented are summarized in Exhibit 3-14. More detailed analyses are provided in the subsequent subsections.

¹⁰ The lifetime of wildlife is not explicitly considered in TRIM.FaTE. The bioenergetic model of mercury accumulation (i.e., based on mercury intake, transformation, and excretion rates by individual animals) used in this application of TRIM.FaTE does not account for loss of mercury from the wildlife compartments by death of individuals due to disease, starvation, or senescence, when the mercury either would be returned to the soil or ingested by scavengers (not modeled here). Moreover, it does not account for loss of mercury from wildlife compartments via emigration (e.g., dispersal of juveniles), with the population size being maintained by immigration of individuals from other, possibly less contaminated areas. Thus, it is possible that modeled mercury accumulation in the wildlife compartments will be somewhat higher than would be the case if the loss of mercury via death and emigration of individuals were included. Because inclusion of the non-predator-associated wildlife death would result in mercury transfers to scavenger species, soil, water, and air, some fraction of this transferred mercury would be re-entrained into the terrestrial food web. Consequently, the extent to which the mercury accumulation in wildlife compartments might be reduced with explicit modeling of organism death (e.g., involving use of species-specific mortality rates for disease, starvation, and senescence) and associated mercury transfers to soil, water, and air is not easily characterized without additional analysis.

¹¹ Monthly and instantaneous results in this section are presented for different lengths of time because the main purpose is to show the different patterns of variation. One year is sufficient for presenting the variation in the bi-hourly instantaneous results, but five years shows the variation more completely for the monthly results. Additionally, a five-year set of bi-hourly data points would be cumbersome to present.

Exhibit 3-14
Descriptions of Instantaneous and Averaged Outputs for Selected Compartments^a

Compartment Type ^b	Compartment	Long-term Temporal Trend	Range of Variation	
			Instantaneous Estimates (year 30)	Monthly Averages (years 26-30)
Air	SSW2 and SSE4	steady	6+ orders of magnitude	~1 order of magnitude
Total deposition flux to surface soil ^b	SW2	steady	10+ orders of magnitude	~1 order of magnitude
Leaf	SW2 (grasses/herbs) and SSE4 (coniferous)	increasing	SW2: +1 order of magnitude; SSE4: factor of 1.6	SW2: ~1 order of magnitude; SSE4: factor of 1.6
Surface soil	SW2, SSE4, E1, SE1	increasing	slight variations	slight variations
Surface water	Swetts, Brewer	increasing	factor of 1.6	factor of 1.5
Water-column herbivore	Swetts	increasing	factor of 1.1	factor of 1.2
Water-column carnivore	Swetts	increasing	none visible	none visible

^a All trends and ranges based on total mercury concentration, except deposition row based on total mercury flux.

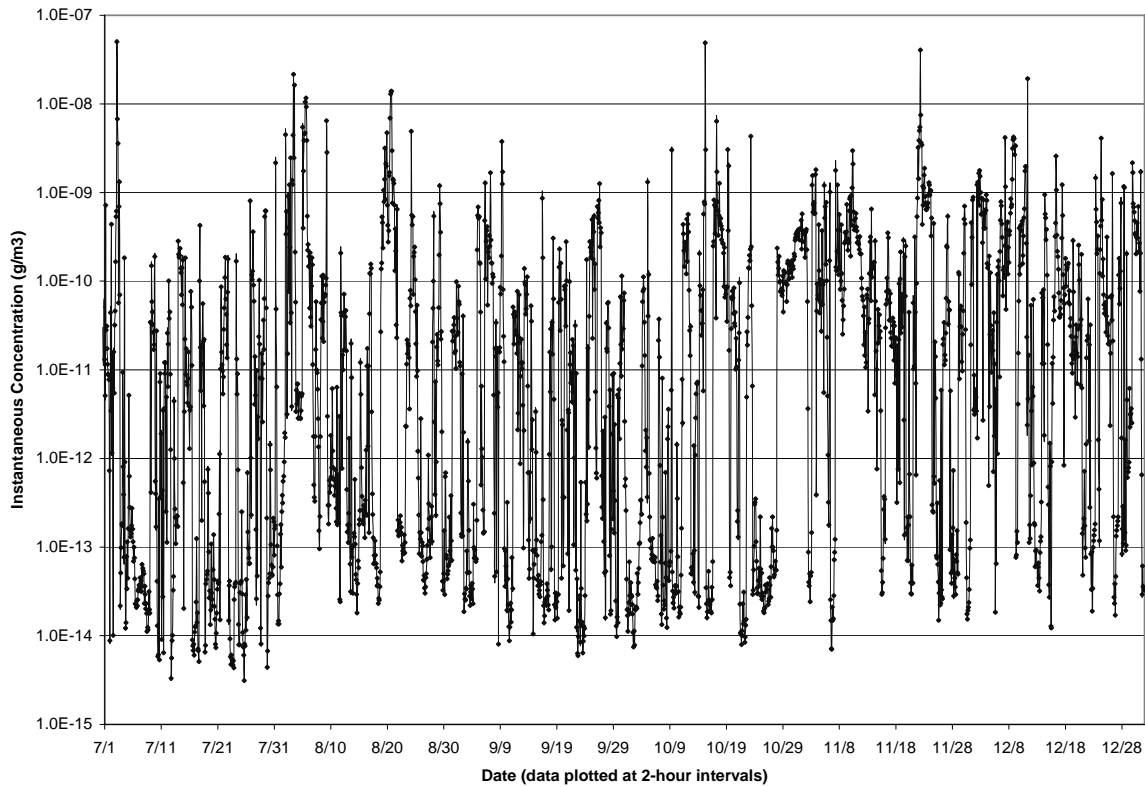
^b All values in this column are compartment types except for total deposition flux to surface soil.

Air

Instantaneous total mercury concentrations in the air compartments vary greatly over the year (six or more orders of magnitude in the compartments analyzed). Exhibit 3-15 shows six months of instantaneous output for air compartment SSE4.¹² This large variability in total mercury air concentration is due to the hour-to-hour variability in meteorological input data and the effect these data have on air concentrations (wind speed and direction and precipitation rate largely determine how much chemical is blown into and removed from a compartment, and mixing height directly affects air compartment volumes and thus chemical concentrations). The monthly average concentrations of total mercury in the air compartments vary by one or more orders of magnitude (SSE4 and SSW2 shown in Exhibit 3-16). Note that the annual average air concentrations discussed in Section 3.2.1 vary less than an order of magnitude (approximately 50 to 60 percent).

¹² Due to the high variability in the instantaneous air concentrations, a graph showing a full year of instantaneous concentration is too cluttered to distinguish the patterns.

**Exhibit 3-15 - Log Scale
Instantaneous Total Mercury Concentration in Air: SSW2 (July to December, Year 30)**



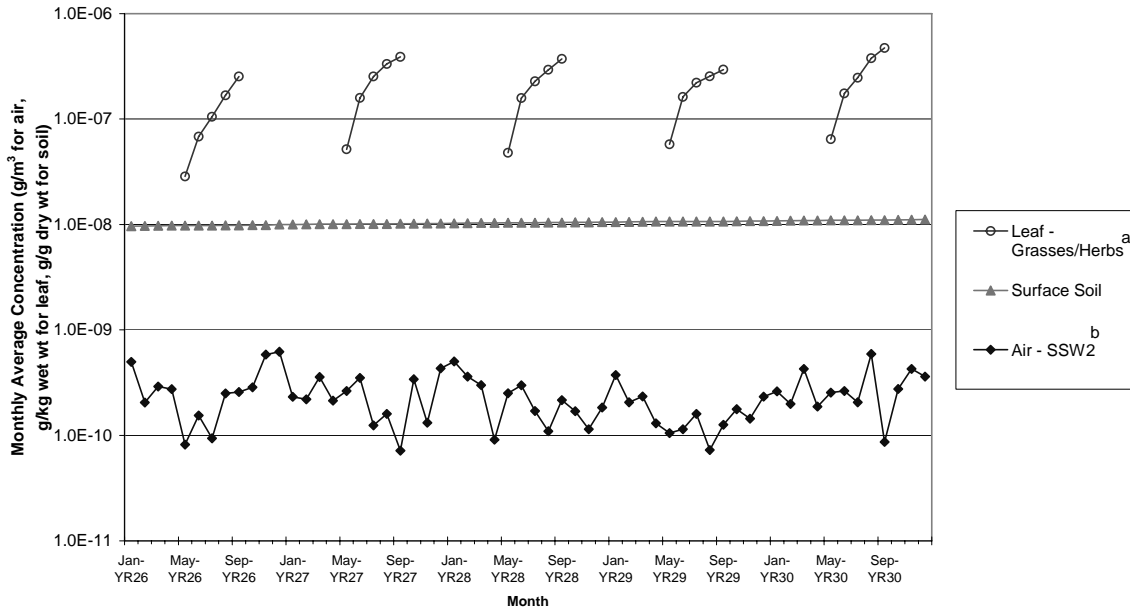
Instantaneous total mercury deposition flux to surface soil varies even more than air concentration, up to 10 orders of magnitude for surface parcel SW2 (not shown on a chart), primarily because wet vapor deposition flux is so highly variable over time (depending for example on whether and how hard it is raining, and which direction the wind is blowing). Dry vapor deposition flux for total mercury is also highly variable, however, with roughly a nine order-of-magnitude range. The reason that dry vapor deposition flux variability is higher than air concentration variability is due to mercury speciation differences – deposition is dominated by divalent mercury, which is more variable in both air concentration and deposition than elemental mercury, which dominates air concentration (i.e., the greater variability in divalent mercury air concentration is swamped by the dominant elemental mercury air concentration).

Surface Soil and Leaves

The instantaneous total mercury surface soil concentrations in compartments SE1 and E1 follow an increasing pattern (Exhibit 3-17; not on log scale), which is expected in all surface soil compartments. The instantaneous concentration shows only slight fluctuations hour-to-hour, which are not significant relative to the amount that the concentrations increase over the year. Most of the larger increases in surface soil concentration (which are still quite small; note scale on Exhibit 3-17) occur around large deposition events (defined here as the top one percent of total deposition fluxes to surface soil occurring during the 30-year simulation), which are indicated on Exhibit 3-17 for the two compartments shown. This is because wet deposition accounts for most

**Exhibit 3-16 – Log Scale
Monthly Average Total Mercury Concentration in Surface Soil, Leaf, and Air
(Years 26 to 30)**

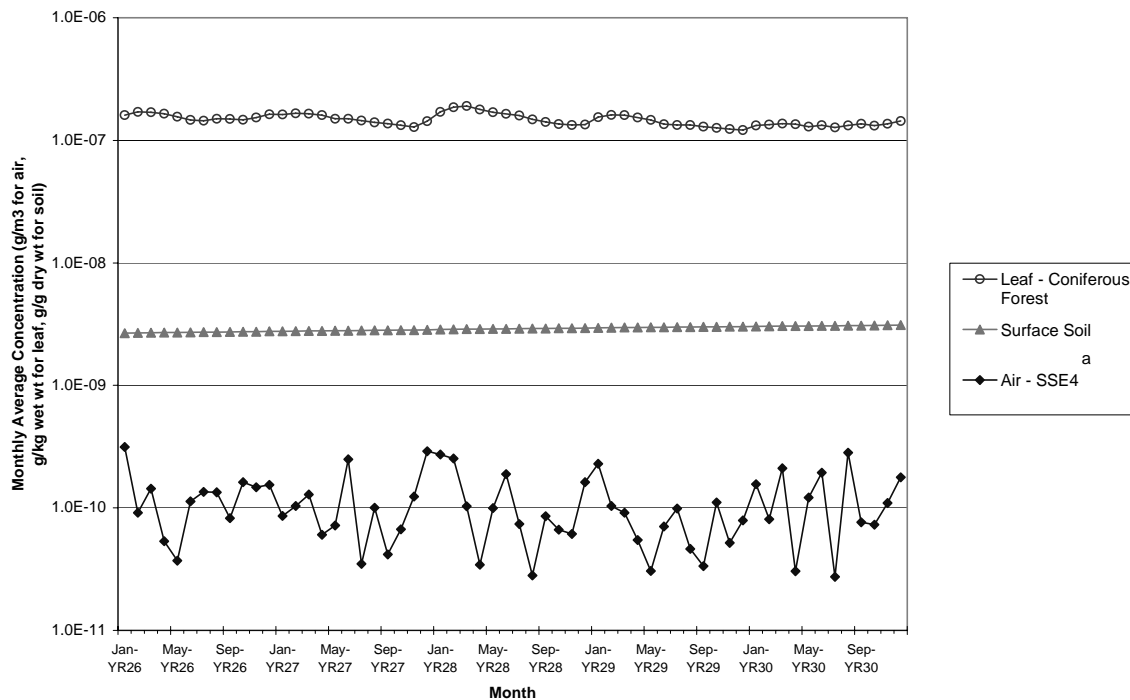
(a) SW2 – Grasses/Herbs



^a Leaf concentrations included are only for months during the growing season, when leaves are present. Furthermore, the average monthly concentration in leaves for the month of May each year is an average of daily concentrations from May 14-31 because no leaves are modeled as present before May 14.

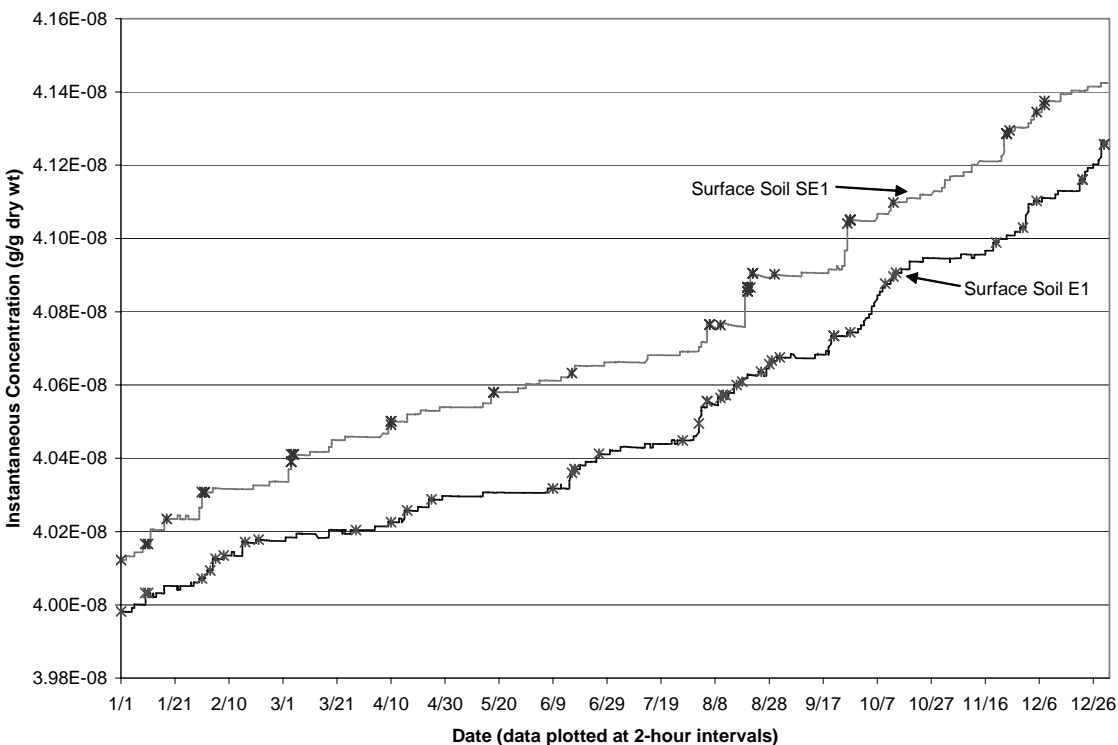
^b Because of the differences in the air and surface parcel layouts, the boundaries of the SSW2 air parcel do not match those of SW2 surface parcel, but there is substantial overlap (see footnote on Exhibit 3-10).

(b) SSE4 – Coniferous Forest



^a Because of the differences in the air and surface parcel layouts, the boundaries of the SSE4 air parcel do not match those of SSE4 surface parcel, but there is substantial overlap (see footnote on Exhibit 3-10).

Exhibit 3-17
Instantaneous Total Mercury Concentration in Surface Soil: E1 and SE1 (Year 30)



Top 1% of hourly deposition fluxes onto surface soil indicated: SE1 *, E1*

of the mercury deposition to the soil surface (see Exhibit 3-9). Therefore, when it rains, a larger amount of chemical mass is transferred from the air to the soil. (Note that not all precipitation events are among the top deposition events for a given compartment, depending on the compartment location relative to the source and the wind direction during the precipitation event. Thus, the top deposition times differ for different compartment locations, as clearly shown in Exhibit 3-17. This is why the top deposition events are indicated on the exhibit rather than the top precipitation events, which do not correlate nearly as well with concentration increases.) The monthly average soil concentrations increase slowly over five years and have very slight yearly fluctuations when examined closely (although they are not apparent on the log scale in Exhibit 3-16). The steadily increasing monthly average concentration of total mercury in surface soil compartments is similar to the pattern seen for annual average mercury concentration (Exhibit 3-10) and is due to the higher rate of mercury input than mercury removal for the surface soil compartment during the 30-year simulation period.

Monthly average total mercury concentrations in grasses/herbs and coniferous forest leaf compartments are shown along with the overlying air and associated surface soil in Exhibit 3-16. The grasses/herbs leaf compartment (Exhibit 3-16a) only has non-zero monthly average concentrations for five months of the year (although the May average only represents half of the month) because those are the only months when leaves are modeled for this vegetation type in this simulation. Each year, the monthly average concentrations increase during these months as the mass transferred into the leaves (e.g., from the air) builds up during the growing season. At

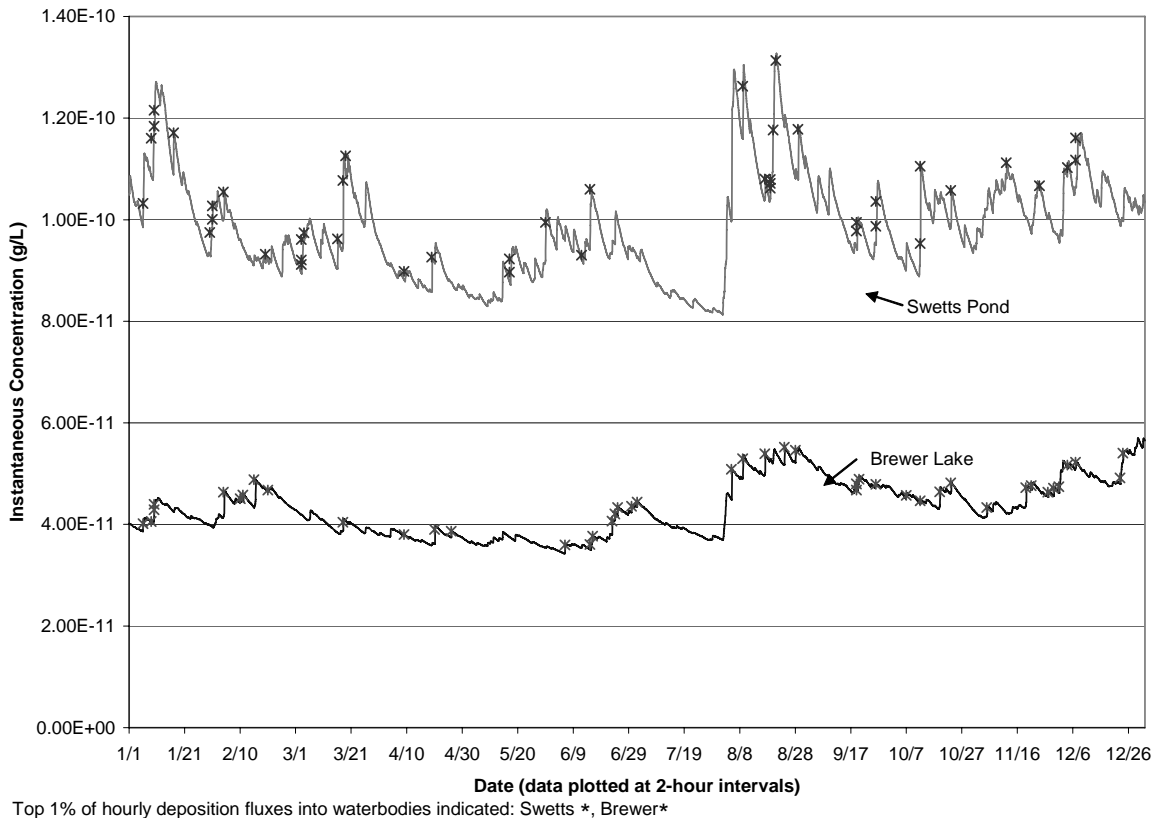
the end of each growing season, any mercury that has accumulated in deciduous plant leaf compartments (and particle-on-leaf compartments) transfers to the surface soil via litterfall.

The monthly average mercury concentrations in the coniferous forest leaf compartment (Exhibit 3-16b) are not increasing and fluctuate slightly over the five-year period. The monthly coniferous leaf time series is much smoother than the monthly air concentrations, but appears to be influenced by peaks in the air concentrations (e.g., around January, Year 28 and January, Year 29). The steady, slightly fluctuating pattern of monthly average concentrations in leaves is similar to the annual average mercury concentration in leaves presented in Section 3.2.1 and Appendix B.

Aquatic Compartment Types

Exhibit 3-18 (not on log scale) shows the instantaneous estimates of total mercury concentrations in Swetts Pond and Brewer Lake for year 30. The instantaneous surface water concentrations in Swetts Pond and Brewer Lake fluctuate by a factor of approximately 1.6 during this year. The fluctuations appear to be associated with large deposition events, which are indicated in the exhibit, although not every increase is accompanied or preceded by one of the top one percent of deposition times. Such increases may result from longer-term deposition events

Exhibit 3-18
Instantaneous Total Mercury Concentration in Surface Water:
Swetts Pond and Brewer Lake (Year 30)



(e.g., lower intensity rain that continues over a long period of time) or deposition events slightly below the one percent threshold used for displaying the top events in the exhibit. (Water temperature does not play a role in the observed fluctuations, given that it was modeled as a constant 293° K.) The larger fluctuations of the surface water concentrations than the surface soil concentrations (compare Exhibits 3-17 and 3-18) may be partially due to the difference in baseline mercury concentration between the two compartment types. Because the total mercury concentration is much higher in the surface soil, the deposition inputs would not be expected to have as much relative impact. Therefore, large deposition events would be expected to cause higher fluctuations in concentration in the surface water than the surface soil. Exhibit 3-19 (not on log scale) displays the monthly average surface water concentrations of total mercury in Swetts Pond over the last five years of the simulation. The Swetts Pond monthly average concentrations vary by a factor of approximately 1.5 over the five years of data. The pattern of monthly averages is very similar to the monthly air concentration pattern for the overlying air parcel (not shown).

Exhibit 3-19
Monthly Average Total Mercury Concentration in Surface Water and Water-column Fish: Swetts Pond (Years 26 to 30)

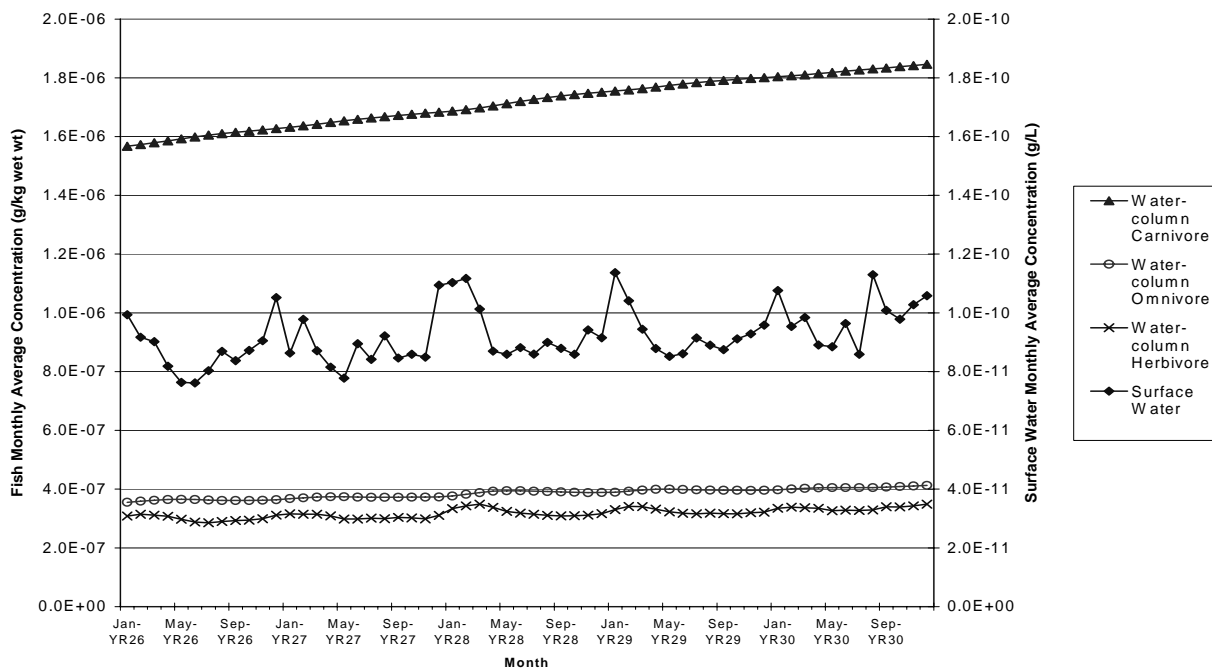
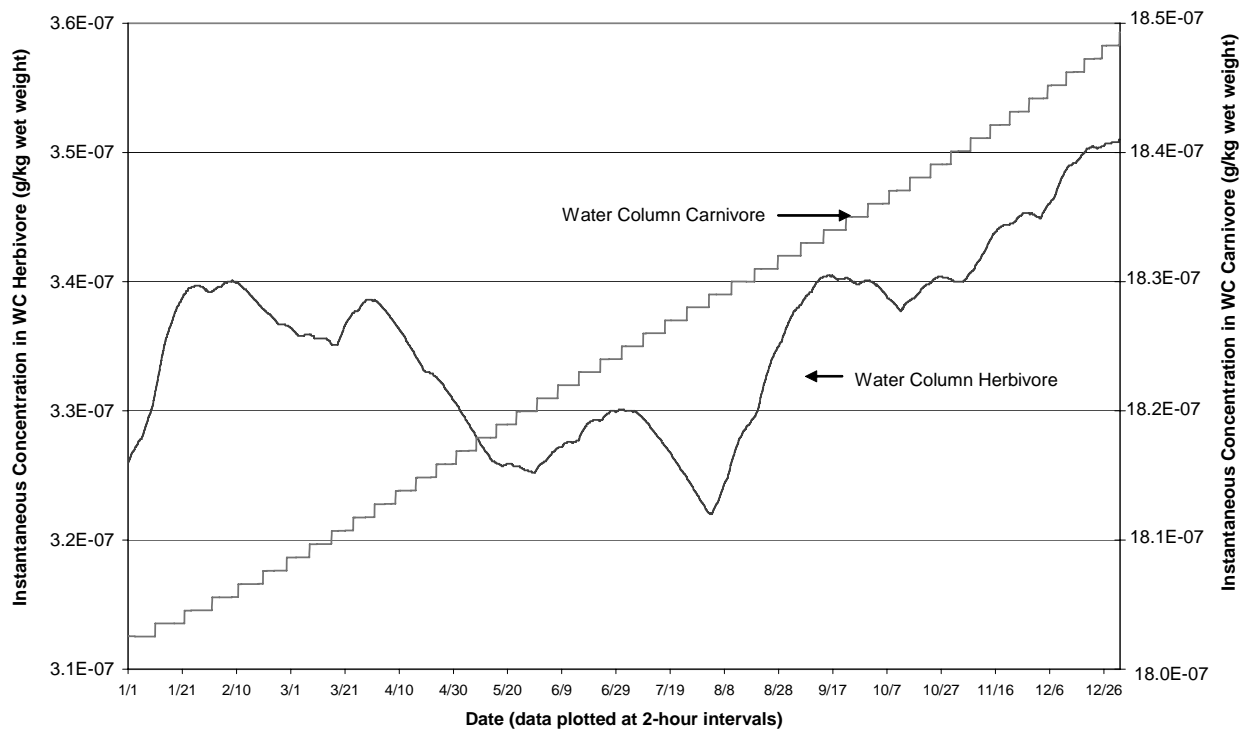


Exhibit 3-20 (not on a log scale) shows the instantaneous total mercury concentrations in water-column herbivores and carnivores in Swetts Pond. The water-column herbivore concentrations fluctuate during the year and appear to track the surface water concentrations, with a slight delay and smoother peaks (e.g., peaks at the end of January, late March, end of June, and early September). This is because the water-column herbivore eats 100 percent algae which is modeled as a phase of the surface water. The water-column carnivore instantaneous concentrations of total mercury increase steadily throughout the year, with no fluctuations. Once again, this is due to the diet of the water-column carnivore (100 percent water-column omnivore)

and its position on the modeled aquatic food chain. Unlike in the case of the water-column herbivore, temporal changes in surface water concentration do not have any direct effect on the time pattern of mercury accumulation in the water-column carnivore. Moreover, the higher mercury concentration in water-column carnivores probably dampens any potential fluctuations from varying mercury inputs.

The apparent stair-step pattern of the time-series results from the small output time step and the fact that TRIM.FaTE instantaneous output concentrations were reported to four significant figures. Each “step” consists of approximately 100 instantaneous concentrations with the same value (at a larger output time step, or if outputs were reported with more significant figures, the line would appear to be a smooth, upward-sloping line). Monthly average total mercury concentrations in the aquatic biota show similar patterns (Exhibit 3-19). The water-column herbivore monthly average concentrations fluctuate with a seemingly seasonal pattern of higher concentrations around January, matching the peaks in the surface water compartment. The water-column omnivore monthly concentrations are smoother than the herbivore with very slight fluctuations. The water-column carnivore concentrations increase steadily throughout the five years with little apparent fluctuation. Note that total mercury concentration in all three fish compartment types increase about the same percentage over the five years, roughly 15 percent.

Exhibit 3-20
Instantaneous Concentration of Total Mercury in Water-column Carnivore and Herbivore:
Swetts Pond (Year 30)

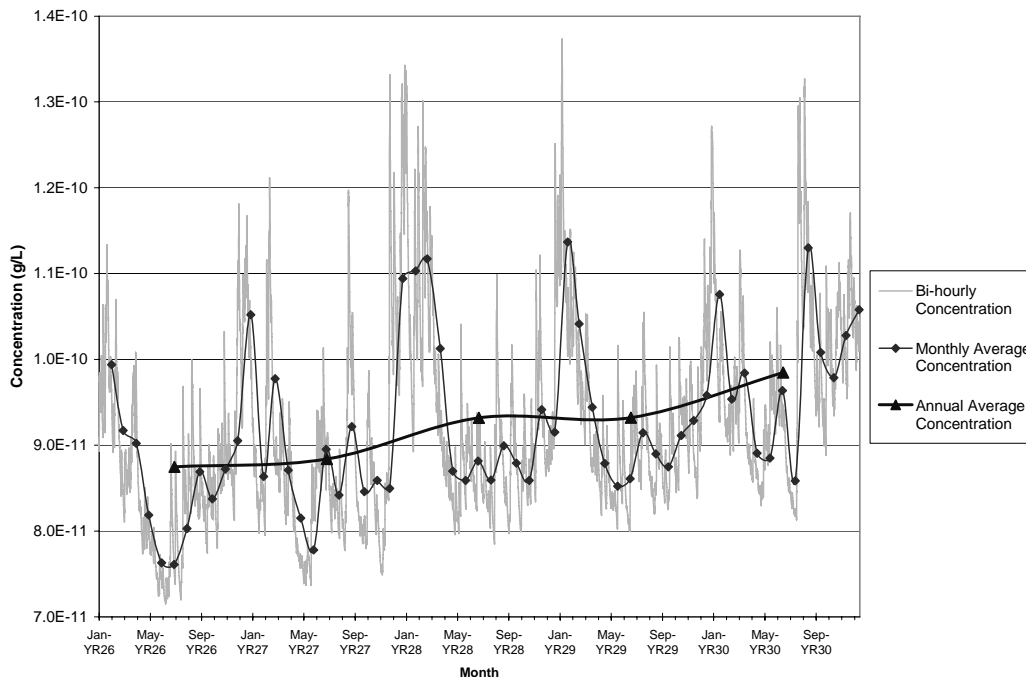


^aNote that the two fish types are plotted on separate y-axes, but the scale increments of the two axes are the same.

Summary of Instantaneous and Monthly Results

Short-term concentration patterns in a compartment are highly influenced by the relationship between the compartment and the air, the turnover rate (i.e., mass transfers in versus mass transfers out) of chemical mass in the compartment, and the pattern of the chemical concentration in the compartment(s) providing mass input to the compartment. As expected, instantaneous concentration results show resolution that is damped in monthly or annual averages, as illustrated in Exhibit 3-21, which shows annual averages, monthly averages, and instantaneous outputs plotted together for surface water of Swetts Pond (not on log scale). Instantaneous fluctuations in concentrations are due primarily to fluctuations in time-varying input data (e.g., meteorological data that directly affect deposition or air concentration). TRIM.FaTE has the flexibility to allow for input data treated as constants in this test case (e.g., surface water properties) to vary over time as well, and additional patterns in short-term concentrations would be expected if more input properties (e.g., surface water parameters such as temperature or depth) varied hourly or seasonally. As expected, monthly averages do not fluctuate as much as instantaneous estimates (but more than annual averages), but do appear to show some seasonal patterns based on seasonal meteorological data patterns.

Exhibit 3-21
Instantaneous and Average Concentration of Total Mercury in Surface Water: Swetts Pond (Years 26 to 30)



3.3 Speciation: How Do Concentrations of Hg⁰, Hg²⁺, and MHg Differ?

This section examines mercury speciation profiles of predicted concentrations in abiotic and biotic compartments for the mercury test case (emission case B). The analyses here focus on the *relative* concentrations of the different mercury species; therefore, for all of the bar charts in this section, a 100 percent stacked column is used. The data used to generate these charts are concentrations of elemental mercury, divalent mercury, and methyl mercury (as mercury). Note that if this analysis focused on *mass* fractionation of mercury species in specific compartments, the results would be identical to the *concentration*-based fractions generated here.

3.3.1 Speciation by Compartment Type

The relative speciation profiles for various compartment types are compared below. These charts are grouped by ecosystem type. Compartments for each ecosystem were selected to compare the overall speciation for compartments that may be related to one another due to food chain and other relationships. Both abiotic and biotic compartment types are included in these analyses. For analyses and charts in Sections 3.3.1 and 3.3.2, the annual average concentrations for each compartment for the 30th modeling year are used.

Aquatic Ecosystem

Mercury speciation is presented for selected compartment types that are included in a typical aquatic ecosystem in the mercury test case. Compartment types included in these analyses are:

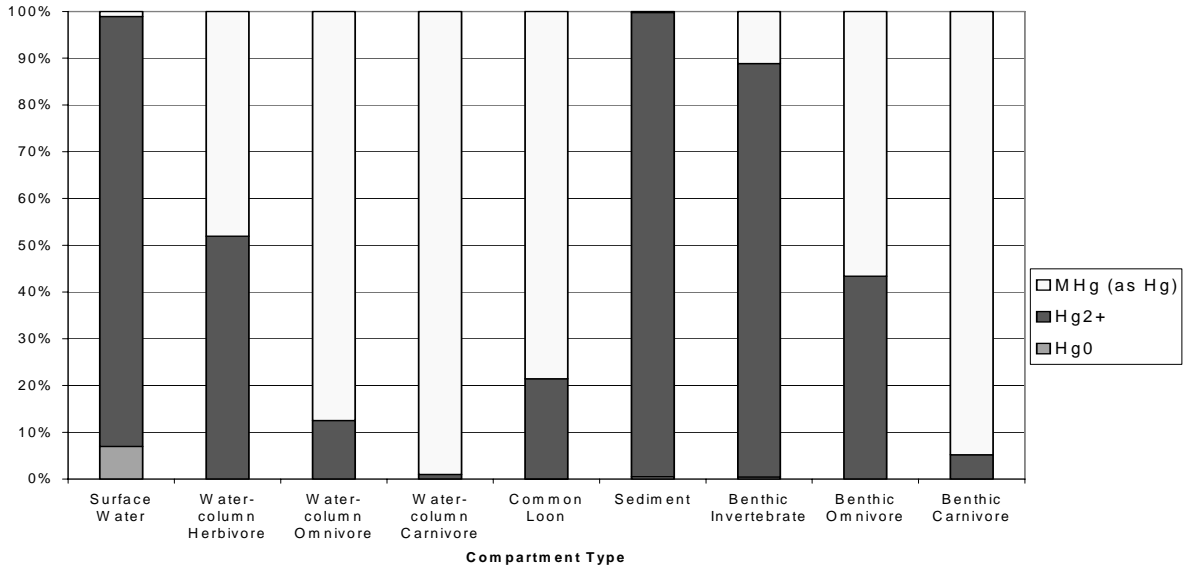
- Surface water;
- Water-column herbivore, omnivore, and carnivore;
- Common loon;
- Sediment;
- Benthic invertebrate; and
- Benthic omnivore and carnivore.

Speciation results for the aquatic ecosystems in Swetts Pond and Brewer Lake are presented in Exhibit 3-22.

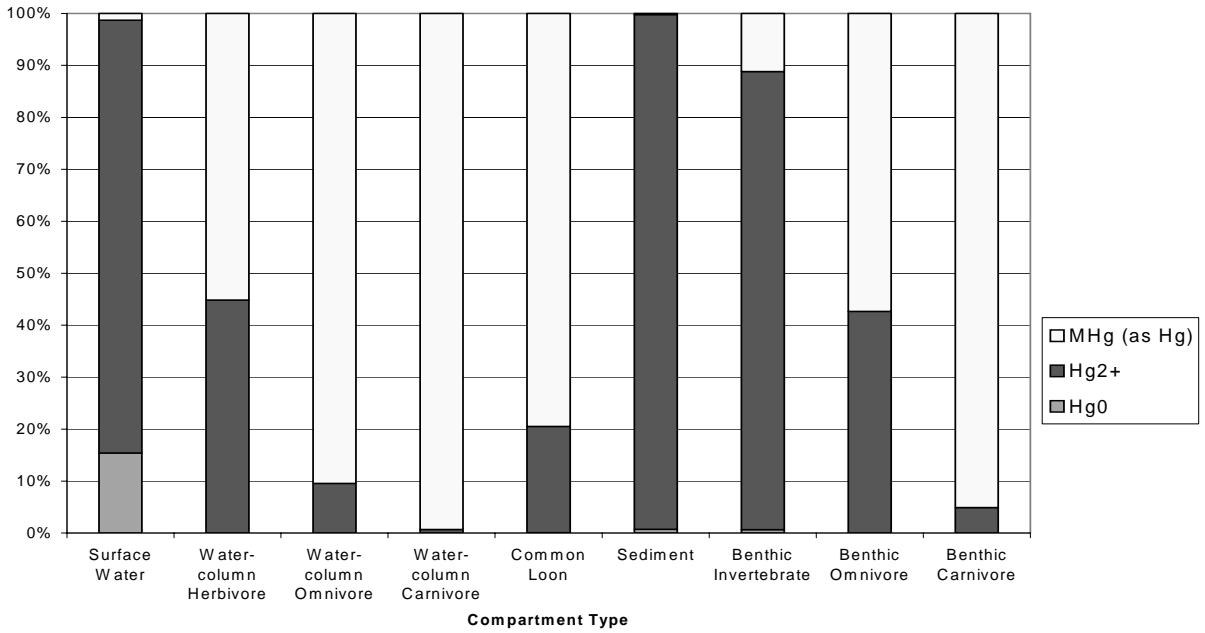
In general, the basic speciation profile is similar for each set of aquatic compartment types across the two water bodies. This trend is evident regardless of the size of the water body; the modeled volume of Brewer Lake is almost 25 times the volume of Swetts Pond, and the modeled depth is eight meters (Brewer) versus three meters (Swetts). However, small differences in speciation profiles between surface water bodies were observed (these variations are discussed in more detail in Section 3.3.2).

Exhibit 3-22
Mercury Speciation Profile of Various Compartment Types Present in Water Bodies:
Year 30 (Annual Average)

(a) Swetts Pond



(b) Brewer Lake



Abiotic Compartments. Most (more than 80 percent) of the mercury in the surface water compartments for these two lakes is estimated to be divalent, with most of the balance being elemental. Nearly all (more than 98 percent) of the mercury in the sediment for both water bodies is divalent. Thus, divalent mercury dominates the speciation in the abiotic compartments for the modeled lakes.

Biotic Compartments. For water-column herbivores in the two lakes shown in Exhibit 3-22, roughly half of the mercury is methyl (48 and 55 percent), with the remainder present in divalent form. A larger fraction of the mercury in water-column omnivores (roughly 90 percent) and carnivores (roughly 99 percent) is methyl mercury. As evident from the bar charts, divalent mercury plays a bigger role in the benthic food chain. For the benthic fish, most of the mercury in the carnivore (roughly 95 percent) is methyl mercury, and mercury in the omnivore is a little more than half methyl (50 to 60 percent). Most (about 90 percent) of the mercury in benthic invertebrates is divalent. The common loon, which feeds on both the water-column and benthic fish, has roughly 80 percent methyl mercury.

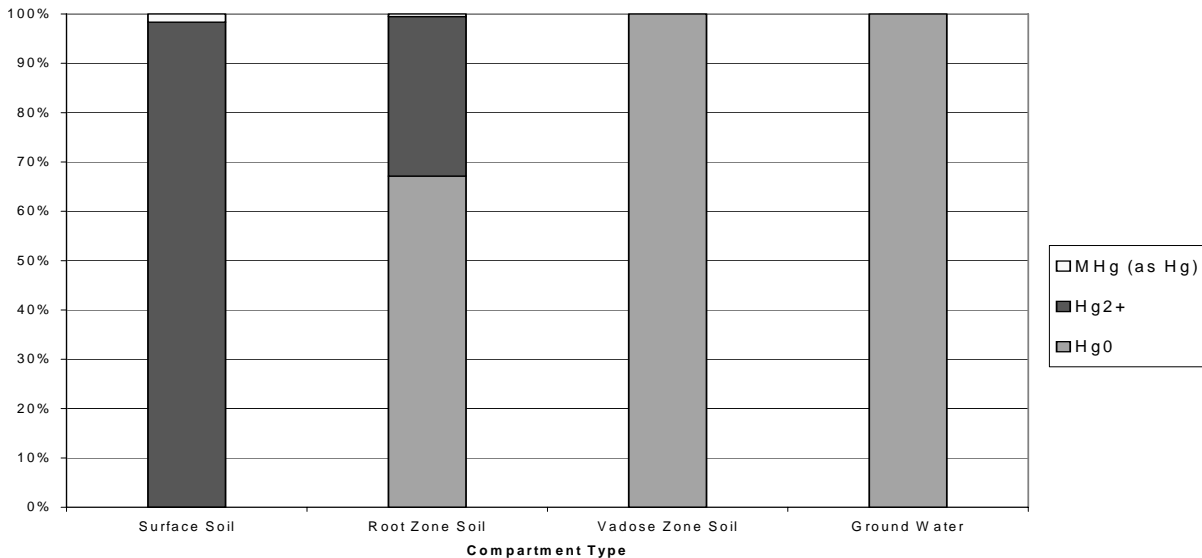
Thus, methyl mercury dominates the modeled speciation in the fish compartments – especially at higher trophic levels – and the semi-aquatic animal compartments with a 100 percent fish diet (i.e., common loon), but the benthic invertebrate compartment has mostly divalent mercury. Based on the literature, methyl mercury is expected to be the dominant species of mercury in predatory fish (Bloom 1992). In the modeling results, methyl mercury is not as dominant in lower trophic levels, consistent with the findings of Mason et al. (2000), who concluded that the overall trophic status of the tested organism was indicated by the percentage of mercury in its tissues that was methyl mercury (i.e., percent methyl mercury increased with increasing trophic status). For example, non-predatory benthic invertebrates had more divalent mercury than methyl mercury in their tissues. Bloom (1992) also suggests that lower percent methyl mercury levels might be found in aquatic biota from non-natural (i.e., contaminated) systems. For example, high percentages of inorganic (i.e., divalent) mercury have been observed in stonerollers, a small fish that feeds exclusively on periphyton (algae often have a relatively high ratio of inorganic to organic mercury), in a mercury-contaminated stream at the Y-12 facility in Oak Ridge (Hill et al. 1996). This finding is consistent with the relatively high divalent mercury fraction in the modeled water-column herbivore, which has a diet of 100 percent algae.

With respect to reported mercury speciation in benthic invertebrates, in Onondaga Lake, NY, only about 25 percent of the mercury in benthic macroinvertebrates was observed to be methyl mercury (Becker and Bigham 1995). A variety of results were reported in studies of Duncan Lake in Northern Quebec (Tremblay et al. 1996), in which seven different aquatic insect taxa were classified by feeding type (i.e., detritivores, grazers, predators, and combinations of these). The percent methyl mercury of total mercury ranged from 10.5 percent for the mayfly (a detritivore) to 75.1 percent for the dragonfly (an obligate predator). The average percent methyl mercury was 31.7 percent for non-predators (4 of 7 taxa), 39.5 percent for non-obligate predators (6 of 7 taxa), and 44.5 percent for all taxa. Biota-sediment accumulation factors for mercury used as inputs for this TRIM.FaTE test case were derived from values for mayfly, and therefore the speciation presented in Exhibit 3-22 (i.e., 11 percent methyl mercury after 30 years; see also Exhibits 3-27 and 3-32) tends to represent that of non-predatory benthic invertebrates.

Terrestrial Ecosystem

Soil Layers and Ground Water. Speciation results are presented for surface soil, root zone soil, vadose zone soil, and ground water compartments associated with parcel SW2 (Exhibit 3-23). Divalent mercury dominates the speciation profile in the surface soil compartment. For subsurface soil and ground water compartments, reduced (elemental) mercury predominates. Mercury in vadose zone soil and ground water compartments is essentially 100 percent elemental mercury, the most mobile form of the three species in soil. Note, however, that there are considerably lower total mercury concentrations in the vadose zone and ground water than in the overlying soil compartments (see, for example, Appendix Table B-8a).

Exhibit 3-23
Mercury Speciation Profile of Soil Layer Compartments in SW2:
Year 30 (Annual Average)



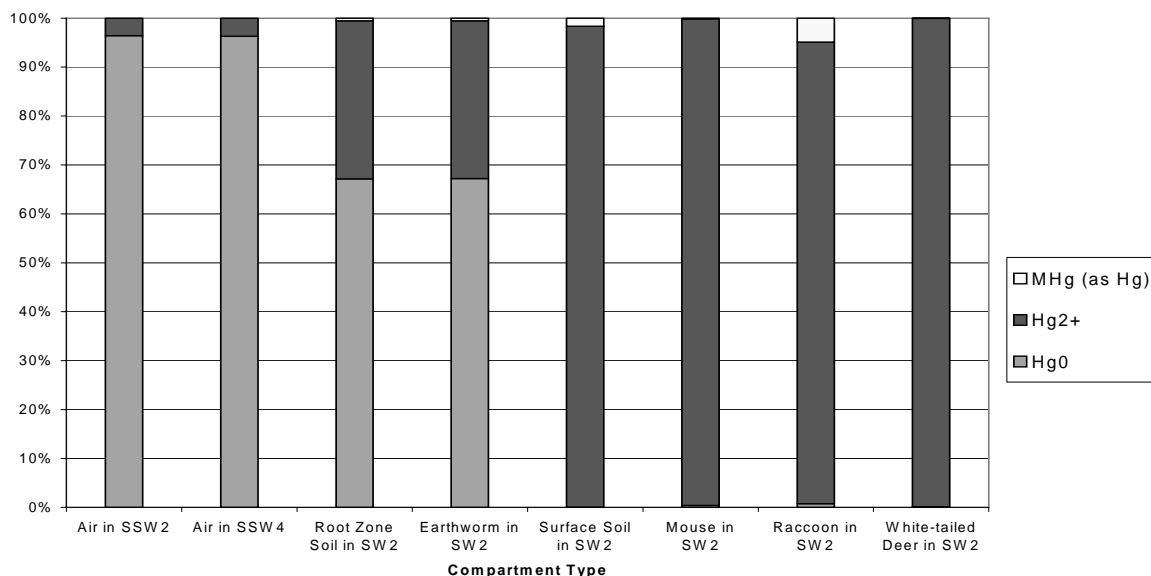
Animals. Mercury speciation for several of the compartment types in a terrestrial ecosystem is presented here, with a focus on the animal compartments.¹³ Compartment types discussed are air, root zone soil, earthworm, surface soil, mouse, raccoon, and white-tailed deer. Exhibit 3-24 presents the speciation profile for these compartment types associated with parcel SW2. Note that air parcels SSW2 and SSW4 both overlay parts of surface parcel SW2.

In general, the bulk (at least 95 percent) of the mercury in surface soil and animals that eat terrestrial diets (e.g., leaves, other land animals) or partial terrestrial diets (e.g., raccoon, which also eats benthic invertebrates and fish) is estimated to be divalent mercury. The majority

¹³ Note that there is more uncertainty associated with the test case results for terrestrial biota compartments relative to the results for aquatic biota compartments. The parameters used in the mercury mass transport and transformation algorithms related to terrestrial biota have been studied less, resulting in greater uncertainty.

(around 60 percent) of the mercury in root zone soil is present as elemental mercury, with the remainder present as divalent mercury. This reflects the lower mobility of divalent mercury relative to elemental mercury in soil (EPA 1997). It is noted that concentrations of total mercury in root zone soil are much lower than those for surface soil (see, for example, Appendix Table B-8a). Speciation for the earthworm compartment mirrors that of the root zone soil, which is consistent with the fact that the earthworm partitions mercury from the root zone soil, not the surface soil. Most of the mercury in air is elemental, similar to the modeled emissions profile.

Exhibit 3-24
Mercury Speciation Profile of Selected Terrestrial Compartments in SW2 and Corresponding Air Parcels: Year 30 (Annual Average)



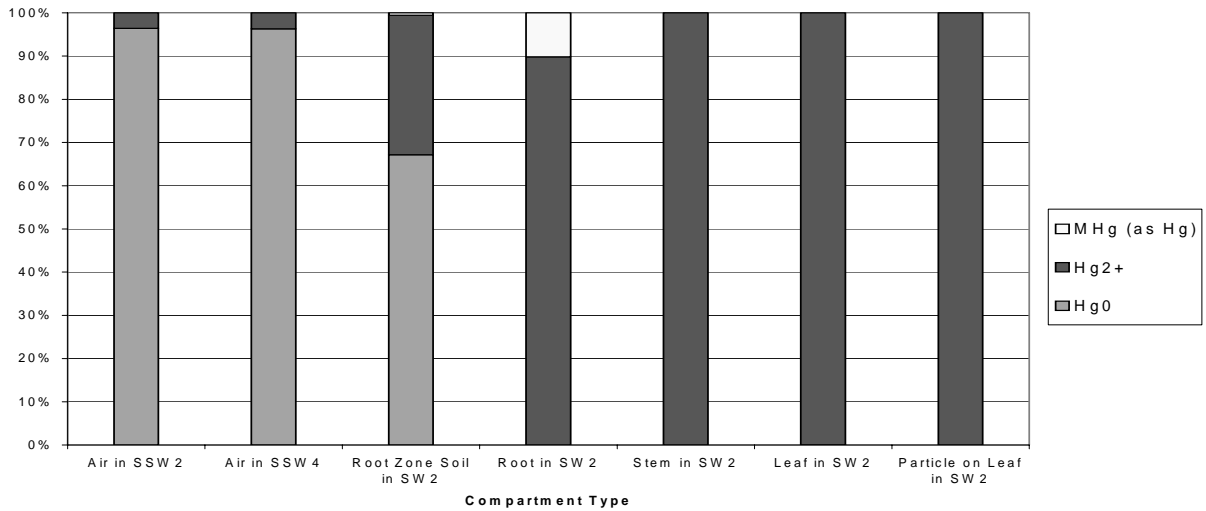
Terrestrial Plants. Mercury speciation for each of the plant compartment types is presented here for a terrestrial ecosystem associated with parcel SW2, where grasses/herbs is the vegetation type (see Exhibit 3-25). Included in this chart are air, root zone soil, and four plant compartment types (root, stem, leaf, particle on leaf). As in the rest of this section, the results presented for air and root zone soil reflect the annual average concentrations for year 30 of the simulation; speciation results for the plant compartments reflect the average concentrations during the growing season only for year 30 (i.e., averages for the three mercury species were calculated from the results for May 13 through September 29 of that year). Air parcels SSW2 and SSW4 both overlay parts of surface parcel SW2.

Most (essentially 100 percent for stem, leaf, and particle on leaf, roughly 90 percent for root) of the mercury in the grasses/herbs plant compartments for parcel SW2 is present as divalent mercury, with some methyl mercury evident in the root compartment. This noticeable presence of methyl mercury in the root compartment, coincident with a lack of noticeable methyl mercury in the root zone soil compartment, likely reflects the difference in partitioning coefficients among the mercury species. The partition coefficient (root zone soil to root) for methyl mercury is

approximately 10 times greater than that for divalent mercury, while the value for elemental mercury is negligible.

The speciation in plant compartments for coniferous and deciduous forests was also examined as a part of this analysis. Only leaf and particle-on-leaf compartments are included in the coniferous and deciduous plant composite compartments; root and stem compartments for woody plants are not included in the test case due to significant uncertainties in modeling transfers to and from those compartments. The speciation profiles for coniferous and deciduous leaf and particle-on-leaf compartments across the modeling region are very similar to the trends observed in the corresponding grasses/herbs compartments (nearly 100 percent divalent mercury). Thus, most of the mercury in each of the plant compartments across the modeling region is present as divalent mercury, with some methyl mercury evident in the root compartments.

Exhibit 3-25
Mercury Speciation Profile of Terrestrial Grasses/Herbs Plant Compartments in SW2 and Corresponding Air Parcels: Year 30 (Annual Average)



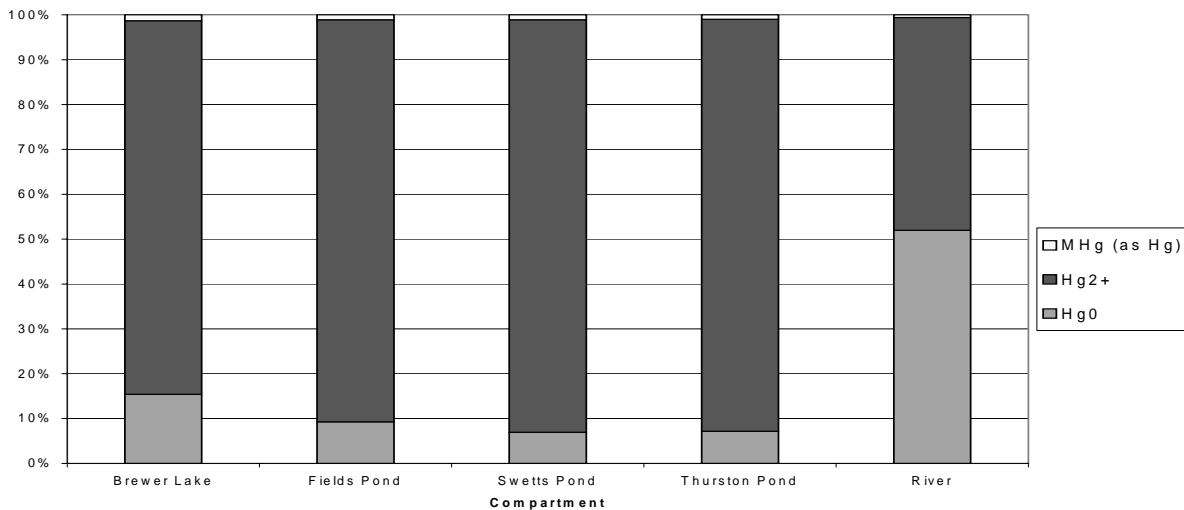
3.3.2 Spatial Variations in Speciation

In general, no major spatial variations in speciation were observed for most abiotic and biotic compartment types included in the mercury test case. The speciation profile for a compartment type is, for the most part, relatively constant across the modeling region. This is to be expected because most of the spatially varying aspects of a scenario, such as air concentration and deposition rate, are not expected to affect mercury speciation for a given compartment type. One divergence from this observation is the variation in speciation profiles for the different water body compartments that were included in the test case.

The surface water compartment type is the only compartment type for which noticeable variations in speciation were observed for compartments located in different parts of the modeling region. It is important to note that the water body compartments in the mercury test case were characterized individually; the property values for water body compartments reflect the site-specific variation between the various water bodies. For example, site-specific surface areas, depths, temperatures, and flow/flush rates were assigned to each surface water compartment. By contrast, the basic properties for other compartment types (e.g., surface soil) were identical or nearly the same for all compartments included in the scenario (e.g., all surface soil compartments were assigned the same depth, soil density, and temperature). Therefore, many of the differences in speciation observed in the various surface water compartments are likely a result of different water body *characteristics* rather than different compartment *locations*.

Speciation profiles for the surface water compartments included in the mercury test case scenario are presented in Exhibit 3-26, based on total water column concentrations (i.e., phase-specific concentrations, such as dissolved mercury, were not considered).

Exhibit 3-26
Mercury Speciation Profile of Various Surface Water Compartments:
Year 30 (Annual Average)



In general, the majority of the mercury in surface water is divalent, with elemental mercury comprising the bulk of the remaining mercury. Among the lakes, speciation differences are fairly small, with the larger (and deeper) ones having higher fractions of elemental mercury. There is a large difference in speciation between mercury in the river and the four lakes, with a considerably higher fraction of elemental mercury in the river. Variations in surface water speciation could be related to the surface area-to-volume ratio, water body depth, residence time, or other characteristics of the water bodies, which can affect the relative amount of elemental mercury that transfers into and out of, and transforms within, a compartment.

Although surface water speciations of mercury do vary for the different water bodies, speciations for sediment and most fish compartment types do *not* appear to vary much across water bodies (see, for example, Exhibit 3-22 for a presentation of the mercury speciation in sediment and fish compartments for Swetts Pond and Brewer Lake). The steady-state results (see Chapter 4 for detailed discussion of the steady-state modeling) for aquatic animal compartments for all four lakes included in the mercury test case are presented in Exhibit 3-27. Methyl and divalent mercury concentration results (elemental mercury is negligible) and the corresponding percent methyl mercury for each of the five fish compartments and the benthic invertebrate compartment are presented in this table. For most of these compartments, the overall variation in percent methyl mercury between water bodies is small (i.e., generally within a few percent); for benthic animals, the speciation fractions are nearly identical. The most notable difference in mercury speciation in fish across water bodies is for the water-column herbivore (100 percent algae diet), which varies more across the lakes, with the percent methyl mercury ranging from 36 to 51 percent (and which also has a considerably higher percent methyl mercury in the river than in the lakes).

Food chain multiplier ratios are presented along the bottom of Exhibit 3-27 for reference; these values are very stable across the four lakes.

Exhibit 3-27

Speciated Mercury Results for Fish and Benthic Invertebrates in Four Lakes/Ponds: Steady-state

	Swetts Pond				Thurston Pond				Brewer Lake				Fields Pond			
	MHg	Hg ²⁺	Total	%MHg	MHg	Hg ²⁺	Total	%MHg	MHg	Hg ²⁺	Total	%MHg	MHg	Hg ²⁺	Total	%MHg
<i>Methyl and Divalent Mercury Concentrations and Percent Methyl Mercury: Steady-state^a</i>																
WC-C^b	1.41E-04	2.26E-06	1.44E-04	98.4%	6.19E-05	1.06E-06	6.29E-05	98.3%	1.00E-04	8.34E-07	1.01E-04	99.2%	8.26E-05	1.11E-06	8.37E-05	98.7%
WC-O	2.70E-05	6.28E-06	3.33E-05	81.1%	1.17E-05	2.94E-06	1.47E-05	80.0%	1.84E-05	2.29E-06	2.07E-05	88.9%	1.58E-05	3.09E-06	1.89E-05	83.7%
WC-H	1.21E-05	2.12E-05	3.33E-05	36.4%	5.22E-06	9.87E-06	1.51E-05	34.6%	8.01E-06	7.58E-06	1.56E-05	51.4%	7.37E-06	1.07E-05	1.81E-05	40.8%
B-C	1.07E-04	5.83E-06	1.13E-04	94.8%	5.08E-05	2.73E-06	5.36E-05	94.9%	4.26E-05	2.18E-06	4.48E-05	95.1%	5.19E-05	2.91E-06	5.48E-05	94.7%
B-O	2.07E-05	1.63E-05	3.71E-05	56.0%	9.75E-06	7.62E-06	1.74E-05	56.1%	7.86E-06	6.01E-06	1.39E-05	56.7%	1.01E-05	8.16E-06	1.82E-05	55.3%
B-I	6.35E-06	5.18E-05	5.90E-05	10.8%	2.94E-06	2.40E-05	2.74E-05	10.8%	2.30E-06	1.86E-05	2.13E-05	10.8%	3.26E-06	2.66E-05	3.03E-05	10.8%
<i>Food Chain Multipliers: Steady-state</i>																
WC-C/WC-O	5.2	0.4	4.3		5.3	0.4	4.3		5.4	0.4	4.9		5.2	0.4	4.4	
WC-O/WC-H	2.2	0.3	1.0		2.2	0.3	1.0		2.3	0.3	1.3		2.1	0.3	1.0	
B-C/B-O	5.2	0.4	3.0		5.2	0.4	3.1		5.4	0.4	3.2		5.1	0.4	3.0	
B-O/B-I	3.3	0.3	0.6		3.3	0.3	0.6		3.4	0.3	0.7		3.1	0.3	0.6	

^a Hg²⁺ concentration results in mg/kg wet weight, MHg and total concentration results in mg/kg wet weight as Hg.

^b WC = water-column, B = benthic, C = carnivore, O = omnivore, H = herbivore, I = invertebrate.

3.3.3 Temporal Variations in Speciation

Abiotic Compartments

Overall, speciation within most of the abiotic compartments included in the mercury test case does not appear to vary much over the time frame of the scenario (i.e., 30 years). The speciation profile for some of these compartments stabilizes relatively quickly at a profile similar (or nearly identical) to the speciation profile calculated from the steady-state simulation results. For example, there are not perceptible variations in mercury speciation in surface soil, surface water, and sediment compartments for years 1, 10, and 30 or the steady-state simulation results. See Exhibits 3-28a, 3-28b, and 3-28c for speciation profiles of the surface soil compartment in SW2 and surface water and sediment compartments in Swetts Pond corresponding to these time points. Speciation profiles in each of these exhibits were calculated from annual average concentrations for years 1, 10, and 30, and from the simulation end results for the steady-state run.

Exhibit 3-28a
Mercury Speciation Profile of Surface Soil Compartment in SW2:
Years 1, 10, 30, and Steady-state

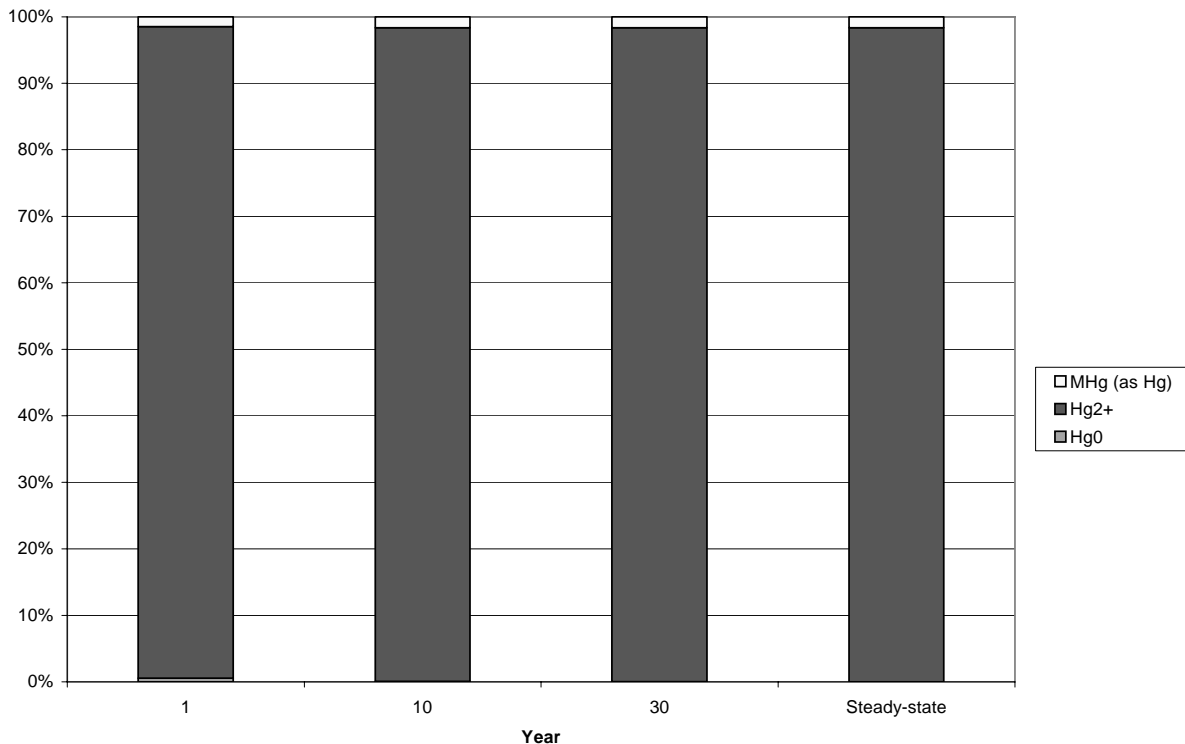


Exhibit 3-28b
Mercury Speciation Profile of Surface Water Compartment in Swetts Pond:
Years 1, 10, 30, and Steady-state

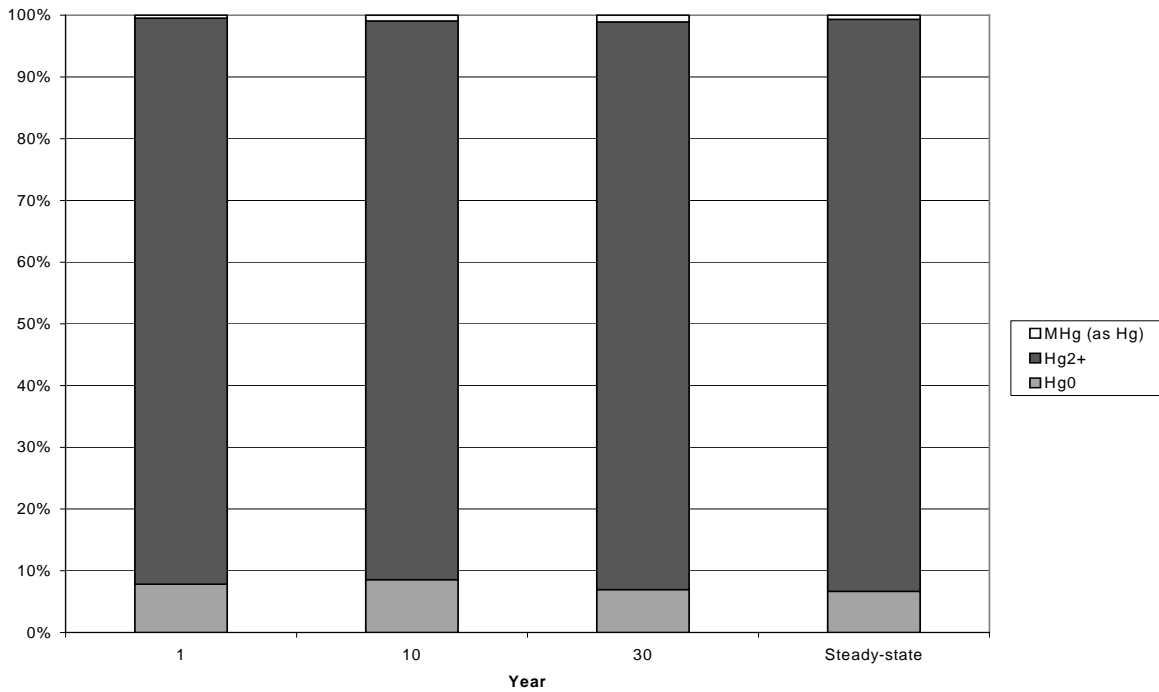
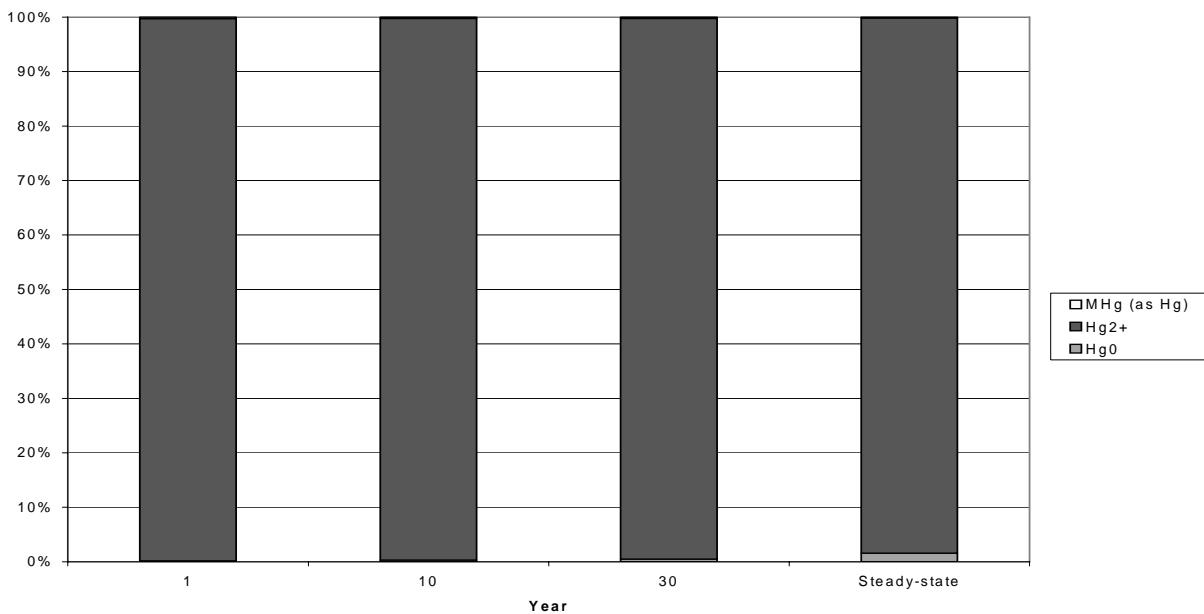


Exhibit 3-28c
Mercury Speciation Profile of Sediment Compartment in Swetts Pond:
Years 1, 10, 30, and Steady-state



Biotic Compartments

Temporal aspects of speciation profiles in some of the biotic compartments are slightly more variable. These changes may be a result of one or more factors, *possibly* including:

- Relationships between biotic compartments and their surrounding abiotic environments (e.g., uptake of mercury via inhalation and ingestion, excretion of mercury to the environment);
- Various mercury transformation reactions that occur at different rates in different biotic compartment types (e.g., methylation, which is an important process affecting mercury speciation in fish); and
- Food web relationships that connect a biotic compartment with multiple other biotic compartments via consumption.

For the fish and common loon compartment types, the fraction of mercury as methyl mercury increases over time. See, for example, the speciation profiles for the water-column herbivore, omnivore, and carnivore compartments and the benthic carnivore compartment in Swetts Pond presented in Exhibit 3-29.¹⁴ The speciation profile for the common loon compartment in Swetts Pond also changes over time (Exhibit 3-30). Possible factors in this temporal increase in methyl mercury fraction include both the slightly higher uptake rate of methyl mercury into algae (compared to divalent mercury) and the slower rate of methyl mercury excretion from fish than that for divalent mercury. For common loons in eastern Canada, Scheuhammer et al. (1998) have observed that the proportion of methyl mercury is 80 to 100 percent of total mercury in the breast muscle but only five to seven percent of total mercury in livers and kidneys. Whole body concentrations generally have not been measured; blood and feather measurements are much more common. The test case modeling results presented in Exhibit 3-30 appear to be consistent with the data reported in Scheuhammer et al.

This trend of increasing percent methyl mercury is not observed for all aquatic biota compartment types. The speciation profiles for the benthic invertebrate and benthic omnivore compartments in Swetts Pond are nearly constant over time (Exhibit 3-31).

Exhibit 3-32 presents detailed speciated mercury results for the aquatic animal compartments for Swetts Pond that are summarized in Exhibits 3-29 and 3-31. This table shows concentration of methyl and divalent mercury (elemental mercury is negligible) over time (and steady-state) for Swetts Pond. The right side of the table provides methyl mercury percentages, and food chain multiplier ratios are provided along the bottom. As shown in the bar charts, the percentage of methyl mercury increases over time (except for benthic invertebrates) and is higher in the higher trophic levels. Also, as expected, methyl mercury concentrations in fish consistently increase up through the food chain (carnivore > omnivore > herbivore), as shown by the food chain multipliers for methyl mercury.

¹⁴ All biotic speciation profiles discussed in this section were calculated from annual average concentrations for years 1 through 10 and year 30, and from the simulation end results for the steady-state model run.

Exhibit 3-29
Mercury Speciation Profile of Aquatic Biota Compartments in Swetts Pond:
Years 1 - 10, 30, and Steady-state

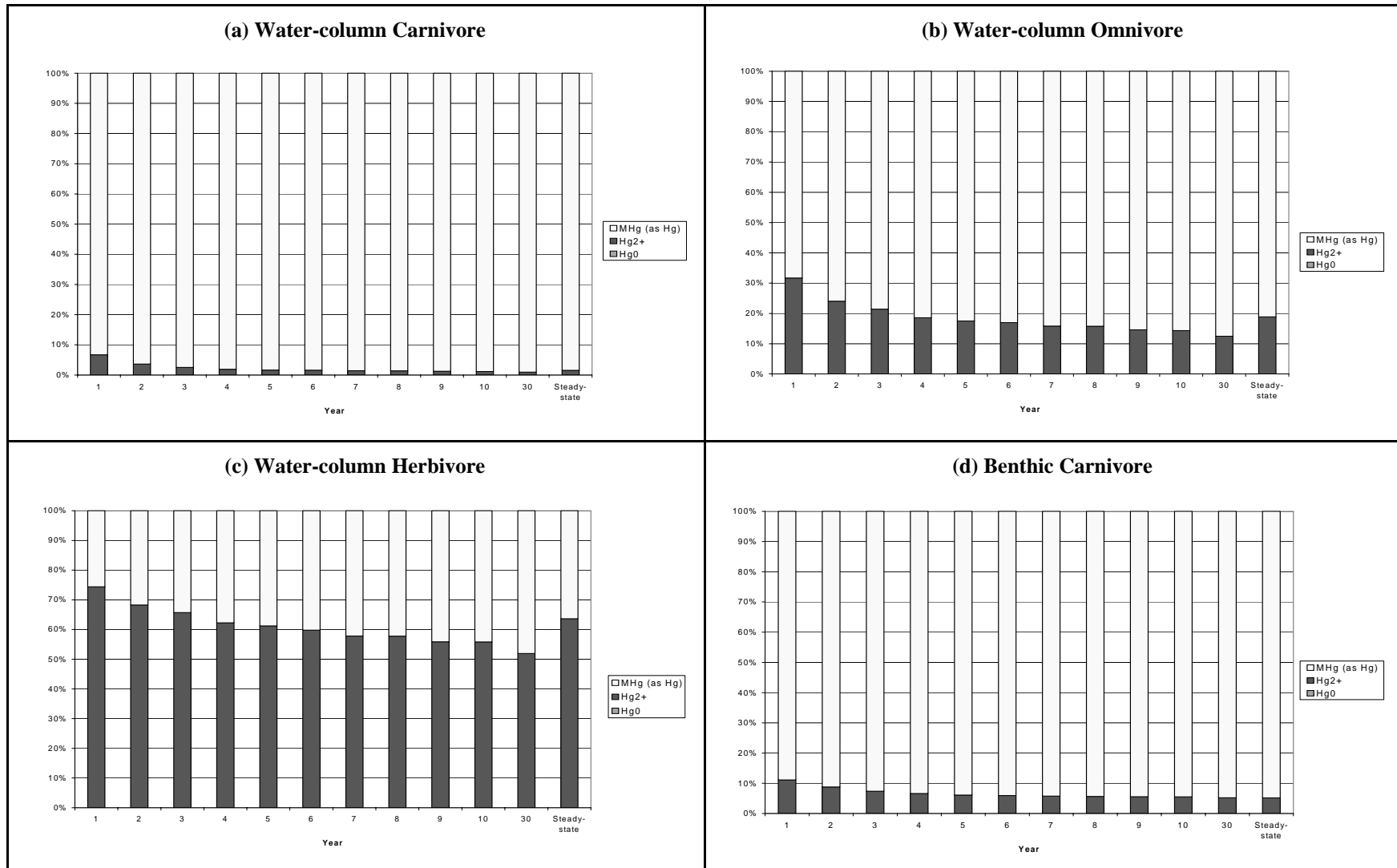


Exhibit 3-30
Mercury Speciation Profile of Common Loon Compartment in Swetts Pond:
Years 1 - 10, 30, and Steady-state

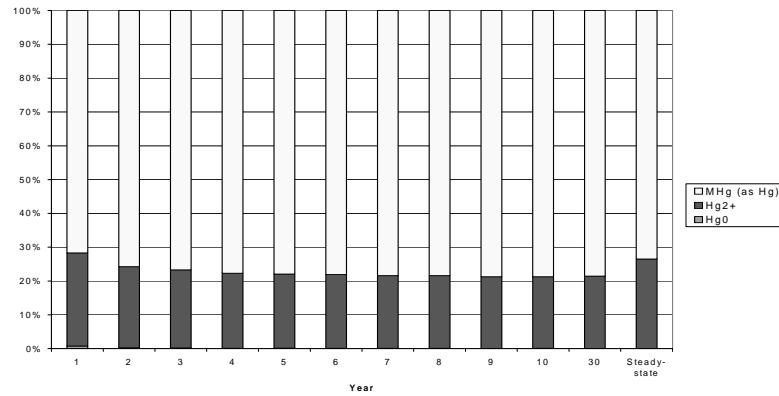
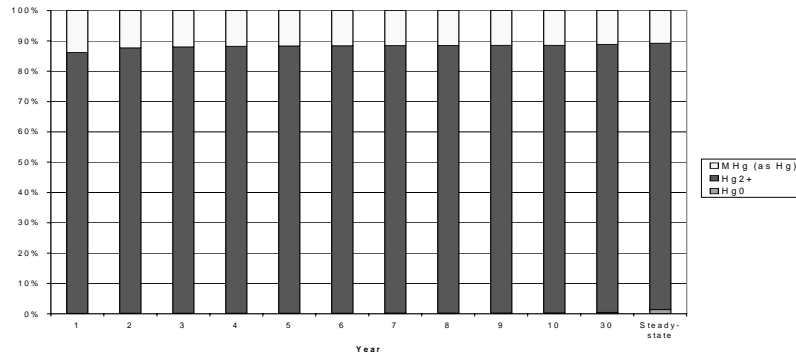


Exhibit 3-31
Mercury Speciation Profile of Benthic Invertebrate and Benthic Omnivore Compartments
in Swetts Pond: Years 1 - 10, 30, and Steady-state

(a) Benthic Invertebrate



(b) Benthic Omnivore

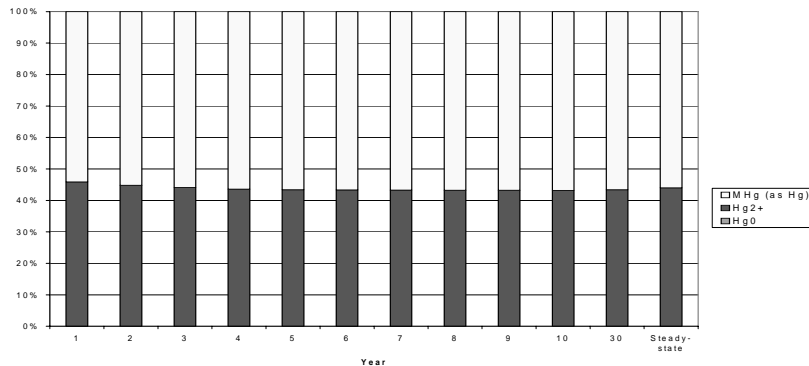


Exhibit 3-32

Speciated Mercury Results for Fish and Benthic Invertebrates in Swetts Pond: Years 1, 10, 30, and Steady-state

Year	MHg (g/kg wet weight as Hg)				Hg ²⁺ (g/kg wet weight)				Total Hg (g/kg wet weight)				Percent Methyl Mercury			
	1	10	30	SS	1	10	30	SS	1	10	30	SS	1	10	30	SS
<i>Concentrations</i>																
WC-C^a	2.01E-08	6.32E-07	1.81E-06	1.41E-04	1.45E-09	7.66E-09	1.79E-08	2.26E-06	2.15E-08	6.40E-07	1.82E-06	1.44E-04	93.3%	98.8%	99.0%	98.4%
WC-O	1.51E-08	1.32E-07	3.55E-07	2.70E-05	7.03E-09	2.20E-08	5.07E-08	6.28E-06	2.22E-08	1.54E-07	4.05E-07	3.33E-05	68.3%	85.7%	87.5%	81.1%
WC-H	1.11E-08	6.13E-08	1.61E-07	1.21E-05	3.23E-08	7.75E-08	1.74E-07	2.12E-05	4.34E-08	1.39E-07	3.35E-07	3.33E-05	25.6%	44.2%	48.1%	36.4%
B-C	3.30E-10	5.35E-08	2.87E-07	1.07E-04	4.12E-11	3.11E-09	1.58E-08	5.83E-06	3.71E-10	5.67E-08	3.03E-07	1.13E-04	88.9%	94.5%	94.8%	94.8%
B-O	2.76E-10	1.20E-08	5.85E-08	2.07E-05	2.34E-10	9.13E-09	4.49E-08	1.63E-05	5.10E-10	2.11E-08	1.03E-07	3.71E-05	54.1%	56.8%	56.6%	56.0%
B-I	1.82E-10	3.92E-09	1.83E-08	6.35E-06	1.14E-09	3.03E-08	1.46E-07	5.18E-05	1.32E-09	3.43E-08	1.65E-07	5.90E-05	13.8%	11.4%	11.1%	10.8%
<i>Food Chain Multipliers</i>																
WC-C/WC-O	1.3	4.8	5.1	5.2	0.2	0.3	0.4	0.4	1.0	4.2	4.5	4.3				
WC-O/WC-H	1.4	2.1	2.2	2.2	0.2	0.3	0.3	0.3	0.5	1.1	1.2	1.0				
B-C/B-O	1.2	4.5	4.9	5.2	0.2	0.3	0.4	0.4	0.7	2.7	2.9	3.0				
B-O/B-I	1.5	3.1	3.2	3.3	0.2	0.3	0.3	0.3	0.4	0.6	0.6	0.6				

^a WC = water-column, B = benthic, C = carnivore, O = omnivore, H = herbivore, I = invertebrate.

3.4 Spatial Variation of Total Mercury Concentration

This section examines spatial variations in total mercury concentrations for emission case B of the test case. The data used to create the tables and charts included in this section are concentrations of total mercury, which are calculated by summing the concentrations of elemental mercury, divalent mercury, and methyl mercury (as mercury) output by TRIM.FaTE. With the exception of the air results, these tables and charts present the average total mercury concentrations for the final (i.e., 30th) year of the emission case B simulation. The tables and charts for the air compartments present the average total mercury concentrations over the final five years of the simulation.¹⁵ This section does not address temporal patterns of mercury mass and concentration or variations in mercury speciation over the modeling region; these topics were addressed in Sections 3.1 through 3.3, respectively, of this report.

3.4.1 Abiotic Compartments

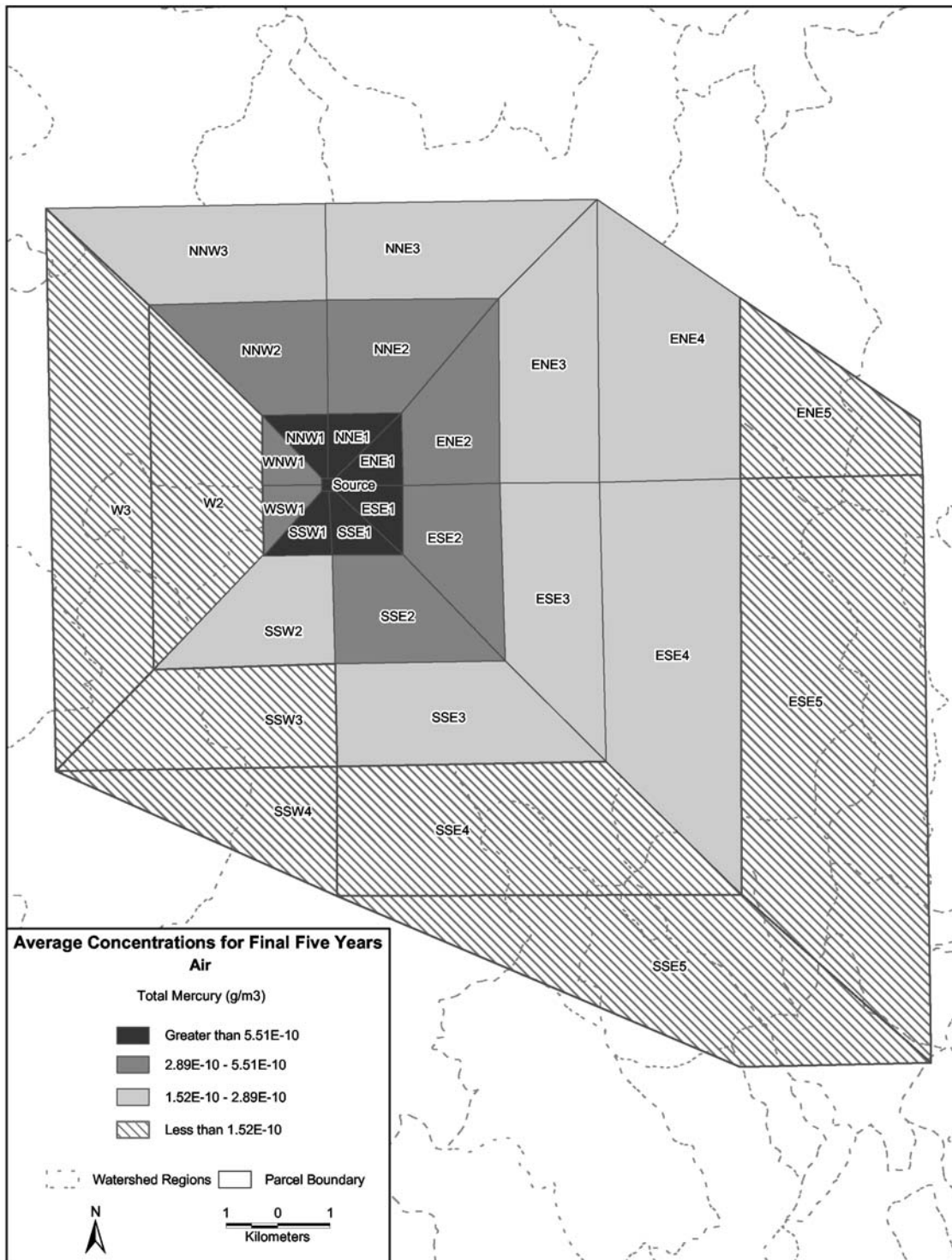
Seven abiotic compartment types were included in the mercury test case simulations: air, surface soil, root zone soil, vadose zone soil, surface water, sediment, and ground water. This section describes the spatial variations in total mercury concentrations for each of these compartment types, with the exception of vadose zone soil and ground water. These two compartment types accumulated very little mercury mass over the 30-year modeling period (see Section 3.1) and have little impact on the endpoints of main interest in this scenario, and thus they were not included in this analysis. In addition to total mercury concentrations in the abiotic compartments, this section also presents the spatial pattern of deposition of total mercury from air to surface soil to help illustrate how chemical mass moves from the air into the rest of the system across the modeled region.

Air

Exhibit 3-33 displays the variation across the air parcel layout of the total mercury concentrations (averaged over the final five years of the simulation) in the air compartments. In general, concentrations decrease as distance from the source increases, with the highest concentration occurring in the source compartment (compartment where mercury mass emitted from source is initially input). This pattern was expected based on the spread of chemical mass over a larger area with increasing distance from the source. Air concentrations east and north of the source tend to be slightly higher than concentrations west and south of the source. This pattern is consistent with the predominant combination of wind speed and wind direction.

¹⁵ This approach to averaging the air concentration data better represents the “ending” concentration for the 30-year modeling period because the air results are highly dependent on the meteorological data used and five years of meteorological input data was repeated throughout the period.

Exhibit 3-33
Spatial Variations in Total Mercury Concentrations: Air Compartments



To illustrate the size of the differences across air compartments, Exhibit 3-34 presents the total mercury concentrations ordered from highest to lowest. These concentrations are inclusive of both the particulate and gaseous fractions of mercury mass (with gaseous fraction predominant). Generally, the highest concentrations in compartments other than the source occur in compartments adjacent to the source (i.e., compartment names ending in "1"), although these concentrations are substantially lower than the concentration in the source compartment. The difference between the source compartment concentration and concentrations in adjacent compartments is approximately an order of magnitude. With additional distance from the source, concentration is further reduced more gradually, dropping by a little over an order of magnitude from the compartments adjacent to the source to the compartment with the lowest concentration (W3, roughly 3 km west of the source).

**Exhibit 3-34
Total Mercury Concentrations: Air Compartments**

Compartment	Average Concentration, Years 26-30 (g/m ³)
Source	2.1E-08
NNE1	1.0E-09
ENE1	1.0E-09
ESE1	1.0E-09
NNW1	8.7E-10
SSE1	8.0E-10
SSW1	7.3E-10
NNE2	4.3E-10
WSW1	4.1E-10
ESE2	3.9E-10
WNW1	3.8E-10
ENE2	3.7E-10
NNW2	3.0E-10
SSE3	3.0E-10
NNE3	2.7E-10

Compartment	Average Concentration, Years 26-30 (g/m ³)
SSW2	2.5E-10
ESE3	2.4E-10
ENE3	2.2E-10
NNW3	1.8E-10
SSE3	1.8E-10
ENE4	1.7E-10
ESE4	1.6E-10
SSW3	1.5E-10
W2	1.3E-10
SSW4	1.3E-10
ENE5	1.3E-10
SSE4	1.2E-10
ESE5	1.1E-10
SSE5	9.2E-11
W3	8.0E-11

Deposition from Air to Surface Soil

The spatial distribution of total mercury deposition flux¹⁶ to the surface soil (averaged over the final five years of the simulation) and the relative contributions from wet and dry deposition to the total deposition flux are displayed in Exhibit 3-35. Like the air concentrations, the deposition fluxes generally decrease with distance from the source. The highest deposition fluxes are found north and south of the source, whereas the highest air concentrations are north and east of the source. Close to the source, the total deposition is higher to the west than the east.

The relative contributions from wet and dry deposition follow a spatial pattern which is related to the meteorological data patterns. The wind speed and direction – which control the direction of mercury advection in air – during precipitation events can highly influence the locations receiving the most wet deposition. Exhibit 3-36 is a wind rose showing the wind speed and direction only during precipitation events. This exhibit shows that during rain events the wind blows predominantly toward the north and southwest and infrequently toward the east. Conversely, the overall predominant wind directions are to the north and southeast, and the wind blows infrequently to the west (see Exhibit 2-7). The difference between the overall wind patterns and the wind patterns when it is raining help to explain how the wet deposition percent of the total is highest to the west and the percent of deposition that is dry deposition is highest to the east. As described in Section 3.2, nearly 70 percent of the deposition of mercury to soil within the modeling region occurs during precipitation events. Therefore, the different spatial pattern in wet and dry deposition helps to explain why the total deposition spatial pattern is slightly different from the air concentration pattern (especially close to the source).

To illustrate the size of the deposition flux differences across surface soil compartments, Exhibit 3-37 shows the total mercury deposition fluxes ordered from highest to lowest. The deposition flux to the source compartment is more than an order of magnitude greater than the deposition flux to the adjacent compartments. The highest deposition fluxes to compartments other than the source occur in compartments adjacent to the source. With additional distance from the source, the deposition flux (like the air concentration) decreases more gradually, dropping a little over an order of magnitude from the compartments adjacent to the source to the compartment with the lowest deposition flux (ESE5, roughly 7 km southeast of the source).

¹⁶ The deposition flux of total mercury was estimated by summing the wet vapor, wet particle, dry vapor, and dry particle deposition fluxes to each surface soil compartment.

Exhibit 3-35
Spatial Variations in Total Mercury Deposition Flux: Surface Soil Compartments

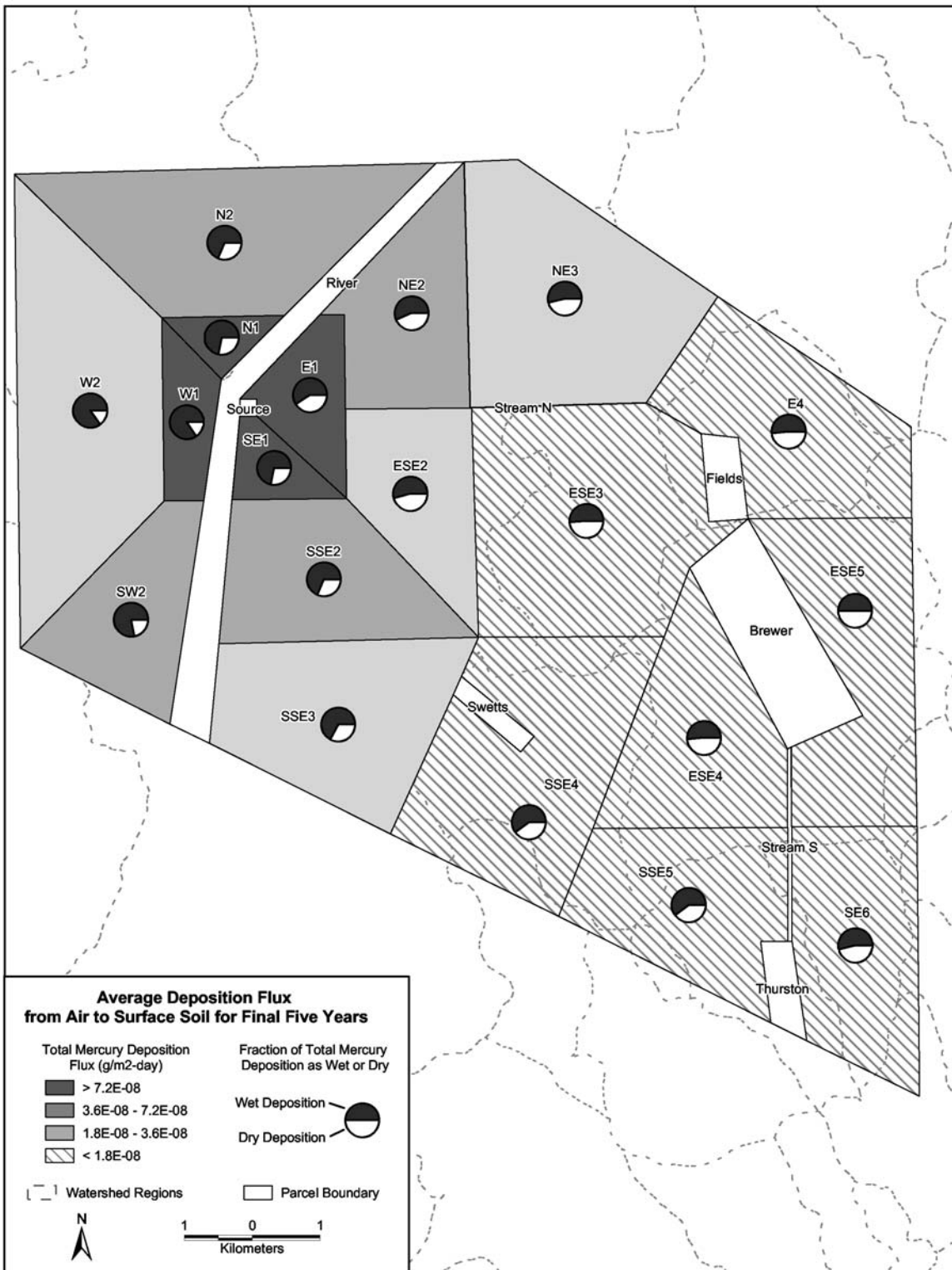


Exhibit 3-36 Wind Rose Representing TRIM.FaTE Five-year Input Data Set During Precipitation Events

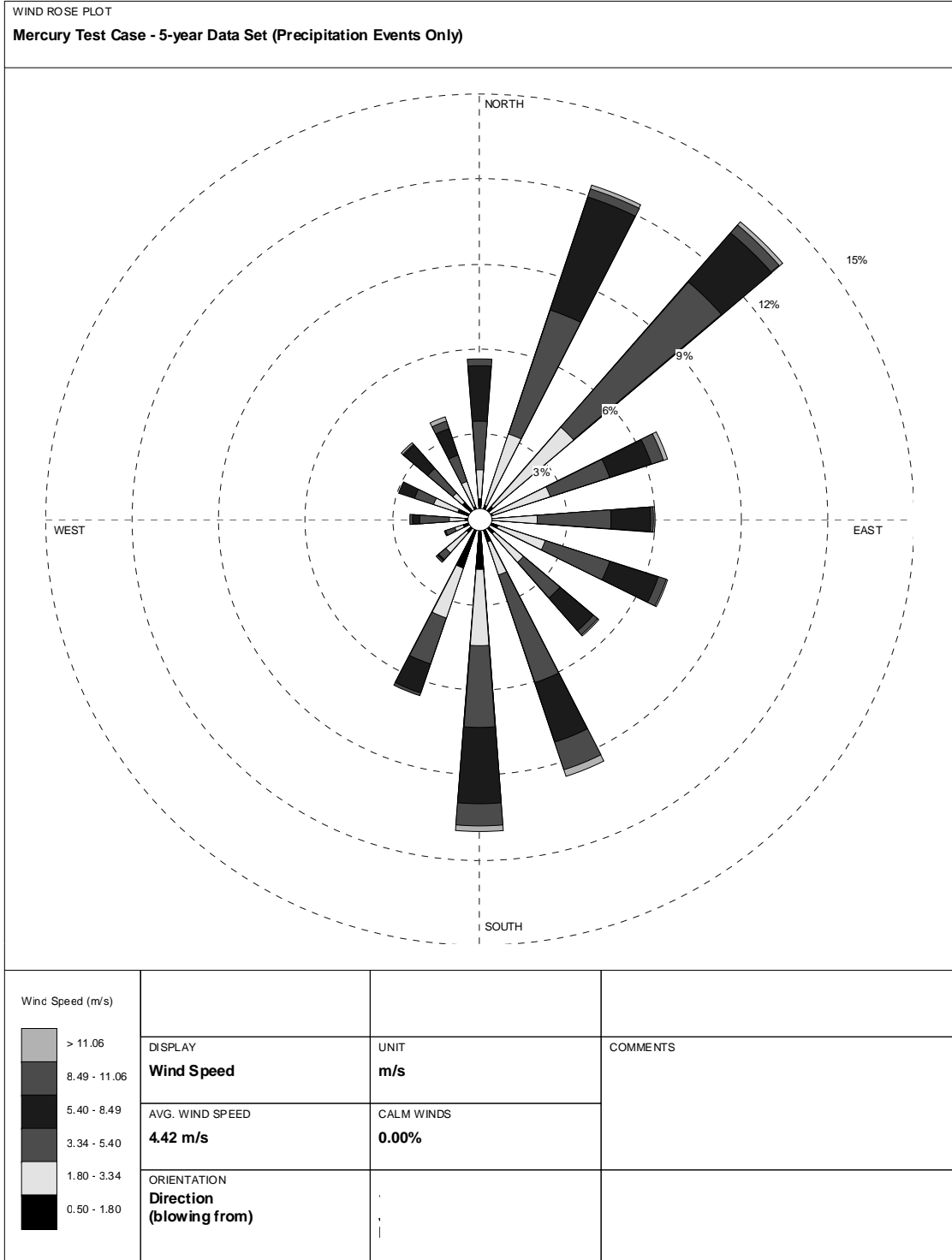


Exhibit 3-37
Total Mercury Deposition Flux: Surface Soil Compartments

Compartment	Annual Average Deposition Flux, Years 26-30 (g/m ² -day)
Source	3.9E-06
N1	1.5E-07
SE1	1.2E-07
W1	1.2E-07
E1	1.1E-07
N2	4.8E-08
SW2	4.1E-08
SSE2	3.8E-08
NE2	3.6E-08
ESE2	3.5E-08

Compartment	Annual Average Deposition Flux, Years 26-30 (g/m ² -day)
W2	3.4E-08
SSE3	2.0E-08
NE3	1.8E-08
ESE3	1.6E-08
SSE4	1.5E-08
ESE4	1.2E-08
SSE5	1.1E-08
E4	1.1E-08
SE6	8.7E-09
ESE5	8.6E-09

Surface Soil

The spatial variation of annual average concentrations of total mercury across the surface soil compartments for the 30th year of the simulation is shown in Exhibit 3-38. This pattern is slightly different from the pattern of concentrations for the air compartments. Like the air compartments, the highest estimated concentration in surface soil is found in the source compartment and concentrations decrease with distance from the source. However, higher surface soil concentrations are generally found to the north and west of the source, whereas the highest air concentrations generally occur to the north and east. Overall, the spatial pattern of surface soil concentrations is consistent with the pattern of deposition described above and its role in transporting chemical mass to the soil from the air compartments.

To illustrate the size of the differences across compartments, Exhibit 3-39 lists the total mercury concentrations ordered from highest to lowest. Because the boundaries of the air and surface soil compartments do not match exactly, it is difficult to compare the order of the compartments in Exhibits 3-34 and 3-39 on a one-to-one basis. However, the general patterns of concentrations can be compared. The overall range of surface soil concentrations across the modeling region (approximately three orders of magnitude) is similar to the range of air concentration results, although the range for soil is a little bigger (and the size of the soil modeling region is smaller than the air modeling region). In addition, like the air compartments, the highest concentrations in surface soil compartments other than the source generally occur with parcels adjacent to the source (i.e., compartment names ending in "1"), although the decrease in surface soil compartment concentration between the source and adjacent soil parcels

Exhibit 3-38
Spatial Variations in Total Mercury Concentrations: Surface Soil Compartments

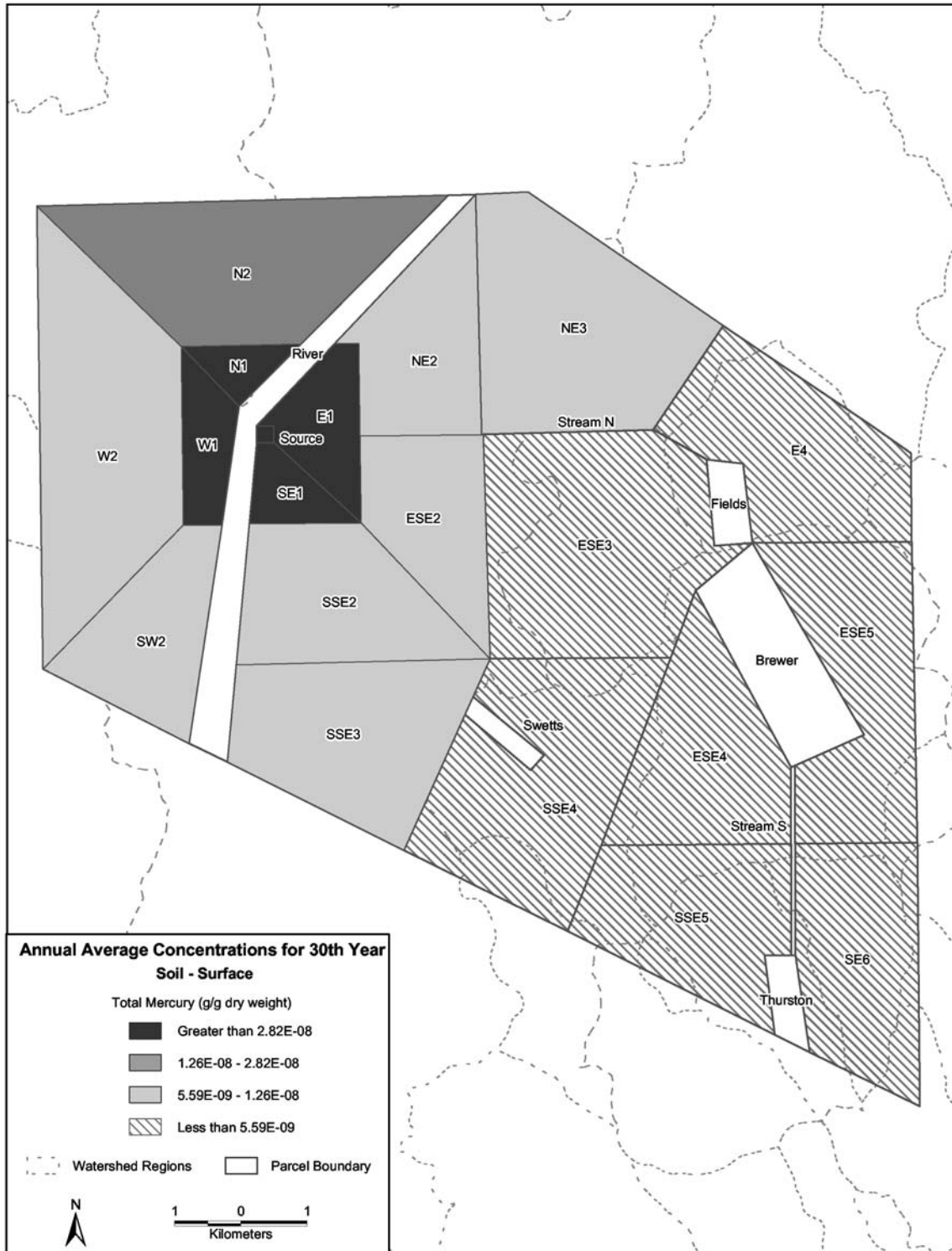


Exhibit 3-39
Total Mercury Concentrations: Surface Soil Compartments

Compartment	Annual Average Concentration, Year 30 (g/g dry weight)	Compartment	Annual Average Concentration, Year 30 (g/g dry weight)
Source	2.2E-06	W2	9.2E-09
N1	6.3E-08	SSE3	6.5E-09
W1	5.0E-08	NE3	5.9E-09
SE1	4.1E-08	ESE3	4.5E-09
E1	4.1E-08	ESE4	4.0E-09
N2	1.4E-08	SSE5	3.6E-09
ESE2	1.2E-08	ESE5	3.1E-09
NE2	1.2E-08	SSE4	3.1E-09
SSE2	1.2E-08	SE6	3.1E-09
SW2	1.1E-08	E4	2.5E-09

is greater (by approximately 1.7 fold) than for air. Additionally, the further decrease in concentration over the remaining distance to the outermost parcels is somewhat greater for surface soil compared to air (e.g., highest-to-lowest compartment concentration ratio, excluding the source compartment, is 25 for surface soil and 13 for air), even though the surface soil parcel layout is smaller than the air layout. Thus, for the test case scenario, the spatial pattern of total mercury concentration in surface soil is generally consistent with the pattern for air and for atmospheric deposition, but surface soil concentrations decrease somewhat more rapidly with distance from the source.

Root Zone Soil

Exhibit 3-40 presents the spatial variation across the surface parcel layout of annual average concentrations of total mercury in the root zone soil compartments for the 30th year of the simulation. The patterns of root zone soil concentrations closely resemble the concentration patterns for surface soil. Given that the great majority of the chemical mass transported into the root zone soil compartments comes directly from the surface soil compartments, the general patterns in the two compartment types are expected to be similar.

To illustrate the size of the differences across root zone soil compartments, Exhibit 3-41 presents the total mercury concentrations ordered from highest to lowest. The ranking of compartments based on concentration for root zone soil compartments is similar to the ranking for surface soil compartments (Exhibit 3-39). The primary difference is that the surface soil concentration in SE1 is higher than in E1, and the root zone soil concentration in E1 is higher than in SE1. For both compartment types, however, the difference between E1 and SE1 is small.

Exhibit 3-40
Spatial Variations in Total Mercury Concentrations: Root Zone Soil Compartments

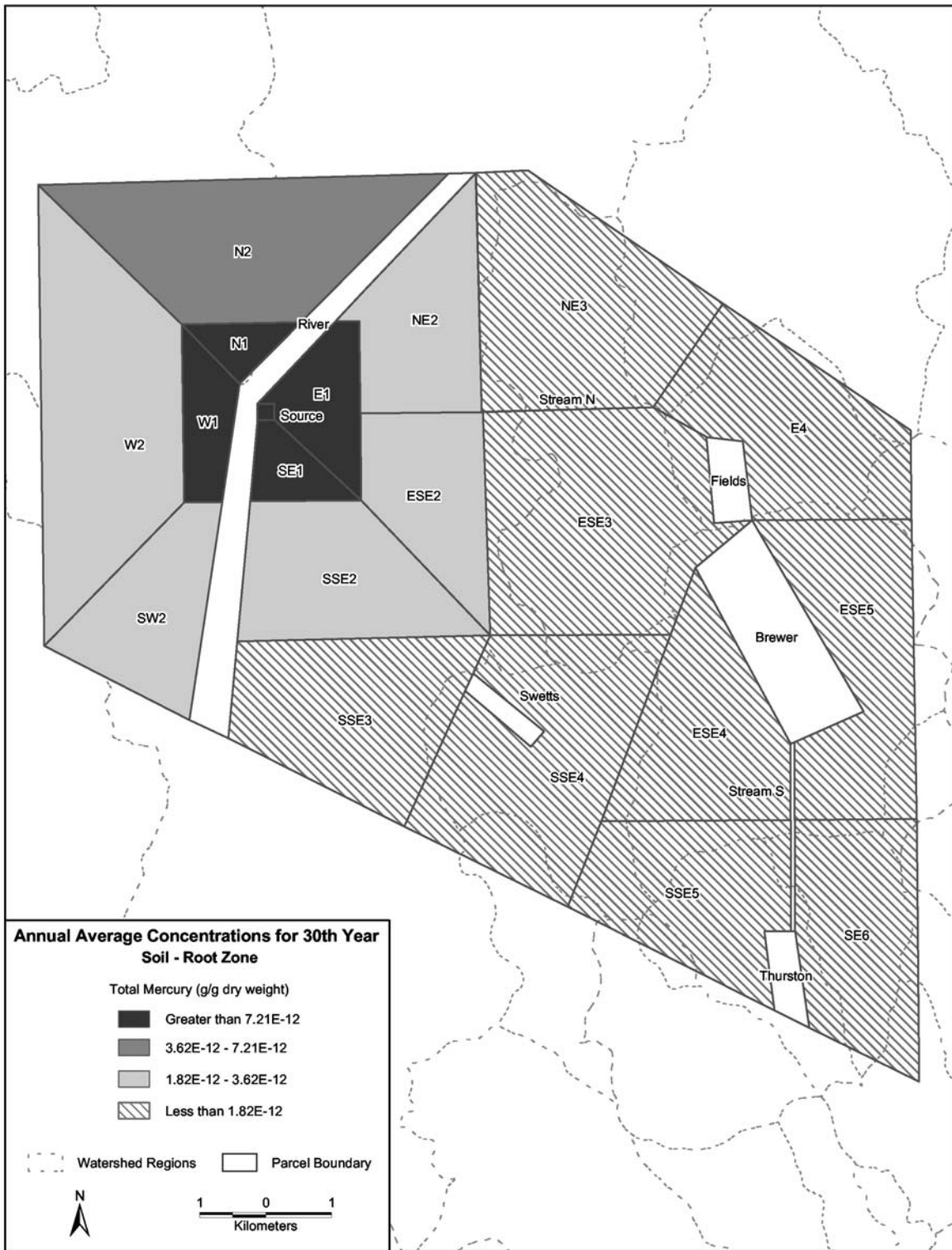


Exhibit 3-41
Total Mercury Concentrations: Root Zone Soil Compartments

Compartment	Annual Average Concentration, Year 30 (g/g dry weight)
Source	4.7E-10
N1	1.4E-11
W1	1.1E-11
E1	1.1E-11
SE1	1.0E-11
N2	3.9E-12
ESE2	3.5E-12
NE2	3.4E-12
SSE2	3.1E-12
SW2	3.1E-12

Compartment	Annual Average Concentration, Year 30 (g/g dry weight)
W2	2.4E-12
SSE3	1.8E-12
NE3	1.8E-12
ESE3	1.5E-12
ESE4	1.2E-12
SSE4	1.1E-12
SSE5	1.1E-12
ESE5	9.4E-13
E4	9.1E-13
SE6	9.1E-13

The only other difference between the ranking of surface soil and root zone soil concentrations is that the SSE4 and E4 parcels have higher rank orders and the SSE5, ESE5, and SE6 parcels have lower rank orders in root zone soil than in surface soil. These slight differences may be explained in part by the spatial differences in the deposition flux of elemental and divalent mercury from air to soil (refer to Section 3.3 for a more detailed description of speciation in soil) or by differences in the assigned plant types at these locations (SSE4 and E4 have coniferous plants and SSE5, ESE5, and SE6 have deciduous plants).

The overall range of root zone soil concentration results is also similar to the ranges of surface soil and air concentration results (approximately three orders of magnitude, with the range for root zone soil smaller than for surface soil and larger than for air). The difference in root zone soil compartment concentrations between the source parcel and adjacent parcels is slightly less than that seen for surface soil, as is the difference in compartment concentrations between adjacent parcels and the outermost parcels. This may be due in part to the fact that there are fewer loss processes for root zone soil than for surface soil; specifically, erosion and runoff are modeled for surface soil but not root zone soil. Overall, for the test case scenario, the spatial pattern of total mercury concentration in root zone soil is very similar to the pattern for surface soil, but concentration in root zone soil decreases more slowly with distance from the source.

Surface Water

The spatial variation of annual average concentrations of total mercury across the surface water compartments for the 30th year of the simulation is shown in Exhibit 3-42.¹⁷ There are a number of different factors that may contribute to the concentration differences between the water bodies, including:

- Air and surface soil concentrations in the parcels adjacent to each water body;
- Surface area and depth of each water body;
- Size of the watershed associated with each water body;
- Incoming and outgoing flow characteristics of the water bodies; and
- Proximity of each water body to the emission source.

The highest surface water concentration is found in the Swetts Pond compartment, which was expected given that it is the closest water body to the source, and, along with Thurston Pond, has the smallest depth (both water bodies are three meters deep).

Sediment

The spatial variation of annual average concentrations of total mercury across the sediment compartments for the 30th year of the simulation is also shown in Exhibit 3-42. The spatial patterns of sediment concentrations are nearly identical to the patterns for the surface water compartment, with the highest concentration in the Swetts Pond compartment. Given that the sediment compartments receive chemical mass solely from the surface water compartments, the similarities between the patterns in surface water and sediment are not surprising.

3.4.2 Biotic Compartments

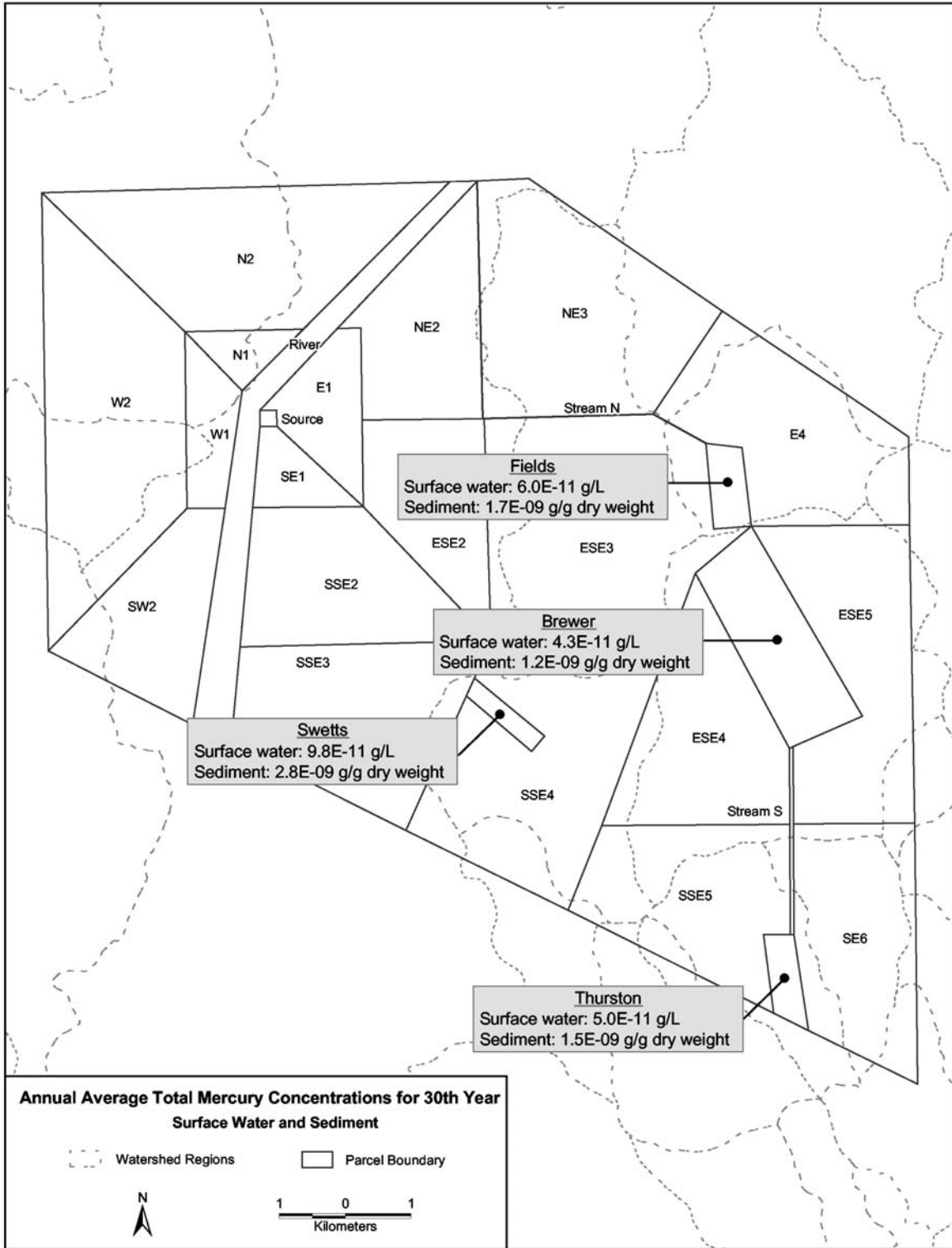
To simplify the presentation of results for the biotic compartment types, they are grouped into the following five categories:

- Terrestrial plants;
- Terrestrial animals;
- Semi-aquatic animals;
- Water-column fish; and
- Benthic animals.

For the terrestrial plant, terrestrial animal, and semi-aquatic animal categories, the discussion focuses on one or two compartment types as examples of the overall spatial variations for the category. To facilitate interpretation of patterns for the terrestrial and semi-aquatic animals, compartment types with fewer numbers of different dietary compartment types are presented. For the water-column fish and benthic animal categories, each compartment type is presented.

¹⁷ Results not shown for the river compartment. This water body, which is an estuary, was modeled as a river in the mercury test case to assist in general model evaluation, but results are not considered representative of the actual conditions.

Exhibit 3-42
Spatial Variations in Total Mercury Concentrations: Surface Water and Sediment
Compartments



Terrestrial Plants

Spatial variation in annual average total mercury concentrations for the leaf compartments in the 30th year of the simulation is presented in Exhibit 3-43.¹⁸ Note that no plants were included in the source volume element, and thus the source compartment is not shaded. In interpreting these results, it is important to consider differences in how litter fall and dormancy were simulated for the different vegetation types in this scenario. For deciduous forest and grasses/herbs vegetation types, litter fall is simulated through the essentially complete transfer of chemical mass from the leaf to the surface soil over one month during the fall. As the chemical mass is transferred from the leaves to the soil, chemical concentrations in the leaf compartments for these vegetation types decrease to zero. In simulation of dormancy, these leaf compartments do not begin accumulating chemical mass again until the spring. For coniferous forest vegetation types, however, litter fall is simulated via a low, constant rate of transfer of chemical mass from the leaf to the surface soil, and no period of dormancy is simulated.

The patterns of spatial variation for the leaf compartments appear to be driven both by proximity to the source and vegetation type. In general, the highest concentrations occur with leaf compartments in parcels close to the source assigned with coniferous vegetation, while parcels assigned deciduous forest and grasses/herbs vegetation, regardless of location, generally have the lowest concentrations. Given the lack of complete litter fall each year and the lack of a period of dormancy for the coniferous forest compartments, it is not surprising that they accumulate more chemical mass than other vegetation types. Additionally, the generally lower concentrations in the deciduous forest leaf compartments are at least partially attributable to the fact that deciduous forest was the vegetation type assigned to the parcels farthest from the source.

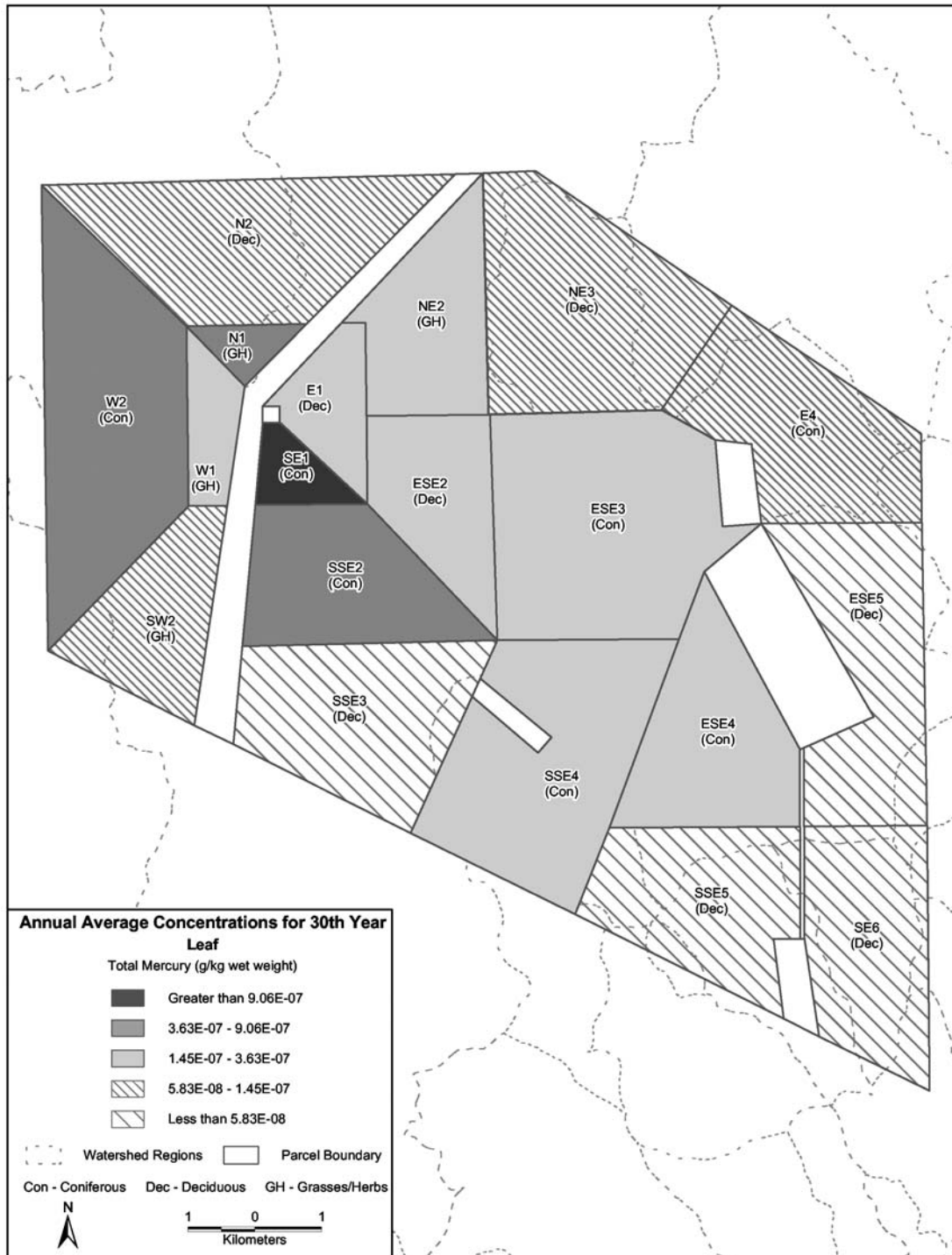
Terrestrial Animals

Spatial variations in total mercury concentration across the surface parcel layout are presented for the white-tailed deer and leaf compartments in Exhibit 3-44. The leaf compartment concentrations are included in this exhibit to help illustrate the relationship between the white-tailed deer and its diet in this scenario (i.e., 100 percent leaves and particles on leaves¹⁹). In general, concentrations of total mercury in the white-tailed deer are closely related to the leaf compartment concentrations. The highest concentrations in white-tailed deer compartments are found with parcels that are assigned coniferous forest vegetation, and the lowest concentrations are found with parcels that are assigned deciduous forest and grasses/herbs vegetation. This pattern is likely due in part to the way the diets of herbivorous animals are modeled in this application of TRIM.FaTE. For deciduous and grasses/herbs vegetation types, there is no

¹⁸ For leaf compartments representing deciduous forest and grasses/herbs vegetation types, annual average concentrations presented in this section were calculated based on modeling results for the entire year (i.e., including zeros for time periods when leaves are absent).

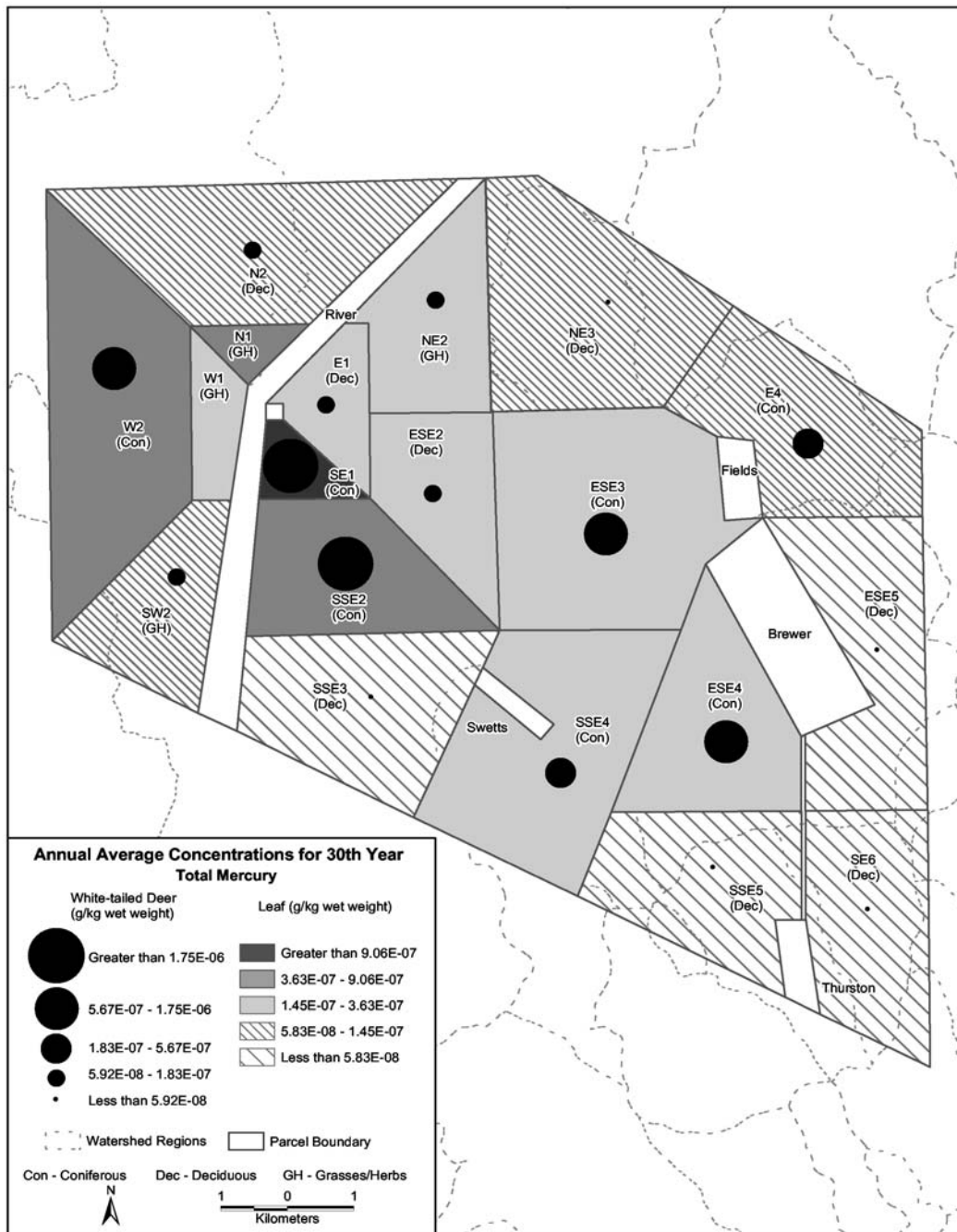
¹⁹ In this scenario, the diets of white-tailed deer were comprised entirely of leaves and particles on leaves, regardless of the type of vegetation present in each surface parcel. As a result, white-tailed deer in parcels assigned coniferous forest vegetation were assumed to consume coniferous leaves, which may not be entirely representative of their actual diets.

Exhibit 3-43
Spatial Variations in Total Mercury Concentrations: Leaf Compartments^a



^aFor all leaf compartments, annual average concentrations were calculated based on modeling results for the entire year (i.e., including, for deciduous and grasses/herbs vegetation types, zeros for time periods when leaves are absent).

Exhibit 3-44
Spatial Variations in Total Mercury Concentrations: White-tailed Deer and Leaf
Compartments^{a, b}



^a For all leaf compartments, annual average concentrations were calculated based on modeling results for the entire year (i.e., including, for deciduous and grasses/herbs vegetation types, zeros for time periods when leaves are absent).

^b White-tailed deer not modeled in volume elements N1 or W1 because these areas are considered too developed.

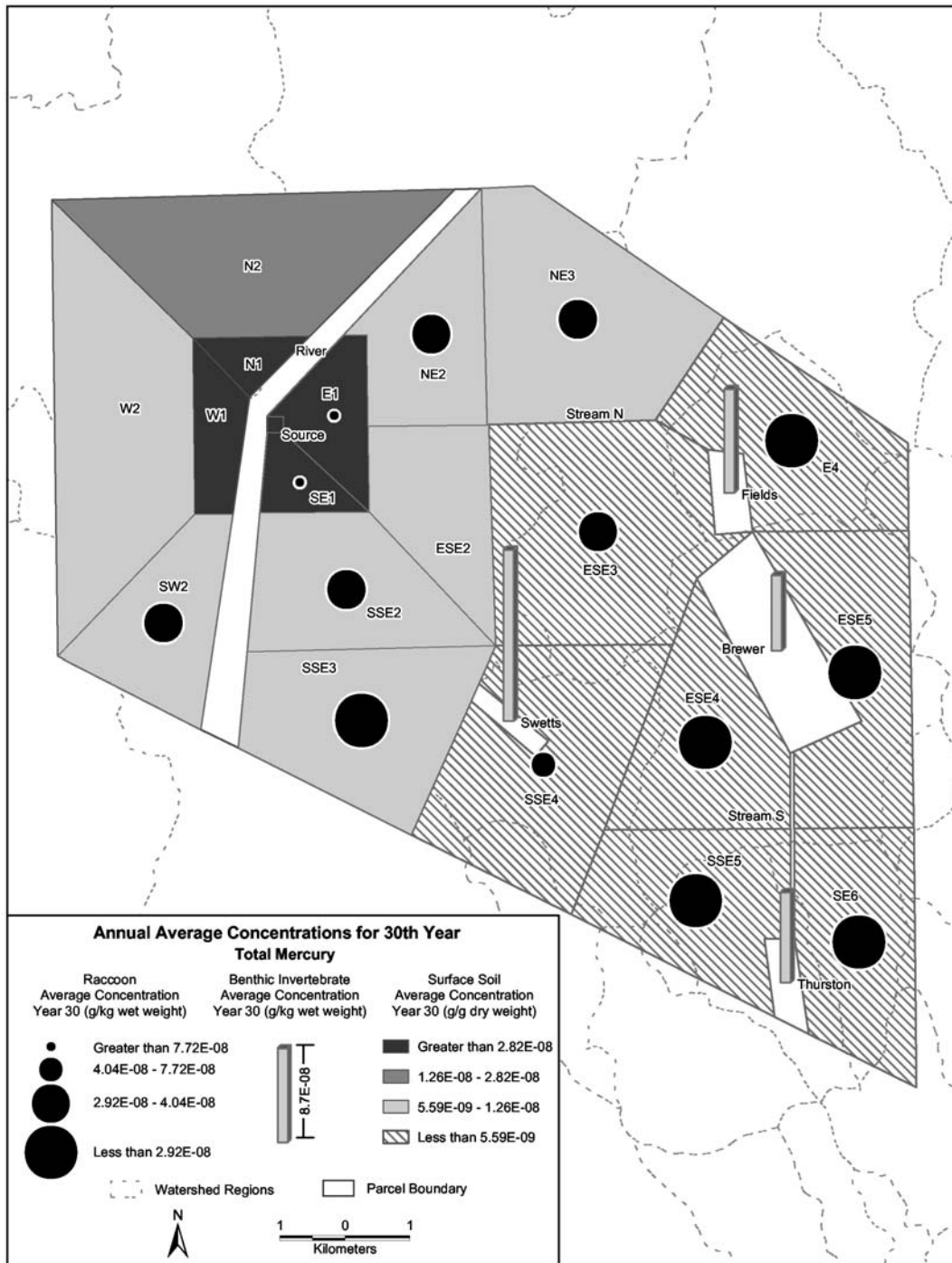
chemical mass in the leaf and particle-on-leaf compartments during the non-growing season because the leaves are assumed to have fallen from the plants during the once-a-year litter fall event. Conversely, the leaf and particle-on-leaf compartments for parcels assigned coniferous vegetation remain on the plants throughout the simulation and therefore contain chemical mass at all times. Because the composition of the diets of herbivorous animals is assumed to be constant for the entire simulation, the white-tailed deer in parcels assigned deciduous and grasses/herbs vegetation do not consume chemical mass during the non-growing season, resulting in lower concentrations than white-tailed deer in a comparable locations assigned coniferous vegetation. In future applications, the diets of herbivorous animals assigned to parcels with vegetation that undergo a single litter fall event per year (e.g., deciduous and grasses/herbs vegetation) may be refined to better reflect the change in the diets of these animals during the non-growing season.

Semi-aquatic Animals

Exhibit 3-45 presents the variation across the surface parcel layout in total mercury concentration for the raccoon, surface soil, and benthic invertebrate compartments. Benthic invertebrate concentrations are included because benthic invertebrates comprise nearly 70 percent of the raccoon's diet in this scenario. Surface soil concentrations are included because the concentrations in the earthworm, the second largest component of the raccoon's diet (21 percent), show correlation with soil concentrations (see Appendix Chart B-2). The spatial pattern of total mercury concentrations in raccoons shows a correlation with the patterns for surface soil and benthic invertebrates. In parcels closer to the source, there appears to be a stronger correlation with soil concentrations, consistent with the modeling result that raccoons in these parcels obtain the majority of their chemical mass from soil or biota associated with the soil. For example, the highest raccoon concentrations occur in the parcels E1 and SE1, which are both adjacent to the source parcel and have the highest soil concentrations among the parcels containing raccoons. Raccoons in these parcels ingest benthic invertebrates from the river, which has the lowest benthic invertebrate concentrations among the water bodies. Conversely, there appears to be a stronger correlation with benthic invertebrate concentrations in parcels further from the source, consistent with the modeling result that raccoons in these parcels obtain the majority of their chemical mass from benthic invertebrates. For example, the third highest raccoon concentration occurs in parcel SSE4, which has some of the lowest soil concentrations in the modeling region, and is adjacent to Swetts Pond (where SSE4 raccoons obtain the aquatic portion of their diet), which has the highest benthic invertebrate concentrations.

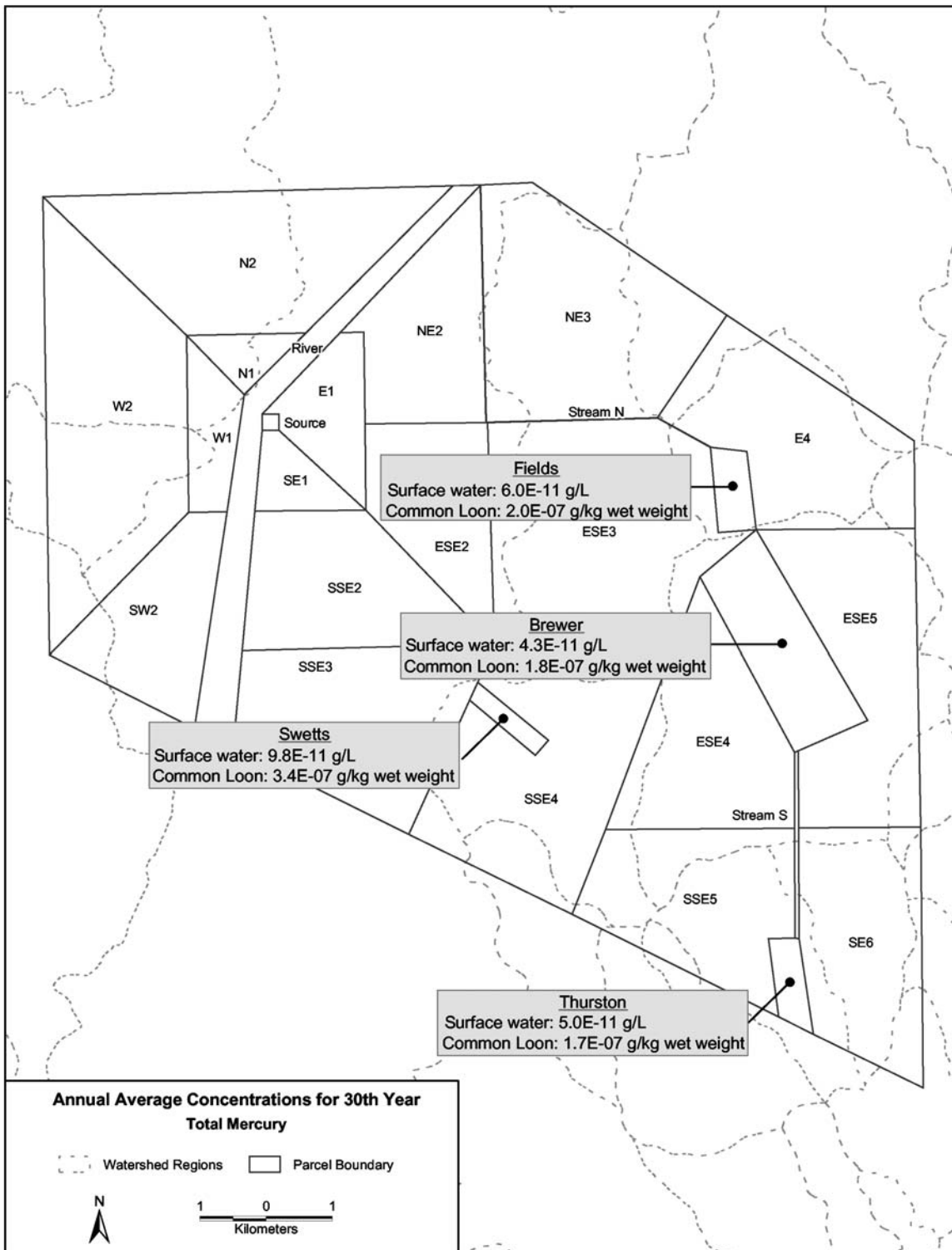
Exhibit 3-46 presents the variation across the surface parcel layout in total mercury concentration for the common loon and surface water compartments. The surface water compartment concentrations are included in this figure to help illustrate their relationship with the common loon compartments. In general, the common loon concentrations appear to be closely related to the surface water concentrations. When ordered from highest total mercury concentrations to lowest, the ranking of compartments for common loon compartments is similar to the ranking for surface water compartments. The only difference in the rankings is that the common loon concentrations are slightly higher in Brewer Lake than Thurston Pond, whereas the surface water concentrations are slightly higher in Thurston Pond than Brewer Lake. These results are reasonable considering that the loon's diet consists entirely of water-column and benthic omnivores (each is 50 percent), water-column omnivores typically have higher total

Exhibit 3-45
Spatial Variations in Total Mercury Concentrations: Raccoon, Surface Soil, and
Benthic Invertebrate Compartments^a



^a Raccoons not included in volume elements N1 or W1 because these areas are considered too developed, or in volume elements W2, ESE2, or NE3 because these areas do not border any surface water bodies containing fish.

Exhibit 3-46
Spatial Variations in Total Mercury Concentrations: Common Loon and Surface Water Compartments



mercury concentrations than benthic omnivores in this scenario, and water-column omnivore concentrations are higher in Brewer Lake than Thurston Pond.

Water-column Fish

The spatial variation in *methyl* mercury concentrations across all three water-column fish compartment types, as well as the variation of total mercury in surface water compartments, is presented in Exhibit 3-47. Because methyl mercury is preferentially accumulated up the water-column fish food chain, the concentrations in the fish compartments are presented as methyl mercury instead of total mercury. This figure uses a slightly different format from the previous figures in that it presents the results for all three fish compartments for each surface water volume element as bar charts (see Appendix Table B-10 for actual values for Swetts Pond and Brewer Lake). These bars show the concentrations in each fish compartment relative to the other compartments of the same type in different volume elements, as well as to the other fish compartment types in the same volume element. The surface water compartment concentrations are included in this exhibit to illustrate the relationships between surface water and water-column fish concentrations.

Overall, the fish concentrations are closely related to the surface water concentrations. When each water body is ranked relative to water-column fish and surface water concentrations, the resulting order is similar. The highest and second highest surface water concentrations of total mercury occur in the same water bodies (Swetts Pond and Fields Pond, respectively) as the highest fish concentrations of methyl mercury. The only difference between the rank orders is that the water-column fish concentrations of methyl mercury are higher in Brewer Lake than Thurston Pond, whereas the surface water concentrations of total mercury are higher in Thurston Pond than Brewer Lake. This difference appears to be related to differences in mercury speciation between the water bodies; specifically, total mercury in Brewer Lake is comprised of a slightly higher percentage of methyl mercury than total mercury in Thurston Pond. Because water-column fish accumulate methyl mercury more rapidly than divalent mercury, this difference in speciation is magnified up the food chain.

The accumulation of methyl mercury with increasing trophic level can be illustrated by the use of food chain multipliers. These ratios show the increase in methyl mercury concentrations across each step of the food chain and are calculated by dividing the concentration in a higher trophic-level organism by the concentration in the next lower trophic-level organism. Exhibit 3-48 presents methyl mercury food chain multiplier values for the water-column fish in the four water bodies. These values were calculated based on annual average concentration for year 30 for the water-column carnivore to water-column omnivore relationship (WCC:WCO) and for the water-column omnivore to water-column herbivore relationship (WCO:WCH). This exhibit illustrates a similar pattern of methyl mercury bioaccumulation across fish trophic levels for the different water bodies. The spatial consistency in these ratios is related to similarities in the characterization of the fish compartments among the various water bodies, as well as to similarities in the predation on these compartments by semi-aquatic animals (e.g., the amount of water-column omnivores consumed by raccoons from a particular water body is relative to the total biomass of water-column omnivores in that water body).

Exhibit 3-47
Spatial Variations in Mercury Concentrations: Water-column Fish and Surface Water Compartments

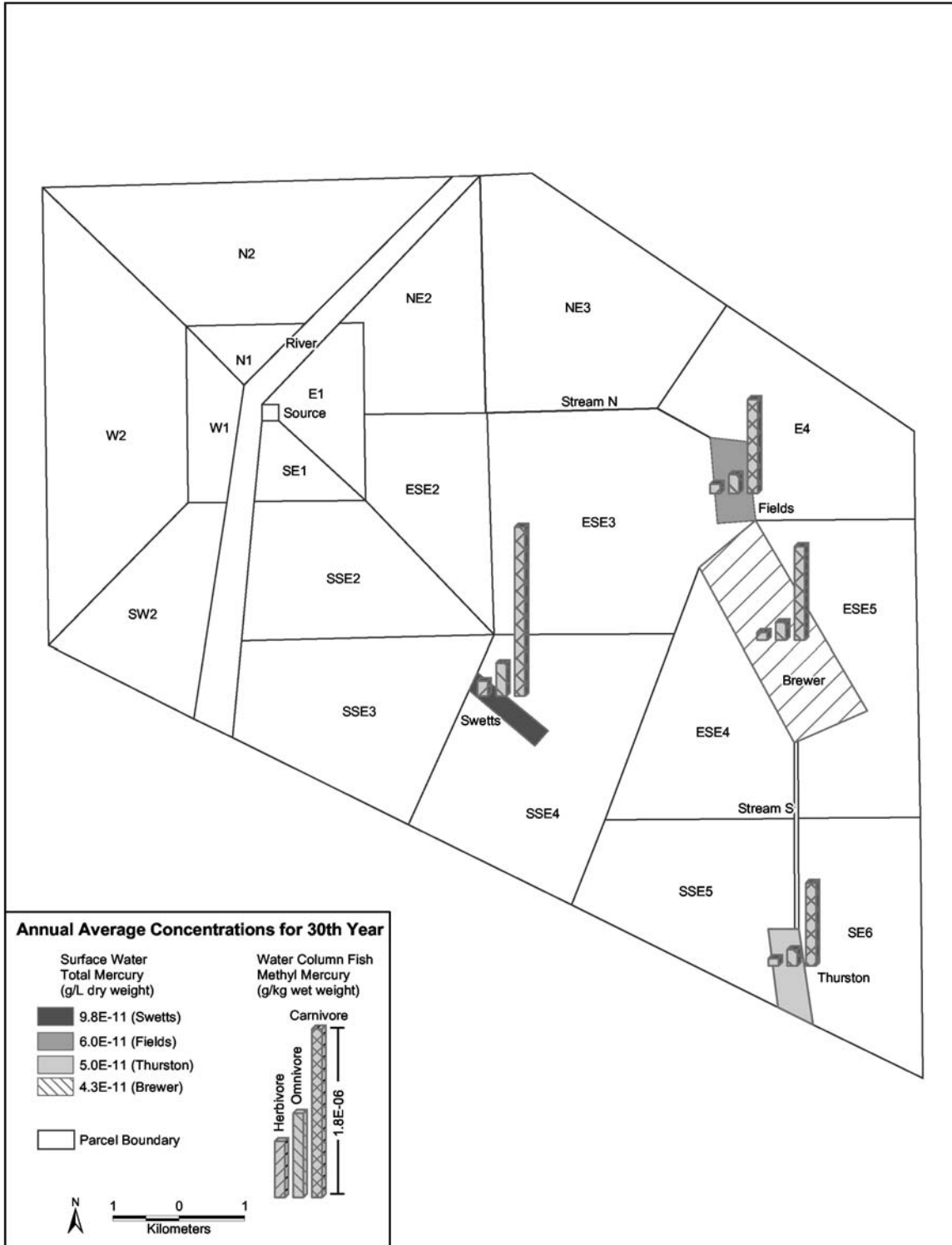


Exhibit 3-48
Water-column Food Chain Multipliers for Methyl Mercury
(Based on Average Concentrations for Year 30)

Water Body	WCC:WCO	WCO:WCH
Brewer Lake	5.4	2.3
Fields Pond	5.1	2.1
Swetts Pond	5.1	2.2
Thurston Pond	5.1	2.2
Average	5.2	2.2
Std. Deviation	0.1	0.1

Benthic Animals

The spatial variation in *methyl* mercury concentrations across all three benthic animal compartment types, as well as the spatial variation in total mercury concentration across sediment compartments, is presented in Exhibit 3-49. Because methyl mercury is preferentially accumulated up the benthic animal food chain, the concentrations in the benthic animal compartments are presented as methyl mercury instead of total mercury. As with the presentation for water-column fish in the previous section, a combination of bar charts and shading are employed to present the concentration results for the benthic animal compartments and the sediment compartment.

Consistent with the modeling approach used in which the sediment compartment is the source of chemical mass to the benthic food chain compartments, the benthic animal concentrations are closely related to the sediment concentrations. When each water body is ranked relative to benthic animal and sediment concentrations, the resulting order is identical. That is, the water body (Swetts Pond) with the highest sediment total mercury concentration also has the highest benthic carnivore, omnivore, and invertebrate concentrations of methyl mercury, and so forth.

Food chain multiplier values were calculated for the benthic food chain, as they were for the water-column food chain. Exhibit 3-50 presents food chain multipliers for the benthic carnivore to benthic omnivore relationship (BC:BO) and for the benthic omnivore to benthic invertebrate relationship (BO:BI). As with the water-column food chain multipliers, this exhibit illustrates a similar pattern of methyl mercury bioaccumulation across fish trophic levels for the different water bodies. As stated in the previous section, the spatial consistency in these ratios is related to similarities in the characterization of the fish compartments among the various water bodies, as well as to similarities in the predation on these compartments by semi-aquatic animals (e.g., the amount of benthic omnivores consumed by raccoons from a particular water body is relative to the total biomass of benthic omnivores in that water body).

Exhibit 3-49

Spatial Variations in Mercury Concentrations: Benthic Animal and Sediment Concentrations

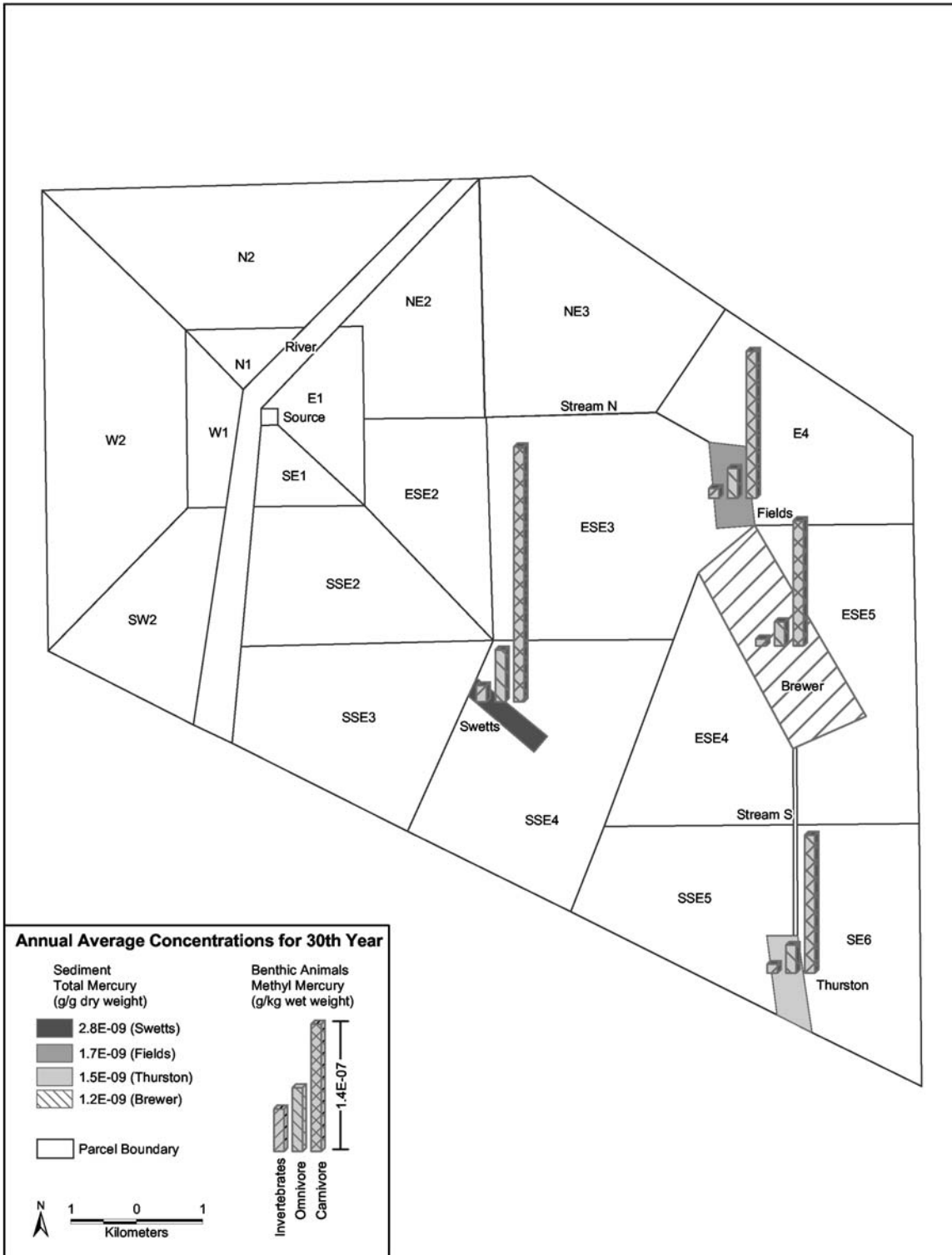


Exhibit 3-50
Benthic Food Chain Multipliers for Methyl Mercury
(Based on Average Concentrations for Year 30)

Water Body	BC:BO	BO:BI
Brewer Lake	5.2	3.3
Fields Pond	4.9	3.0
Swetts Pond	4.9	3.2
Thurston Pond	5.0	3.2
Average	5.0	3.2
Std. Deviation	0.1	0.1

3.5 Comparison of Emission Cases

This section compares the dynamic modeling results for the different emission cases:

- Case A – only Hg^{2+} emitted (17.663 g/day), with *no* initial media or biota concentrations of mercury and *no* boundary contributions;
- Case B – both Hg^{2+} and Hg^0 emitted (17.663 and 335.6 g/day, respectively), with *no* initial media or biota concentrations of mercury and *no* boundary contributions (results for this case are the focus of the other sections of Chapter 3 and of Chapters 4 and 5); and
- Case C – both Hg^{2+} and Hg^0 emitted (17.663 and 335.6 g/day, respectively), with initial media and biota concentrations of mercury and boundary contributions of mercury in air.

First, case A is compared with case B to examine the incremental effect that including elemental mercury air emissions has on multimedia concentrations of various mercury species. Then, case B is compared with case C to examine the impact of including contributions of “background” (i.e., not from the test case plant emissions) mercury on the modeled multimedia concentrations. Most comparisons in this section are based on annual average concentrations for individual compartments for year 30, although some time series charts are presented as well.

3.5.1 Emission Case A vs. Emission Case B

Case A was included in the test case mainly to serve as the basis for comparisons of TRIM.FaTE results with 3MRA results (see Chapter 6). However, case A also was compared with case B – which is the primary case analyzed in this report – to assess whether elemental mercury emitted to air along with divalent mercury produces substantially different multimedia modeling results local to the source (i.e., within 10 miles) than divalent mercury emitted alone. Because divalent mercury deposits from air to soil and surface water at a much faster rate than elemental mercury (i.e., over a given distance, a larger fraction of divalent mercury in air will deposit than elemental mercury in air), and because both cases have the exact same emissions of divalent mercury, major differences between the cases were not expected for most non-air compartments. (See Section 3.2 for comparison of modeled deposition fluxes for divalent and elemental mercury.)

Air Compartments

Of all the TRIM.FaTE compartment types modeled, air has by far the largest differences in total mercury concentrations between case A and case B. Divalent mercury concentrations in air for case A and case B are very similar, which makes sense given that the same emission rate was used for divalent mercury and no rapid transformations in air were modeled (oxidation of elemental mercury to divalent mercury was modeled at a relatively slow rate, which has limited effect over the distances modeled). Thus, the differences in case B total mercury concentrations are a direct result of the additional elemental mercury emitted from the source. Note that the ratio of total mercury emissions mass for case B to case A is 20.

Case B air concentrations of total mercury are higher than case A concentrations by a range of 21 times (for the source compartment) to 35 times (for air compartments ESE4 and ESE5). The ratio is lowest at the source compartment and increases with distance from the source, with a small dropoff at the edges of the modeling region. It is suspected that this spatial pattern results because divalent mercury deposits from air to land and surface water much more rapidly than elemental mercury, which tends to stay in the air over the modeling distances used in this test case. Thus, divalent mercury concentrations in air tend to decrease faster with distance from the source than elemental mercury, which results in case B:case A air concentration ratios for total mercury getting higher as the distance from the source increases (i.e., total mercury concentration in air drops off more slowly with distance in case B (mostly elemental) than in case A (mostly divalent)). The reason that the ratio decreases in the edge air compartments is that these compartments are not fully underlain by surface compartments, which are the main source of elemental mercury in air for case A – thus, this result is an artifact of the compartment layout.

Case B:case A air concentration ratios for divalent mercury are very close to 1.0 (always greater) throughout the modeling region, though they do increase very minimally with distance from the source (highest ratio is 1.01 for air compartment ESE5), possibly as a result of the slow oxidation of the elemental mercury emitted to air in case B to divalent mercury.

Compartments Other than Air

Key differences between case A and case B for other compartment types are summarized in Exhibit 3-51. Out of 33 compartment types modeled in this test case, only seven (other than air) have any appreciable differences for total mercury, and only three for divalent mercury. For all compartment types other than air and those shown in Exhibit 3-51, there is less than 10 percent difference between case A and case B in year 30 average concentrations for total mercury and for divalent mercury *in any compartment modeled* (i.e., at any location). Thus, for those compartment types, the emission of elemental mercury to air has minimal impact (relative to concurrent emission of divalent mercury at five percent of the total) on long-term modeled concentrations of either divalent or total mercury at locations near the source.

Exhibit 3-52 shows the total mercury concentrations for one of the differing compartment types, root zone soil, at one location over the full 30-year modeling period, illustrating the time series results for the two cases. The differences in both magnitude and time pattern of the results are attributable to the effects of the emitted elemental mercury in case B, which is considerably more mobile in soils than divalent mercury. (Other total mercury time series charts are not presented here for case A, given the similarity of most of them to the charts presented for case B (see Section 3.2 and Appendix B.2). Some additional time series charts for case A are shown in Chapter 6.)

The explanation of the case A versus case B results appears to be reasonably straightforward for the various soil layers, which are the compartment types (other than air) where case B has the greatest relative impact. The spatial patterns of the case B to case A relationship for all soil layers follow the pattern for air (i.e., higher ratios farther from the source), and for a related reason to that explained above for air. Similar to the air concentrations,

Exhibit 3-51
Case B:Case A Ratios for Compartment Types Other than Air^a

Compartment Type	Total Hg Range of Case B: Case A Ratios ^b	Hg ²⁺ Range of Case B: Case A Ratios ^b	Comments
Root zone soil	1.3 - 2.2	All ~ 1.0	Source always lowest, ratio increases with distance (follows air pattern)
Vadose zone soil	2.1 - 5.9	All ~ 1.0	Source always lowest, ratio increases with distance (follows air pattern)
Ground water	2.5 - 8.0	2.8 - 9.5	Source always lowest, ratio increases with distance (follows air pattern)
Surface water	1.0 - 2.1	All ~ 1.0	Only river >1.0 for total Hg
Macrophyte	1.0 - 3.6	1.0 - 3.8	Only river >1.0 for total Hg and Hg ²⁺ ; total Hg ratio tracks Hg ²⁺ closely (total Hg ~90% Hg ²⁺)
Earthworm	1.4 - 2.2	All ~ 1.0	Earthworm matches root zone soil exactly (except source compartment, with 1.3 ratio for root zone soil, was not modeled for earthworm)
Tree swallow	1.0 - 1.9	1.0 - 1.8	Total Hg ratio tracks Hg ²⁺ closely (total Hg ~75% Hg ²⁺)

^a Only compartment types with at least a 10 percent difference in at least one compartment are shown.

^b All ratios based on annual average concentrations for individual compartments for year 30.

the air deposition of elemental mercury drops off more slowly with distance than the air deposition of divalent mercury. Thus, the contribution of airborne elemental mercury to soil in case B drops off more slowly with distance than the contribution of airborne divalent mercury to soil in both cases, and for the deeper soil layers elemental mercury is an important contributor to total mercury. As a result, the case B:case A total (and elemental) mercury ratios are higher for compartments more distant from the source.

As shown in Exhibit 3-51, the impact of the elemental mercury emitted in case B on total mercury concentrations gets larger as the soil layers get deeper, with negligible percent difference for surface soil (not shown in Exhibit 3-51, see Exhibit 3-53 for an example) and highest percent difference for ground water. A small amount of the elemental mercury in air in case B deposits to the surface soil, where it quickly either re-volatilizes to air or, because it is mobile in soils, infiltrates to deeper soil levels. The small additional amount of elemental mercury in surface soil is swamped by the much greater level of divalent mercury, and thus there is negligible effect on total mercury in surface soil. Conversely, as a portion of the elemental mercury moves downward through the soil it has much greater relative impact because divalent mercury levels drop off so quickly with depth in soil (divalent mercury is relatively immobile in soils) (see also the speciation results for soil layers in Section 3.3). Exhibit 3-53 illustrates these spatial and vertical patterns with a detailed example of the soil concentration results for two

specific compartment locations, one at the edge of the modeling region (E4) and one adjacent to the source (E1). For both locations, the ratios for total mercury match divalent mercury for surface soil, they match elemental mercury for vadose zone soil and ground water, and they are intermediate for root zone soil (i.e., both divalent and elemental mercury are important in root zone soil).

Exhibit 3-52
Case A vs. Case B: Time Series of Total Mercury Concentrations, Root Zone Soil in SW2

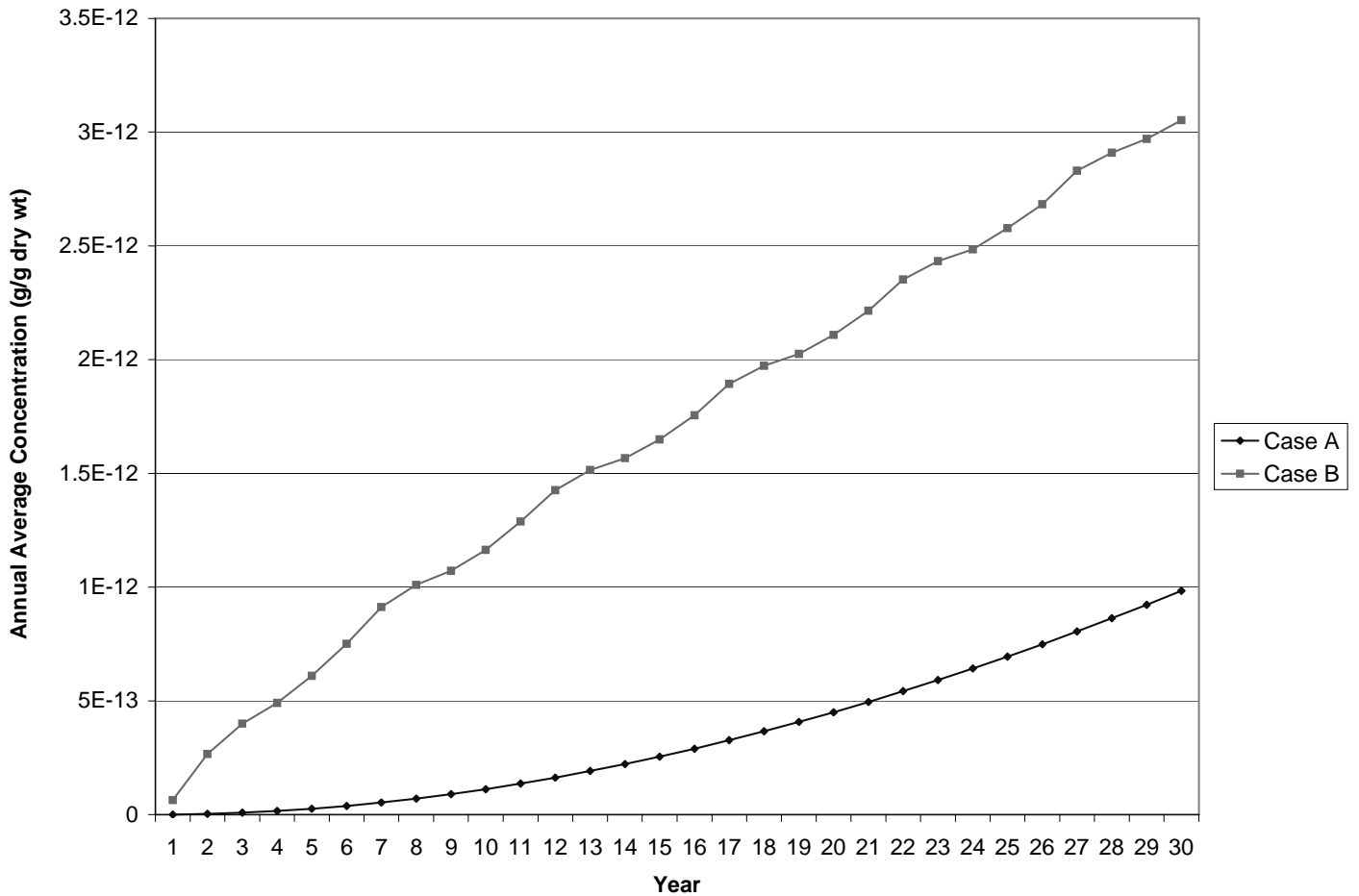


Exhibit 3-53
Detailed Example of Soil Concentration Results for Case A vs. Case B^a

Compartment Type/Location	Elemental Mercury		Divalent Mercury		Total Mercury	
	Conc B/ Conc A	Ratio	Conc B/ Conc A	Ratio	Conc B/ Conc A	Ratio
Surface soil/E4	8.8E-13/ 2.3E-13	3.8	2.4E-9/ 2.4E-9	1.0	2.5E-9/ 2.5E-9	1.0
Root zone soil/ E4	6.9E-13/ 1.9E-13	3.6	2.2E-13/ 2.2E-13	1.0	9.1E-13/ 4.1E-13	2.2
Vadose zone soil/E4	4.5E-15/ 7.6E-16	5.9	5.6E-20/ 5.5E-20	1.0	4.5E-15/ 7.6E-16	5.9
Ground water/ E4	3.0E-18/ 3.7E-19	8.1	8.6E-23/ 9.1E-24	9.5	3.0E-18/ 3.7E-19	8.1
Surface soil/E1	8.4E-12/ 3.8E-12	2.2	4.0E-8/ 4.0E-8	1.0	4.0E-8/ 4.0E-8	1.0
Root zone soil/ E1	7.0E-12/ 3.0E-12	2.3	3.6E-12/ 3.6E-12	1.0	1.1E-11/ 6.7E-12	1.6
Vadose zone soil/ E1	4.1E-14/ 1.2E-14	3.4	9.2E-18/ 9.2E-18	1.0	4.1E-14/ 1.2E-14	3.4
Ground water/ E1	2.6E-17/ 6.2E-18	4.2	7.4E-22/ 1.5E-22	4.9	2.6E-17/ 6.2E-18	4.2

^a All concentrations are annual average values for year 30, in g/g dry wt.

The apparently anomalous result that case B has considerably higher divalent mercury in ground water than case A, while there is negligible difference in divalent mercury concentrations in the other soil layers, possibly results from a simplification in the way ground water is modeled in TRIM.FaTE. (Note: Because of its focus on air pollutants of priority concern for multimedia exposures, which in general are highly bioaccumulative and relatively immobile in soil systems, the TRIM.FaTE library includes relatively simple ground water transfer algorithms.) Certain ground water compartments are not linked to any other compartment and behave essentially as a partial sink – any chemical mass that reaches those compartments stays there (subject to transformation or degradation, as applicable) throughout the modeling period. Because there is a very slow transformation rate of elemental to divalent mercury in ground water, some of the additional elemental mercury that reaches ground water in case B gets transformed to divalent mercury over the 30-year modeling period. Even though this is an extremely small amount, the amount of divalent mercury that reaches ground water via downward advection from surface soil (i.e., the amount in case A) is so low that even a very small amount of transformed elemental mercury may possibly make a difference.

With respect to other compartment types, earthworm tracks root zone soil almost exactly (i.e., the case B:case A ratios for every compartment location are virtually identical), which

reflects the rapid partitioning approach used to model earthworm accumulation of mercury. The additional elemental mercury in root zone soil in case B appears to be directly responsible for the additional elemental mercury observed in earthworms in case B.

For surface water and macrophytes (which accumulate mercury via partitioning with surface water), the additional elemental mercury emitted in case B has a sizable impact on total mercury concentration for the river compartment, but only a small impact (<5 percent increase) on the pond compartments. Primarily because it is closer to the source, the contribution of elemental mercury via air deposition is more important (relative to other inputs of mercury mass) for total mercury in the river compartment than in the other surface water compartments; thus, the difference between case B and case A is larger for the river. For surface water the total mercury increase in case B appears to result directly from higher elemental mercury levels deposited from air. In the case of macrophytes, the higher total mercury in case B appears to be because elemental mercury is transferred to macrophytes via partitioning from surface water and rapidly transformed to divalent mercury, which is then accumulated.

The results for the tree swallow compartment type are more complicated. The only case B:case A total mercury ratios greater than 1.1 for tree swallows are for compartments where the food source (tree swallow diet modeled as 100 percent benthic invertebrates, which represent emerging benthic insects) is the river. However, the benthic invertebrate results do not vary much at all in case B versus case A, so the food source does not appear to fully explain the variation in tree swallow results. The compartments for which the tree swallow food source is the river also are closer to the emission source than those compartments where the food source is one of the ponds. Detailed examination of the mass flux results for individual compartments in case B indicates that inhalation of elemental mercury can be an important source of total mercury for tree swallows for certain compartments, depending on their proximity to the source and the contribution of mercury from their food source. For compartments more distant from the source, inhalation is strongly dominated by ingestion of benthic invertebrates. Thus, the much higher elemental mercury levels in air in case B have a notable impact on total mercury in tree swallows near the source (where airborne elemental mercury is highest), with much less impact as elemental mercury disperses with distance. Further complicating these relationships is the simulation of a fairly rapid transformation of elemental mercury in tree swallows to divalent mercury, which explains the similar spatial relationship seen for divalent mercury as for total mercury.

3.5.2 Emission Case B vs. Emission Case C

Case C was included in the test case modeling runs mainly to serve as the basis for comparisons of TRIM.FaTE results with available measurement data for mercury for the modeling region (see Chapter 7). However, case C also was compared with case B – which is the primary case analyzed in this report – to assess the impact of the modeled “background” (i.e., not from the test case facility emissions) mercury in air relative to mercury emitted from the test case facility.

In viewing the mercury concentration results for case C relative to case B, it is helpful to know the differences in the mercury inputs used for the two cases. Exhibit 3-54 summarizes the mercury mass inputs over 30 years for case B and case C. The two cases have identical inputs

from the industrial facility being modeled (same amounts of mercury, same forms, same time pattern of emissions). However, case C also has a relatively small amount of mercury present in environmental media and biota at the start of the modeling period (i.e., historical “background” contamination of the modeling region that originates from contaminated air flowing into the region prior to modeling) and a relatively large input of mercury over the 30-year modeling duration from air boundary contributions (i.e., concurrent “background” contamination from contaminated air flowing into the region during modeling). In fact, roughly 24 times more total mercury (4.7 times more divalent mercury) enters the modeling system from air boundary contributions than from the test case facility air emissions. Just like the mass emitted from the test case facility, the vast majority of the input mass originating in boundary contributions is elemental mercury that ends up in air sinks (i.e., leaves the modeling region before deposition and uptake into the ecosystem). Note that, based on the available modeling results, it generally is not possible to differentiate the relative impacts of the initial concentrations portion of “background” from the boundary contributions portion (e.g., how much of the mercury concentration in a given compartment results from which portion).

Exhibit 3-54
Summary of Mercury Mass Inputs in Cases B and C (over 30 years)

Source of Mass	Case B (kg)		Case C (kg)	
	Total	Divalent	Total	Divalent
Test case facility air emissions	3,871 ^a	194	3,871 ^a	194
Initial mass present in media/biota	0	0	41 ^b	39
Air boundary contributions	0	0	91,674 ^c	907
Total mass inputs	3,871 ^a	194	95,586 ^d	1,140

^a Assumed to be 95 percent Hg⁰ and 5 percent Hg²⁺.

^b Roughly 96 percent Hg²⁺, 3 percent Hg⁰, and 1 percent MHg.

^c Assumed to be 99 percent Hg⁰ and 1 percent Hg²⁺.

^d Roughly 99 percent Hg⁰ and 1 percent Hg²⁺.

In addition to the differences in mercury mass inputs for the two cases, the boundary contributions in case C are a different kind of source than the test case facility. The test case facility is modeled as a point/area source at a fixed location within the modeling compartment grid. The air boundary contributions, in contrast, are modeled as a volume source that moves when the wind shifts direction and that over the course of time entirely surrounds the modeling region boundary (i.e., wind-blown mercury in air enters the region from all directions over time, changing with the wind direction). Thus, most of the mercury mass in case C enters into the eight air compartments at the edges of the modeling region, while all of the mercury mass in case B enters into the air source compartment near the center.

Many of the patterns seen in comparing case C with case B result from these two key differences in the mercury mass inputs. As expected, the 30-year annual average concentrations are *always* higher in case C than in case B (case C can be viewed simply as additional mercury mass inputs overlaid on case B). The amount of differences and percent differences vary by

compartment type, compartment location, and mercury species. Among all 417 compartments, the median case C:case B concentration ratio for total mercury at year 30 is 8.1 (i.e., for more than half the compartments modeled, the total mercury concentration difference is less than a factor of 10), the 75th percentile is 18, and the 90th percentile is 29. For roughly 79 percent of the compartments modeled, the case C total mercury concentration is within a factor of 20.

Exhibit 3-55 shows the range of case C:case B ratios (i.e., relative differences) for all compartment types modeled except meadow vole, which was only modeled as present in two compartments (and therefore the range is not comparable). In terms of percent increase, the highest impacts of the case C “background” contributions are seen in two groups:

- The root zone and vadose zone soil and ground water compartment types, plus the soil invertebrates (which partition mercury from root zone soil); and
- Sediment, benthic invertebrates/fish, and tree swallow (diet is 100 percent benthic invertebrates).

Case C produces the smallest increases in the terrestrial plant, terrestrial mammal and bird, and mallard compartments (terrestrial plants are a key part of the food chain for mallards and the terrestrial mammals and birds), with air, surface water, macrophytes, water-column fish, and most semi-aquatic animals in the middle. Many of the same compartment type relationships are seen here as evident in other analyses in this chapter (e.g., very close tracking of results for surface water/macrophyte, root zone soil/earthworm, tree swallow/benthic omnivore, sediment/benthic invertebrate, weasel/hawk).

There is much less spatial variability in mercury concentrations in land-based compartment types in the case C results than in the case B results. Spatial variability is damped in case C because most of the mass inputs come fairly evenly from all directions around the modeling region boundary, rather than 100 percent from one central source as in case B. For example, the maximum:minimum concentration ratios for total mercury for selected compartment types are as follows:

- Air – 13 for C, 236 for B (1.8 for C, 12 for B excluding source compartment);
- Root zone soil – 21 for C, 510 for B (2.1 for C, 16 for B excluding source compartment);
- Mouse – 33 for C, 219 for B;
- Short-tailed shrew – 2.1 for C, 16 for B; and
- White-tailed deer – 36 for C, 233 for B.

A similar result – less overall spatial variability in total mercury concentrations within a compartment type for case C than case B – is seen for compartment types in the four ponds that were modeled. In relative terms, case C has much lower effect on the river compartments than on those in any of the ponds, probably at least in part due to its location relative to the edge of the modeling region.

Exhibit 3-55
Case B vs. Case C: Range of Differences in Total Mercury Concentration
by Compartment Type ^a

Land-based Compartment Type ^b	Lowest C:B ratio	Highest C:B ratio
Air (30)	1.1	24
Surface soil (20)	1.0	22
Root zone soil (20)	1.0	34
Vadose zone soil (20)	1.1	57
Ground water (20)	1.3	120
Leaf (19)	1.6 conif	8.0 conif
Particle-on-leaf (19)	1.6 conif	8.0 conif
Root (4)	3.2	10
Stem (4)	1.4	3.9
Arthropod (17)	2.8	43
Earthworm (19)	3.1	34
Black-capped chickadee (17)	1.6	13
Mouse (17)	1.6	14
White-tailed deer (17)	1.6	13.
Short-tailed shrew (17)	1.9	22
Red-tailed hawk (17)	1.6	13
Long-tailed weasel (17)	1.7	13
Raccoon (15)	2.0	27
Bald eagle (17)	1.7	21
Mink (15)	1.6	16
Tree swallow (17)	3.4	31

Water-based Compartment Type ^b	Lowest C:B ratio	Highest C:B ratio
Surface water (7)	5.0	24
Sediment (7)	3.4	37
Macrophyte (5)	5.7	21
Water-column herbivore (5)	3.3	20
Water-column omnivore (5)	3.4	19
Water-column carnivore (5)	3.5	19
Benthic invertebrate (5)	3.4	31
Benthic omnivore (5)	3.4	31
Benthic carnivore (5)	3.4	32
Mallard (5)	1.6	4.1
Common loon (5)	3.5	21

^a All ratios based on annual average concentrations for individual compartments for year 30.

^b Number of compartments modeled for each type shown in parentheses.

When viewed on a percent difference basis, all of the air, land, and land-based biota compartment types have the greatest percent increase at the edges of the modeling grid – compartment locations SE6, SSE5, and ESE5 have the highest case C:case B ratios. Likewise, the lowest percent increase is always seen at the center of the grid, either the source compartment or (for compartment types not modeled as present in the source compartment) compartment locations SE1, E1, or N1. This pattern results from a combination of two factors: (1) case B concentrations for these compartment types are usually higher near the source and decline with distance (toward the edges); and (2) the mass contributions across the boundaries in case C produce relatively low spatial variation because they enter the system from all directions over time (as the wind direction changes) and not from a single fixed location. Thus, the roughly similar increases in mass from case C produce higher percent increases in concentration at the edges (where case B is lower) than at the center (where case B is higher).

For the water-based compartment types, Thurston Pond always has the highest case C:case B ratio and the river always has the lowest. The spatial pattern for water-based compartments is suspected to be at least partly due to the same factors playing a role in the land-based compartments, as described above – proximity to the edge of the modeling region is associated with higher ratios.

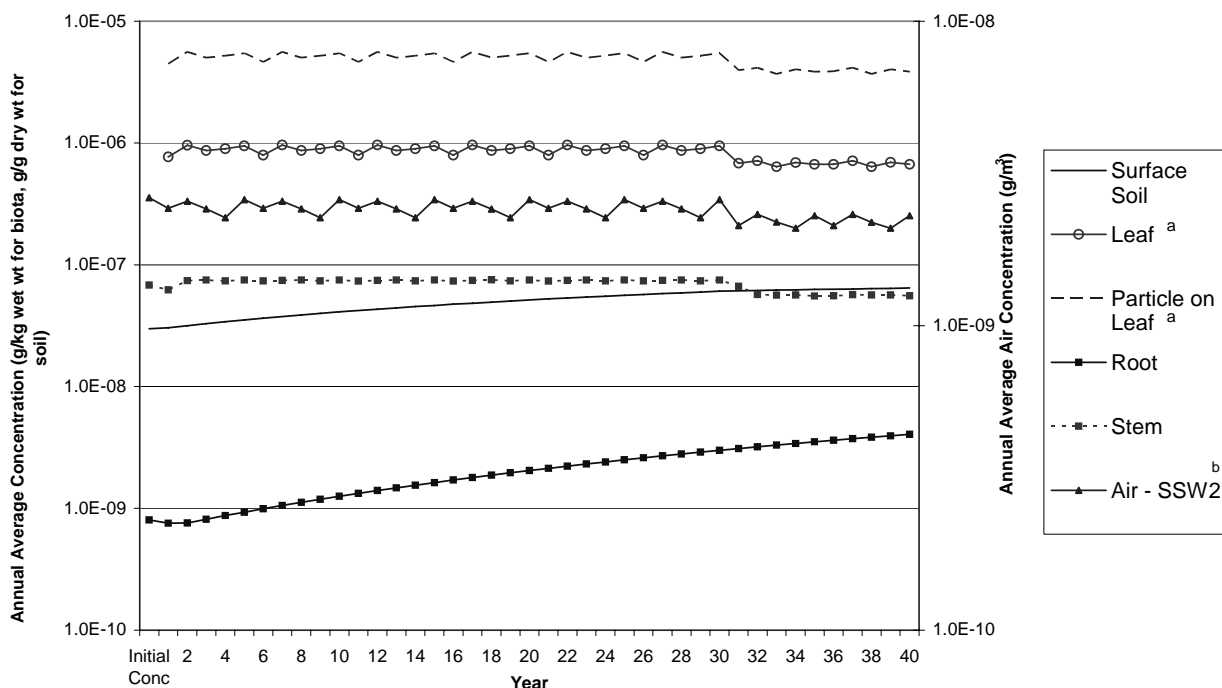
As noted in Chapter 2, the case C modeling duration is 40 years, including 10 years following the shutoff of source emissions at the end of year 30. Exhibits 3-56 through 3-58 illustrate for case C the time series patterns of total mercury concentration in selected compartment types over the 40 years (compare with Exhibits 3-10, 3-11, and 3-13 for case B). The basic time patterns – spiking versus smooth, increasing versus flat – for the various compartment types in case C are similar to case B, with case C always higher in concentration. The order of the compartment types on a chart, from high to low concentration, also is the same for the two emission cases. There are, however, some differences apparent from examination of the charts.

- In case C, some compartment types (e.g., air, leaf, particle on leaf, stem, terrestrial and some semi-aquatic animals) show a concentration drop after the halt of emissions from the source at year 30. These compartment types are the ones that have a non-increasing pattern over the first 30 years. The dropoff is not dramatic, indicating that the boundary contributions (which continue after year 30) are more important quantitatively than the source emissions for the compartment locations shown. The size of the dropoff would be expected to vary depending on a compartment's position relative to the source and the modeling region boundary. Note that soil, surface water, sediment, and related biotic compartments, which have increasing concentrations before year 30, continue to rise after year 30, although in some cases less rapidly than before.
- Compartment types with smoothly increasing plots (e.g., soil, sediment) tend to increase more slowly in case C (i.e., look flatter on the charts), reflecting the fact that case C starts at an initial concentration based on 30 years of air boundary (“background”) contributions rather than at zero. Thus, the relatively rapid increases in early years in case B are not seen in case C. For example, the total mercury concentration in root increases about three and a half orders of magnitude in 30 years in case B, but less than one order of magnitude in 40 years in case C.

- Compartment types with spiking in the time pattern of annual average concentrations show less spiking in case C, for a similar reason to that explaining the lower spatial variability. Temporal variability is damped in case C because most of the mass inputs come more evenly over time from the boundary contributions, rather than from a single central source. No matter what the wind direction, there is always some boundary contribution to a given compartment in case C. This is not true for the source contribution, which is dependent on wind direction and thus more time variable.

Note that in the case B charts, the initial concentration, which is always zero, is not plotted. If it were, there would be a steep increase in year 1 for all compartment types, which differs from most of the case C plots, where there is not much change in year 1 from the initial concentration. However, because deciduous leaves in TRIM.FaTE return to zero mercury concentration each year after litter fall, animal compartment types that have deciduous leaves in their diet show a large increase in year 1 in case C (because initial mercury concentrations of such animal compartments are an instantaneous concentration on December 31, when deciduous leaf concentrations equal zero, and are considerably lower than the annual average concentrations that follow, which reflect both growing (leaf concentration greater than zero) and non-growing (leaf concentration equals zero) seasons).

Exhibit 3-56 - Log Scale
Case C Total Mercury Concentration in Air, Soil, and Plants vs. Time:
SW2 (grasses/herbs)

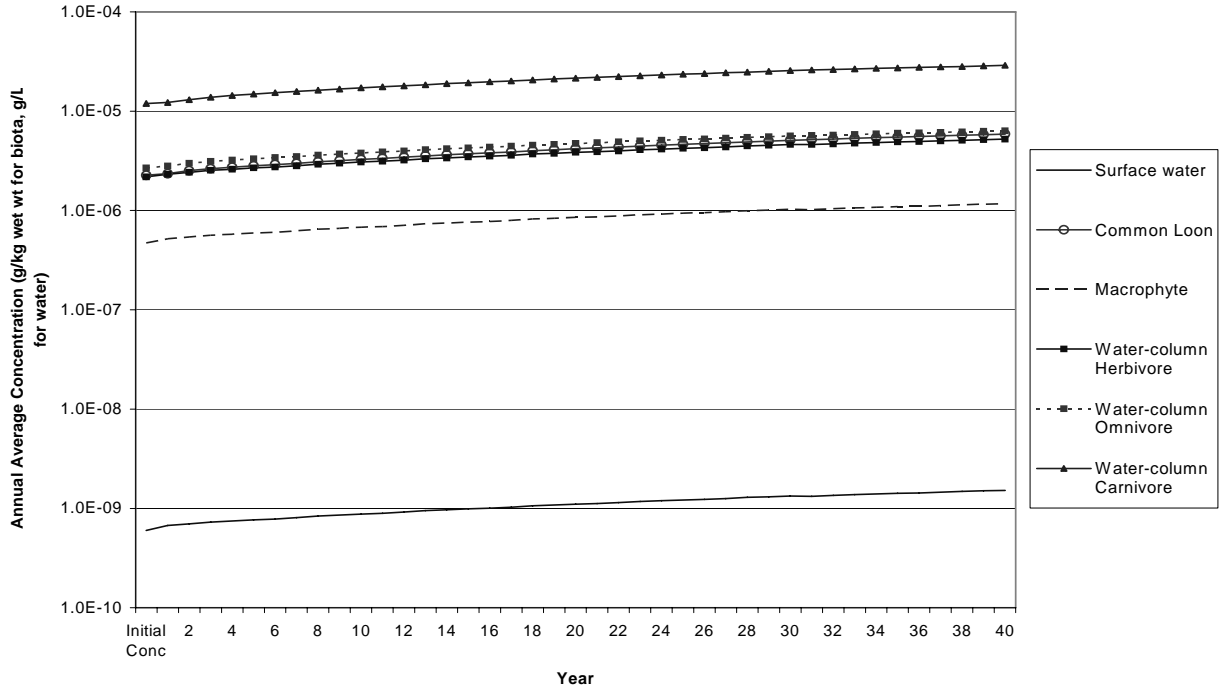


^a Each annual average data point shown for leaf and particle on leaf is the average of values during the days (May 13 to September 29 each year) for which leaves were modeled as present (i.e., represents a growing season average). Initial concentration is set to zero (not plotted).

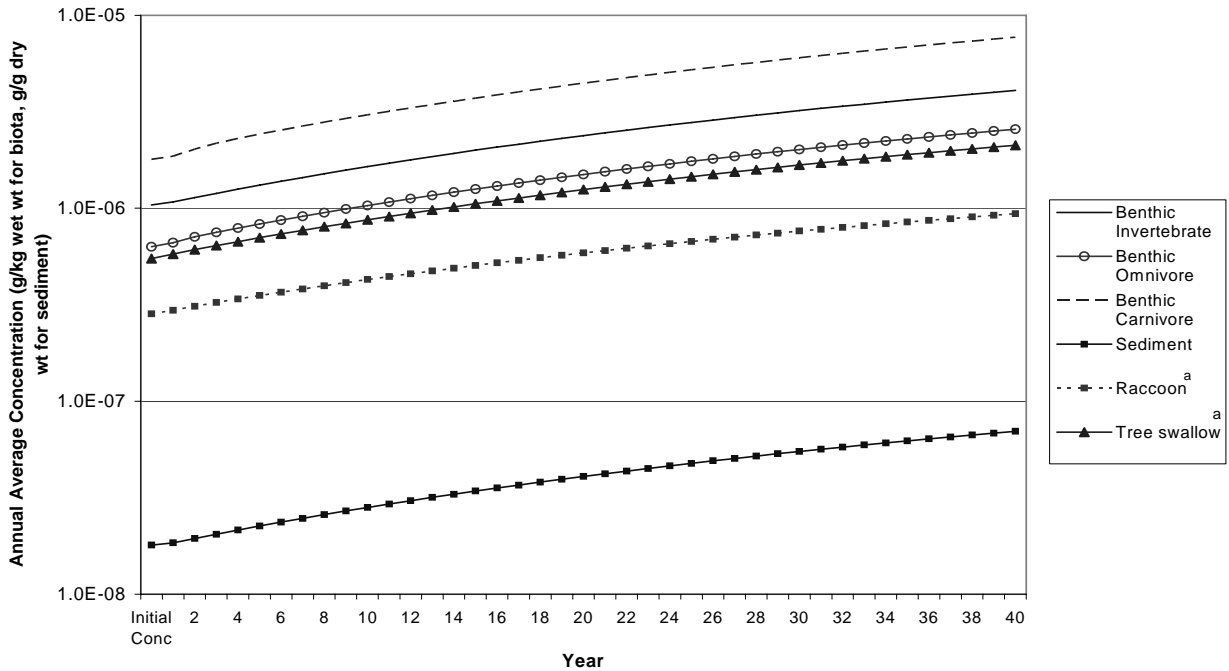
^b Because of the differences in the air and surface parcel layouts, the boundaries of the SSW2 air parcel do not match those of the SW2 surface parcel (see Exhibits 2-1 and 2-2), but this air parcel does have substantial overlap with the surface parcel (among air parcels, SSW2 has the most overlap with surface parcel SW2).

Exhibit 3-57 - Log Scale Case C Total Mercury Concentration in Surface Water and Related Biota vs. Time: Swetts Pond

(a) Water-column and Related Biotic Compartments



(b) Benthic and Related Biotic Compartments

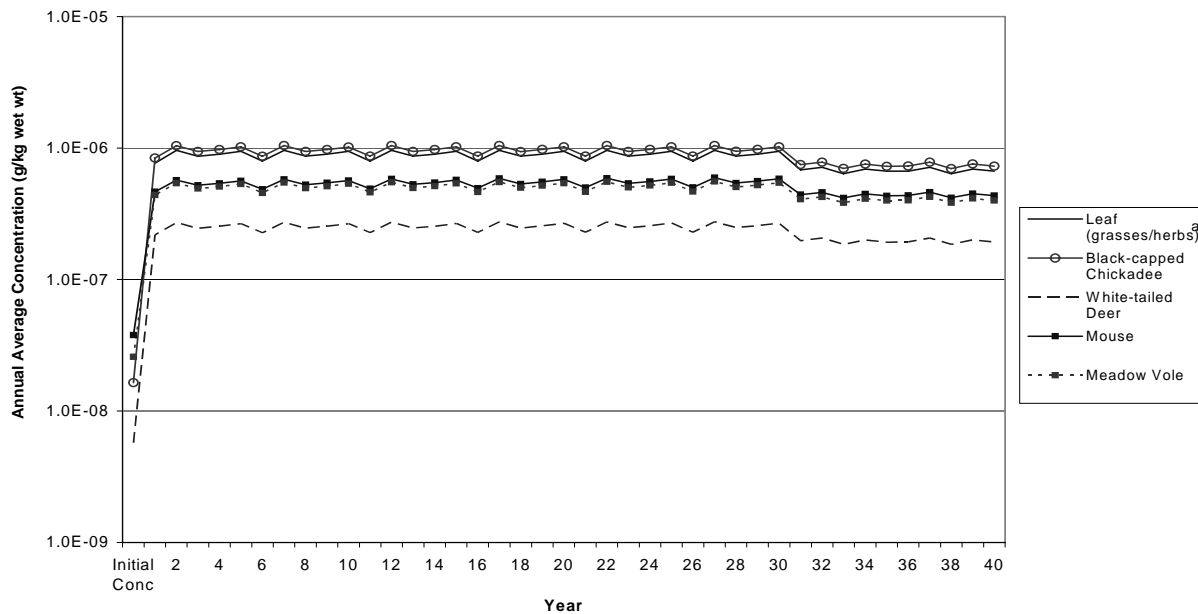


^a Results shown for compartment SSE4, where semi-aquatic animals feed from Swetts Pond.

Exhibit 3-58 - Log Scale

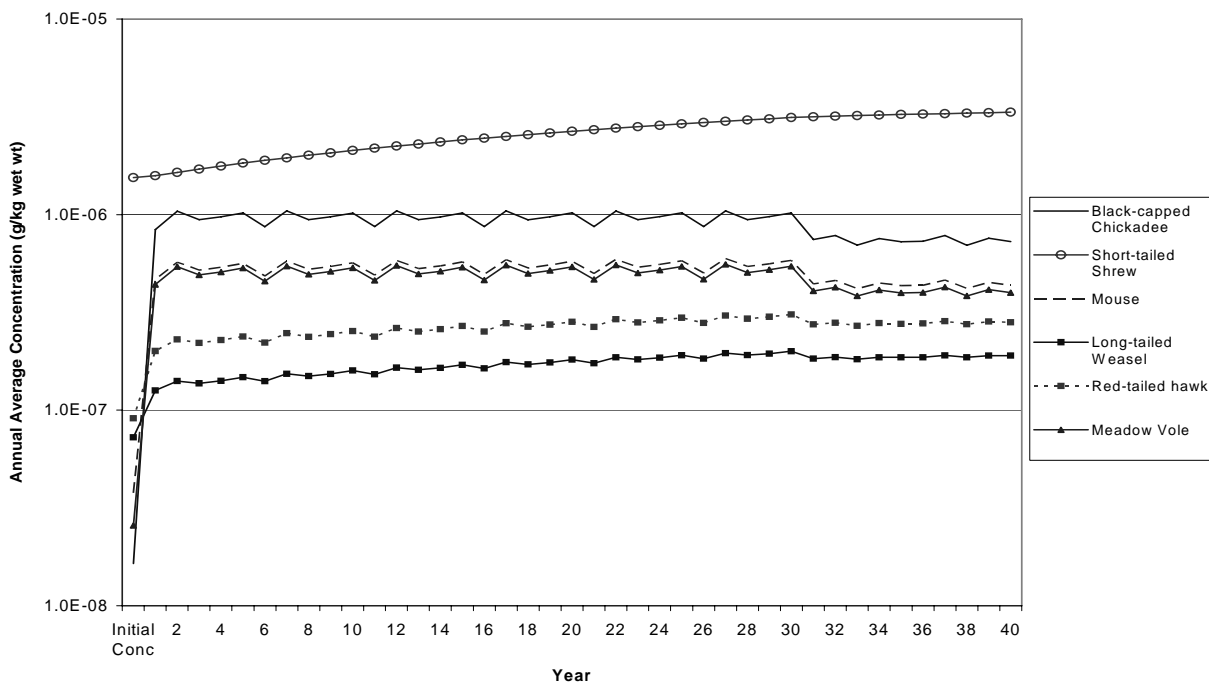
Case C Total Mercury Concentration in Terrestrial Animals vs. Time: SW2 (grasses/herbs)

(a) Terrestrial Herbivore and Omnivore Compartments



^a Each annual average data point shown for leaf and particle on leaf is the average of values during the days (May 13 to September 29 each year) for which leaves were modeled as present (i.e., represents a growing season average). Initial concentration is set to zero (not plotted).

(b) Terrestrial Carnivore (Weasel and Hawk) Compartments



4. RESULTS AND DISCUSSION: STEADY-STATE MODELING

The TRIM.FaTE model can be run in two different modes: *dynamic mode*, which estimates pollutant concentrations in each compartment over time at user-defined intervals; and *steady-state mode*, which estimates the pollutant concentrations in each compartment at steady-state (i.e., when the distribution of mass within the modeling system is no longer changing given a constant source term or emission rate). This chapter presents the TRIM.FaTE steady-state modeling results for the mercury test case. The main purpose of this chapter is to provide an overview of the steady-state results and give a sense of how these steady-state results compare to the results from the dynamic simulations. The steady-state mode is used as the basis for the sensitivity analysis of TRIM.FaTE described in Chapter 5. For additional description of the steady-state mode, refer to the *TRIM.FaTE Technical Support Document* (EPA 2002b,c) and *TRIM.FaTE User's Guide* (EPA 2003b).

Section 4.1 describes how the TRIM.FaTE scenario used for the mercury test case was configured to run in steady-state mode and highlights how this configuration differed from that of the dynamic simulations. Section 4.2 provides an overview of the results from the steady-state simulation, and Section 4.3 discusses these results in the context of the results from the dynamic simulations.

4.1 Configuring a TRIM.FaTE Scenario for Steady-state Mode

To generate steady-state results using TRIM.FaTE, no model inputs can be assigned time-varying values. Therefore, all time-varying inputs in a dynamic scenario must be replaced with representative constant values to generate steady-state results for that scenario. In the dynamic scenarios for the mercury test case, the following inputs were assigned time-varying values:

- Air temperature;
- Wind speed;
- Wind direction;
- Mixing height;
- Precipitation rate;
- *isDay* (0 at night, 1 during the day);
- *AllowExchange* (0 during non-growing season, 1 during growing season);
- Litter fall rate (for deciduous forest and grasses/herbs, user-specified rate during litter fall and zero at all other times); and
- River flush rate (i.e., flow) and current velocity.

In order to provide a sound basis of comparison with the results from the dynamic simulations, constant values for these inputs were calculated with the objective that the resulting steady-state conditions closely approximate the system modeled in the dynamic simulations. Several of the constant values are simply arithmetic averages of the time-varying values. The resulting constant values used in the steady-state analysis are provided in Exhibit 4-1. The methodology used to calculate these values is provided in Appendix C.1.

Exhibit 4-1
Constant Input Values for Time-varying Properties
Used in Steady-state Modeling

Input	Steady-state Value
Air temperature	280 K
<i>AllowExchange</i> (for air-to-plant algs.)	0.426
<i>AllowExchange</i> (for other plant algs.)	0.386
River current velocity	0.166 m/s
River flush rate	531.24 /yr
Wind speed	3.64 m/s
<i>isDay</i> (for air-to-plant algs.)	0.552
<i>isDay</i> (for other plant algs.)	0.609
Litter fall rate	0.013 /day
Precipitation rate	0.0041 m/day
Mixing height	887 m

All of the algorithms used in the steady-state simulation were identical to those used in the dynamic mode, with the exception of the algorithms that estimate air-to-air advective transfers. Using a constant wind speed and direction with the air-to-air transfer algorithms that were developed for the dynamic mode can result in a much different spatial distribution of chemical mass than is estimated when wind speed and direction are allowed to vary. Therefore, a new air-to-air advective transfer algorithm that does not require wind speed and direction was developed for the steady-state mode. The new algorithm uses a constant transfer factor (first-order rate constant, in units of "per day") for each direction across each air-to-air interface in the modeling area. These steady-state transfers were estimated by averaging the hourly air-to-air advective transfers (for each interface) calculated using the dynamic mode of TRIM.FaTE over the five-year meteorological input data period.¹ Because wind direction is only used in the air-to-air advective transfer algorithm that was replaced, this input is not required to run TRIM.FaTE in steady-state mode and thus is not included in Exhibit 4-1. (The wind speed, however, is still used in algorithms for volatilization from surface water.) The resulting steady-state transfer factors for the air-to-air advection algorithm are provided in Appendix C.1 along with additional details on the development of the steady-state algorithms.

¹ Simple averaging (arithmetic mean) of transfers across each interface was used in the mercury test case. Other approaches to developing the "most representative" steady-state transfers may be investigated in the future.

The next step in configuring TRIM.FaTE to run the mercury test case in steady-state mode was to set up the scenario. This process was identical to that used to set up a dynamic scenario, with the following exceptions.

- The steady-state scenario used constant values for time-varying inputs (as described above).
- The steady-state scenario used the air-to-air advection algorithm developed for steady-state simulations (as described above).
- All outgoing links from ground water compartments were disabled. Because the ground water compartments in the mercury test case have extremely slow chemical loss processes, TRIM.FaTE is not able to calculate a steady-state solution for the modeled system unless the ground water compartments are treated as virtual sinks (i.e., compartment that can gain pollutant mass, but not lose it). This is accomplished by disabling all of the outgoing links from the ground water compartments, which essentially eliminates all of the processes by which ground water compartments lose mass. Because TRIM.FaTE cannot estimate steady-state solutions for sinks, it does not estimate a steady-state solution for the ground water compartments after these links are disabled.

4.2 Steady-state Results

After configuring TRIM.FaTE as described in Section 4.1, a steady-state simulation was performed for emission case B (i.e., source emissions of divalent and elemental mercury, no boundary contributions, and no initial concentrations) using the same model configuration as the dynamic simulation described in detail in Chapter 3 (e.g., same spatial layout, same chemicals), with the exception of the inputs and air-to-air transfer algorithm described in Section 4.1. This section summarizes the results from the steady-state simulation. The data described in this section are masses and concentrations of total mercury, which are calculated by summing the mass and concentrations of elemental mercury, divalent mercury, and methyl mercury (as mercury) output by TRIM.FaTE.

Exhibit 4-2 summarizes the mass and concentration results from the steady-state simulation. The total mercury mass in each compartment type was estimated by summing the mass of all three mercury species across all compartments of each compartment type. Likewise, the average total mercury concentration in each compartment type was estimated by averaging the total mercury concentrations across all compartments of each compartment type (note: averages not weighted by size of compartment). Appendix C.2 presents the compartment-specific total mercury mass and concentration results. The remainder of this section summarizes the results of the steady-state simulation with respect to the mass results. The concentration results are described within the context of the dynamic results in Section 4.3.

Exhibit 4-2
Steady-state Simulation Mass and Concentration Results by Compartment Type

Compartment Type	Total Mercury Mass		Total Mercury Concentration	
	Mass (g)	% of Total in Modeling System ^a	Ave. Conc.	Units
<i>Abiotic Media</i>				
Air	2.7E+01	7.4E-03%	3.8E-10	g/m ³
Soil - surface	1.7E+05	46.1%	3.7E-07	g/g dry weight
Soil - root zone	5.6E+04	15.5%	1.9E-09	g/g dry weight
Soil - vadose zone	2.9E+03	0.81%	5.6E-11	g/g dry weight
Surface water	1.8E+02	0.05%	6.7E-09	g/L
Sediment	1.4E+05	37.5%	5.8E-07	g/g dry weight
<i>Terrestrial Plants</i>				
Leaf - deciduous forest	1.2E+01	3.2E-03%	4.7E-07	g/kg wet weight
Leaf - coniferous forest	1.0E+02	0.03%	1.5E-06	g/kg wet weight
Leaf - grasses/herbs	4.7E+00	1.3E-03%	7.1E-07	g/kg wet weight
Particle-on-leaf - decid. forest	6.0E-04	1.6E-07%	3.0E-06	g/kg wet weight
Particle-on-leaf - conifer. forest	7.5E-03	2.1E-06%	3.2E-05	g/kg wet weight
Particle-on-leaf - grasses/herbs	1.4E-03	3.9E-07%	4.1E-05	g/kg wet weight
Root - grasses/herbs	5.8E+00	1.6E-03%	5.2E-07	g/kg wet weight
Stem - grasses/herbs	1.0E-01	2.9E-05%	4.0E-08	g/kg wet weight
<i>Terrestrial Animals</i>				
Earthworm	1.2E-01	3.3E-05%	3.5E-08	g/kg wet weight
Arthropod	4.4E-03	1.2E-06%	1.7E-07	g/kg wet weight
Short-tailed shrew	1.0E-02	2.8E-06%	8.5E-06	g/kg wet weight
Meadow vole	9.6E-04	2.7E-07%	3.7E-07	g/kg wet weight
White-tailed deer	4.3E-01	1.2E-04%	1.5E-06	g/kg wet weight
Black-capped chickadee	1.9E-04	5.2E-08%	6.0E-06	g/kg wet weight
Mouse	1.2E-02	3.3E-06%	3.2E-06	g/kg wet weight
Long-tailed weasel	4.9E-05	1.3E-08%	5.9E-07	g/kg wet weight
Red-tailed hawk	7.1E-05	2.0E-08%	1.1E-06	g/kg wet weight
<i>Semi-aquatic Animals</i>				
Tree swallow	1.3E-02	3.6E-06%	6.6E-06	g/kg wet weight
Mallard	2.5E-04	6.8E-08%	3.1E-06	g/kg wet weight
Mink	6.0E-05	1.7E-08%	2.4E-06	g/kg wet weight
Raccoon	2.3E-03	6.2E-07%	3.4E-06	g/kg wet weight
Common loon	2.6E-05	7.2E-09%	2.1E-05	g/kg wet weight
Bald eagle	7.4E-05	2.0E-08%	8.9E-06	g/kg wet weight
<i>Aquatic Plants^b</i>				
Macrophyte	3.4E+01	9.5E-03%	4.3E-06	g/kg wet weight
<i>Aquatic Animals</i>				
Water-column carnivore	9.5E-02	2.6E-05%	7.9E-05	g/kg wet weight
Water-column herbivore	1.5E-01	4.3E-05%	1.7E-05	g/kg wet weight
Water-column omnivore	6.6E-02	1.8E-05%	1.8E-05	g/kg wet weight
Benthic carnivore	6.1E-02	1.7E-05%	5.3E-05	g/kg wet weight
Benthic omnivore	1.7E-01	4.7E-05%	1.7E-05	g/kg wet weight
Benthic invertebrate	5.3E+00	1.5E-03%	2.8E-05	g/kg wet weight

^a Calculated relative to mass within the modeling system not including the mass in sinks because TRIM.FaTE does not generate steady-state results for sinks. Thus, the sum of the values in the column labeled “% of Total in Modeling System” equals 100 percent.

^b Algae are not represented as aquatic plants in this simulation; rather they are represented in the surface water estimates as a phase of surface water compartment instead of as a separate compartment.

As shown in Exhibit 4-2, most of the mercury mass at steady-state is in the abiotic compartments, particularly the soil and sediment compartments.² Overall, the abiotic compartments comprise over 99.9 percent of the total mercury mass in the modeling region. Among abiotic media, surface soil has the most mercury at steady-state (approximately 46 percent of the mercury in the modeling region), followed by sediment (approximately 38 percent), root zone soil (16 percent), and vadose zone soil (0.81 percent).³ The remaining abiotic compartment types, surface water and air, contain 0.05 percent and less than 0.01 percent, respectively, of the mercury in the modeling region.

The amount of mercury mass in biota is much lower than in the abiotic media, which is in part a result of the lower relative volume of the biotic compartments. Of the biotic compartments, the leaf, root, macrophyte, and benthic invertebrate compartments contain the most mercury mass. The coniferous leaf compartments contain the most mass among the biotic compartments, likely due in part to the fact that coniferous plants are not assumed to lose all of their foliage each year like deciduous and grasses/herbs plants. The benthic invertebrate compartments have substantially higher amounts of mercury than the rest of the animals associated with benthos and surface water, likely due in part to the higher amounts of mercury mass in the sediment compartments and higher biomass of the benthic invertebrates.

4.3 Comparison of Steady-state and Dynamic Results

In this section, the results from the steady-state simulation described in Section 4.2 are compared to the corresponding dynamic simulation results described in Chapter 3. As in Section 4.2, this comparison is based on the masses and concentrations of total mercury from each simulation. The first part of this section compares the overall distribution of mass for the steady-state and dynamic simulations, and the second section compares the concentrations for selected compartment types estimated by the steady-state and dynamic simulations.

Comparison of the Overall Distributions of Mass

Although the results from steady-state and dynamic simulations cannot be directly compared for sinks, the relative distribution of mass among the compartments provides some insight into how the steady-state mode compares to the dynamic mode. Generally, the distribution of mass in the steady-state simulation is similar to the distribution in the dynamic simulation. In both simulations, the abiotic compartments contain nearly all of the total mercury mass in the non-sink compartments. The primary difference between the steady-state and dynamic results with regard to the distribution of mass among the abiotic compartments is that the estimated total mercury mass in the root zone soil, vadose zone soil, sediment, and surface water compartments is considerably higher relative to the other abiotic compartments in the

² Note that TRIM.FaTE does not generate steady-state estimates for sinks; therefore, the information on distribution of pollutant mass in the steady-state simulation results is limited to the compartments in the modeling region.

³ For comparison, roughly 94 percent of the total mercury mass in the compartments is in surface soil at year 30 in the dynamic modeling results, with 4 percent in sediment, 2 percent in root zone soil, and 0.01 percent in vadose zone soil. See Section 4.3 for discussion.

steady-state simulations. This result is not surprising as the mass in these compartment types appears to be increasing more rapidly than the other abiotic compartment types at the 30th year of the dynamic simulation (i.e., these compartment types are “farther” from steady-state at year 30).

For biotic compartments, the pattern of mercury mass accumulation in the steady-state simulation is slightly different from the pattern in the dynamic simulation. For the steady-state simulation, the pattern is:

terrestrial plants >> aquatic plants > aquatic animals > terrestrial/semi-aquatic animals

whereas the pattern for the dynamic simulation is:

terrestrial plants >> aquatic plants ~ terrestrial/semi-aquatic animals > aquatic animals

The difference between these mass accumulation patterns is reasonable because, based on the results from the dynamic simulation, the total mercury mass in aquatic plants and animals appears to be increasing more rapidly at the 30th year of the dynamic simulation than the mass in the terrestrial and semi-aquatic animals.

The distribution of mass among the plant compartments in the steady-state simulation was also slightly different from the distribution in the dynamic simulation. At the end of the dynamic simulation, the leaf compartments contain the majority of the mass, followed (in order) by the stem, root, and particle-on-leaf compartments. In the steady-state simulation, the leaf compartments also contain the majority of the mass, but the root compartments contain substantially more mass than the stem and particle-on-leaf compartments. This result is likely due to the strong relationship between the root concentration and the concentration in the root zone soil, which is still increasing at year 30 of the dynamic simulation.

Comparison of Compartment Concentrations

Exhibit 4-3 compares the arithmetic average steady-state concentrations (in the column labeled “Steady-state”) for each compartment type to the arithmetic average concentrations for each compartment type for the 30th year of the dynamic simulation (in the column labeled “Dynamic”). Additionally, the “SS : Dynamic” column of Exhibit 4-3 presents the average of the compartment-specific ratios of steady-state to dynamic results for each compartment type. A similar pattern of results is seen when comparing the mass results for the two modes (not shown).

With a few notable exceptions, the steady-state concentrations are higher than the dynamic concentrations. For some abiotic compartment types, such as root zone soil, vadose zone soil, and sediment, the steady-state:dynamic ratio is high because the dynamic concentrations for these compartment types are still increasing at the end of the dynamic simulation, indicating that the compartments have not reached steady-state. Likewise, some of the biotic compartment types with higher steady-state:dynamic ratios (e.g., earthworm, root, benthic invertebrate) are closely tied to these abiotic compartment types and would be expected to have similar concentration patterns.

Exhibit 4-3
Comparison of Steady-state (SS) Concentrations to 30th Year
Dynamic Concentrations, by Compartment Type

Compartments	Units	Total Hg Concentrations			Ratios		
		SS	Dynamic ^a	Dynamic w/SS Inputs ^a	SS : Dynamic ^b	SS : Dynamic w/SS Inputs ^b	Dynamic w/SS Inputs : Dynamic ^b
Air ^c	g/m ³	3.8E-10	1.1E-09	3.8E-10	0.7	1.0	0.6
Soil - surface	g/g dry	3.7E-07	1.3E-07	1.2E-07	16	3.3	5.1
Soil - root zone	g/g dry	1.9E-09	2.7E-11	2.3E-11	290	90	3.3
Soil - vadose zone	g/g dry	5.6E-11	8.5E-14	5.8E-14	2,000	1,000	2.1
Surface water	g/L	6.7E-09	1.0E-10	7.0E-10	77	12	5.9
Sediment	g/g dry	5.8E-07	2.9E-09	2.0E-08	230	37	6.1
Leaf - decid. forest ^c	g/kg wet	4.7E-07	8.8E-08	4.7E-07	5.8	1.0	5.8
Leaf - conif. forest ^c	g/kg wet	1.5E-06	6.4E-07	1.5E-06	2.5	1.0	2.5
Leaf - grasses/herbs ^c	g/kg wet	7.1E-07	4.1E-07	7.0E-07	3.3	1.0	3.2
Particle-on-leaf - decid. forest ^c	g/kg wet	3.0E-06	5.8E-07	3.0E-06	5.6	1.0	5.6
Particle-on-leaf - conif. forest ^c	g/kg wet	3.1E-05	1.4E-05	3.1E-05	2.4	1.0	2.4
Particle-on-leaf -grasses/herbs ^c	g/kg wet	4.1E-05	9.1E-05	4.0E-05	2.6	1.0	2.6
Root - grasses/herbs	g/kg wet	5.2E-07	8.9E-10	2.1E-09	640	220	3.3
Stem - grasses/herbs ^c	g/kg wet	4.0E-08	6.9E-08	3.9E-08	0.8	1.0	0.8
Macrophyte	g/kg wet	4.3E-06	4.2E-08	2.7E-07	87	14	5.6
Earthworm	g/kg wet	3.4E-08	1.3E-10	3.6E-10	300	91	3.5
Arthropod	g/kg wet	1.7E-07	2.0E-10	9.8E-10	1,000	170	5.8
Short-tailed shrew	g/kg wet	8.5E-06	5.7E-07	2.7E-06	18	3.2	5.7
Meadow vole ^c	g/kg wet	3.7E-07	1.8E-07	3.2E-07	2.0	1.2	1.7
White-tailed deer ^c	g/kg wet	1.5E-06	6.8E-07	1.5E-06	2.3	1.1	2.1
Black-capped chickadee ^c	g/kg wet	6.0E-06	2.6E-06	5.8E-06	2.5	1.2	2.1
Mouse ^c	g/kg wet	3.2E-06	1.4E-06	3.0E-06	2.8	1.3	2.2
Long-tailed weasel	g/kg wet	5.9E-07	1.3E-07	3.4E-07	7.0	2.2	3.1
Red-tailed hawk	g/kg wet	1.1E-06	3.1E-07	7.5E-07	6.1	2.1	2.9
Tree swallow	g/kg wet	6.6E-06	3.1E-08	1.6E-07	130	23	3.8
Mallard	g/kg wet	3.1E-06	2.0E-06	7.0E-07	15	7.2	1.7
Mink ^c	g/kg wet	2.3E-06	1.9E-07	4.7E-07	32	9.6	2.7
Raccoon	g/kg wet	3.4E-06	4.2E-08	2.1E-07	110	17	5.4
Common loon	g/kg wet	2.1E-05	1.8E-07	1.3E-06	97	15	6.3
Bald eagle ^c	g/kg wet	8.9E-06	2.2E-07	7.9E-07	45	8.9	3.6
Water-column herbivore	g/kg wet	1.6E-05	1.7E-07	1.3E-06	78	12	6.2
Water-column omnivore	g/kg wet	1.8E-05	2.2E-07	1.6E-06	69	10	6.4
Water-column carnivore	g/kg wet	7.8E-05	9.9E-07	7.3E-06	67	10	6.3
Benthic invertebrate	g/kg wet	2.8E-05	9.0E-08	6.0E-07	260	41	5.9
Benthic omnivore	g/kg wet	1.7E-05	5.6E-08	3.8E-07	260	41	5.9
Benthic carnivore	g/kg wet	5.3E-05	1.7E-07	1.1E-06	260	42	5.9

^a Average concentrations for dynamic simulations are based on average concentration for the 30th year of the simulation, unless otherwise noted.

^b These values represent the averages of the various ratios calculated for all compartments for each compartment type, not the ratios of the corresponding average concentrations. Therefore, these values are not exactly equal to the ratios of the concentrations in the previous two columns (i.e., average of ratios does not equal ratio of averages).

^c Indicates dynamic concentration was average of years 26-30, rather than year 30 (all leaf and particle on leaf averaged for entire year, zeros included, to facilitate comparison to steady-state).

However, some of the differences between the steady-state and dynamic simulations cannot be easily attributed to compartments that had yet to reach their steady-state values in the dynamic simulation. For example, many of the individual compartment results showed steady-state values less than dynamic values (e.g., air compartments), which was not an expected result. In light of this, an additional dynamic simulation (referred to as “dynamic with steady-state inputs”) was performed to help determine which differences are attributable to compartments that had not reached steady-state after 30 years and which are due to the constant input values used in place of dynamic values for the steady-state simulation (i.e., which are “modeling” differences vs. which are “input” differences). This new simulation used the exact same constant inputs and algorithms as the steady-state simulation (including the steady-state air-to-air advection algorithm), but was run for 30 years using the dynamic mode instead of using the model’s steady-state solution. The results of this simulation, as well as comparisons of these results to the steady-state (in the column “SS : Dynamic w/SS Inputs”) and dynamic results (in the column “Dynamic w/SS Inputs : Dynamic”), are presented in Exhibit 4-3. A more detailed comparison of these results is presented in Appendix C.3.

Assuming the model is performing as expected, the differences between the steady-state results and dynamic with steady-state inputs results should be strictly due to compartments not reaching steady-state within 30 years of the dynamic simulation. There are no ratios of steady-state to dynamic with steady-state inputs results less than one (which would have indicated that the model was not performing as expected), and many of the compartment types that appear to reach steady-state within 30 years (e.g., air, leaves) have ratios for all compartments of exactly one (meaning the results for the two runs are identical). Furthermore, the largest ratios are found in compartments that are expected, based on the results of the dynamic simulation, to take much longer than 30 years to reach steady-state (e.g., root, vadose zone soil). Therefore, when TRIM.FaTE is supplied the exact same constant inputs for both steady-state and dynamic modes, the steady-state concentration is always equal to or greater than the average dynamic concentration, as would be expected, and the magnitudes of the differences appear to be logical.

Likewise, the differences between the dynamic results and dynamic with steady-state inputs results should be strictly due to the approximation of time-varying inputs with constants in the latter simulation. Both simulations used TRIM.FaTE’s dynamic mode and ran for 30 years with the same configuration, except the dynamic with steady-state inputs simulation used constants instead of time-varying values for the properties listed in Exhibit 4-1. With a few exceptions (e.g., air compartments), the dynamic with steady-state inputs results are generally higher than the dynamic results and there appears to be a spatial pattern in the ratios of these results for the individual compartments (see Appendix C.3). The ratios of dynamic with steady-state inputs results to dynamic results are consistently highest to the south and east of the facility and lowest to the north and west.

The differences between the dynamic and dynamic with steady-state inputs simulations appear to be driven, at least in part, by the combination of the constant advective transfers between air compartments and the constant precipitation rate used in the dynamic with steady-state inputs simulation. For both simulations, the primary route for transport of mercury from air to surface soil and surface water is wet deposition. Several of the primary inputs used in calculating when, where, and how much wet deposition will occur (i.e., precipitation rate, wind speed, and wind direction) are time-varying inputs for which constant approximations were used

in the dynamic with steady-state inputs simulation. The methodology used to approximate these constant values did not account for the possibility that there may be a correlation between rain events and wind direction.

Further analysis of the dynamic meteorological data indicates that in fact the overall predominant wind direction is not the same as the predominant wind direction when it is raining (i.e., the predominant wind directions are from the south and northwest, and the predominant wind directions when it is raining are from the south and east). As expected based on these findings, the highest total mercury concentrations in air occur to the east of the source and the highest deposition occurs to the north and west of the source. The predominant wind direction in the dynamic with steady-state inputs simulation is roughly from the northwest (based on the amount of total mercury in the air advection sinks), which is consistent with the predominant wind direction in the dynamic simulation and reasonable considering the methodology used to estimate the constant advective transfers in this simulation (see Appendix C.1 for an explanation of this methodology).

Based on these results, there appears to be a correlation between wind direction and precipitation in the dynamic meteorological data that may not have been captured in the estimation of the precipitation rate and constant advective transfers between air compartments for the steady-state inputs. Because the dynamic with steady-state inputs simulation uses a constant precipitation rate, it is likely that more deposition occurred in the direction of the predominant winds (i.e., towards the southeast of the source) in this simulation. The increased deposition in the dynamic with steady-state simulation may explain the higher concentrations in soil and surface water and lower concentrations in air in this simulation because more chemical mass is being removed from the air and deposited onto the soil and surface water than in the dynamic simulation. Furthermore, because the spatial layout used in this scenario is not symmetrical and includes more parcels (and covers more distance) to the southeast of the source, more mercury accumulation occurred within the modeling domain in the dynamic with steady-state inputs simulation. This is consistent with the fact that the concentrations in surface soil, surface water, and biotic compartments that are closely tied to surface soil and surface water are generally higher in the dynamic with steady-state simulation than in the dynamic simulation.

Overall, the steady-state mode appears to be operating as expected based on these comparisons. When identical inputs and algorithms are used to run TRIM.FaTE in steady-state and dynamic modes, the ratios of the steady-state results to the comparable dynamic results seem reasonable. However, it appears that the methodology for estimating constant values for time-varying inputs, particularly estimation of the constant advective transfer factors for air and the precipitation rate, might not be fully capturing the variations in and correlations between the time-varying properties. Replacing time-varying values with constant values within a complex model is quite complicated and additional research may be needed to determine if there are methods that could be used to more accurately capture these temporal variations with constant values. Nevertheless, these comparisons show that the steady-state results for the mercury test case, as a whole, approximate the dynamic results well enough that sensitivity results generated using the steady-state mode can be generalized to dynamic scenarios, although these results will not capture any changes in model sensitivity over time. However, because some compartments, such as sediment and vadose zone soil, may take thousands of years to reach steady-state, the

steady-state results may not be appropriate for evaluating impacts on compartments that are not expected to reach steady-state within the expected duration of the emission source.

5. SENSITIVITY ANALYSIS

This chapter presents an evaluation of the sensitivity analysis performed for the mercury test case using TRIM.FaTE. The main purpose of this evaluation is to answer the following questions.

- Which properties have the largest influence on model results?
- Are the findings consistent with expectations based on the algorithms used in the simulation and the natural processes being modeled?

To evaluate their relative importance, the properties included in the analysis were ranked on the basis of their influence on or contribution to the variation in model outputs. This analysis and the resulting rankings will help in prioritizing future data collection efforts for similar TRIM.FaTE applications. Further, the results of this sensitivity analysis were evaluated to determine if they are consistent with expectations based on the scientific principles underlying the model. Unusual results were investigated to determine if they point to deficiencies in the model algorithms or selected input values.

This chapter begins with a description of the analysis design and methodology (Section 5.1). Then, Section 5.2 describes the most influential properties with regard to mercury concentration in selected compartment types. The input properties that are influential with regard to mercury concentration in a number of different compartment types are described in Section 5.3. Section 5.4 provides a brief summary and a discussion of possible follow-up sensitivity analyses. For additional description of the input properties used in TRIM.FaTE, along with a key between common names used for properties and their TRIM.FaTE code names, see Module 16 of the *TRIM.FaTE User's Guide* (EPA 2003b) and the technical support documents (EPA 2002b,c).

5.1 Analysis Design/Methods

The sensitivity of model outputs to changes in approximately 800 properties relevant to the mercury test case simulation was assessed in this analysis. The properties included in the analysis all use numeric values (versus equations) in the mercury test case, and so are sometimes referred to as “input” properties. A complete list of the properties assessed is provided in Appendix D.1.¹ The impact of changes to the values of these properties on model predictions is estimated by performing a TRIM.FaTE simulation for each model input property in which the value of the property is varied and comparing the results of that simulation with results from the base case simulation (i.e., the simulation using all original/unchanged property values). The

¹ All TRIM.FaTE numerical input properties relevant to the mercury test case scenario were included in the sensitivity analysis, with a few exceptions: (1) spatial layout inputs, such as volume element depth, (2) inputs that are fractions that sum to 1.0, such as diet fractions for animals, and (3) convergence properties for the differential equation solver. Time-varying inputs, such as rainfall rate, were included as constant values, as explained in Chapter 4 and Appendix C.1. Of the more than 1,000 input properties varied as part of the sensitivity analysis model runs, approximately 800 are applicable to the compartment types selected for assessment and are listed in Appendix D.1.

theoretical approach for this sensitivity analysis is described in more detail in Chapter 6 of Volume I of the *TRIM.FaTE Technical Support Document* (EPA 2002b).

This sensitivity analysis was performed for emission case B (source emissions of both divalent and elemental mercury, no boundary contributions or initial concentrations) using TRIM.FaTE's steady-state mode and the scenario described in Chapter 4 and Appendix C.1.² The steady-state mode was selected for this analysis because of its much faster execution time (several minutes compared to several days for the dynamic mode) and the large number of simulations needed for this analysis (over 1,000, one for each property varied). As described in Chapter 4, the steady-state configuration of the mercury test case site approximates the results of the dynamic simulations well enough that the results from this analysis can be generalized to dynamic scenarios and provide a reasonable basis for evaluation of the most influential input properties for the mercury test case. Limitations in using the steady-state mode are discussed in Section 5.1.4.

5.1.1 How Input Values Were Varied

As described above, one TRIM.FaTE simulation was performed for each mercury test case input property varied in the sensitivity analysis. In each simulation, the base value of one of these properties was reduced by **one percent** and the resulting changes in output values were recorded. This amount of variation was chosen because it keeps most properties within their range of reasonable values and introduces enough variation to reveal an effect if there is one.³ The values for each property were varied simultaneously in all compartments (i.e., all locations) where they are used. For example, values for the water temperature property were varied in all water bodies in a single simulation instead of performing separate simulations for each water body.

5.1.2 Measures of Sensitivity

After the TRIM.FaTE simulations (one for each input property varied) were completed, the outputs were compared to the outputs from the base case to produce measures of the change in TRIM.FaTE results associated with changes in each of the property values. Two measures of sensitivity, the elasticity and the sensitivity score, were calculated by TRIM.FaTE from the results of these simulations. Elasticity indicates “structural” sensitivity, while sensitivity score

² The sensitivity analysis model runs were completed a few months earlier than all the other model runs described in this report, and there are differences in one algorithm (mercury uptake by algae from surface water) and a few input values (mercury uptake rate by algae, soil ingestion rate for five animal species). Moreover, a different set of wind data was used. However, the steady-state modeling scenario used for the sensitivity analysis is judged to be appropriate for evaluating the relative influence of different properties on the model results, though care should be taken when interpreting results related to algae uptake and soil ingestion (e.g., properties related to algae uptake may be more influential than indicated here because of subsequent changes to the mercury uptake by algae algorithm).

³ Although varying property values by a larger percentage or in the opposite direction (i.e., positive relative to the base value) could possibly generate additional useful results, such investigations were beyond the scope of the current analysis, and one percent was determined to be adequate for the current analysis. In addition, it was anticipated that an input variation of one percent would result in a model response that was approximately linear (the elasticity, as calculated for this analysis, is based on the assumption that the input-output relationship is linear).

indicates “actual” sensitivity after accounting for the estimated variability in an input property. The elasticity provides information useful for understanding how the model operates and is used to compare with expected results, given knowledge of the model and the processes being simulated. The sensitivity score is useful in the context of assessing the influence of input properties, or how the variability of the input property affects the variability of the results.

For this report, calculations of elasticity and sensitivity score were based on the mercury **concentration** results. TRIM.FaTE also has the capability to produce these calculations based on either mercury mass or moles results (TRIM.FaTE mass transfer and transformation calculations are performed on the basis of moles). Sensitivity analysis results are the same for moles and mass (except for the molecular weight property, which is used to convert moles to mass), but results calculated based on concentration differ for any properties used in the conversion from mass to concentration, which varies for different compartment types. For example, for surface soil the concentration-based results differ from the mass-based results for properties included in the conversion, including solids density, soil water content, and soil air content. Therefore, in interpreting the results presented in this chapter, it is important to keep in mind that they are based on mercury concentrations.

Elasticity is the percent change in a model output value resulting from a one percent change in the value of a particular property, with all other properties unchanged. A positive value of elasticity results from an increase in an input value giving an increased output value, or a decrease in an input value giving a decreased output value. A negative value of elasticity means that an input increase resulted in an output decrease, or vice-versa. The equation for elasticity is provided below.

$$Elasticity = \frac{\frac{\Delta y}{y^0}}{\frac{\Delta p}{p^0}}$$

where:

y^0	=	model output value, base case
Δy	=	change in model output value
p^0	=	model input property value, base case
Δp	=	change in model input property value

For example, if a decrease of 1.0 percent in the input property “algae growth rate” results in a 1.1 percent increase in methyl mercury concentrations in fish, then the elasticity is -1.1.

The **sensitivity score** is the elasticity weighted by a normalized measure of the variability and/or uncertainty of the model input property, which takes the form of a normalized range or normalized standard deviation of the input property. It provides a measure of the variation in the output value resulting from the natural variability and uncertainty of the input property by weighting the elasticity by the coefficient of variation (CV) of the input property. The CVs quantify the degree of natural variability of the input property and the uncertainty of the estimate

of the input property. It is equal to the standard deviation divided by the mean of the property, where the standard deviation reflects both variability and uncertainty. The equation for sensitivity score is provided below.

$$\text{Sensitivity Score} = \frac{\Delta y}{\Delta p} \times \frac{p^0}{y^0} \times CV$$

where:

- $\Delta y/\Delta p$ = change in output y per change in input p
- p^0/y^0 = ratio of base case values of the input (p) and output (y)
- CV = coefficient of variation of input p (standard deviation/mean)

The CVs were estimated for each of the model input properties analyzed. Where available, CVs from the literature were assigned to the model input properties. The remaining properties were assigned to classes (i.e., A, B, C, or D) according to their estimated degree of combined variability and uncertainty. Quantitative values for these estimated CVs were assigned according to Exhibit 5-1. Note that these are preliminary estimates of CVs, which can be refined as additional information becomes available.

Exhibit 5-1
CVs Assigned for Each Class of Properties

Variability and Uncertainty	CV Class	CV Value
Low	A	0.05
Moderate	B	0.3
High	C	1.0
very high	D	3.0

The discussion of the sensitivity results in this report focuses on the elasticity estimates because they provide an assessment of the impact each input property has on the model outputs without being affected by the CV estimates, many of which are based on professional judgment. Sensitivity scores are provided in Appendix D.2 for all properties assessed.

5.1.3 Limitations

As described above, the design of this analysis involved varying input property values by a set percentage of their nominal values and comparing the resulting outputs to the base case outputs. This approach is not amenable to assessing the sensitivity of model outputs to model structure (e.g., the overall mass balance design of TRIM.FaTE), formulas or algorithms, or spatial layout of the scenario. In particular, although the TRIM.FaTE sensitivity analysis feature

has capabilities that allow examination of some of these kinds of user inputs,⁴ the sensitivity analysis performed for the mercury test case and described here does not address:

- Model algorithms (e.g., alternative formulations for a given process);
- Spatial layout of the scenario (i.e., size, shape, orientation, and number of parcels; dimensions and numbers of volume elements; links between compartments);
- Ecosystem and food webs defined by the user;
- Time-varying inputs;
- Inputs that are fractions that sum to 1.0, such as diet fractions for animals;
- Step function inputs (e.g., chloride and pH in the formula for partitioning of mercury in surface water with algae); and
- Convergence properties for the differential equation solver.

This sensitivity analysis also does not explicitly address correlations among model input properties, although a number of likely correlations are recognized in the analytic design (e.g., in the development of certain steady-state input values for time-varying properties; see Appendix C.1) and some are discussed in the results section. Also, because the sensitivity analysis is conducted around a single point (i.e., using a constant nominal value for each parameter, which may exist within the parameter space for a short time), the interpretation of the results is technically limited to the specific conditions of the simulation. Furthermore, inputs applicable only to compartment types not included as endpoints for this assessment (e.g., macrophytes, roots and stems, various animal species) are not addressed.

In addition, there are some limitations imposed by the use of the steady-state mode. A steady-state approach by definition cannot evaluate the sensitivity of results for different years or seasons. Further, inherent in our use of the steady-state mode here is the presumption that sensitivity results for the steady-state mode are informative to the dynamic mode, and that the steady-state scenario developed truly represents the steady-state form of our dynamic scenario (see Chapter 4 and Appendix C). The sensitivity to changes in time-varying input values (e.g., changes in precipitation rate) and to the resolution of input data time steps (e.g., meteorological data) cannot be evaluated using the steady-state mode.

For example, *AllowExchange* properties for the terrestrial plant compartment types are specified as 0 or 1 (and can switch back and forth) for the duration of a dynamic model run. These properties are assigned a constant, intermediate value for the purpose of steady-state model runs. Specifying a percentage change in the constant value does not make mechanistic

⁴ For example, the TRIM.FaTE sensitivity analysis can be run in dynamic as well as steady-state mode, and in dynamic mode the sensitivity of outputs to time-varying inputs can be assessed. Also, different kinds of sensitivity analyses using TRIM.FaTE could be designed to assess changes in step function inputs or spatial layout.

sense in the dynamic context. However, the sensitivity analysis results for *AllowExchange* properties give clues about how the model would respond to changes in times or dates on which processes are turned on or off (e.g., litter fall).

5.1.4 Endpoints Analyzed

The mercury test case includes 417 abiotic and biotic compartments, 33 of which were selected for analysis of sensitivity results (Exhibit 5-2).⁵ Compartments were selected to provide

**Exhibit 5-2
Output Compartments Selected for Analysis of Sensitivity Results**

Compartment Type	Compartments ^a
<i>Abiotic</i>	
Air	ESE1, SSE1, SSE3
Soil	SSE4, SW2
Surface water	River, Swetts Pond
Sediment	River, Swetts Pond
<i>Terrestrial Plants</i>	
Leaf - coniferous forest	SSE4
Leaf - grasses/herbs	SW2
<i>Terrestrial Biota</i>	
Herbivore (white-tailed deer)	SSE4, SW2
Omnivore (mouse)	SSE4, SW2
Soil detritivore (earthworm)	SSE4, SW2
<i>Semi-aquatic Biota</i>	
Piscivore (common loon)	River, Swetts Pond
Omnivore (raccoon)	SSE4, SW2
<i>Aquatic Biota</i>	
Water-column carnivore	River, Swetts Pond
Water-column omnivore	River, Swetts Pond
Water-column herbivore	River, Swetts Pond
Benthic carnivore	River, Swetts Pond
Benthic omnivore	River, Swetts Pond
Benthic invertebrate	River, Swetts Pond

^a See Exhibits 2-1 and 2-2 for maps of compartment locations.

⁵ Note that results were generated by TRIM.FaTE for all 417 compartments in these sensitivity simulations; however, measures of sensitivity were only estimated and analyzed for the 33 selected compartments.

breadth of coverage across the different media, with consideration of how the compartments interact, and with a focus on the aquatic food chain because it is of particular interest for this analysis. In total, 17 different compartment types are included (note that the two different vegetation types included for leaf, coniferous forest and grasses/herbs, are counted here as separate compartment types). Two different locations were selected for each compartment type, except three for air and one for each of the two leaf compartment types. Results were analyzed for elemental mercury (Hg^0), divalent mercury (Hg^{2+}), and methyl mercury (MHg), except that elemental mercury was not analyzed for the three water-column fish compartment types because of its extremely low modeled concentrations.

5.2 Influential Input Properties for Individual Compartment Types

A review of the elasticity values for the relationship between individual properties and the model results for specific compartment types of interest can provide confidence in how the model is performing. This section discusses the most influential properties, as defined by absolute elasticity values, with regard to model results for the compartment types selected for evaluation (see Exhibit 5-2). Each subsection focuses on a particular compartment type or group of compartment types and includes one or more exhibits presenting those properties for which elasticity values are above 0.1 (absolute value). In this chapter, the focus is primarily on the compartments associated with surface parcel SW2 or Swetts Pond, although other locations are discussed as appropriate. For a more detailed record of elasticities and sensitivity scores for all the compartments and mercury species examined, refer to Appendix D.2. Following the exhibit(s) in each section there is a discussion of the individual properties and what is known about their relationship to the compartment results (e.g., explaining why the elasticity values make sense, or in a few cases where further investigation may be needed to fully explain the results obtained).

5.2.1 Air

This section describes findings regarding the elasticity of the relationship between model properties and divalent and elemental mercury concentration results for three air compartments, SSE3 (overlies Swetts Pond), ESE1, and SSE1.⁶ An overview of the elasticity values for these air compartments is provided first, followed by a more detailed discussion of the chemical-specific elasticities for elemental and divalent mercury for these compartments.

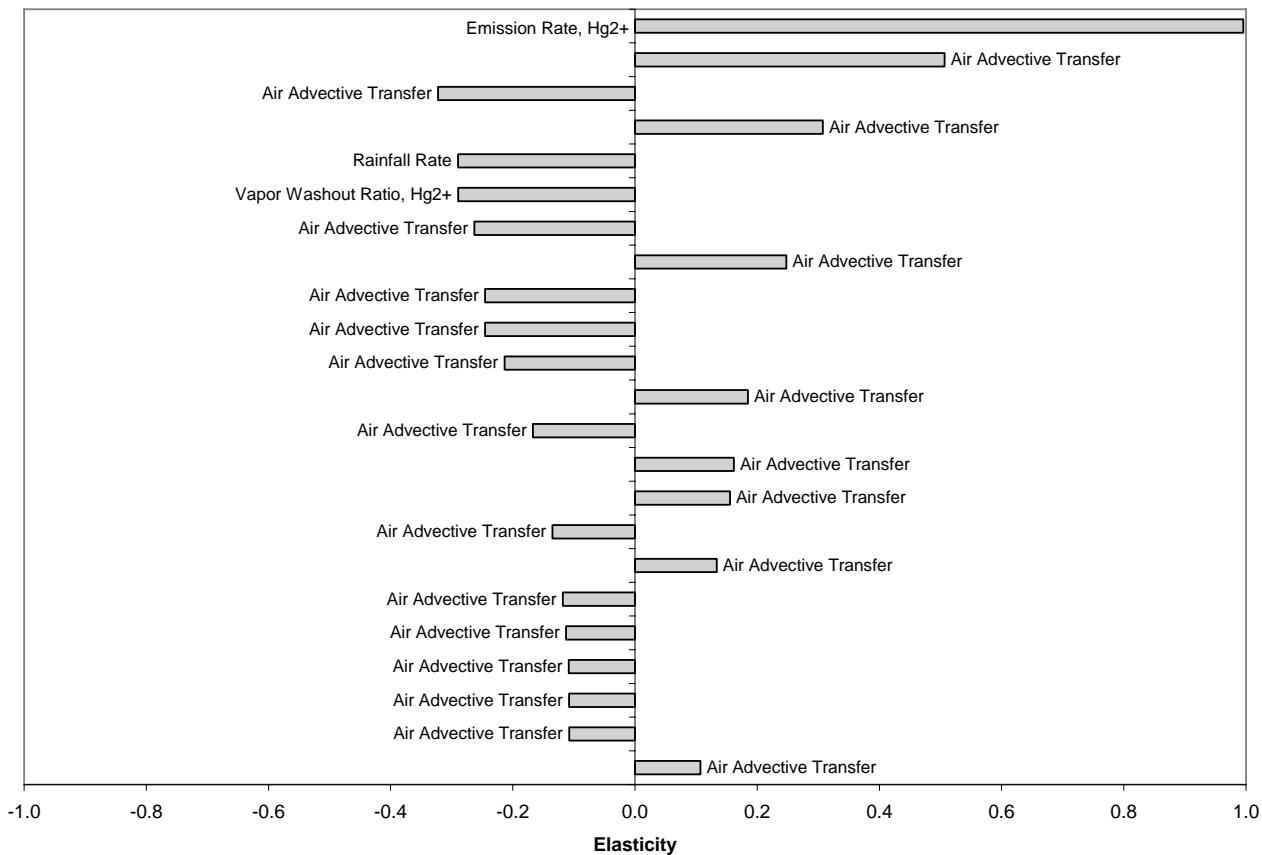
Overall Trends

For both divalent and elemental mercury concentrations in air, most of the properties with the highest elasticities are steady-state air advective transfers (referred to as air advective transfers on charts and remaining text) between various pairs of compartments. In Exhibit 5-3, this is illustrated for divalent mercury in the SSE3 air compartment. For divalent mercury, there are only three properties other than air advective transfers across all three locations (i.e., SSE3,

⁶ Sensitivity analysis results for methyl mercury in air are presented in Appendix D.2. In this and all following sections, the focus is on the dominant mercury species, in most cases divalent mercury. Results for the other mercury species are included in Appendix D.2.

ESE1, and SSE1) that rank among the top 30 properties with the highest elasticities (emission rate of divalent mercury, rainfall rate, and vapor washout ratio of divalent mercury). In these air compartments, emission rate of divalent mercury has the highest elasticity for divalent mercury concentrations. Similarly, emission rate of elemental mercury has the highest elasticity for elemental mercury concentrations in all three air compartments.⁷

Exhibit 5-3
Input Properties with Absolute Elasticity Value > 0.1 –
Divalent Mercury Concentration in Air Compartment SSE3



The sensitivity of the TRIM.FaTE air algorithms (and associated model outputs) to changes in the air advective transfer properties is not surprising because these properties – which are constants used in the TRIM.FaTE steady-state mode to represent time-varying wind speed and direction data (see Appendix C.1) – are the primary drivers of transport of chemical mass between air compartments.⁸ The range of elasticity values for these properties, which includes

⁷ Mixing height (i.e., height of the air compartment layer) would also be expected to have a high elasticity for divalent and elemental mercury concentrations because it directly influences the compartment volume (which, in turn, directly affects the predicted air concentration). As described above, however, none of the spatial properties were varied in the sensitivity analysis.

⁸ For the mercury test case, 124 air advective transfer properties were used: two for each internal boundary between air parcels (one in each direction), and one for each external boundary (outward direction only).

both positive and negative elasticities, is also not surprising. For example, a positive change in a particular air advective transfer property value would be expected to increase transport of mass from the sending to receiving compartment and thus result in an overall reduction in mass in the sending compartment (negative elasticity) and an overall increase in mass in the receiving compartment (positive elasticity). It is important to note, however, that the air advective transfer property values were varied one at a time. This approach does not fully represent the impact of changes in wind speed and/or direction because it only measures the impact of the change across **one** interface of a compartment, whereas a change in wind speed and/or direction would impact advection across **all** interfaces of that compartment. It is possible that this approach results in overestimating the maximum impact of these properties because it only captures, for example, an increase in chemical mass moving into a compartment across a particular interface (which would increase the compartment concentration and thus result in a higher elasticity) and not the associated increase in mass moving out of the compartment across another interface (which would decrease the compartment concentration and thus result in a lower elasticity). A more in-depth examination of the sensitivity of air concentrations to changes in wind speed and direction was beyond the scope of this initial, broadly scoped sensitivity analysis.

In the remainder of the exhibits in this chapter, the elasticities associated with all air advective transfer factor properties are combined into a single bar (instead of multiple bars, as presented in Exhibit 5-3) that extends from the most negative elasticity value associated with an air advective transfer to the most positive elasticity value, with a tick mark on the bar for each absolute elasticity value greater than 0.1. This provides a simple summary of the range of impacts associated with changes in these properties without obscuring the impacts of other properties. Although not as dominant as for the air concentration results, these properties are relatively influential for concentrations of most of the mercury species and compartment types examined, reflecting the importance of wind speed and direction for “downstream” media concentrations of mercury that originate in deposition from air. In most cases, the air advective transfer property results are not discussed further in the following sections about compartment types other than air, but the elasticity values are shown on the exhibits and in Appendix D.2.

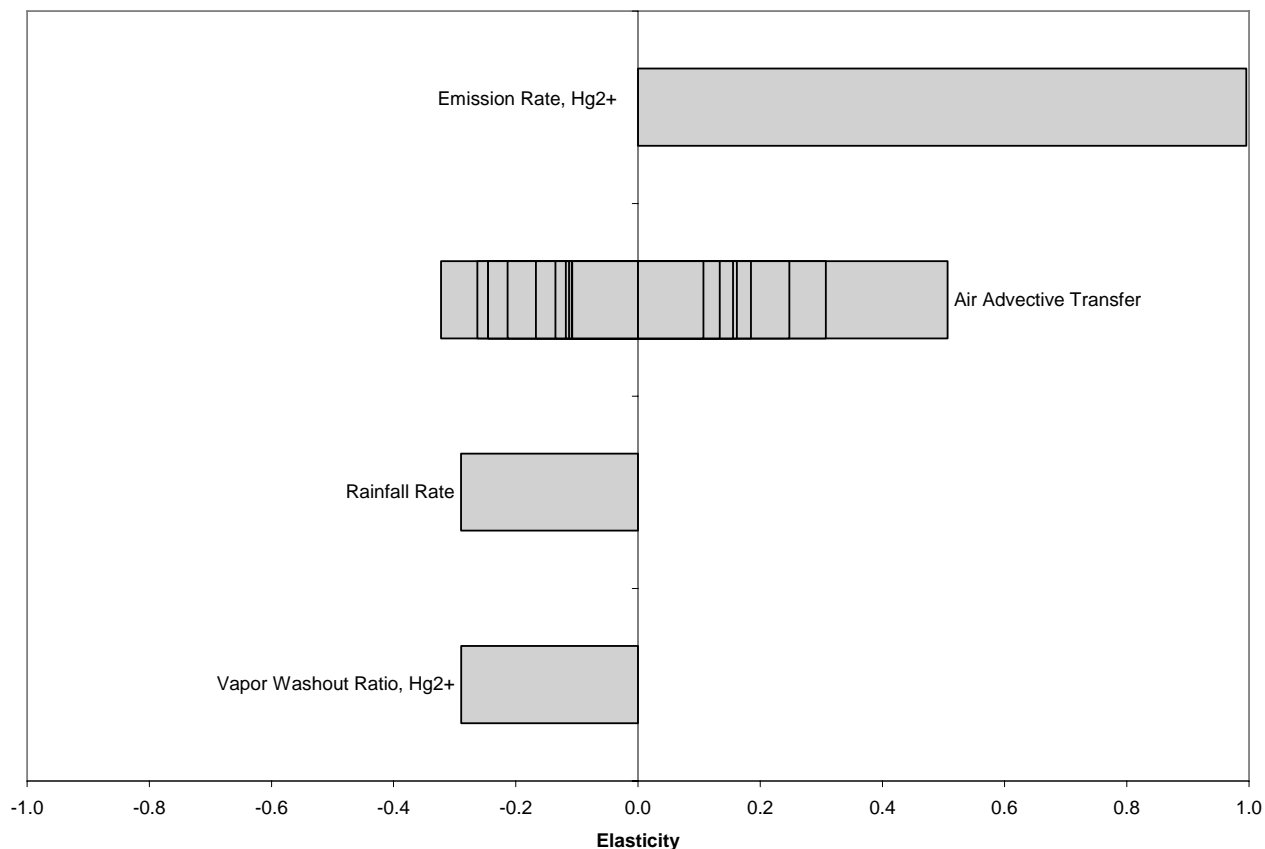
Divalent Mercury Concentration

As mentioned in the previous section, there are only three properties other than air advective transfers that rank among the 30 properties with the highest elasticities for divalent mercury concentrations in air compartments (emission rate of divalent mercury, rainfall rate, and vapor washout ratio of divalent mercury). The elasticity values for these three properties are much higher than those for any other properties (see Exhibit 5-4 for the SSE3 air compartment). Of these, emission rate has by far the highest elasticity value. The elasticities for rainfall rate and vapor washout ratio are identical, reflecting their multiplicative relationship in the equations where they both occur. These findings are consistent with the modeling of wet deposition as the dominant removal process (other than air advection, which is reflected in the air advective transfer properties) of divalent mercury in air and source emissions as the dominant addition process.

The elasticity for the relationship between the emission rate of divalent mercury and divalent mercury concentration in air is +1.0 for all three locations. As expected the elasticity is positive, which means as the emissions of divalent mercury increase, so do the divalent mercury

concentrations in air. The magnitude of the elasticity indicates that air concentrations of divalent mercury are directly proportional to emissions of divalent mercury (e.g., for every one percent increase in emission rate of divalent mercury, the concentration of divalent mercury in each of these three air compartments increases one percent).

Exhibit 5-4
Input Properties with Absolute Elasticity Value > 0.1 –
Divalent Mercury Concentration in Air Compartment SSE3 (Air Advective Transfers
Collapsed into One Bar)



The elasticities for rainfall rate and vapor washout ratio of divalent mercury are identical to each other at each location (-0.1 at SSE1, -0.12 at ESE1, and -0.29 at SSE3). The negative values are expected given that as the amount of precipitation increases, so does the wet deposition, which removes divalent mercury from the air. Likewise, as the vapor washout ratio increases, more divalent mercury is removed from the air by a given amount of precipitation and deposited. It also makes sense that the elasticities of these two properties are identical because they are both multipliers in the numerator of the wet deposition of vapor algorithm. The difference in elasticity values across the different locations may be related to the distance from the source (SSE3 is farther from the source than ESE1 and SSE1). As concentrations of divalent mercury decrease with distance from the source, the relative importance of properties related to deposition increases.

Elemental Mercury Concentration

The only property other than air advective transfers that ranks among the 30 properties with the highest elasticities for elemental mercury concentrations in air compartments is emission rate of elemental mercury. The absolute elasticity values for all other properties are less than 0.1. This suggests a simple modeling relationship for elemental mercury in air, with emission rate the single dominant factor (beyond the wind-related air advective transfer properties).

The elasticity for emission rate of elemental mercury is +1.0 for SSE1 and ESE1 and +0.99 for SSE3. The elasticity is positive, which means as the emissions of elemental mercury increase, so do the elemental mercury concentrations in air. Elemental mercury deposits from air at a much lower rate than divalent mercury (which explains why more elemental mercury, relative to the amount emitted, ends up in the air advection sinks than divalent mercury – see Sections 3.2 and 6.2.2 for additional discussion of relative deposition of different forms of mercury), and therefore deposition processes (and their associated properties) do not have a big impact on elemental mercury concentrations in air. Likewise, transformation processes do not have a substantial impact on elemental mercury concentrations in air, which is consistent with the low transformation rate used for elemental mercury in air. Therefore, it appears reasonable that the elemental mercury concentrations in air are not very sensitive to any properties other than emission rate and air advective transfers (i.e., removal of elemental mercury by processes other than air advection is minimal relative to the addition of elemental mercury).

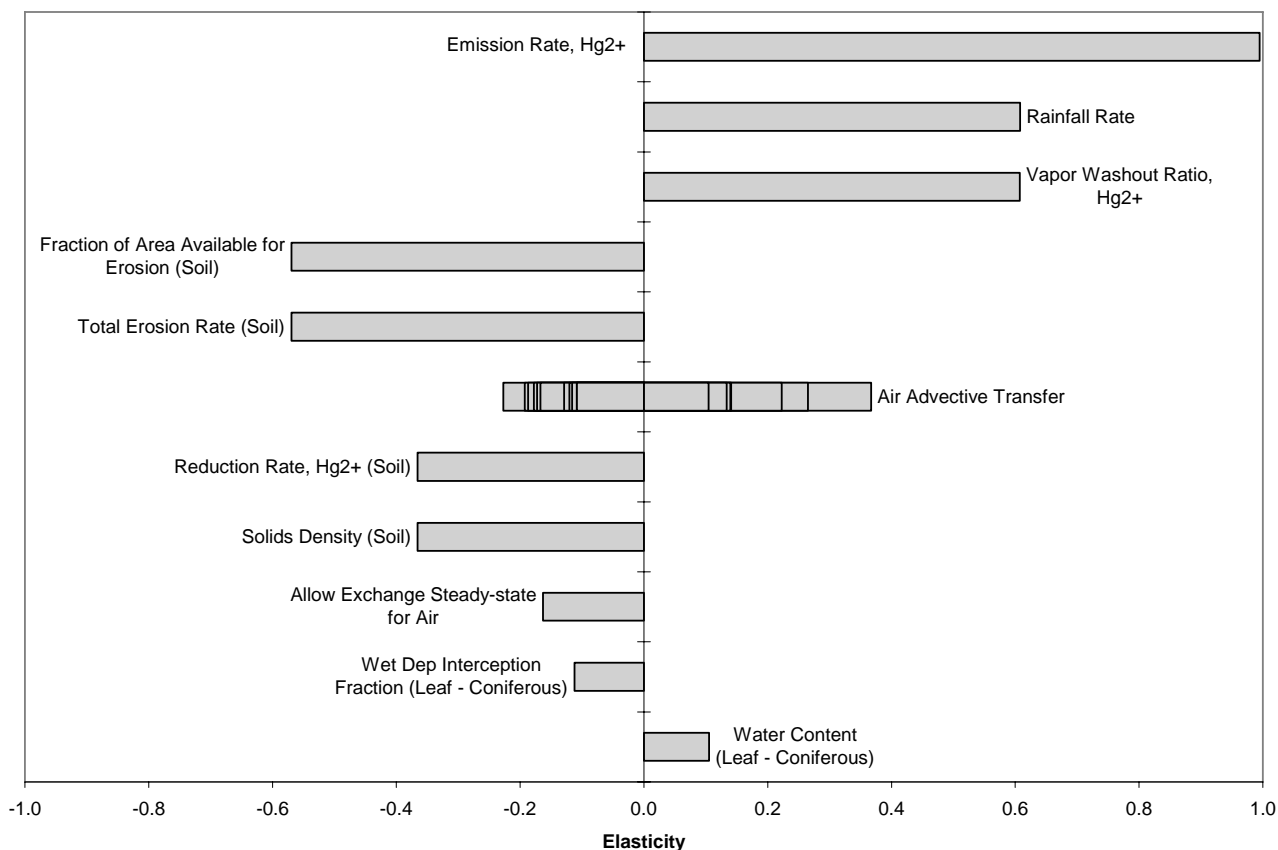
5.2.2 Surface Soil

This section describes findings regarding the elasticity of the relationship between input properties and divalent mercury concentration results in two surface soil compartments, SW2 and SSE4. Emission rate of divalent mercury has the highest elasticity value among the included properties for divalent mercury concentrations in the analyzed surface soil compartments. The next highest elasticity values are for two properties used to estimate wet deposition of vapor (rainfall and vapor washout ratio of divalent mercury) and two other properties used to estimate erosion of surface soil (fraction of area available for erosion and total erosion rate). The properties with the highest elasticity values are generally very similar between the two locations; however, the elasticity values are generally higher for results associated with the SSE4 surface soil compartment. All of the properties with absolute elasticities greater than 0.1 for divalent mercury concentrations in the SSE4 surface soil compartment are presented in Exhibit 5-5.

The properties exhibiting high elasticity values are logical, and those with the three highest values are also the three with highest elasticity for divalent mercury concentrations in the air compartments (see Section 5.2.1). The high, positive elasticity of divalent mercury in surface soil to the emission rate of divalent mercury (elasticities of +1.0 in SW2 and +0.99 in SSE4) appears to reflect the fact that the air is the primary source of chemical mass in soil. The second and third highest elasticity values are for properties that impact wet deposition, rainfall rate and the divalent mercury vapor washout ratio (both with elasticities of +0.69 for SW2 and +0.61 for SSE4). These properties have positive elasticities for divalent mercury concentrations in surface soil, whereas they have negative elasticities for air concentrations. This is consistent with the algorithms used because increasing these property values results in more removal from air

(therefore lower air concentrations) and more deposition to surface soil (therefore higher surface soil concentrations). The elasticities for these two properties are identical because they are both used as multipliers in the numerator of the wet deposition of vapor from air to surface soil algorithms.

Exhibit 5-5
Input Properties with Absolute Elasticity Value > 0.1 –
Divalent Mercury Concentration in Surface Soil Compartment SSE4



The properties with the next two highest elasticities, fraction of area available for erosion and total erosion rate (both with elasticities for divalent mercury of -0.56 for the SW2 surface soil compartment and -0.57 for the SSE4 surface soil compartment), play a role in the algorithms simulating pollutant transfers associated with erosion. These elasticities are negative, which means that increasing the amount of area from which erosion can occur or increasing the erosion rate results in a net reduction in the concentration of divalent mercury in surface soil compartments at these locations (although there is some gain and some loss). This is consistent with erosion as a loss process for surface soil compartments, although it is possible that for some compartments, depending on the spatial layout used and a particular compartment's location in the layout, elasticity values for these properties could be positive (i.e., erosion could be a net gain process for a given surface soil compartment). It is also reasonable that the elasticities for these properties are the same because they are both used as multipliers in the numerator of the same algorithms (i.e., erosion from surface soil to surface soil, surface soil sink, and surface

water). Their relatively high magnitude (especially compared to runoff-related parameters) appears reasonable given that divalent mercury in soil is mostly in the solid phase.

The properties with the sixth and seventh highest elasticity values for divalent mercury in surface soil are divalent mercury reduction rate (with elasticities of -0.38 in SW2 and -0.37 in SSE4) and solids density in surface soil (with elasticities of -0.38 in SW2 and -0.37 in SSE4). The elasticities to these properties are negative and approximately the same in both locations. Their magnitudes are identical, although this appears to be a coincidence as they are not used in the same algorithms. The negative elasticity for divalent mercury reduction rate is consistent with the algorithms used, in which a higher reduction rate equates to more divalent mercury transforming to elemental mercury, resulting in lower divalent mercury concentrations. The negative elasticity for solids density of surface soil is due to its use in the equation used by TRIM.FaTE to convert the surface soil outputs from moles (the units used internally by TRIM.FaTE) to concentration (in g/g dry weight). When elasticity for the solids density property is calculated based on divalent mercury moles in surface soil, the elasticity values are positive in both analyzed locations (+0.69 in SW2 and +0.63 in SSE4). The positive elasticities for solids density are consistent with how this property is used in algorithms associated with erosion (i.e., higher solids density results in a slower erosion velocity, which results in less chemical loss via erosion).

Starting with the ninth highest elasticity, the rank order of the properties becomes increasingly different for the two locations. Because many of these properties are involved in calculating mercury transfers involving plants, this could be related, at least in part, to the fact that the two parcels are assigned different types of vegetation (coniferous plants for SSE4 and grasses/herbs for SW2). The leaf properties *AllowExchange* for air (elasticity of -0.16 in SSE4 and -0.01 in SW2), wet deposition interception fraction (elasticity of -0.11 in SSE4 and -0.0085 in SW2), and water content (elasticity of +0.11 in SSE4 and +0.0054E-03 in SW2) are ranked between 8 and 10 for SSE4 and between 15 and 18 for SW2.

AllowExchange is a key property in the algorithms describing pollutant transfers involving plants. This property indicates the presence of viable vegetation and in a dynamic simulation is a time-varying value alternating between 0 (indicating dormancy) and 1 (indicating the growing season). For steady-state simulations, however, *AllowExchange* is set to a constant value between 0 and 1 reflective of the fraction of the year that plants exchange mass with other compartments (see Section 4.1). Therefore, vegetation with higher *AllowExchange* values in steady-state simulations receives more chemical mass via air deposition than vegetation with lower *AllowExchange* values. Specifically, an increase in *AllowExchange* for air for both locations/types of vegetation (coniferous and grasses/herbs) results in more interception of deposition by the plants, which increases the amount of accumulated mass in plants and decreases the amount deposited to surface soil. Thus, it is reasonable that elasticities for this property are negative in both locations. It also appears reasonable that the absolute value of the elasticity for SSE4 is greater than for SW2 because the value of *AllowExchange* for air is greater for SSE4. Several other properties (e.g., litter fall rate, wet mass per area) also have different values for the two vegetation types, which may also be contributing to the observed differences in elasticity.

Likewise, an increase in wet deposition interception fraction for both locations/types of vegetation (coniferous and grasses/herbs) results in more of the wet deposited divalent mercury being deposited to plants instead of soil, resulting in less divalent mercury depositing to soil and therefore lower soil concentrations. It is therefore reasonable that elasticities for this property are negative in both locations. It also appears reasonable that the absolute value of the elasticity for SSE4 is greater than for SW2. The SSE4 surface soil compartment (in which coniferous trees are located) has higher *AllowExchange* values than SW2 (in which grasses/herbs are located). This results in more interception by plants, relatively speaking, in SSE4 than in SW2. Thus, the same relative change (e.g., one percent) in wet deposition interception fraction in both locations would have a more substantial relative impact in SSE4 than in SW2, which is consistent with the results.

An increase in leaf water content for both locations/types of plants (coniferous and grasses/herbs) results in a decrease in the dry deposition interception fraction, resulting in more divalent mercury depositing to soil and therefore higher soil concentrations. Therefore, as expected, the elasticities for this property are positive at both locations. It also appears reasonable that the elasticity for SSE4 is greater than for SW2. Due to the differences in *AllowExchange* values for the two locations (described above), the same relative increase (e.g., one percent) in water content in both locations would have a more substantial relative impact in SSE4 than in SW2, which is consistent with the results.

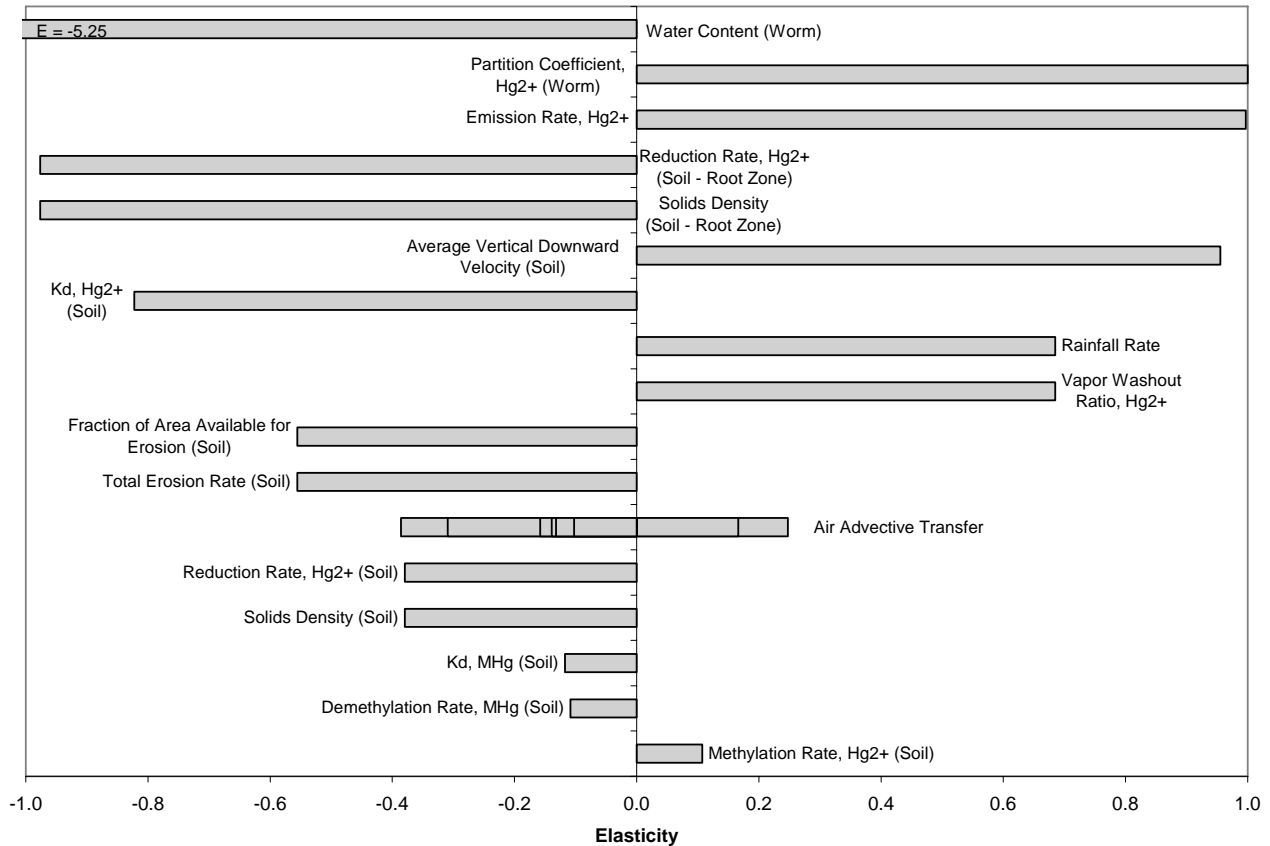
5.2.3 Earthworm

This section describes findings regarding the elasticities of the relationships between model properties and divalent mercury concentration results in the earthworm. The properties demonstrating absolute elasticity values greater than 0.1 for divalent mercury in the SW2 earthworm compartment are presented in Exhibit 5-6 and discussed below. Except for the first two, most of these are soil properties, reflecting the modeling approach based on partitioning of divalent mercury from soil to earthworm.

The most influential property affecting the concentration of divalent mercury in the earthworm, expressed on a wet-weight basis, is water content. The high negative elasticity for this property (-5.25) reflects the very strong influence of water content (percent water) on the wet-weight concentration of divalent mercury in worms. This property is used to convert the worm/soil dry-weight partition coefficient (a separate input property) to a wet-weight partition coefficient (higher water content yields lower wet-weight partition coefficient, hence the negative elasticity), which is then used to calculate the soil-to-worm transfer factor. The water content of earthworms in nature can vary substantially and is generally high (e.g., 80 to 85 percent; 84 percent is the base value for this scenario). The reason for the high magnitude of the elasticity relates to the form of the equation using water content – a $(1 - \text{water content})$ term is used as a multiplier – and the base value of 0.84. At this base value, a 1 percent reduction in water content results in a 5.25 percent increase in $(1 - \text{water content})$.⁹

⁹ Note that if TRIM.FaTE was designed to use as an input a partition coefficient based on lab-measured wet-weight soil and worm concentrations, the worm water content would have no influence on the wet-weight concentration of divalent mercury in the worm (assuming algorithms had not been added to correct for differences in water content for TRIM.FaTE soil and earthworm compartments compared with the original data).

Exhibit 5-6
Input Properties with Absolute Elasticity Value > 0.1 –
Divalent Mercury Concentration in Earthworm Compartment SW2



Following water content, the next two properties, the worm/soil dry-weight partition coefficient and the facility emission rate for divalent mercury, show equally high positive elasticities (+1.0). The worm/soil dry-weight partition coefficient is the property in TRIM.FaTE that defines the net extent of divalent mercury uptake by worms from the soils. Similar findings for facility emission rate (close to directly proportional effect of divalent mercury emissions on divalent mercury concentrations) are seen in other compartment types as well. This reflects the fact that facility emissions (no boundary contributions and no initial concentrations) are the only source of mercury to this simulation.

The root zone soil properties reduction rate and solids density both have high negative elasticities (-0.98) for divalent mercury concentrations in the earthworm. Higher values for the divalent mercury reduction rate in root zone soil result in lower amounts and concentrations of divalent mercury in the root zone soil, and less divalent mercury to partition into earthworms. The relatively high negative elasticity for solids density here is consistent with the relationship seen for this property in surface soil. At higher values for solids density in soil, concentrations

of divalent mercury in the soil on mass/mass-basis are lower (see Section 5.2.2).¹⁰ Hence, because the partitioning is modeled as a concentration-driven process, less divalent mercury partitions into earthworms.

The next four most influential properties on divalent mercury concentration in the earthworm (i.e., average vertical downward velocity, +0.96; divalent mercury Kd, -0.82; vapor washout ratio, +0.69; and rainfall rate, +0.69) reflect the propensity of divalent mercury to reach the root zone soil (three positive elasticities) and the propensity of divalent mercury to remain sorbed to surface soil particles (negative elasticity), and hence to remain in the surface soil layer rather than to move to subsurface soil layers via diffusion or percolation. At higher values for the average vertical downward velocity of water percolating through surface soil, the amount of divalent mercury reaching the subsurface soil layers (including the root zone soil layer where the earthworms are located in TRIM.FaTE) is larger; hence, the large positive elasticity. It is reasonable that Kd would have a relatively large negative elasticity because at higher values for divalent mercury Kd in surface soils, more divalent mercury is sorbed to surface soil particles, and less is available dissolved in water to percolate downward to the root zone soil. Additionally, it makes sense that both rainfall rate and vapor washout ratio have relatively high positive elasticities, as they do for surface soil. At higher values for both of these properties, the higher the amount of divalent mercury that is deposited to surface soils per unit time; hence, more divalent mercury is available for percolation to the subsurface soil layers, including the root zone layer, where some of it is available for uptake by earthworms.

Following these properties, the next four most influential properties (excluding air advective transfers, discussed in Section 5.2.1) on divalent mercury concentrations in earthworms are the fraction of area available for erosion, total erosion rate, solids density in surface soil, and divalent mercury reduction rate in surface soils. As the fraction of area available for erosion and the total erosion rate increase, the concentration of divalent mercury in surface soil decreases as more divalent mercury sorbed to surface soil particles is removed from a given surface soil compartment (for this particular compartment location, losses via erosion are greater than gains via erosion). Hence, less divalent mercury can percolate into the root zone soil layer, and a moderate negative elasticity (-0.56) for both properties results. Likewise, as the solids density and divalent mercury reduction rate in surface soil decrease, the concentration of divalent mercury in the surface soil increases. Hence, more divalent mercury can diffuse and percolate from the surface soil into the root zone soil, where it is taken up by earthworms, with a resulting moderate negative elasticity (-0.38) for both properties. Note that the reason surface soil solids density is influential on divalent mercury concentration in earthworms differs from the reason discussed in Section 5.2.2 for surface soil. Rather than being related to the units conversion from moles to dry-weight concentration (which uses solids density in the denominator), in this case the reason is that solids density is used in the denominator of the equation for Z_{solid} , which is then used to calculate Z_{total} , which is then used to calculate the effective advection rate from surface to root zone soil (see TRIM.FaTE TSD Volume II for more

¹⁰ The negative elasticity of solids density for divalent mercury concentration in soil is due to its use in the TRIM.FaTE equation that converts the surface soil outputs from moles (the units used internally by TRIM.FaTE) to concentration (in g/g dry weight).

details). Thus, higher solids density in surface soil yields lower advection (percolation) to root zone soil, which leads to lower divalent mercury concentrations in the earthworm.

The remaining properties with absolute elasticity values that exceed 0.1 are discussed below.

- The relatively small negative elasticity associated with the relationship between methyl mercury K_d in surface soil and the concentration of divalent mercury in earthworm (-0.12) is reasonable. At higher values of the methyl mercury K_d in surface soils, a higher proportion of the methyl mercury would be sorbed to soil particles. Although most of the mercury in surface soils is in the divalent form, a higher proportion of the methyl mercury in surface soil being sorbed to soil particles means less methyl mercury reaching the root zone soil layer where demethylation would convert it to divalent mercury.
- The small negative elasticity for demethylation rate of methyl mercury in surface soils (-0.11) seems puzzling initially. At higher rates of demethylation in surface soils, the amount of divalent mercury, the product of methyl mercury demethylation, also should be higher. Therefore, the amount of divalent mercury that reaches the subsurface layers would be expected to increase also. However, the K_d for divalent mercury (50,000) is much higher than the K_d for methyl mercury (3,000). Higher demethylation rates in surface soil means higher ratios of divalent to methyl mercury in surface soil, which means that less mercury overall is in the aqueous phase and available for diffusion or percolation to subsurface layers. Thus, less methyl mercury reaches the root zone, where it is available for transformation to divalent mercury and uptake into earthworms.
- At higher rates of divalent mercury methylation in surface soils, the proportion of mercury in surface soil that is in the divalent form compared with the methylated form is lower. Given the much higher K_d for divalent mercury than methyl mercury, as discussed above, at higher methylation rates the ratio of methyl to divalent mercury is higher, meaning that more mercury overall is in the aqueous phase and available for diffusion and percolation to the root zone soil layer. Thus, more methyl mercury reaches the root zone, where it is available for transformation to divalent mercury and uptake by the earthworm, resulting in a positive elasticity (+0.11). This is an inverse relationship to the one described above for demethylation rate.

5.2.4 Leaf

This section describes findings regarding the elasticity of the relationships between input properties and divalent mercury concentration results for the leaf compartments. Properties with absolute elasticity values greater than 0.1 for divalent mercury in the SSE4 leaf compartment (coniferous forest) and SW2 leaf compartment (grasses/herbs) are shown in Exhibits 5-7 and 5-8 and discussed below. For the most part, the same properties have absolute elasticity values greater than 0.1 for both vegetation types. Differences in elasticity between the two compartments are largely due to the different vegetation types, not the different locations. The two vegetation types have different base values for many of the compartment properties, such as litter fall rate, wet mass per area, leaf dimensions, and *AllowExchange*, and thus comparing leaf

Exhibit 5-7
Input Properties with Absolute Elasticity Value > 0.1 -
Divalent Mercury Concentration in Coniferous Forest Leaf Compartment SSE4

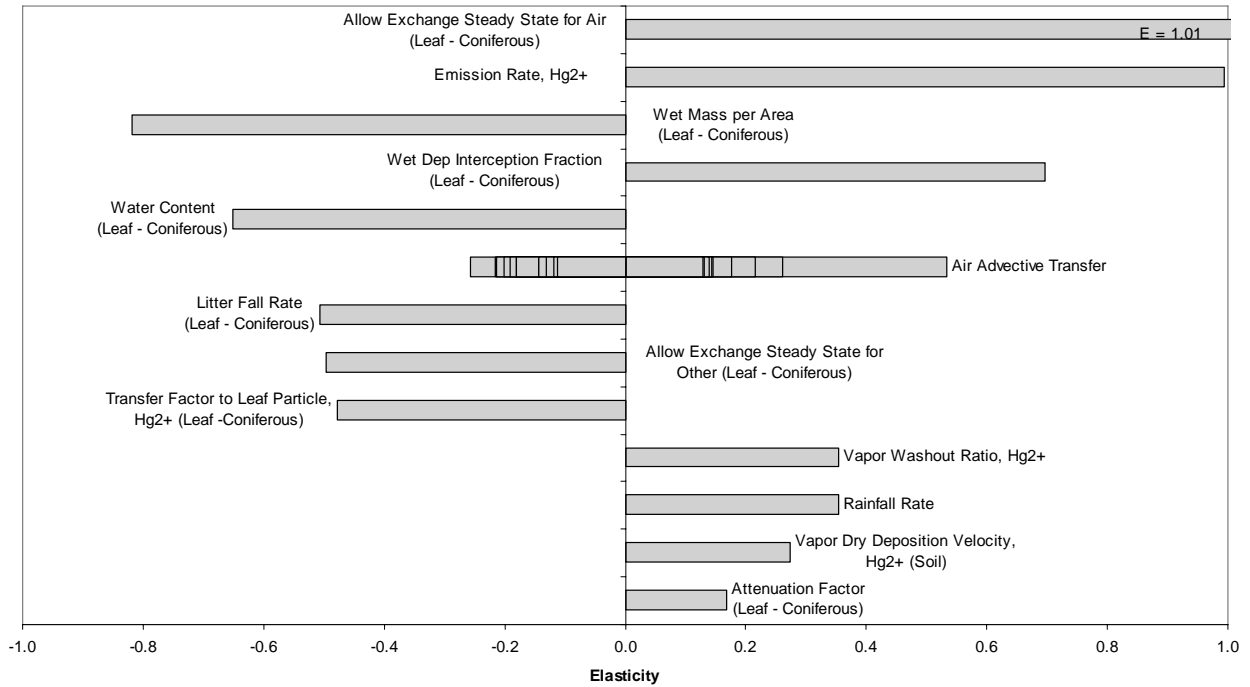
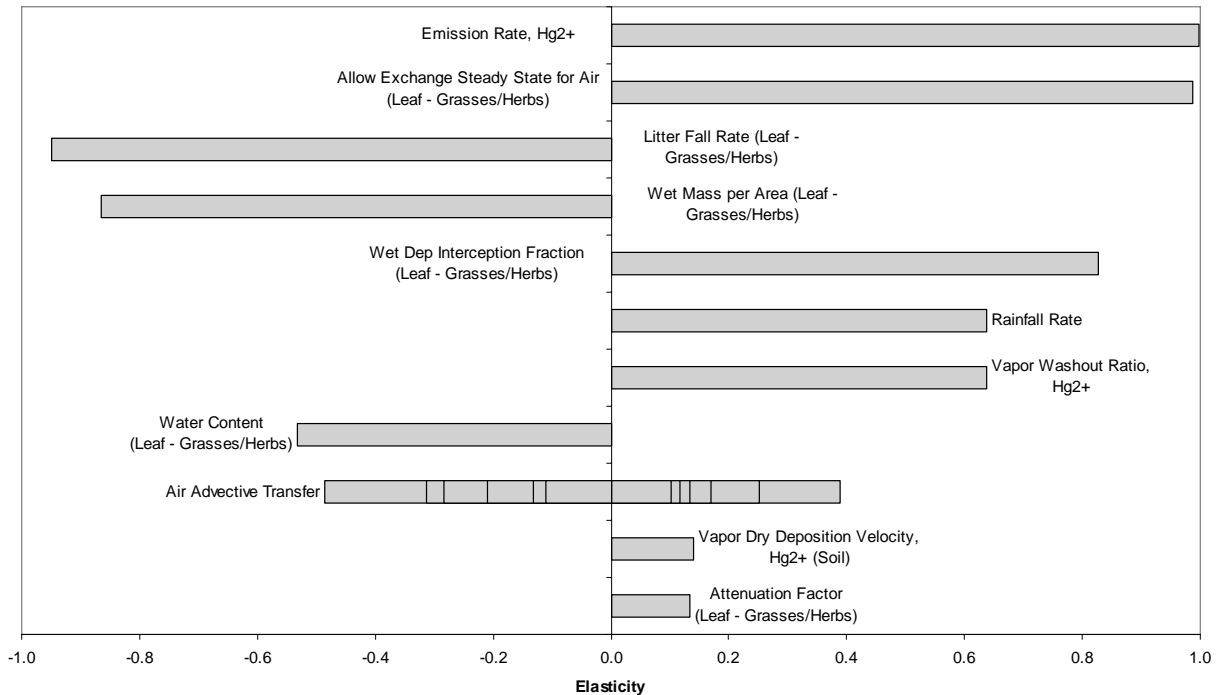


Exhibit 5-8
Input Properties with Absolute Elasticity Value > 0.1 -
Divalent Mercury Concentration in Grasses/Herbs Leaf Compartment SW2



results for these two locations is more like comparing the two surface water bodies (which have significantly different property base values) in Section 5.2.5 than like comparing the different locations for the other compartment types (e.g., air, surface soil, mammals).

The rank order of properties influencing the concentration of divalent mercury in leaves of grasses/herbs and coniferous forest compartments is consistent with expectations. As with other compartment types, the concentration of divalent mercury in the leaf is directly proportional to the facility emission rate of divalent mercury (i.e., +1.0 for both coniferous forests and grasses/herbs). The concentration of divalent mercury in leaves is also highly or moderately sensitive to wet mass per area (elasticity of -0.82 for coniferous forests and -0.87 for grasses/herbs); transfer factor to leaf particle (coniferous forest -0.48, grasses/herbs -0.05); litter fall rate constant (coniferous forest -0.51, grasses/herbs -0.95); and several other properties that control exchange of mercury between leaves and air under rain and non-rain conditions.

The wet mass per area property has a large negative influence on the concentration of divalent mercury in leaves. The larger the wet biomass of leaves per unit surface area, the lower the concentration of divalent mercury in leaves for a given deposition (and uptake) rate owing to dilution of mercury in the leaves by their increased biomass. Note that deposition of mercury from air to leaf occurs on a per-surface-area basis, not per-mass.

The elasticity for the transfer factor to leaf particle property is much larger for conifers than for grasses/herbs. This could possibly be due to the fact that the *AllowExchange* for other property value is higher for conifers (base value of 1.0 versus 0.386 for grasses/herbs), reflecting that coniferous leaves (needles) are present 12 months of the year whereas the leaves of grasses/herbs are present a fraction of the year. The *AllowExchange* for other property is a factor in all exchanges between leaf and non-air compartments, such as the leaf particle, herbivores, and stems. The elasticity for the litter fall rate property is higher for grasses/herbs than conifers, reflecting the six times higher base value used for grasses/herbs. For both vegetation types, as litter fall rate increases, the divalent mercury mass in the leaf compartment decreases (hence, the negative elasticity).

Several other properties that control exchange of mercury between leaves and air under rain and non-rain conditions also are influential on divalent mercury concentrations in leaves, including *AllowExchange* for air (coniferous forest and grasses/herbs, +1.0); wet deposition interception fraction (coniferous forest +0.70, grasses/herbs +0.83); vapor washout ratio and rainfall rate (coniferous forest +0.35, grasses/herbs +0.64); attenuation factor (coniferous forest +0.17, grasses/herbs +0.13); water content (coniferous forest -0.65, grasses/herbs -0.53); and vapor dry deposition velocity (coniferous forest +0.27, grasses/herbs +0.14).

5.2.5 Surface Water and Sediment

This section describes findings regarding the elasticity of the relationships between input properties and divalent mercury concentrations in surface water and sediment compartments. Properties with elasticity values greater than 0.1 for divalent mercury in Swetts Pond surface water and sediment compartments are shown in Exhibits 5-9 and 5-10, respectively. Elasticities relevant to methyl and elemental mercury in these compartments and to all three mercury species in the river surface water and sediment compartments are presented in Appendix D.2.

In the subsections that follow, properties are discussed in the following categories:

- (1) Properties with similar influence on divalent mercury concentrations in both surface water and sediment compartments; and
- (2) Properties with influence on divalent mercury concentrations in either surface water or sediment compartments (but not both).

Influential Properties in Both Surface Water and Sediment Compartments

All 18 properties that are influential on divalent mercury concentrations in surface water (i.e., elasticity greater than 0.1) are also influential on divalent mercury concentrations in sediment. These properties affect the overall input or removal of divalent mercury mass to the surface water/sediment system.¹¹ For all but the suspended solids particle density in surface water (represented by rho in the TRIM.FaTE library), these properties affect input to and removal of divalent mercury mass from the surface water, and the mass to/from sediment “follows” (chemical mass can only reach the sediment by traveling “through” surface water). Suspended solids particle density influences removal of chemical mass from sediment (see discussion further below) which in turn affects total chemical mass in the surface water/sediment system.

Eight properties that are influential on divalent mercury concentrations in both surface water and sediment compartments at Swetts Pond have elasticities that are similar to those observed for surface water and sediment at the river.

- The positive elasticity of nearly 1.0 associated with emission rate of divalent mercury is reasonable because the emission rate dictates the total mass of divalent mercury in the system. Divalent mercury is the species that dominates deposition, and therefore this species also drives the transfer of mercury mass from air to surface water/sediment systems. The positive elasticity near 1.0 indicates a directly proportional relationship.

¹¹ All references to surface water and sediment concentrations in this section refer to total (dissolved + sorbed to suspended or benthic sediment) chemical concentrations, unless otherwise specified.

Exhibit 5-9
Input Properties with Absolute Elasticity Value > 0.1 -
Divalent Mercury Concentration in Surface Water Compartment Swetts Pond

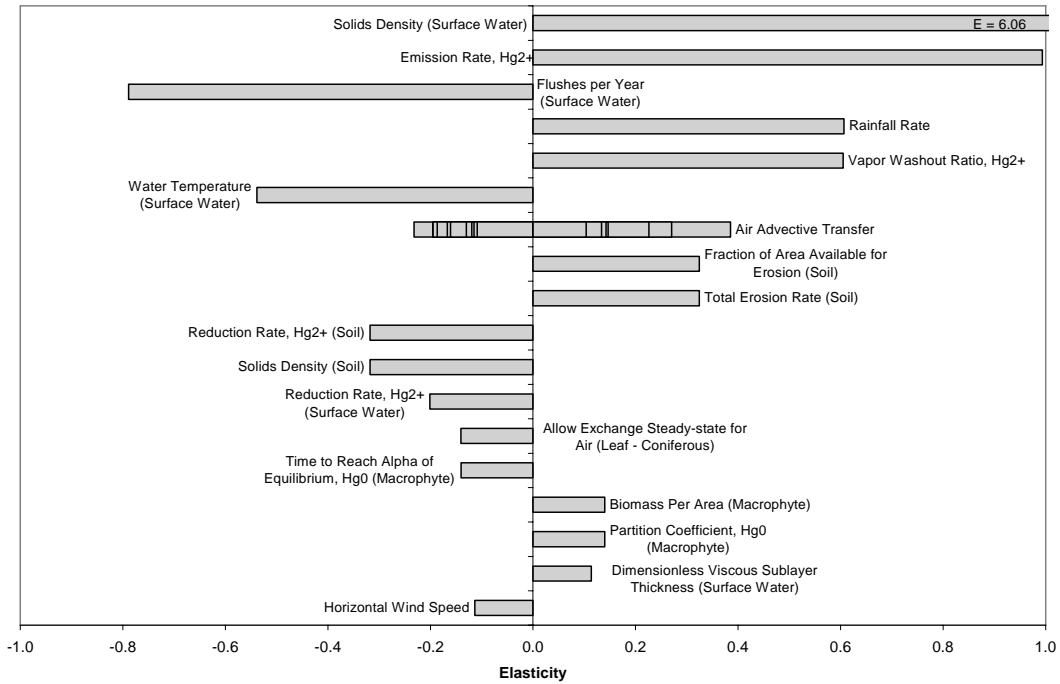
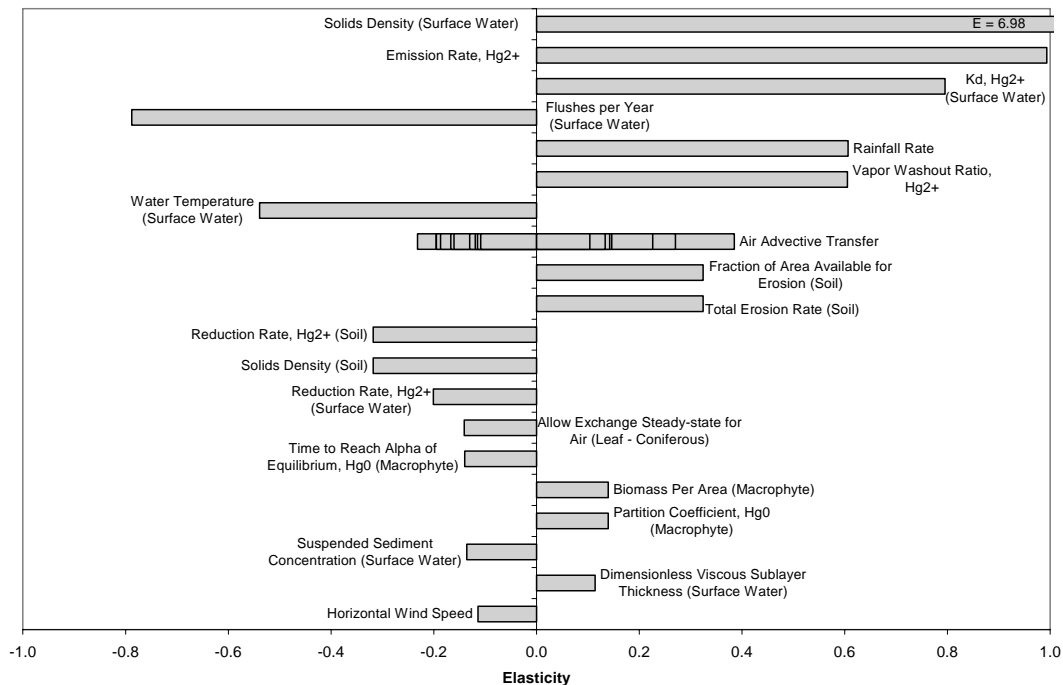


Exhibit 5-10
Input Properties with Absolute Elasticity Value > 0.1 -
Divalent Mercury Concentration in Sediment Compartment Swetts Pond



- Flushes per year of the surface water compartment has a large negative elasticity for both surface water and sediment compartment types. This is logical because this property directly affects the amount of mass removed from the surface water/sediment system. Higher elasticities were evident for this property in the river compartments with regard to divalent mercury (see Appendix D.2). This is consistent with the larger role of flushing in mercury removal from the river. Advection to a flush rate sink accounts for nearly 90 percent of the mass removal from river surface water but only 7 percent of the mass removal from Swetts surface water (not counting “removal” of divalent mercury via reduction reactions).
- Elasticities for rainfall rate and divalent mercury vapor washout ratio are positive and nearly identical for concentrations in surface water and sediment at Swetts Pond (and similar for Swetts Pond and river compartments). Two other properties – fraction of soil area available for erosion and total erosion rate – also have very similar positive elasticities for concentrations in both surface water and sediment. These results are consistent with expectations because input of divalent mercury to a given system is positively proportional to the transfers from air to surface water/surface soil driven by these properties (i.e., wet deposition of divalent mercury for rain and vapor washout ratio, as described in Section 5.2.1, and input to surface water from eroding soil for fraction of area available and total erosion rate, as described in Section 5.2.2).
- The negative elasticities for reduction rate in surface soil and soil solids density seem reasonable. The similarity of the elasticities for these two properties appears to be a coincidence as they are not used in the same algorithms. A decrease in the value for reduction rate would be expected to result in an increase in the amount of divalent mercury in surface soil available for transfer to the aquatic system. A decrease in solids density results in a higher erosion velocity, which results in more chemical transferred to the surface water via erosion. The elasticities for both of these properties – as well as fraction of soil area available for erosion and total erosion rate, which also influence concentrations in soil – are discussed in more detail in Section 5.2.2 (surface soil compartments). For solids density, note that although a negative elasticity is observed for this property for chemical *concentrations* in surface soil (due to the conversion from moles to concentration), a positive elasticity is calculated for chemical *moles* in surface soil. This results in the negative elasticities for these two properties for divalent mercury concentrations in surface water and sediment.

For these eight properties, the differences between the elasticities observed for divalent mercury concentrations in Swetts Pond and the river are small despite the differences in the configuration of each system. Differences between Swetts pond and the river include different input values for some water body characteristics that affect mass transfer rates (e.g., flush rate, suspended sediment concentration, and depth, which affects the surface area to volume ratio) and a different parcel layout (which in turn affects the surface area of soil comprising the effective watershed for the receiving surface water compartment). A plausible explanation for the similar elasticities may be that these eight properties all primarily affect processes that occur outside of the water body system (i.e., transfers from air to surface soil/surface water; transfers from surface soil to surface water, primarily through erosion). The exception to this is flush rate,

which directly affects mass removal from the system, and for which the largest differences in elasticities were observed.

Six properties are relatively influential (i.e., absolute value of elasticity 0.1 to 0.5) for divalent mercury concentrations in Swetts Pond surface water and sediment but much less influential for divalent mercury concentrations in river surface water and sediment (i.e., elasticity absolute values less than 0.01). These include:

- Water temperature;
- Reduction rate of divalent mercury in surface water;
- Steady-state *AllowExchange* property for conifer leaf compartments (*AllowExchange* dictates active plant growth and presence of leaves);
- Time to reach alpha of equilibrium of elemental mercury in macrophyte;
- Biomass of macrophytes per area; and
- Partitioning coefficient for dissolved elemental mercury in the water column and macrophyte.

For all of these properties, elasticities for divalent mercury concentrations in surface water and sediment compartments in Swetts were very similar. In contrast to the eight properties discussed previously, these six properties all appear to influence processes that occur within the surface water/sediment system. Therefore, it seems reasonable that different elasticities for these properties are observed for Swetts Pond and the river due to the differences in the two systems (especially flush rate). Possible reasons for specific differences are discussed below.

The three properties related to macrophytes (partitioning time, biomass per area, and partitioning coefficient) are all involved in the uptake of mercury by macrophytes in the surface water, and the difference in values between locations suggest that this process is relatively more important for Swetts Pond than for the river. Indeed, the transfer rate of divalent mercury from surface water to macrophytes is about four times larger for Swetts Pond than the river and also comprises a much larger fraction of the total divalent mercury mass transfer out of surface water (35 percent of total transfer factor for mass transfer from Swetts Pond, versus less than 1 percent of transfer factor from the river, based on the detailed mass transfer output for the test case steady-state scenario). Reasons for the difference in surface water to macrophyte transfer rate (and presumably the reverse transfer as well, i.e., back into macrophytes) are not entirely clear but are quite possibly due to differences in residence time driven by the input value for flush rate (see next paragraph). Additionally, the total macrophyte mass is actually greater for the river (because the area of the surface water volume element is larger), but the dissolved fraction of divalent mercury mass in the surface water is greater and the total surface water volume is smaller at Swetts Pond (which would both result in increased transfer to macrophytes based on the use of these properties in this algorithm).

As noted previously, the input value for flushes per year is very different for these two locations (4.3 per year for Swetts Pond surface water, versus 531 per year for the river). This difference seems like a possible explanation for the difference in elasticities of these six properties with regard to divalent mercury concentrations in Swetts Pond and the river. For example, advective flushing to a sink is the dominant mass transfer process for removal of mercury from the river surface water compartments, and this contributes to lower residence times for mercury in the river (thus reducing potential for transfers into macrophyte or sediment). This explanation may also be relevant to the difference between the two systems with regard to elasticities for reduction rate (i.e., the residence time of mercury is much shorter in the river, and therefore reduction of divalent mercury is comparatively less in the river than in Swetts Pond). In short, the much larger water flow rate through the river system “swamps” other processes that are more important in the more static Swetts Pond.

AllowExchange of the conifer leaf compartments influences the amount of mercury transferred from air to the leaf compartment. As shown in Exhibit 5-5, this property inversely affects the amount of mass deposited to surface soil and that is then available for transfer to Swetts Pond surface water via erosion and runoff. It is hypothesized that differences in vegetation types (and the associated *AllowExchange* values) for the watersheds around Swetts Pond and the river may be a factor in the different sensitivities of model outputs to these properties for the two locations.

The higher elasticity for water temperature in Swetts Pond compartments (elasticity of -0.54 for divalent mercury concentrations in both surface water and sediment) than in river compartments (elasticity of -0.01 for both compartments) may be related to the classification of Swetts Pond as a lake rather than a flowing water body. The algorithms used for lakes to describe mercury transfers between air and surface water include a role for water temperature (i.e., Henry’s law constant and the water Schmidt number vary with temperature). An increase in water temperature results in a decrease in transfer from water to air (which matches the negative elasticity observed in this analysis). For flowing water bodies, a different algorithm is used that does not depend on temperature. However, it should be noted that diffusion to air comprises an extremely small fraction of the total divalent mercury mass transfer out of the surface water compartment at steady-state (less than 10^{-4} percent for both sites). Therefore, it is expected that these concentrations would be sensitive to water temperature via these processes only if the small change in temperature leads to an extremely large (relative) change in the transfer factor. Water temperature is also used in the algorithms for ingestion of food and excretion by aquatic biota (see Section 5.2.6), but it is not clear how these algorithms might affect Swetts Pond and the river differently. Overall, the reasons for the differences in elasticity for water temperature between the two systems may need further examination.

Solids density of suspended particles in surface water is a highly influential property (elasticities up to +6 and higher) for concentrations of divalent mercury in surface water and sediment compartments at Swetts Pond. Mercury concentrations in fish compartments and some biotic compartments that obtain their food from the aquatic environment (e.g., raccoons) are also highly sensitive to this property due to their relationship through the food chain to surface water and sediment concentrations. An investigation of TRIM.FaTE algorithms involving solids density in surface water suggest that the sensitivity of this property is a special situation related to the configuration of the TRIM.FaTE test case library (see accompanying text box). Although

not incorrect, these very high elasticities could be misleading if not interpreted in the context of this situation.

Solids density in surface water is much more influential for concentrations in Swetts Pond compartments than for river compartments. This suggests that sediment burial, which is affected by solids density in surface water, plays a larger role proportionally in removing mass from the surface water at Swetts Pond than at the river. This is consistent with the observation that advection via flushing plays a larger role in the river than in Swetts Pond and appears to swamp out some other processes.

Influential Properties in Sediment Compartment Type Only

Two properties were identified as particularly influential on divalent mercury concentrations in sediment but much less so on concentrations in surface water. It appears that these two properties directly influence processes that dictate chemical concentrations in sediment, whereas properties discussed previously in this section directly influence chemical concentrations in surface water (which then affect chemical concentrations in sediment via deposition/resuspension and other processes). Mercury concentrations in sediment seem to be closely correlated with concentrations in surface water but the reverse does not appear to be true. In other words, processes that directly affect chemical concentrations in sediment have much less impact on concentrations in surface water, probably because there are other, more dominant processes occurring in surface water.

K_d (partitioning coefficient) of divalent mercury in surface water is particularly influential for divalent mercury concentrations in Swetts Pond sediment but much less so and in a negative direction for surface water (elasticities of +0.8 for sediment, -0.04 for surface water). The directions of these results make sense because increasing K_d results in increased chemical sorption to the solid phase in surface water and therefore more divalent mercury mass available for transfer to the sediment via deposition from surface water. The much larger absolute elasticity for K_d for concentrations in sediment compared to concentrations in surface water also seems logical. The dominant mass transfer process that influences chemical concentrations in sediment is deposition (for which K_d directly affects amount of mass transferred), while the sediment resuspension that occurs in reverse may be less significant for surface water chemical concentrations relative to other processes that affect divalent mercury transfers into and out of the surface water. The elasticity for K_d is about twice as large for chemical concentrations in Swetts Pond sediment than those in river sediment. This may be due to the greater dominance of flush rate for the river with regard to mercury removal from the surface water, making it unavailable for transfer to the sediment. Conversely, transfer of chemical mass from surface water to sediment via deposition is more dominant (relative to total mass transferred out of surface water) in Swetts Pond than in the river. As a result, in Swetts Pond, a larger fraction of the total mercury mass in the system resides in the sediment (i.e., the sediment to surface water mass ratio is about four times larger in Swetts Pond than in the river), which is consistent with the higher sensitivity for K_d for Swetts Pond. More investigation is needed to fully explain these observations.

Solids Density of Suspended Particles in Surface Water

High elasticities for surface water solids density are related to the use of this property in the algorithm representing movement of mass from sediment to a sediment burial sink (i.e., “permanent” burial of chemical below the sediment layer). The TRIM.FaTE library for the mercury test case is set up to maintain a constant volume of unconsolidated benthic sediment in order to satisfy the condition that the depth of the volume element sediment layer remains constant. Any net increase in the volume of sediment particles added to the benthic sediment via deposition of suspended sediment in the surface water is offset by a corresponding transfer of sediment volume to a sediment burial sink representing the consolidated sediment. The chemical mass burial rate to this sink is in turn calculated based on the amount of chemical sorbed to benthic sediment particles.

In calculating mass transfers via sediment deposition, resuspension, and burial, several user-specified properties (i.e., sediment deposition velocity, suspended sediment concentration, benthic sediment concentration, solids density of suspended particles, and solids density of benthic sediment particles) are used to calculate resuspension velocity and volumetric deposition and resuspension rates. For the mercury test case, including the sensitivity analysis base case, sediment burial does not occur because (based on the user-specified property values used in the test case) the suspended sediment volumetric deposition rate is exactly equal to the benthic sediment resuspension rate. There is no increase in benthic sediment volume; consequently, sediment transfer to the burial sink (and the corresponding transfer of chemical mass) is zero.

For the sensitivity analysis, solids density in surface water is decreased by one percent while the solids density of benthic sediment particles remains the same. This difference in particle density (in combination with the formula properties used in the TRIM.FaTE library) results in a deposition rate greater than the resuspension rate. In order to maintain constant benthic sediment volume, the net difference is offset by a positive transfer of sediment to the sediment burial sink. As a result, mercury mass is also transferred from the benthic sediment to the sink, resulting in a net removal of chemical mass from the surface water/sediment system. The presence of this mass removal process results in a decrease in sediment and surface water concentrations that drives the high positive elasticity for surface water and sediment compartments (i.e., a decrease in solids density in surface water results in lower mercury concentrations in surface water and sediment compartments).

Separate test runs indicate that if the solids densities for both surface water and sediment are reduced in parallel, the elasticities of concentrations in Swetts Pond surface water and sediment are significantly less than the values obtained in the sensitivity analysis (elasticities of about +1.0 for sediment concentrations and +0.1 or less for surface water concentrations). This occurs because the volumetric deposition and resuspension rates are affected in the same proportions, and no sediment burial occurs (i.e., the transfer factor for the mass transfer to the sediment burial sink is zero). These results reflect the correlation between surface water and sediment solids density in the context of model sensitivity and suggest that the values for these properties should be selected carefully in any model applications.

Further testing indicates that the mercury test case scenario is not sensitive to *increases* in surface water solids density. In other words, the sensitivities of mercury concentrations in surface water, sediment, and other compartments to solids density in surface water are nonlinear around zero. This is the result of a conditional statement in the TRIM.FaTE algorithm for transfer to a sediment burial sink that prevents the calculation of a negative burial rate. If the volumetric resuspension rate is greater than the suspended sediment deposition rate – the condition that results from increasing surface water solids density – the model assumes a value of zero for sediment burial to prevent the occurrence of a negative transfer factor. Testing also confirms that surface water and sediment concentrations are sensitive to benthic sediment particle density by the same amount but in the opposite direction – in other words, increasing the sediment solids density by one percent results in larger elasticities for concentrations in surface water and sediment similar to those observed for a one percent decrease in surface water solids density.

Suspended sediment concentration in surface water is a relatively influential property on divalent mercury concentrations in the river sediment compartment but less influential on concentrations in Swetts Pond sediment (elasticities of -0.6 for river sediment, -0.14 for Swetts sediment). It is not intuitive why this elasticity is negative (i.e., a lower value for this property results in a higher divalent mercury concentration in benthic sediment). Possibly, the decreased suspended sediment in surface water might result in a shift in “loss” transfers from surface water from particle deposition to advection out of surface water to the flush rate sink. Alternatively, decreased suspended sediment in the surface water might result in less of the chemical remaining in the suspended sediment due to a decrease in surface area in suspended sediment, thereby resulting in more chemical mass transferred to the benthic sediment via other processes (i.e., diffusion and deposition of algae). This property is not influential for chemical concentrations in surface water in either system, possibly because sediment deposition/resuspension processes drive chemical concentrations in sediment, while other processes dictate chemical concentrations in surface water. Alternatively, the total chemical loss rate from surface water does not change but simply shifts some mass transfer from deposition (to sediment) to advection (to the sink). The difference between the river and Swetts Pond may be related to the input values assigned for suspended sediment concentration – the suspended sediment concentration in surface water is much larger for the river than for Swetts Pond (river > Swetts by 10 times). Consequently, the fraction of total divalent mercury mass in the surface water column that is sorbed to suspended sediment is greater at the river than at Swetts Pond. The different flush rates for these two systems may also play a role in the different elasticities that are observed. However, more investigation of the roles of specific processes and algorithms is needed to fully explain the elasticity values for this property.

5.2.6 Aquatic Food Chain

This section describes findings regarding the elasticities of the relationships between model input properties and methyl mercury concentrations in benthic invertebrates, benthic carnivores, benthic omnivores, water-column carnivores, water-column herbivores, and water-column omnivores in Swetts Pond. The properties demonstrating absolute elasticity values greater than 0.1 for methyl mercury in the Swetts Pond benthic invertebrate and water-column carnivore compartments are presented in Exhibits 5-11 and 5-12, respectively, and are discussed below. In comparison with the other TRIM.FaTE compartment types and mercury species examined, more properties are influential on methyl mercury concentration (i.e., absolute elasticity > 0.1) in the aquatic food chain compartment types.

The scenario analyzed included two independent food chains, a benthic food chain and a water-column food chain (see Appendix I-B in EPA 2002a). The benthic invertebrate compartment (Exhibit 5-11) represents the base of the benthic food chain. The water-column carnivore (Exhibit 5-12) is the top aquatic predator in the aquatic food chain.

This section is organized in four main parts by the type of property that influences the results: (1) abiotic properties, (2) properties related to fish compartment biomass, (3) algal and benthic invertebrate compartment properties, and (4) other properties of biotic compartments.

Abiotic Properties

In general, the elasticities of the relationships between abiotic properties and methyl mercury concentrations in the benthic invertebrate and water-column carnivore compartments of Swetts Pond seem appropriate. The discussion in this section is organized as follows. First, properties that most influence (i.e., absolute elasticity values > 0.1) results for both compartment types are discussed. Then properties that most influence methyl mercury concentrations in the benthic invertebrate compartment, but not the water-column carnivore compartment, are discussed. Finally, properties that most affect results in the water-column carnivore compartment, but not the benthic invertebrate compartment are discussed.

Exhibit 5-11
Input Properties with Absolute Elasticity Value > 0.1 –
Methyl Mercury Concentration in Benthic Invertebrate Compartment Swetts Pond

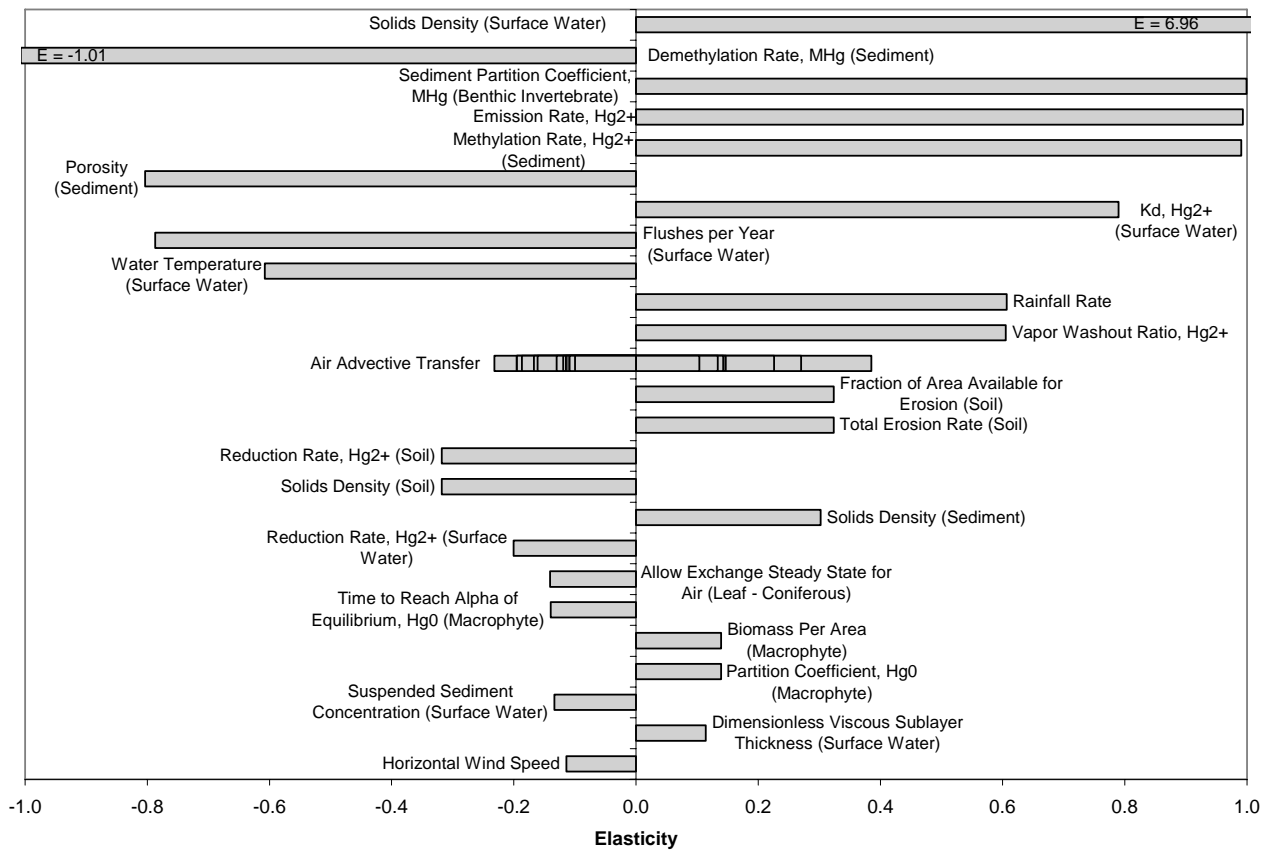
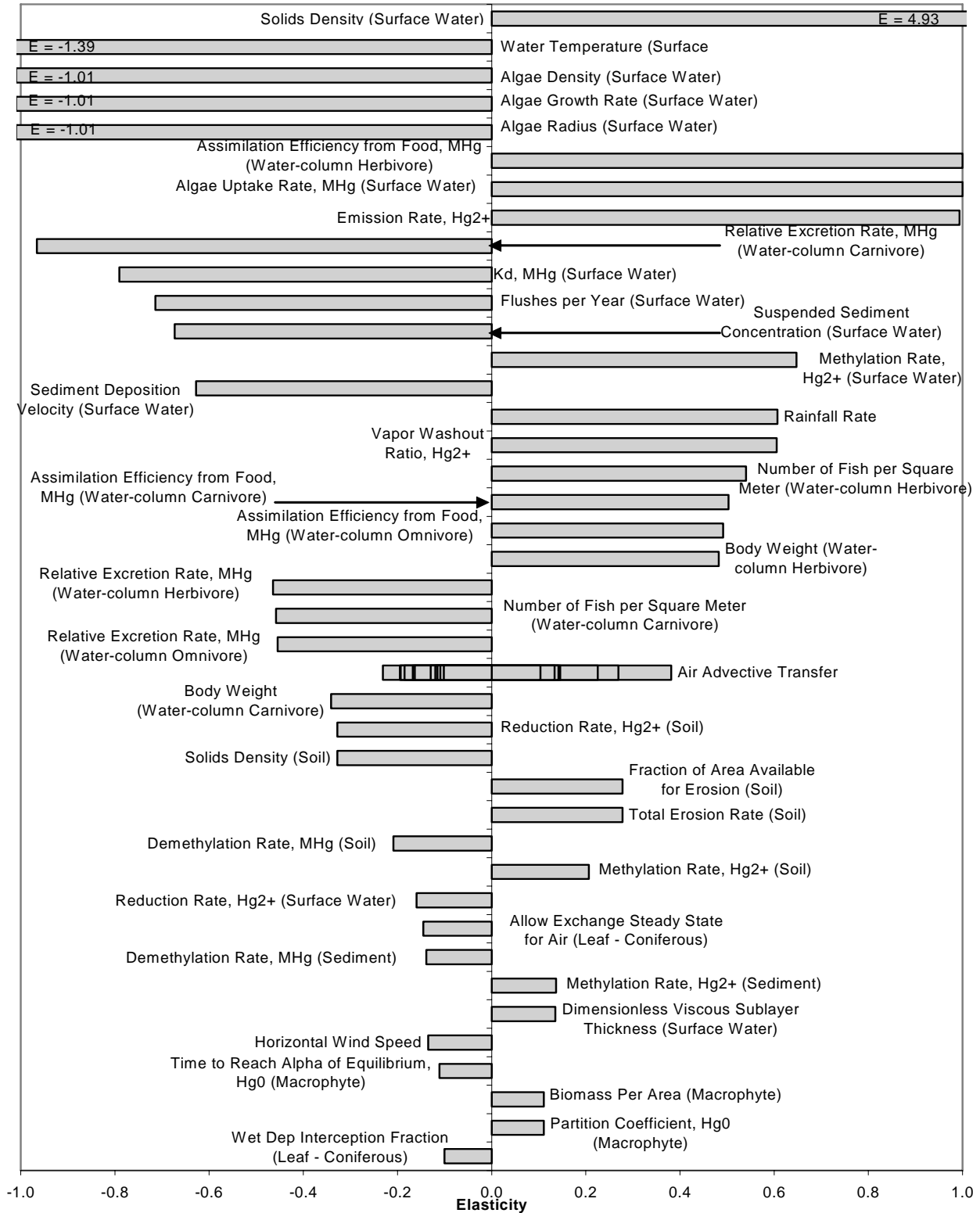


Exhibit 5-12
Input Properties with Absolute Elasticity Value > 0.1 –
Methyl Mercury Concentration in Water-column Carnivore Compartment Swetts Pond



Properties Influencing Methyl Mercury Concentrations in Both Benthic and Water-column Compartments. For methyl mercury concentrations in both the benthic invertebrate and water-column carnivore compartment types, the most influential property is solids density (represented by rho in the TRIM.FaTE library) for the particles suspended in the surface water (elasticity of +7.0 for benthic invertebrates and +4.9 for water-column carnivores). An investigation of TRIM.FaTE algorithms involving solids density in surface water suggests that the sensitivity of results to this property is a special situation related to the configuration of the TRIM.FaTE test case library (see text box in Section 5.2.5).

As shown in Exhibits 5-11 and 5-12, five other abiotic properties – emission rate, water temperature, flushes per year, rainfall rate, and divalent mercury vapor washout ratio – exhibit a relatively high degree of influence on methyl mercury concentrations in both compartments. As with many of the compartment types, the mercury concentrations, including methyl mercury concentrations, in all aquatic organism compartments are directly proportional to the facility emission rate for divalent mercury (elasticity of +1.0). The moderate negative influence of water temperature on methyl mercury concentrations in the benthic invertebrate compartment may be the result of higher rates of volatilization of elemental and divalent mercury from the surface water into the air with higher water temperatures, resulting in lower mercury concentrations in the aquatic system. The large negative influence of the water temperature property on the methyl mercury concentrations in the water-column carnivore (elasticity value of -1.4) and the other fish compartments (see Appendix D.2) may reflect both the previous relationship and the fact that water temperature is in the exponential position in the equation that estimates food ingestion rates for fish. The property flushes per year determines the surface water dilution rate; thus, the higher the number of flushes per year and dilution rate, the lower the concentrations of methyl mercury in the surface water, sediments, and aquatic biota. The high positive elasticity for the relationships between both rainfall rate and divalent mercury vapor washout ratio and concentrations of methyl mercury in the aquatic animal compartments is expected. Similar to the findings for surface soil, higher values for both of those properties result in more divalent mercury being deposited from the air to surface water (and then to sediments).

Four soil properties related to the movement of mercury in soils to surface water via erosion – divalent mercury reduction rate, surface soil solids density, fraction of area available for erosion, and total erosion rate – exhibited moderate degrees of influence on methyl mercury concentrations in the benthic invertebrate and fish compartments. The negative elasticity values for the influence of divalent mercury reduction rate in soils on methyl mercury concentrations in aquatic organisms indicate that at lower rates of transformation of divalent to elemental mercury in soil, more divalent mercury remains in the soil for transport to surface water via erosion. (Elemental mercury tends to volatilize back into the air from surface soil.) The negative elasticity for soil solids density on methyl mercury concentrations in aquatic biota is consistent with the findings for the surface soil compartment on the relationship between soil solids density and mercury concentrations in soil. Lower values for soil solids density results in higher soil mercury concentrations (see Section 5.2.2), hence more mercury is available for erosion into the surface water. The positive elasticities for fraction of area available for erosion and total erosion rate on methyl mercury concentrations in the aquatic biota is expected because as more soil erodes, more of the total mercury mass sorbed to soil particles will be transferred to surface water (and sediments), where it can enter the aquatic food chains.

Properties Influencing Methyl Mercury Concentrations in Benthic Food-chain

Compartments. Methyl mercury concentrations in the benthic invertebrate compartment (and the fish compartments in the benthic food chain) are sensitive to several abiotic properties that affect methyl mercury concentrations in sediments – mercury methylation and demethylation rates in sediment, K_d for divalent mercury (surface water), and divalent mercury reduction rate in surface water. Methyl mercury concentrations in benthic invertebrates are directly proportional to the sediment methylation rate and inversely proportional to the sediment demethylation rate, as expected. At higher values for the divalent mercury K_d in surface water, methyl mercury concentrations in benthic invertebrates are higher. This result is expected because at higher values of divalent mercury K_d , more of the divalent mercury entering the surface water is sorbed to suspended sediment particles, and more divalent mercury reaches the sediments (where it is methylated) through deposition of suspended sediment particles. The moderate negative relationship between the reduction rate of divalent mercury in surface water and methyl mercury concentrations in benthic invertebrates reflects the fact that higher reduction rates in surface water transform more of the divalent mercury into elemental mercury, which leaves the surface water via volatilization into the air.

Similarly, sediment porosity and sediment solids density influence methyl mercury concentrations in the benthic invertebrate compartment but not the water-column carnivore compartment. A high negative elasticity exists between sediment porosity and methyl mercury concentrations in benthic invertebrates. The less porous the sediment, the higher the fraction of the sediment volume that is comprised of solid particles to which methyl mercury tends to sorb. Because the partitioning coefficient that defines the extent of methyl mercury uptake from sediments by benthic invertebrates is based on bulk sediments (not the interstitial water), lower values of sediment porosity result in higher concentrations of methyl mercury in bulk sediments and benthic invertebrates. A moderate positive elasticity holds for the relationship between the sediment solids density property and concentrations of methyl mercury in benthic invertebrates because of the positive influence of sediment solids density on the concentration of mercury in bulk sediment (see Section 5.2.5).

Properties Influencing Methyl Mercury Concentrations in Water-column Food-chain

Compartments. Methyl mercury concentrations in the water-column fish compartments are sensitive to variation in several properties that influence the dissolved concentration of mercury in surface water. Three properties that influence the rate at which mercury is removed from the water column by sedimentation exhibit strong negative relationships to methyl mercury concentrations in the water-column fish: methyl mercury K_d in surface water, suspended sediment concentration, and sediment deposition velocity. The negative elasticity for methyl mercury K_d in surface water and methyl mercury concentrations in the water-column carnivore is appropriate. The lower that K_d value, the less mercury is “scavenged” from the water column by sorption to sediments and deposition to the sediment bed, and the more mercury remains in the water-column for transport into and through the water-column food chain. The negative elasticity values associated with both the suspended sediment concentration and sediment deposition velocity properties reflect the same process.

The positive elasticity associated with the relationship between divalent mercury methylation rate in surface water and methyl mercury concentrations in the water-column carnivore is expected for all of the water-column fish compartments. Similarly, the elasticity

values for the other properties that affect methyl mercury concentrations in the water-column carnivore compartment (i.e., demethylation and methylation rates in soil, reduction rate of divalent mercury in surface water, demethylation and methylation rates in sediment, and the dimensionless viscous sublayer thickness for surface water) are similar to those for the other water-column fish compartments.

Fish Compartment Biomass Properties

For the aquatic ecosystems in this application, a food chain was constructed with a trophic pyramid of biomass in fish intended to reflect that of northern lakes in the US (see Appendix I-B in EPA 2002a). Because this application used a bioenergetics model to simulate mercury transfers through the food chains, the distribution of biomass among trophic levels affects the distribution of contaminant amount and concentration in each trophic level. In an ecosystem with a different pyramid of biomass, a different distribution of contaminants across trophic levels would be expected.

The discussion in this section explores the influence of biomass at the different trophic levels on mercury concentration in all fish compartments. In this scenario, the biomass (per unit area) for the fish compartments was set as the product of two properties: body weight (BW) and number of fish per square meter (# of fish). Exhibit 5-13 illustrates the influence of biomass in each Swetts Pond fish compartment on methyl mercury concentrations in each Swetts Pond fish compartment. The scenario analyzed included two independent food chains, a benthic food chain and a water-column food chain.

The elasticity values in Exhibit 5-13 reveal three general patterns of influence of fish compartment biomass properties on methyl mercury concentrations in the fish compartments: influence of biomass changes at the bottom of the food chain, influence of biomass changes at the top of the food chain, and influence of biomass changes in the middle of the food chain.

Biomass in the fish compartments at the bottom of the fish food chain (i.e., benthic omnivore in the benthic food chain and water-column herbivore in the water-column food chain, respectively) demonstrate a positive influence on methyl mercury concentrations in all fish compartments (positive elasticity values). A greater biomass in the bottom food chain compartments results in higher methyl mercury concentrations in those fish compartments. The reason for this is because the greater the biomass in a bottom-trophic-level-fish compartment, the more methyl mercury is transferred from its food source into that fish compartment. However, given the same biomass of higher-trophic level fish, a smaller proportion of the total methyl mercury in the bottom trophic level fish can be removed each day the higher-trophic level fish. That results in higher methyl mercury *concentrations* in the bottom trophic level compartments. Those higher concentrations are transferred up the food chain, so that concentrations in the upper trophic levels are also positively affected by biomass of the bottom trophic level compartments.

Exhibit 5-13
Analysis of Influence of Biomass in One Trophic Level on Methyl Mercury Concentrations in Other Trophic Levels of the Aquatic Food Chain

Biomass Properties for:	Influence on Methyl Mercury Concentrations in:	(Sign) and Elasticity Value for BW / # of Fish ^a
<i>Benthic Food Chain</i>		
Omnivore	Carnivore	(+) 0.32 / 0.34
Omnivore	Omnivore	(+) 0.32 / 0.34
Carnivore	Carnivore	(-) < 0.1 / 0.22
Carnivore	Omnivore	(-) 0.23 / 0.27
<i>Water-column Food Chain</i>		
Herbivore	Carnivore	(+) 0.48 / 0.54
Herbivore	Omnivore	(+) 0.48 / 0.54
Herbivore	Herbivore	(+) 0.48 / 0.54
Omnivore	Carnivore	< 0.1
Omnivore	Omnivore	< 0.1
Omnivore	Herbivore	(-) 0.44 / 0.51
Carnivore	Carnivore	(-) 0.46 / 0.34
Carnivore	Omnivore	(-) 0.43 / 0.50
Carnivore	Herbivore	< 0.1

^a All data for Swetts Pond compartments.

Biomass in the fish compartments at the top of a fish food chain (i.e., carnivore compartments in both food chains, respectively) demonstrates a negative influence on methyl mercury concentrations in all fish compartments in that food chain. A greater biomass in a top carnivore compartment results in lower methyl mercury concentrations in that fish compartment. That result occurs because the greater the biomass of the top carnivore, the more methyl mercury they remove each day from their prey compartment. That results in lower methyl mercury concentrations in the prey, and therefore lower concentrations of methyl mercury in the top carnivore. The negative elasticity values are larger for the relationships observed in the water-column food chain (i.e., maximum of -0.50) than for the relationships observed in the benthic food chain (i.e., maximum of -0.27). That is because the starting biomass of the water-column carnivore is approximately 30 percent of the biomass of the water-column omnivore, while the starting biomass of the benthic carnivore is approximately 10 percent of the biomass of the benthic omnivore.

The effect of changes in the properties related to biomass for a middle-trophic-level compartment (i.e., the water-column omnivore) is only pronounced (i.e., exhibits an absolute

elasticity value greater than 0.1) for methyl mercury concentrations its prey compartment (i.e., the water-column herbivore). The negative elasticity of that relationship is similar to that for the relationship between the biomass of the top carnivore and methyl mercury concentrations in its prey compartment. The starting biomass of the water-column omnivore compartment is 36 percent of the biomass of the herbivore compartment. The lack of a pronounced effect of water-column omnivore biomass on methyl mercury concentration in that compartment (and therefore the higher trophic level compartment) probably reflects opposing influences related to the higher and lower trophic level compartments on methyl mercury in the middle-trophic-level-fish compartment.

Algal and Benthic Invertebrate Properties

Algae forms the base of the water-column food chain, while benthic invertebrates form the base of the benthic food chain. Several algal and benthic invertebrate-related properties influence methyl mercury concentrations in the compartments in the water-column and benthic food chains, respectively.

The concentration of methyl mercury in all water-column fish is inversely proportional to the value of several algal properties (i.e., algal density, algal growth rate, and algae radius, elasticity -1.0) and directly proportional to the algae uptake rate for methyl mercury from surface water (elasticity +1.0). The former three properties together affect algae biomass, with higher values for the algal density, algal growth rate, and algae radius properties resulting in a higher algae biomass. For a fixed algae methyl mercury uptake rate *not* normalized to algae biomass, the higher the algae biomass, the lower the concentration of methyl mercury in algae, and hence the lower the concentration of methyl mercury in the water-column fish. The opposite is true for the algae uptake rate property. At higher values of that property, the mass and concentration of methyl mercury in algae are higher, and hence the methyl mercury concentrations in all fish in the water-column food chain are higher.

The concentration of methyl mercury in benthic invertebrates (and in the benthic fish compartments, see Appendix D.2) is directly proportional to the benthic invertebrate sediment partition coefficient (elasticity +1.0), which reflects the extent to which methyl mercury in bulk sediment concentrates in the benthic invertebrate compartment. Unlike the role of the bottom-trophic-level fish compartment biomass, benthic invertebrate biomass exerts little influence on methyl mercury concentrations in higher trophic level compartments (elasticity values $<|0.1|$). That is because the biomass of the benthic omnivore compartment is only five percent of the biomass of the benthic invertebrate compartment.

Other Biotic Properties

Several other properties of the aquatic biotic compartments influence methyl mercury concentrations in those and other biotic compartments. Methyl mercury concentrations in all aquatic biota compartments are somewhat sensitive (i.e., absolute elasticity values ~ 0.1) to three macrophyte properties that influence the extent to which elemental mercury in the water column partitions into the macrophytes rather than remains available for oxidation to divalent mercury (and methylation to methyl mercury) and transfer to the sediments via sedimentation and diffusion. Those three properties are the time to reach alpha (i.e., 95 percent) of equilibrium for

elemental mercury in macrophytes, the macrophyte/water partition coefficient for elemental mercury, and the biomass of macrophytes per unit area. For shorter times to equilibrium and higher macrophyte/water partition coefficients, higher concentrations of mercury in macrophytes result. The reason that the macrophyte biomass and partition coefficient properties have a positive influence on concentrations of methyl mercury concentrations in water-column carnivores is probably related to speciation and transformation of mercury in the surface water and in macrophytes, although additional analysis would be needed to determine the reasons for this positive elasticity with confidence. Increasing the amount of elemental mercury uptake into macrophytes changes the mercury speciation profile in surface water (less elemental, more divalent and methyl), which affects the uptake of methyl mercury into fish.

Methyl mercury concentration in the water-column carnivore fish compartment is sensitive to two biotic properties associated with fish compartments in addition to the biomass-related properties described above. These are the chemical assimilation efficiency from food and relative excretion rate for methyl mercury. As expected, the concentration of methyl mercury in water-column carnivores increases with increasing assimilation efficiency of methyl mercury by all three water-column fish compartments, with that for the water-column herbivore being the strongest relationship (positive elasticity of 1.0 for the herbivore property vs ~0.50 for the assimilation rate of the other two water-column fish compartments). An opposing influence is exhibited by the excretion rate for methyl mercury property for all three water-column fish compartments.¹² In this case, the strongest relationship is for the water-column carnivore excretion rate (negative elasticity of ~1.0 vs ~0.5 for the excretion rate associated with the water-column herbivore and omnivore compartments). Similar trends are seen in the other fish compartments (see Appendix D.2).

One terrestrial plant property for the leaf compartment type – *AllowExchange* for air – has a negative influence on methyl mercury concentrations in aquatic biota. As described in Section 5.2.2, at lower values of the *AllowExchange* property, higher concentrations of mercury occur in surface soil. *AllowExchange* indicates the presence of viable vegetation, and in a dynamic simulation its value varies by season. For the steady-state mode, its value was set to a constant reflecting the proportion of the year that is the growing season. The negative elasticity values for the relationship of that property to methyl mercury concentrations in the benthic invertebrate and water-column carnivore compartments indicates that at higher values of *AllowExchange*, mercury concentrations in surface water and sediments are lower. Higher values of *AllowExchange* mean that mercury is tied up in the vegetation for longer periods of time (i.e., in the steady-state mode, more mercury is associated with the vegetation), and less mercury is reaching the soil surface. The lower concentrations of mercury in surface soil results in a lower input of surface soil mercury to surface water via erosion.

¹² See Appendix A.1.3 of TRIM.FaTE TSD Volume II for details of how excretion is estimated. In addition to evaluating the relative excretion rate *for divalent mercury* and *for elemental mercury* properties (base value set to 3.0 for both), the relative excretion rate *for methyl mercury* property (base value set to 1.0) was varied to examine the influence of the algorithm used to calculate methyl mercury excretion rate. As expected, this excretion rate has a large influence on methyl mercury concentration for the applicable compartment type, and lesser influence for compartment types representing higher trophic levels (e.g., excretion rate for carnivores has high negative elasticity for carnivores, excretion rate for omnivores and herbivores has smaller negative elasticity for carnivores).

5.2.7 Terrestrial Mammals

This section describes findings regarding the elasticities of the relationships between model properties and divalent mercury concentration results in the mouse, raccoon, and deer compartments in SW2. The properties demonstrating absolute elasticity values greater than 0.1 for divalent mercury in those compartments are presented in Exhibits 5-14, 5-15, and 5-16, respectively, and discussed below.

Exhibit 5-14
Input Properties with Absolute Elasticity Value > 0.1 –
Divalent Mercury Concentration in Mouse Compartment SW2

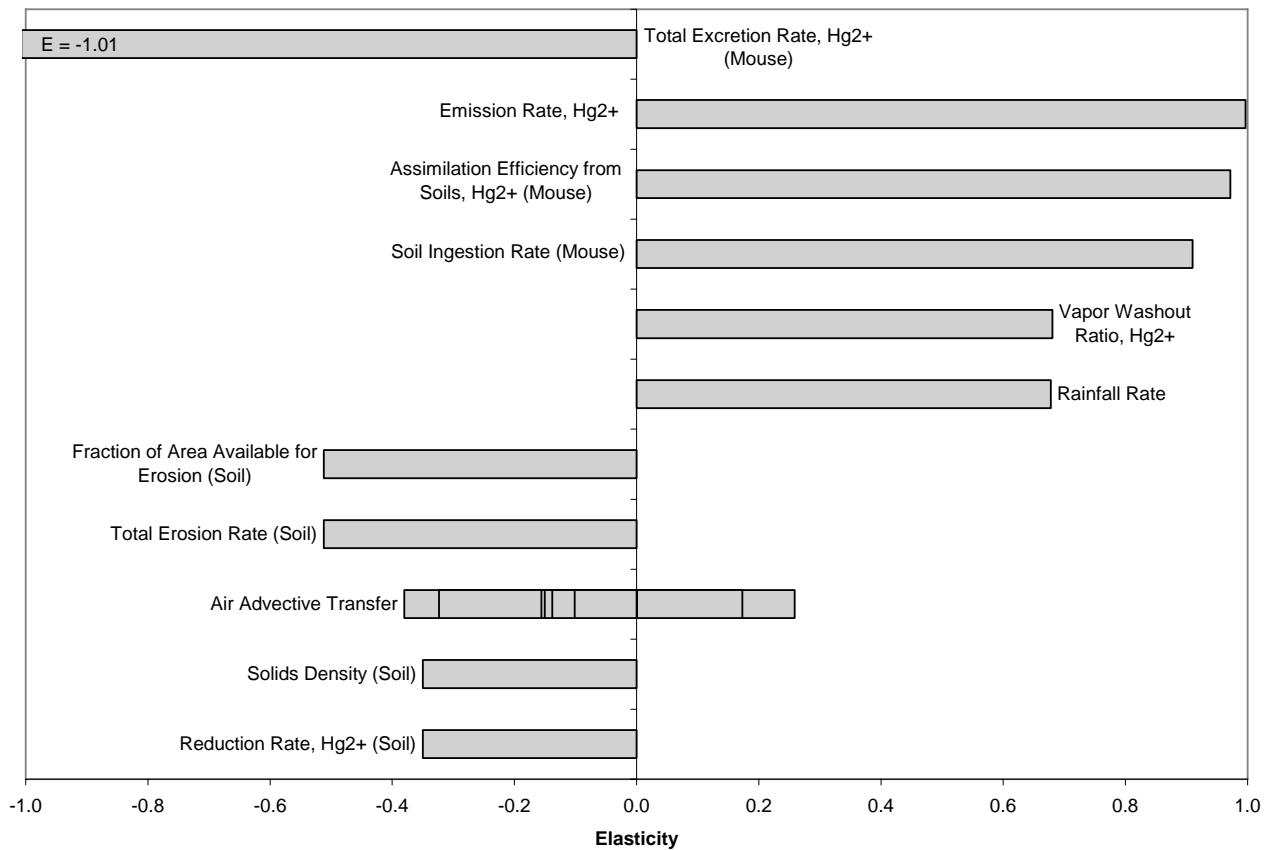


Exhibit 5-15
Input Properties with Absolute Elasticity Value > 0.1 –
Divalent Mercury Concentration in White-tailed Deer Compartment SW2

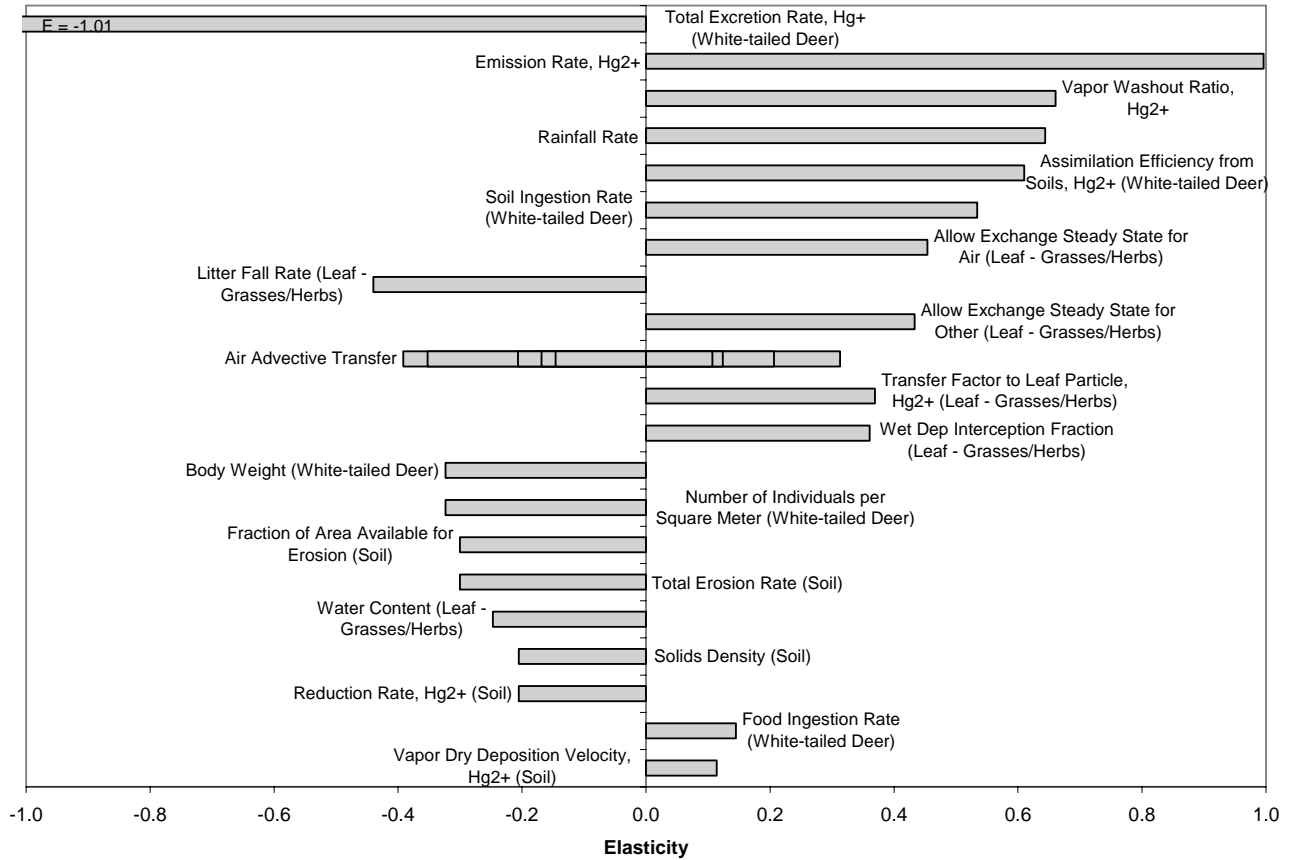
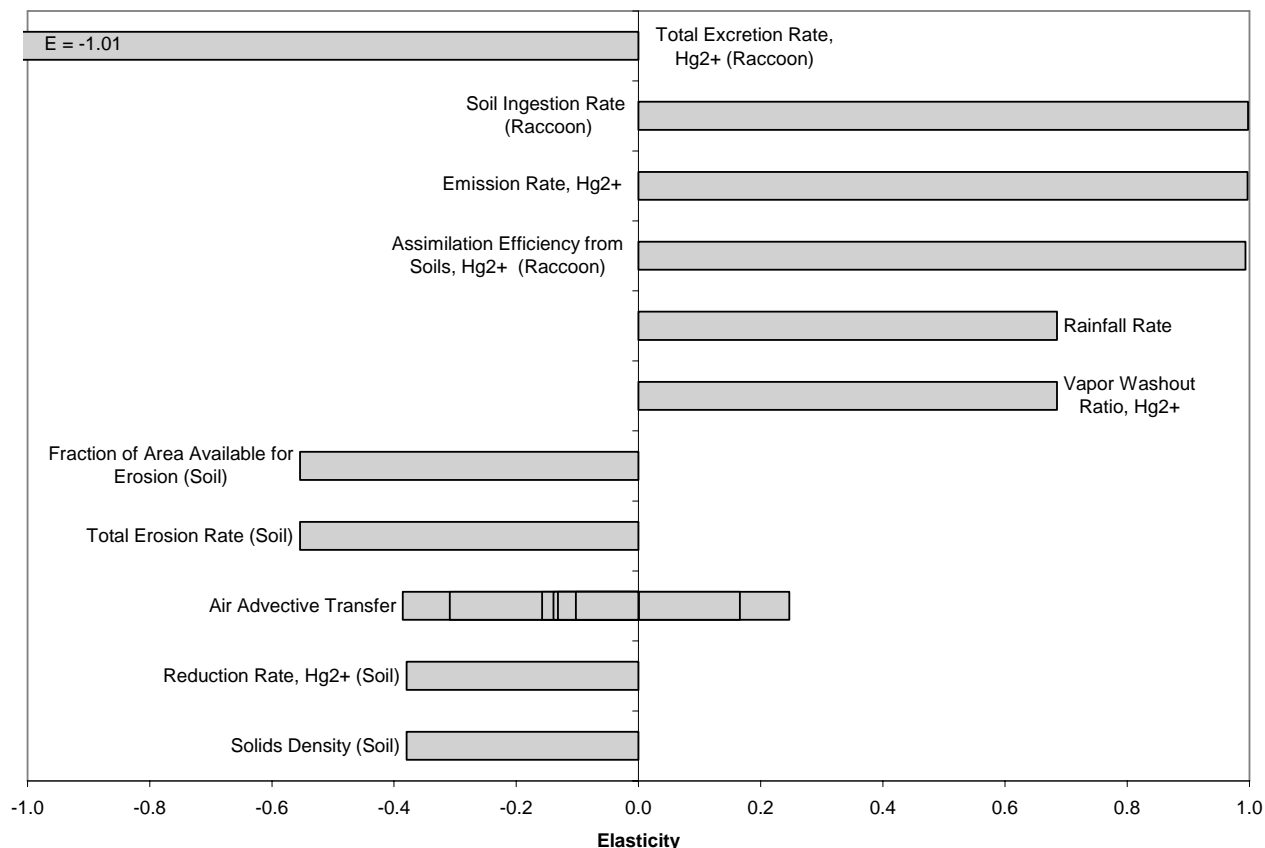


Exhibit 5-16
Input Properties with Absolute Elasticity Value > 0.1 –
Divalent Mercury Concentration in Raccoon Compartment SW2



The top two most influential properties for divalent mercury concentrations in all three terrestrial mammals are facility emission rate of divalent mercury and total excretion rate of divalent mercury. As with many of the other compartment types, the facility emission rate for divalent mercury has a directly proportional positive influence on divalent mercury concentrations in terrestrial animal compartments (elasticity value of +1.0). The effect of total divalent mercury excretion rate on the concentrations of divalent mercury in the three mammal compartment types (elasticity values of -1.0) is logical because excretion is the only modeled process by which the mammals can eliminate divalent mercury from their bodies.

The relative sensitivity of divalent mercury concentration in the three mammalian species to the remaining input properties varies according to the relative soil ingestion rate, body weight, diet, and food ingestion rate for the three species.

For all three mammal compartment types, the next four most influential properties are ones that strongly influence the incidental intake of divalent mercury in the soil, either directly (assimilation efficiency from soils, soil ingestion rate) or indirectly by influencing the amount of divalent mercury in surface soil (vapor washout ratio, rainfall rate). The fact that the concentration of divalent mercury in all three mammals is much more sensitive to the assimilation efficiency from soils and soil ingestion rate properties than to the food ingestion rate

property indicates that, in the scenario modeled, incidental ingestion of divalent mercury sorbed to soil particles is a more important exposure route for divalent mercury for these species than ingestion of divalent mercury in food. That reflects the overall lower concentration of divalent mercury in biota than in soils at steady-state.¹³ Each species is discussed in turn below.

The positive elasticity values for assimilation efficiency from soils (+0.97) and soil ingestion rate (+0.91) are reasonable for the mouse given its relatively high direct soil ingestion rate (0.02 kg/kg-day used in the sensitivity analysis). The higher sensitivity of mouse divalent mercury concentration to soil ingestion properties than to food ingestion properties indicates that at steady-state the majority of divalent mercury intake by the mouse is the incidental ingestion of divalent mercury in soil. The positive elasticity values for vapor washout ratio for divalent mercury and rainfall rate (both +0.68) reflect the influence of those properties on the amount of divalent mercury deposited to the soil (and also to leaves) per unit time. The higher the values for those two properties, the higher the soil (and leaf) concentration of divalent mercury, which then is taken up by the mouse through incidental ingestion of soil (and in some cases ingestion of leaves).

The concentration of divalent mercury in the raccoon is as sensitive to soil ingestion rate and assimilation efficiency from soils as it is to facility emission rate, whereas concentration in the mouse was slightly less sensitive to those two properties than to the facility emission rate. This reflects the slightly higher body-weight-normalized soil ingestion rate for the raccoon (0.094 kg/kg-day used in the sensitivity analysis) than for the mouse. The positive elasticity values for the vapor washout ratio for divalent mercury and rainfall rate are nearly identical to the values for the mouse.

The elasticity values for the same four properties (i.e., assimilation efficiency from soils, soil ingestion rate, vapor washout ratio, and rainfall rate) for the white-tailed deer differ slightly from values for the mouse and raccoon. The higher importance of vapor washout ratio and rainfall rate over the soil intake properties for the deer probably reflects the importance of vapor washout ratio and rainfall rate not only for deposition of divalent mercury to soils, but also for deposition of divalent mercury to leaves, which comprise 100 percent of the diet of deer (only 50 percent of the diet of the mouse). Also, deer have a much lower incidental soil ingestion rate (0.001 kg/kg-day used in the sensitivity analysis) than the raccoon or mouse.

The similarities between the raccoon and mouse results compared with the white-tailed deer results end after the first six most influential properties. The next four most influential properties (aside from the air advective transfer property, not discussed in this section) are the same for both the raccoon and mouse – both compartment types have the same relative negative elasticity values for the fraction of area available for erosion, total erosion rate, surface soil solids density, and divalent mercury reduction rate in surface soil properties. These four properties all relate to the incidental ingestion of soil. The elasticity values for the raccoon are

¹³ As described in Section 5.1, a previous version of the TRIM.FaTE library was used for the sensitivity analysis. That version inadvertently had soil ingestion rates for some animals that were higher than appropriate for the modeled scenario. The modeled rate for raccoon was 32 times too high, for mouse was 20 times too high, and for deer was 7.7 times too high.

slightly more negative than for the mouse, as expected given the raccoon's somewhat higher soil ingestion rate. Higher values for the fraction of area available for erosion and total erosion rate properties result in lower concentrations of divalent mercury in surface soil, because more divalent mercury sorbed to surface soil particles is removed (by erosion) from a given surface soil compartment. Lower values for both the solids density and divalent mercury reduction rate properties in surface soil result in higher divalent mercury concentrations in soil, as described in Section 5.2.2.

In contrast to the raccoon and mouse, the next five most influential properties (after the top six) for the white-tailed deer are ones affecting the concentration of divalent mercury in plant leaves: litter fall rate, *AllowExchange* (both properties), transfer factor to leaf particle, and wet deposition interception fraction. Because the deer has a relatively low soil ingestion rate compared with the raccoon and mouse, and because its diet is 100 percent plant leaves, it makes sense that the concentration of divalent mercury in deer would be relatively more sensitive to the concentration of divalent mercury in leaves.

- The moderately negative elasticity (-0.44) for litter fall rate indicates that the lower the value used for steady-state litter fall rate in the sensitivity analysis (i.e., the lower the amount of divalent mercury transferred from the leaf compartment to the soil compartment), the higher the amount of divalent mercury remaining in leaves, and the higher the rate of divalent mercury ingestion with leaves by the deer.¹⁴
- The moderate positive elasticities for the three properties *AllowExchange* for air, *AllowExchange* for other, and wet deposition interception fraction are reasonable. Lower values for those properties result in lower concentrations of divalent mercury in leaves, as already discussed for the sensitivity analysis for plant leaf compartments (Section 5.2.4).
- The moderate positive elasticity for the transfer factor [from the leaf] to leaf particle property (+0.37) means that lower values for that transfer factor results in lower concentrations of divalent mercury in the deer. Thus, as more divalent mercury moves from the leaf to the leaf particle, the deer is ingesting more divalent mercury. Given that the deer eats both the leaves and leaf particles, the sensitivity to the transfer factor to leaf particle is not a result of a redistribution of divalent mercury between the leaf and particle-on-leaf compartments. Further investigation would be needed to pinpoint the exact reason for this result. One possibility is that after divalent mercury is transferred from the leaf to leaf particles, it can sorb to the particles and is less available for diffusion back into the air or for exchange with the stem compartment than is the divalent mercury that remains in the plant leaves. Note that the lack of sensitivity of divalent mercury in the deer to other properties related to divalent mercury in particles on leaves indicates the relatively low absolute mass of divalent mercury in particles on leaves compared to in leaves.

¹⁴ The vegetation in SW2 is grasses/herbs. Litter fall for this type of vegetation reflects the dieback of grass stems and leaves at the end of the growing season rather than leaves actually falling, as is the case for deciduous trees. In the steady-state mode used for the sensitivity analysis, a single value is used for litter fall rate, which accounts for the fraction of the year that leaves are present. See Appendix C.1 for details.

For both the raccoon and the mouse, none of the remaining properties exhibit an absolute elasticity value greater than 0.1. For the deer, several additional properties show moderate elasticity values, with some of these properties reflecting the fact that the biomass of the deer is sufficient to influence the distribution of divalent mercury between the deer and the plants.

Both the deer body weight (BW) and the number of individuals per square meter (N) properties show moderate negative elasticity values (elasticity for both is -0.32). Thus, at lower values for deer biomass (i.e., lower values for either BW or N), the divalent mercury in the grasses/herbs reflects the lower total mass of divalent mercury transferred from the leaf compartment to the deer compartment via grazing, and concentrations of divalent mercury in the grasses/herbs leaf compartment are higher. Fewer deer ingesting grasses with a higher concentration of divalent mercury achieve higher body divalent mercury concentrations than more deer grazing on grass with lower concentrations of divalent mercury; hence, the negative elasticity.¹⁵ This result is consistent with the guidance to users of TRIM.FaTE that it is important to include the major herbivores in the system being modeled because they can influence the distribution of mercury mass in the system.

Moderate negative elasticity values resulted for the fraction of area available for erosion (-0.30), total erosion rate (-0.30), surface soil solids density (-0.21), and divalent mercury reduction rate (-0.21) properties, as was the case for the mouse and raccoon; the values are just lower in magnitude than the values for those properties for the mouse and raccoon and lower in relative influence on deer divalent mercury concentrations than other properties. This reflects the relatively lower importance of soil ingestion as a route of divalent mercury intake for deer compared with the mouse and raccoon and compared with ingestion of divalent mercury in leaves by the deer.

At higher values for water content in grasses/herbs, the dry deposition interception fraction by plant leaves is lower according to the equation of Baes et al. (1984) (Equation 7-2 in TRIM.FaTE TSD Volume II), thus decreasing the concentration of divalent mercury in leaves and in deer (elasticity -0.25). There is a moderate positive elasticity for food ingestion rate (+0.14), which appears reasonable given the importance of ingestion of divalent mercury in the leaves of grasses/herbs for the deer. A similar positive elasticity for vapor dry deposition velocity for divalent mercury to soil (+0.11) also makes sense. The same positive elasticity for that property is evident for both the mouse and the raccoon, however it ranks as the 12th most influential property for those species, while it ranks as the 21st most influential property for the deer.

¹⁵ Note that an alternative hypothesis that the concentration of divalent mercury in deer decreases because the deer compartment biomass increases, thereby diluting the divalent mercury mass in the deer compartment, cannot be true because the deer food ingestion rate is normalized to deer body weight (i.e., kg grass ingested per kg deer biomass per day). In other words, the total mass of grass (and divalent mercury) ingested by the deer increases linearly in direct proportion to increasing deer biomass, leaving the ratio of mercury ingested/deer biomass the same.

5.3 Broadly Influential Properties

Previous discussion in this chapter has focused on influential properties for selected compartment types. In this section, test case sensitivity analysis results are analyzed to highlight broadly influential properties. More specifically, the focus of this section is on properties to which mercury concentrations in numerous compartments and compartment types are particularly sensitive, using elasticity as a measure of sensitivity. These results are expected to contribute to the overall performance evaluation of the model. In addition, because of their broad influence, identification of these properties could be useful for setting data collection priorities for similar TRIM.FaTE applications or focusing future TRIM.FaTE research.

5.3.1 Approach

The following criterion was used to identify a subset of properties with notable influence on mercury concentrations in multiple types of compartments.

Properties with absolute elasticities greater than 0.5 for concentration results for at least one of the three mercury species in at least *five different compartment types* were considered to be broadly influential.

These properties are the primary focus of the discussion in this section. As with the analysis of individual compartment types, the results of this analysis reflect the specific output compartments selected for inclusion in the sensitivity analysis (see Exhibit 5-2). For example, if concentrations in aquatic biota are sensitive to changes in a particular property, that property could be interpreted as more broadly influential than properties that affect semi-aquatic biota because more aquatic biota compartment types were included in the detailed evaluation of the sensitivity analysis. However, as described at the beginning of this chapter, output compartments were selected for this sensitivity analysis both to provide a breadth of coverage *and* to focus on results of interest, such as the aquatic food chain. In general, it is expected that the results presented here are useful for providing overall conclusions regarding broadly influential parameters in the context of the current application. It should not be concluded that properties *not* identified here as broadly influential are unimportant for individual compartment types (see previous sections) or for TRIM.FaTE applications using a different scenario (e.g., different input values, different algorithms, different compartment types).

5.3.2 Summary of Observations

A summary of the broadly influential properties for the mercury test case based on the two criteria defined above is presented in Exhibit 5-17. For each property listed in this table, three values are reported:

- Number of different compartment types (out of the 17 total that were assessed) for which the concentration results for at least one of the three mercury species demonstrated an absolute elasticity greater than 0.5;

- Total number of simulation outputs (out of the 93 total that were assessed) with an absolute elasticity value greater than 0.5 (where an output is the concentration of one of the three mercury species in one of the 33 different compartments); and
- Mean absolute elasticity of the values greater than 0.5 (i.e., those identified in the previous bullet).

In addition, the mercury species included in the outputs with absolute elasticity greater than 0.5 are listed in the column next to the total number of outputs. A complete list of properties for which at least one absolute elasticity value greater than 0.5 was obtained (regardless of how many compartment types were affected) is presented in Appendix D.3.

Exhibit 5-17
Summary of Broadly Influential Properties Based on Elasticity

Property	Number of Compartment Types > 0.5	Outputs > 0.5		Mean Absolute Elasticity ^a
		Number of Outputs	Hg Species Affected	
Emission rate, Hg ²⁺	17	78	all 3	0.98
Vapor washout ratio, Hg ²⁺	17	71	all 3	0.65
Rainfall rate	17	71	all 3	0.65
Solids density (rho) of surface water solids	14	47	all 3	4.69
Water temperature	12	38	all 3	3.63
Emission rate, Hg ⁰	11	15	Hg ⁰	0.84
Suspended sediment deposition velocity	11	13	Hg ⁰ , MHg	0.73
Flush rate (per year) of surface water body	10	48	all 3	0.88
Suspended sediment concentration	10	29	all 3	0.67
Henry's Law constant, Hg ⁰	10	12	Hg ⁰	0.80
Kd in surface water, Hg ²⁺	9	19	all 3	0.74
Demethylation rate in surface soil, MHg	8	11	MHg	0.96
Methylation rate in surface soil, Hg ²⁺	8	11	MHg	0.95
Air temperature	7	13	Hg ⁰ , MHg	1.07
Porosity of sediment	6	25	all 3	1.13
Fraction of surface soil area available for erosion	6	20	all 3	0.55
Total erosion rate of surface soil	6	20	all 3	0.55
Demethylation rate in sediment, MHg	6	11	MHg	1.00

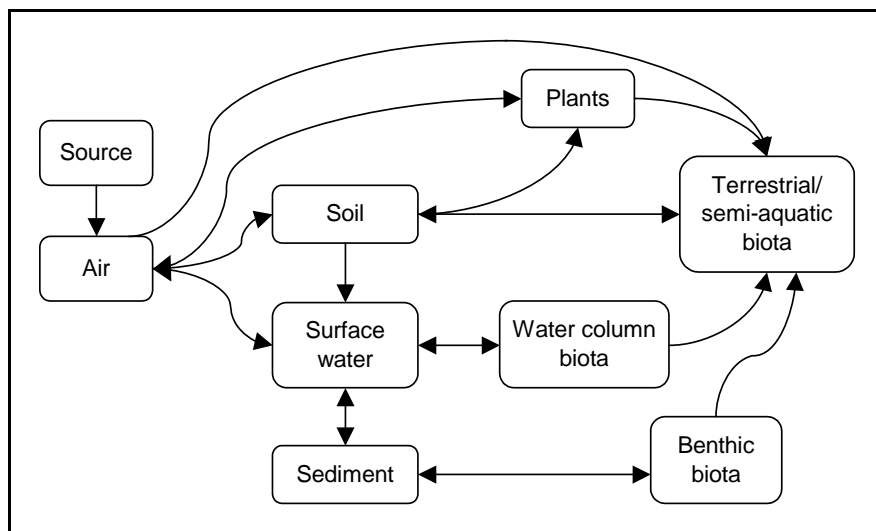
Property	Number of Compartment Types > 0.5	Outputs > 0.5		Mean Absolute Elasticity ^a
		Number of Outputs	Hg Species Affected	
Methylation rate in sediment, Hg ²⁺	6	11	MHg	0.95
Kd in surface water, MHg	6	11	MHg	0.72
Methylation rate in surface water, Hg ²⁺	6	8	MHg	0.66
Steady-state air advective transfer factor	5	10	all 3	0.53
Sediment partition coefficient for benthic invertebrates, Hg ²⁺	5	9	Hg ²⁺	0.85
Sediment partition coefficient for benthic invertebrates, MHg	5	9	Hg ⁰	0.99
Solids density (rho) of sediment particles	5	8	Hg ⁰	0.98
Reduction rate in sediment, Hg ²⁺	5	5	Hg ⁰	0.87

^a Mean absolute elasticities reported here are calculated using only elasticities with an absolute value > 0.5.

Specific reasons for why mercury concentrations in a given compartment type are sensitive to particular properties are not discussed in this section; that information is presented in Section 5.2. However, some general observations can be made regarding the properties included in Exhibit 5-17. Many of the most broadly influential properties influence concentrations of two or three mercury species. In addition, most of the properties presented in this table are broadly influential because they influence concentrations in “upstream” compartments that, in turn, affect concentrations in other, “downstream” compartment types. Although the relationships between compartment types in the mercury test case can be complex (e.g., multiple mass transfer processes can exist on a single link between compartments; mass can flow both ways on a link via different processes and at different rates due to competing or feedback mechanisms represented by the algorithms), the *overall* flow of mass through the whole collection of compartments in the test case can be generalized. A simplified conceptual model of mass flow through the main compartment types/categories included in the mercury test case is presented in Exhibit 5-18.

As a result of these relationships, properties that are influential on mercury concentrations in upstream compartments (generally, compartments closer to the left-hand side of Exhibit 5-18) can also be influential on downstream compartment concentrations due to the predominant movement of mercury mass through the compartments included in the test case scenario. For example, if high elasticity is observed between a property and concentration in air, this property may also be influential on concentrations in soil and surface water because the mercury mass in these downstream compartments is transferred from air compartments via deposition and other processes. If the elasticity for this property is also high for soil concentrations, elevated elasticities may in turn be observed for concentrations in compartments further downstream, such as plants and terrestrial biota. In general, properties to which upstream compartments are highly sensitive are more broadly influential (based on the criteria used for this analysis) than properties to which only downstream compartments are highly sensitive.

Exhibit 5-18
Simplified Mass Flow Diagram – Mercury Test Case Scenario



Properties used in the test case also can be broadly influential if they are used in more than one model algorithm (i.e., for modeling multiple fate and transport processes). For example, Henry’s Law constant – which influences partitioning of mercury from the air to rain, thereby driving the deposition rate to soil/water – is also used in the calculation of other fugacity capacities (i.e., Z-values) that drive partitioning in compartment types other than air. In addition, water temperature influences fish ingestion and excretion rates (elasticities are very large due to the use of temperature in the exponent) and may also affect partitioning between surface water and air or sediment.

A generalized summary of the relationships between the broadly influential properties and the various types of compartments is presented in Exhibit 5-19. Note that this table presents a very general overview and includes numerous simplifications (e.g., some properties may be influential on concentrations on just one mercury species in downstream compartments; some properties are not influential on all downstream compartments). For more detailed information on specific elasticities for these properties and reasons and discussion regarding the quantitative sensitivities, refer to Section 5.2.

The total number of outputs (i.e., compartment-chemical combinations included in the sensitivity analysis) for which the elasticity associated with each identified property is greater than 0.5 is also presented in Exhibit 5-17. Although this value was not used to rank or group the properties discussed here, it does provide an additional indication of influence. For a given property, a large total number of outputs for which the elasticity is high (in this case, > 0.5) can reflect that property’s influence on multiple mercury species and/or at multiple locations. For example, the divalent mercury emission rate is influential to 78 outputs across 17 compartment types. By contrast, the emission rate for elemental mercury is influential to a smaller number of compartment types (11) and a much smaller number of outputs (15). Divalent mercury is more

Exhibit 5-19
Downstream “Mass Flow” Effects – Influential Properties and Compartment
Types Potentially Affected

Property	Compartment Type Directly Affected	“Downstream” Compartment Types Potentially Affected
Emission rate, Hg ²⁺ and Hg ⁰ Vapor washout ratio, Hg ²⁺ Rainfall rate Henry’s Law constant, Hg⁰ ^a Air temperature Steady-state air advective transfer factor	Air	All other compartment types
Demethylation rate in surface soil, MHg Methylation rate in surface soil, Hg ²⁺ Total erosion rate of surface soil Fraction of surface soil available for erosion	Surface soil	Terrestrial animals and plants, surface water, sediment
Solids density (rho) of surface water solids Suspended sediment deposition velocity Flush rate (per year) of surface water body Suspended sediment concentration Kd in surface water, Hg ²⁺ and MHg Methylation rate in surface water, Hg ²⁺ Water temperature ^a	Surface water	Water-column and benthic food-chain biota, sediment
Porosity of sediment Demethylation rate in sediment, MHg Methylation rate in sediment, Hg ²⁺ Solids density (rho) of sediment particles Reduction rate in sediment, Hg ²⁺	Sediment	Benthic food-chain biota, surface water
Sediment partition coefficient for benthic invertebrates, Hg ²⁺ and MHg	Benthic invertebrate	Other benthic food-chain biota

^a These are examples of properties that directly affect a variety of compartment types beyond those listed here.

reactive; it follows that the emission rate for this species is ultimately more broadly influential on multimedia mercury concentrations in this sensitivity analysis than the emission rate for elemental mercury. By the same reasoning, it is logical that non-chemical-specific properties that influence concentrations of all three mercury species can also be more broadly influential than chemical-specific properties. For example, sediment porosity and demethylation rate of methyl mercury in sediment are both sediment properties that have substantial influence (at least one elasticity value > 0.5) on six compartment types. However, porosity affects concentrations of all three mercury species at multiple locations and is highly influential on 25 outputs, while demethylation rate affects only methyl mercury concentrations and, as a result, is highly influential on only 11 outputs.

5.3.3 Conclusions

Although other methods for sorting, grouping, and analyzing the sensitivity results may also be appropriate, the elasticity-based analysis described here was considered to be a logical approach that provides useful observations for the purposes of model evaluation. In general, the results of this analysis seem appropriate – the most broadly influential properties are generally those that influence concentrations in “upstream” compartments (e.g., air), where the concentration/mass influences concentrations in other compartments. These results are also consistent with the sensitivity observations for specific compartment types discussed in Section 5.2 (i.e., mercury concentrations in “downstream” compartments such as fish are generally sensitive to a larger number of properties than “upstream” compartments like air). Additionally, there is a small subset of properties (e.g., Henry’s Law constant, air temperature) that directly influence concentrations in a variety of compartments.

One use of this analysis, in conjunction with the compartment-specific sensitivity analysis presented in Section 5.2, is to be able to give priority to the more influential properties in data collection efforts for similar TRIM.FaTE applications. It is noted, however, that the use of elasticity values (rather than sensitivity scores) in these analyses precluded consideration of the uncertainty and variability associated with the property values, as represented by their coefficients of variation. As described at the beginning of this chapter, sensitivity scores (which take into account the estimated uncertainty and variability associated with a parameter by multiplying elasticity by the CV) were also calculated for each property/output combination included in the sensitivity analysis. These sensitivity scores can be grouped in the same way that absolute elasticity values were used to define another set of broadly influential properties (i.e., absolute sensitivity scores greater than 0.5 could be considered as “influential”). A complete list of the broadly influential properties for the mercury test case based on sensitivity scores is presented in Appendix D.4. In general, many of the same properties are influential when sensitivity scores rather than elasticities are used to define “influence.” However, note that some properties in Exhibit 5-16 that are broadly influential based on elasticity are less influential when sensitivity scores are used to quantify influence. For example, rainfall rate is a less influential property when influence is based on sensitivity scores rather than elasticity because the CV assigned to rain is low (0.1) relative to the CVs assigned to other broadly influential properties (e.g., emission rate, with a CV of 1 for both mercury species; vapor washout ratio for Hg^{2+} , with a CV of 3). These sensitivity results can be useful for focusing data collection efforts, assuming there is a relatively high degree of confidence in the CVs assigned. Note that some properties were assigned preliminary CVs if literature values were not identified; these CV estimates may need to be refined prior to drawing strong conclusions based on sensitivity score.

5.4 Summary of Sensitivity Analysis

The sensitivity analysis described in this chapter, which follows a relatively simple analytic design befitting an initial, broadly scoped investigation of TRIM.FaTE's sensitivity to changes in model inputs, provides much useful information that contributes to model evaluation. The results indicate that the model appears to be working as expected, given the physical, chemical, and biological processes being modeled and the algorithms and input values in place for the mercury test case, thus increasing the overall confidence that the model is performing as designed. As explained throughout the chapter, most results appear to be logical, reasonable, and in line with expectations given the algorithms and prior knowledge of the processes being modeled. Thus, this analysis fortifies the evaluation results and strengthens confidence in TRIM.FaTE's performance. Evaluation of the sensitivity analysis results also has led to enhanced understanding of how various aspects of the model are working in real applications (e.g., the surface water solids density results discussed in Section 5.2.5).

These results affirm that many different input properties can have a strong influence on the modeling results, depending on the compartment type and chemical under consideration. Compartment types farther removed from the point of pollutant entry into the modeling scenario (i.e., "downstream" compartment types) typically have a large number of influential properties, sometimes much larger than the more "upstream" compartment types. As an example, contrast the results for air and surface soil to those for water-column carnivore. Water-column carnivore has 41 properties with elasticity value > 0.1 compared with four for air and 11 for surface soil. The large number of potentially influential properties underscores the number and complexity of processes and compartment interactions being modeled by TRIM.FaTE.

Some properties have a strong influence, characterized by a high elasticity for an individual compartment type, and a subset of these properties has a broad influence as well, characterized by a high elasticity for multiple compartment types. Among the properties that are broadly influential are mercury emission rates from the source, air deposition-related properties, mercury transformation rates, K_d values, and water and air temperature. An important caveat to these results is that other properties not identified here also can be influential, depending on the modeling scenario (e.g., compartment types, spatial layout, algorithms, input values selected by the user) being evaluated. Moreover, as described in the limitations discussion in Section 5.1, not all properties were considered in this sensitivity analysis.

These sensitivity analysis results can inform data collection for future TRIM.FaTE applications, as well as help focus areas for further model development. For TRIM.FaTE applications similar to the mercury test case, properties near the top of the tornado charts in Section 5.2 (and tables in Appendix D.2), especially those appearing on Exhibit 5-17, should be given careful consideration in data collection and the selection of input values. Information on variability and uncertainty associated with properties, such as sensitivity score information, should also be considered. If one or two compartment types are the major focus of an application, then properties influential for those should be given primary attention.

Additional sensitivity and related analyses could be done to build on these findings, including:

- Analyses assessing sensitivity to properties not considered here;
- More detailed studies focused on individual compartments, properties, and chemicals of interest (some such analyses were done in the course of investigating the results reported here);
- More complex studies designed to account for known correlations among properties;
- Studies of sensitivity to changes in spatial layout;
- Studies of sensitivity to different representations of the biota in an ecosystem;
- Studies of sensitivity to time-varying inputs, using TRIM.FaTE's dynamic mode;
- Studies of how sensitivity may change over time, using TRIM.FaTE's dynamic mode; and
- Monte Carlo analyses of variability and uncertainty based on sampling property values from specified distributions.

6. INITIAL COMPARISONS OF TRIM.FaTE AND 3MRA MODELING RESULTS

This chapter presents an initial set of comparisons between TRIM.FaTE modeling results for the mercury test case and corresponding results from a somewhat customized application of 3MRA, an EPA multimedia fate and transport, exposure, and risk model developed originally for analysis of hazardous waste management policies. This set of modeling analyses and comparisons is an important part of EPA's evaluation plan for both of these models.¹ The ultimate objective of this work is to enhance the level of confidence in both models. The immediate objective of the initial comparative work reported here was to identify similarities and differences between the models through comparisons of results, and then identify areas for further investigation and areas where refinement of inputs or algorithms may be appropriate.

This chapter describes the first set of comparisons between these two multimedia models. Further analysis and comparison of TRIM.FaTE and 3MRA is envisioned, leading to increased confidence in both models. Note that the current analysis focuses on *comparisons of modeling results for a specific application* and is not intended to be a comprehensive comparative review of all modeling concepts, structures, algorithms, and data inputs for these two complex models. Extensive documentation is available for both models via EPA's website (see Chapters 1 and 2 for TRIM.FaTE references; see next subsection for 3MRA references).

Following an introductory overview of 3MRA to provide context for the comparison of model results, Section 6.1 describes the approach taken for this analysis. Sections 6.2 through 6.5 present and compare the modeling results for related groups of media – air and leaf (Section 6.2), surface soil, roots, and earthworm (Section 6.3), surface water, benthic sediment, and fish (Section 6.4), and wildlife (Section 6.5).

Overview of 3MRA

3MRA is an environmental modeling system designed to facilitate site-based human and ecological risk assessments at local, regional, and national scales. 3MRA combines data bases containing chemical, climatological, and site data with a series of 17 science-based simulation models within a fully integrated software architecture to provide a user the ability to execute Monte Carlo-based assessment methodologies. See Appendix E for a discussion of the overall systems design of 3MRA and a list of the system processors that collectively manage the execution of the 3MRA modeling system.

Within 3MRA, the Multi-media Simulation Processor (MMSP) manages the invocation, execution, and error handling associated with the 17 individual science models that simulate source release, multimedia fate and transport, foodweb dynamics, and human/ecological exposure and risk. Exhibit 6-1 illustrates the 3MRA multimedia model design contained within

¹ In addition to the work reported in this document and *TRIM.FaTE Evaluation Report: Volume I* (EPA 2002a), other evaluation activities for TRIM.FaTE include comprehensive test cases with PAHs and dioxins/furans, which include comparisons with other EPA multimedia modeling methods (EPA 2004, EPA 2005b, other documentation in preparation).

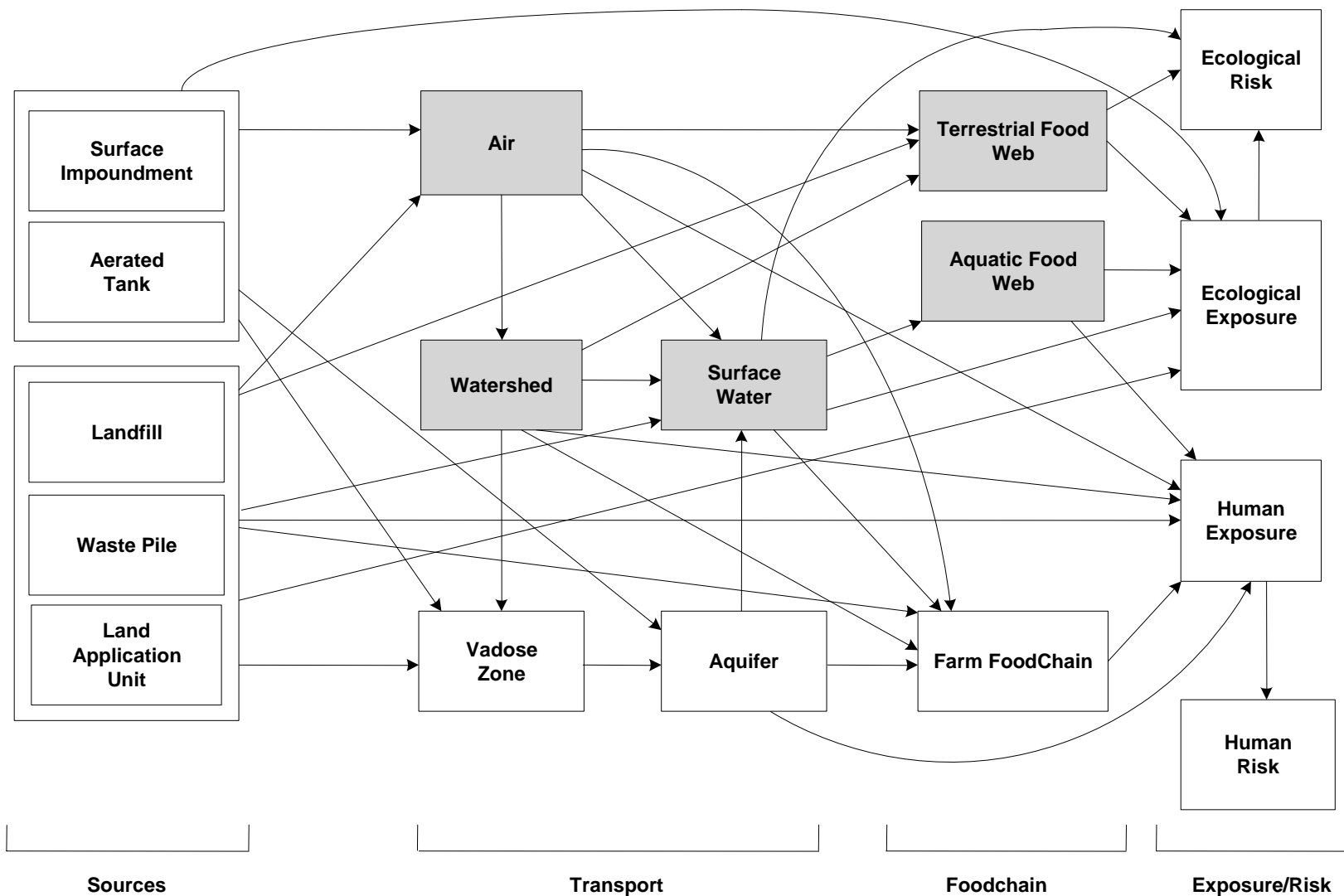
the MMSP, highlighting the modules that were used as part of this model comparison study. The science modules used in this assessment are: the atmospheric, watershed, and surface water modules (which simulate the fate and transport of contaminants through the multimedia environment) and the terrestrial food web and aquatic food web modules (which simulate the contaminant uptake through the food web). The modules not used are the vadose zone, aquifer, farm food chain, human and ecological exposure, and human and ecological risk modules. The modules included in 3MRA represent a “linked media” model, meaning that individual simulation modules, representing each element of a risk assessment, are executed in a logical sequence from source to fate and transport to food web to exposure and risk (when they are all implemented in the simulation). Although certain components of 3MRA’s chemical fate and transport modules maintain a mass balance, it is not a mass balance model in the same sense as TRIM.FaTE.

To download the 3MRA model and access a series of documents describing the 3MRA modeling system in detail, the reader is referred to the following web sites:

- <http://www.epa.gov/ceampubl/mmedia/index.htm> (modeling system); and
- <http://www.epa.gov/epaoswer/hazwaste/id/hwirwste/risk.htm> (documentation).

In addition to employing only a subset of the 3MRA modules, there were several aspects of this application of 3MRA which differ from their description in the documents cited above. These differences are noted within this chapter.

Exhibit 6-1. Linkages Among the Source, Fate, Transport, Exposure, and Risk Modules for the 3MRA Modeling System ^a



^a 3MRA modules used in this model comparison are shaded.

6.1 Approach to Comparison of Modeling Results

Through a series of discussions beginning in 2002, the TRIM.FaTE team and the 3MRA team designed the overall approach for the initial comparisons of modeling results described here. The TRIM.FaTE mercury test case site was chosen as the modeling location. One important decision was that the two teams would, after initial consultations on comparison goals and endpoints and the setting of a few ground rules (e.g., emission rate, time period), work independently in setting up and running the models. The two teams independently developed conceptual site layouts and model input data, with no attempt made to match the layouts or to reconcile the input data (with a few exceptions, noted in Section 6.1.2). The reasoning behind this decision was that the comparison would be most informative if both teams set up and applied their models in the way they judged best for this application, rather than trying to match the model set up and input data as closely as possible.² Thus, rather than a fairly narrow comparison focused on the algorithms, the approach provides a broad comparison of model set up, model algorithms, and model input data. Of course, the selected approach results in a more complex comparison of results – there are more possible explanations for any differences observed – but also allows for a more robust analysis. To date, the teams have only begun the process of reconciling the extent to which comparisons of model outputs that are presented here are driven by differences in conceptual site layout, modeling assumptions and algorithms, and the model input data used.

One initial determination was the selection of the chemicals and endpoints to be compared – which chemicals in which media and at which locations would be the focus of the comparison. Because of the significance of mercury, and given that both models have the capability to handle mercury and that much prior work had been done with TRIM.FaTE related to mercury, it was selected as the chemical on which to focus (U.S. EPA 2002a). Exhibit 6-2 lists the comparison endpoints. Endpoints were selected based on several criteria, including:

- To provide a broad set of media, including both abiotic and biotic, for comparison;
- To provide multiple locations so that spatial trends/differences could be examined; and
- To cover media of particular interest, such as upper trophic-level fish, and locations of particular interest, such as Swetts Pond.

For this application, 3MRA modeled methyl mercury (MHg) in fish; total mercury in wildlife; elemental (Hg^0), divalent (Hg^{2+}), and methyl mercury in surface water and sediment; and divalent mercury in all other media. TRIM.FaTE modeled all three forms of mercury in all media, based on reversible first-order transformation processes. In some cases, the transformation between mercury forms was presumed negligible and transformation rates for the TRIM.FaTE application were set to zero. For many of the media compared here, the focus is on divalent mercury because it is considered to be the most significant environmental form for those media. For fish, the comparison focuses on methyl mercury for the same reason. For surface water and benthic sediment, all three forms of mercury are compared, given that all can be

² Note that for some processes, 3MRA was set up in a simplified form to facilitate the comparison.

important and both models were set up to model all three forms. For wildlife, the comparison focuses on total mercury, largely because of substantial uncertainties in modeling speciation (see Section 6.5). Because both models are designed primarily for long-term (years rather than months or days) applications, it was decided that all comparisons would be based on annual average mercury concentrations.

**Exhibit 6-2
Endpoints Selected for Comparison of Modeling Results**

Medium	Mercury Species	Comparison Locations ^a	
		3MRA	TRIM.FaTE
Air	Hg ²⁺	Watershed 4 → Watershed 10 → Watershed 11 → Watershed 14 →	SSE3, SSE4 SSE1, ESE1 W2, SSW2 W2, NNW2
Surface soil	Hg ²⁺	Watershed 4 → Watershed 10 → Watershed 11 → Watershed 14 → Watershed 9 →	SSE4 SE1, E1 SW2 N2, W2 NE2, E1
Surface water (whole water)	Hg ⁰ , Hg ²⁺ , MHg, Total Hg	Swetts Pond (1,7) → Brewer Lake (1, 11) →	Swetts Pond Brewer Lake
Benthic sediment	Hg ⁰ , Hg ²⁺ , MHg, Total Hg	Swetts Pond (1,7) → Brewer Lake (1, 11) →	Swetts Pond Brewer Lake
Fish	MHg	Swetts Pond (1,7) → Brewer Lake (1, 11) →	Swetts Pond Brewer Lake
Terrestrial plant-leaf Terrestrial plant-root	Hg ²⁺ Hg ²⁺ , Total Hg	Watershed 11 (Habitat 3) → Watershed 11 (Habitat 3) →	SW2 SW2
Earthworm	Hg ²⁺ , Total Hg	Watershed 4 (Habitat 11) → Watershed 9 (Habitat 9) → Watershed 11 (Habitat 3) → Watershed 14 (Habitat 8) →	SSE4 NE2, E1 SW2 N2, W2
Birds	Total Hg	Watershed 4 (Habitat 11) → Watershed 11 (Habitat 3) →	SSE4 SW2
Mammals	Total Hg	Watershed 4 (Habitat 11) → Watershed 9 (Habitat 9) → Watershed 11 (Habitat 3) → Watershed 14 (Habitat 8) →	SSE4 NE2, E1 SW2 N2, W2

^a See maps in Exhibits 6-4 (air), 6-5 (soil and water), and 6-6 (habitat) for locations. Two TRIM.FaTE parcels were used in cases where the 3MRA location was on or near a parcel boundary.

6.1.1 Inherent Differences/Similarities in Spatial Resolution of Model Outputs

For this comparison, 3MRA and TRIM.FaTE take different approaches to estimating chemical concentrations over space. As a result of the underlying model design, TRIM.FaTE outputs inherently are values associated with a volume of space, or the associated biotic population. In contrast, most outputs from this application of 3MRA are values associated with a point in space, or the biotic population at that point. Note that in other applications of 3MRA, some of these point-based outputs are more typically based on spatially averaged areas.

For all abiotic media, TRIM.FaTE (in its deterministic mode, as run here) estimates a single value for chemical concentration that applies over the volume associated with a given compartment at a given point in time.³ For surface water and benthic sediment, 3MRA follows a comparable approach. For air, however, 3MRA estimates a concentration at a point in space, which in this application is ground level at the centroid of selected delineated watersheds. Therefore, the air comparisons are between essentially a volume-average value from TRIM.FaTE and a value at a point in space from 3MRA. For soil, 3MRA estimates an average concentration within a soil core of particular depth at a specific location (which is the same as the air location). Thus, the soil comparisons are between essentially a volume-average concentration from TRIM.FaTE and a depth-averaged concentration at a specific location from 3MRA.

The spatial resolution for biota, conceptually, is more similar between the two models. Both TRIM.FaTE and 3MRA estimate a single chemical concentration that applies to a particular population⁴ that may have associations with one or more spatial locations (e.g., pertaining to residence, grazing, predation). For fish, the similar spatial resolution of the two models for surface water and sediment leads to spatial comparability in the results. For land-based biota, a simplified approach was taken in the application of 3MRA such that the spatial associations and their role in the conceptual approach to pollutant transfers into wildlife differ between the two models. This difference is described in Section 6.5. It is notable here, however, that for this model comparison application the 3MRA wildlife population results were directly derived from the 3MRA soil results, which as described above are for a specific point location⁵ (versus being derived for a particular area by TRIM.FaTE). Similarly, the 3MRA vegetation results are also for a specific point location (based on soil and air predictions there)

³ TRIM.FaTE estimates the chemical mass in a compartment associated with an environmental medium volume element (e.g., air, surface water, soil layer) or a biological population (e.g., raccoon, earthworm). Because in TRIM.FaTE the chemical mass is assumed to be homogeneously distributed within a compartment's volume or population, compartment concentrations generally may be considered to be average concentrations for the volume or population represented.

⁴ Neither TRIM.FaTE nor 3MRA attempt to model population dynamics. The populations modeled represent the same species living in a defined area.

⁵ The 3MRA module that was used to model the wildlife accumulation, the Terrestrial Food Web, calculates chemical concentrations in biota based on media concentrations and empirical BAFs. The Ecological Exposure module, which was not used in this 3MRA model simulation, calculates biota intake rates based on diet and food chain for predator species.

versus the TRIM.FaTE compartment approach for a particular area. The differing approaches to spatial resolution in modeling mercury concentrations are summarized in Exhibit 6-3.

Given the above differences in basic approach, particularly for abiotic media, combined with the fact that the spatial layouts for the two models were designed independently, it is not possible to get an exact spatial match for comparing the modeling results. The comparison locations were selected to provide the best possible spatial matching, but would not be expected to yield perfectly matched results even if the models worked in exactly the same way. In other words, there is some built-in incompatibility (i.e., expectation of different results) in the approaches because of the inherent differences in spatial resolution of the results. In many cases, two TRIM.FaTE locations are compared to a single 3MRA location in an attempt to bound the 3MRA location using the closest spatial matches.

Given the differences described above, the general approach for selecting matched locations for comparison across the two models' results (see Exhibit 6-2 for the location matches) differed by medium, as described below.

- For surface water, benthic sediment, and fish, the same water body was selected. In this case, there is both a good location match (same water body) and good comparability between the spatial aspects of the measure (in effect, both models provide spatial-average concentrations for the same location).
- For air and soil, the TRIM.FaTE parcel that the 3MRA estimation point (watershed centroid) falls within was selected. If a 3MRA point falls near a boundary, multiple TRIM.FaTE parcels were selected to bound the 3MRA location. An important difference between the air concentration estimates from the two models is that the TRIM.FaTE concentrations are essentially volume averages (based on dividing the mass in a compartment by the compartment volume) while the 3MRA concentrations are point concentrations at ground level.
- For land-based biota, the animal and plant compartments associated with the TRIM.FaTE parcel in which the 3MRA estimation point (watershed centroid matched to relevant biota habitat) is located were selected. Consistent with the matching approach for soil, if a 3MRA point falls near a TRIM.FaTE parcel boundary, multiple TRIM.FaTE parcels were selected.

Exhibit 6-4 is a map showing the TRIM.FaTE air parcel layout along with the 3MRA estimation points, which are at the centroids of the watersheds delineated in the 3MRA set-up process. Exhibit 6-5 is a similar map showing the TRIM.FaTE surface parcel layout along with the 3MRA estimation points for soil, which also are at the centroids of the 3MRA-delineated watersheds. Note that the TRIM.FaTE parcel layouts differ for air and surface, but the 3MRA estimation points are the same on both maps (meaning that the deposition flux to a surface point in 3MRA is directly correlated with the air point above, while the deposition flux to a TRIM.FaTE surface parcel could be affected by multiple air compartments if more than one air compartment overlaps it). Exhibit 6-6 is a map overlaying the 3MRA-defined habitats on the TRIM.FaTE surface parcel layout, with the 3MRA watershed centroid locations shown as well.

Exhibit 6-3
General Approach to Spatial Resolution in Modeling of Mercury Concentrations

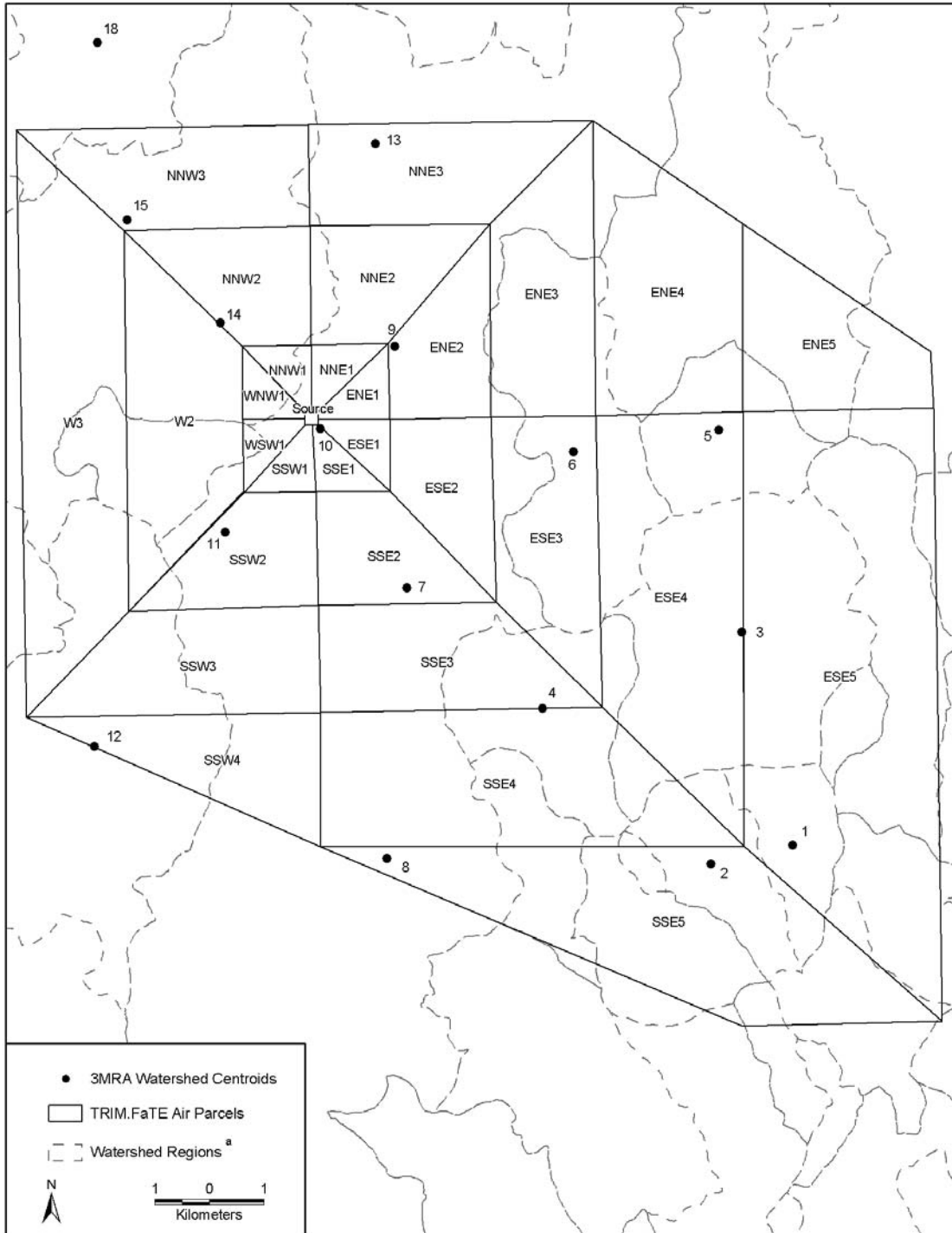
Medium/Biota	TRIM.FaTE	3MRA (in this application)
Air	Estimate for volume of air associated with an air compartment ^a	Point estimate at ground level at watershed centroid
Soil	Estimate for volume of soil associated with a soil (surface or root zone) compartment	Depth-averaged point estimate (e.g., for top 1 cm, or for top 5 cm) at watershed centroid
Surface water	Estimate for volume of surface water associated with a surface water compartment	Estimate for full volume of water body
Sediment	Estimate for volume of sediment associated with a sediment compartment	Estimate for full volume of water body sediment
Fish	Estimate for fish compartment representing a population of given type (e.g., benthic carnivore) and size in a water body	Estimate for all fish of given type (e.g., T4) in a water body
Leaf	Estimate for leaf compartment associated with a surface soil parcel	Point estimate associated with a pair of soil and air point concentrations at watershed centroid ^b
Root	Estimate for root compartment associated with a surface soil parcel	Point estimate associated with a pair of soil and air point concentrations at watershed centroid ^b
Earthworm	Estimate for earthworm compartment associated with a surface soil parcel	Point estimate associated with a soil point concentration at watershed centroid ^b
Mammal/bird	Estimate for mammal or bird compartment representing a population of a given species and size associated with a given parcel (and perhaps linked to food, water, and predators in other parcels)	Point estimate for given species associated with a soil point concentration at watershed centroid ^b

^a In TRIM.FaTE it is assumed that chemical mass within a compartment is homogeneously distributed. Consequently, the compartment concentration generally may be considered to be an average for the associated volume of media or biological population.

^b This approach is different from 3MRA's usual application, in which it derives spatially averaged values for vegetation, earthworms, mammals, and birds based on extent of overlap of a delineated habitat with soils having different modeled concentrations.

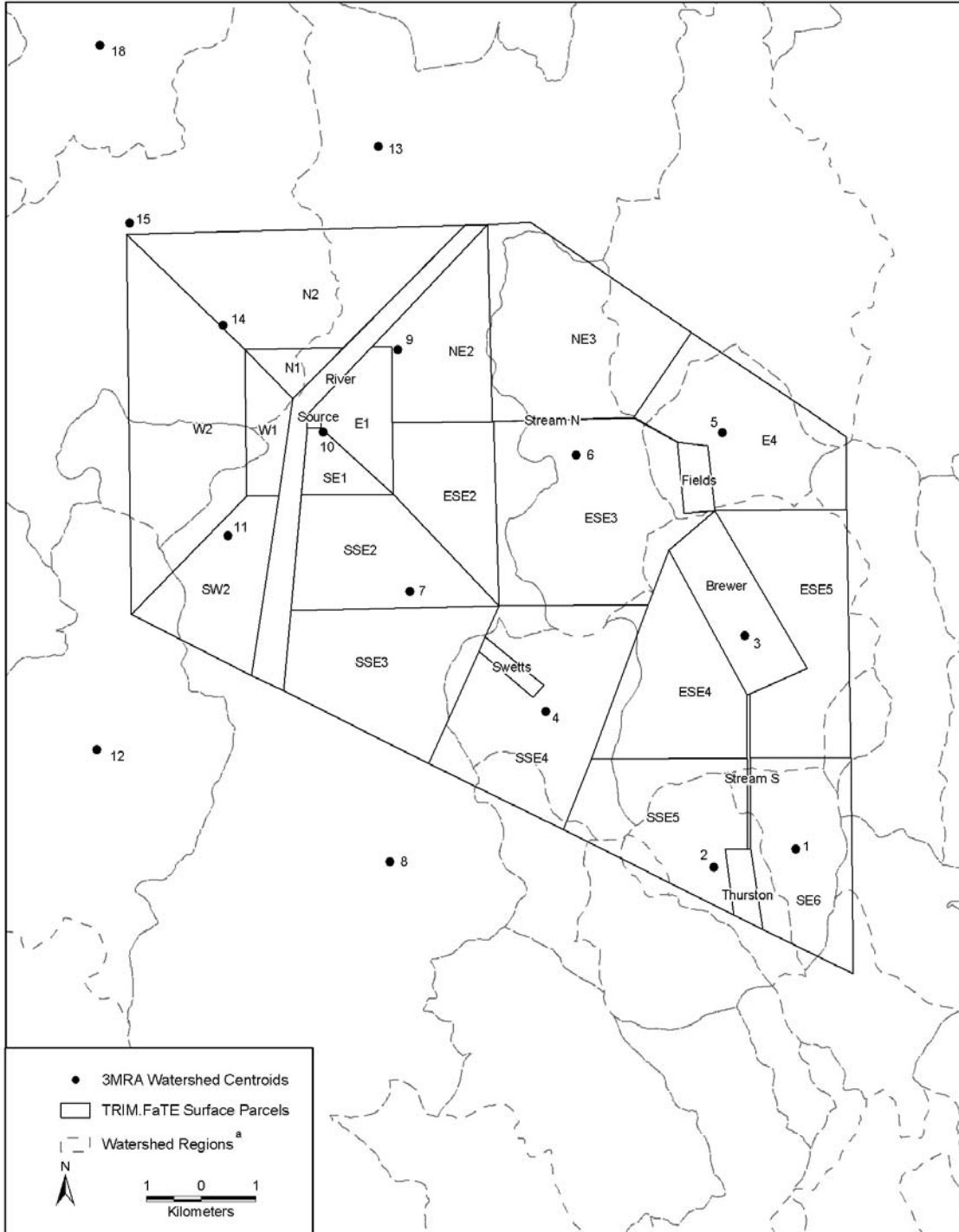
For this application, in order to simplify the layout, the 3MRA team matched each habitat with a single watershed centroid, which was then used to estimate mercury concentrations for the land-based plants and animals associated with that habitat (see Exhibit 6-2 for the habitat-watershed matches relevant to this model comparison and Section 6.1.2 for a description of the habitats).

Exhibit 6-4 Spatial Layout for Air – Both Models



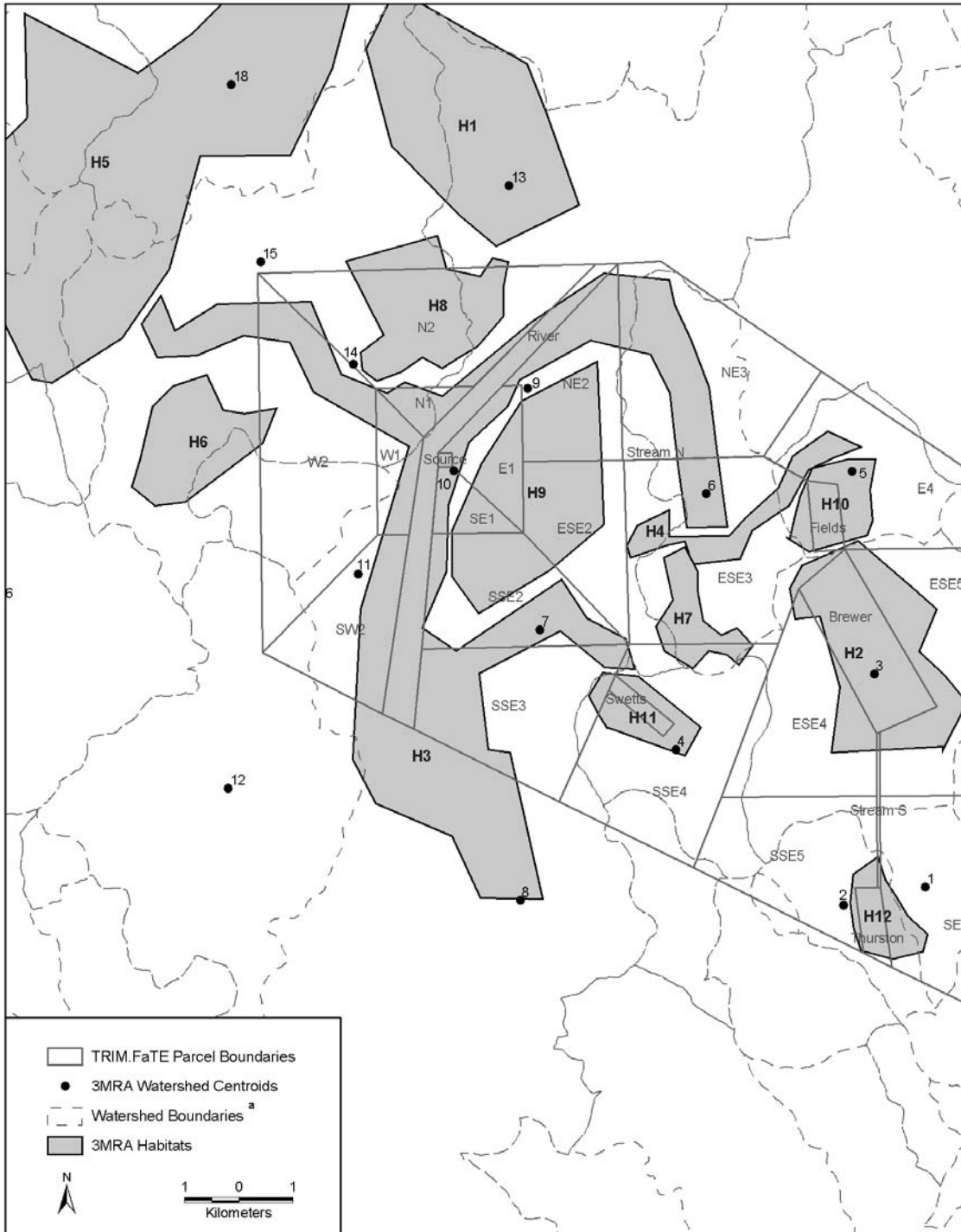
^a Not all watershed boundaries are shown. See Exhibit 6-9 for additional delineation of the watersheds.

Exhibit 6-5
Spatial Layout for Surface Soil and Surface Water – Both Models



^a Not all watershed boundaries are shown. See Exhibit 6-9 for additional delineation of the watersheds.

Exhibit 6-6 Overlay of 3MRA Habitats on TRIM.FaTE Surface Layout



^aNot all watershed boundaries are shown. See Exhibit 6-9 for additional delineation of the watersheds.

6.1.2 Model Set-up and Input Data

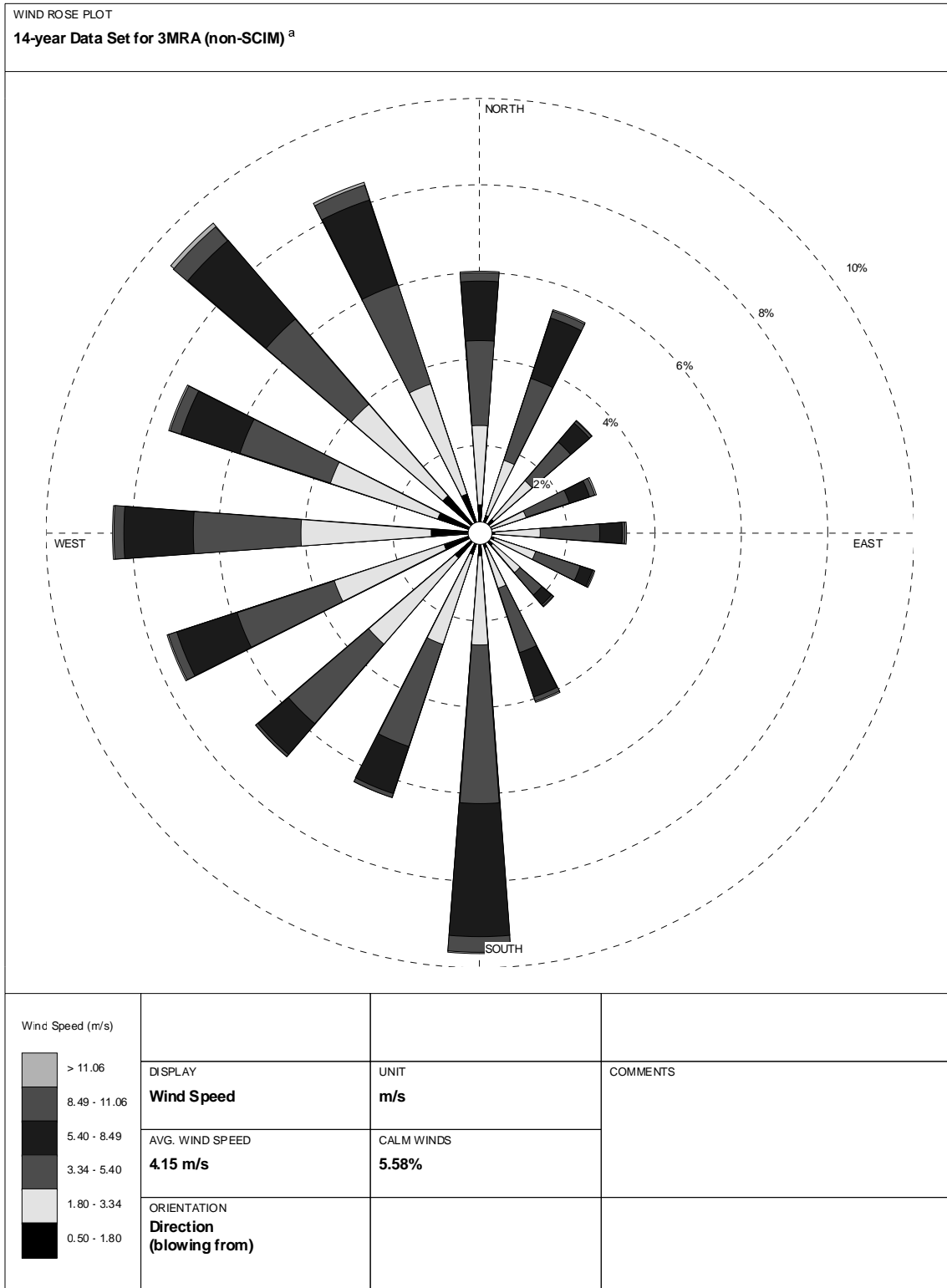
As noted in the introduction, the site conceptualization and model set-up were done independently for the two models, as was the selection of most input data. The TRIM.FaTE set-up is described in Chapters 1 and 2, and the input data used are documented in Appendix A. The 3MRA set-up process is described in a separate subsection below. TRIM.FaTE emission case A (constant and continuous emission of 17.663 grams per day of divalent mercury from ground-level fugitive sources for 30 years, with no initial chemical concentrations or boundary contributions) is used as the basis for all comparisons to the 3MRA simulation, which matched the TRIM.FaTE source characteristics. The emissions simulation time period that was selected for comparison was 30 years, even though 3MRA was run for an additional 170 years after the source was shut off to provide additional information to the 3MRA team (total of 200 years). The focus of the results comparison reported here is on the 30-year source operating period that was modeled by both 3MRA and TRIM.FaTE.⁶

Although it is most frequently applied in a Monte Carlo analysis mode, 3MRA was used in a deterministic mode for this initial comparative analysis – that is, a single set of parameter inputs was used to calculate one set of model outputs. Most of the parameter input values used for 3MRA were selected randomly from the parameter frequency distributions contained in 3MRA for the region corresponding to the test case site location. These distributions are described in the previously referenced 3MRA documentation. Consistent with the original design of this comparison, no attempt was made to match (or even compare) most data inputs, other than the location of the emission source. One prominent exception, as noted above, is the emission pattern and rate, which was set equal to that used for TRIM.FaTE. For both models, a guiding principle for developing all aspects of the model set-up and selecting all input data was to follow the approach that would most likely be used to apply each model to the given site, using the data bases and methods that have been developed for each model.

Although the same location (i.e., source coordinates) was used as a basis for developing meteorological data, the two teams identified and processed their meteorological data inputs separately. Thus, this important set of inputs differs between the models. For TRIM.FaTE, a five-year (1987 to 1991) data set was repeated through the 30-year modeling period. The data set is a composite from three meteorological data measurement stations – wind speed and direction and air temperature from a nearby station, precipitation rate from a different nearby station with more complete records, and the upper air data needed to estimate mixing height from a station roughly 100 miles to the southwest. For 3MRA, 14 years (1961 to 1964, 1979 to 1982, 1984 to 1989) of data were compiled from one station – the station used for TRIM.FaTE's upper air data (100 miles southwest of the source) – and run in the air model (ISCST3). The resulting air concentrations and deposition fluxes were averaged at each location to generate single representative air concentration and deposition values. Wind roses derived from both full data sets are provided to give a sense of the comparability of the input wind data used for the two models (Exhibit 2-7 for TRIM.FaTE, Exhibit 6-7 for 3MRA). Overall wind direction patterns

⁶ The 3MRA simulation involved first running the air model (ISCST3) for a 14-year period using the selected hourly meteorological data. The resulting hourly mercury air concentrations and deposition rates were averaged over the entire 14-year period to obtain constant values at each location. These estimates were then used as constant air concentration and deposition inputs to the other 3MRA modules for the 200-year period.

Exhibit 6-7 Wind Rose Representing 3MRA 14-year Input Data Set



^aThis wind rose represents the entire set of meteorological data used for the 3MRA application. Thus it is labeled “non-SCIM” – it was not produced using the Sampled Chronological Input Model (SCIM) option which pulls a sample of the meteorological data.

look generally similar (peaks from the south and northwest, very low frequency from the east), but there are noticeable differences. The average wind speed for the 3MRA input data is a little higher than for the TRIM.FaTE input data, 4.15 m/sec versus 3.64 m/sec. As shown below (in centimeters), the annual rainfall totals input for the two models are similar with respect to cumulative total, average, and variability, although there are notable year-to-year differences (and likely greater differences at smaller time scales):

- TRIM.FaTE: 93, 78, 112, 123, 113 (cumulative 30-year rainfall = 3,114 cm; mean annual rainfall = 104 cm; standard deviation of mean = 18 cm); and
- 3MRA: 99, 118, 98, 88, 156, 86, 116, 101, 123, 87, 113, 104, 111, 106 (cumulative 30-year rainfall = 3,227 cm; mean annual rainfall = 108 cm; standard deviation of mean = 18 cm).

In addition to source location and emissions, the other input parameters that were matched between the two modeling simulations were the solids:water partition coefficients (Kd) used for the three mercury species in surface water and in benthic sediment. For both models this parameter was set to values used in EPA's *Mercury Study Report to Congress* (EPA 1997).

- Surface water: $\text{Hg}^0 = 1,000$, $\text{Hg}^{2+} = 100,000$, $\text{MHg} = 100,000$ L/kg; and
- Benthic sediment: $\text{Hg}^0 = 3,000$, $\text{Hg}^{2+} = 50,000$, $\text{MHg} = 3,000$ L/kg.

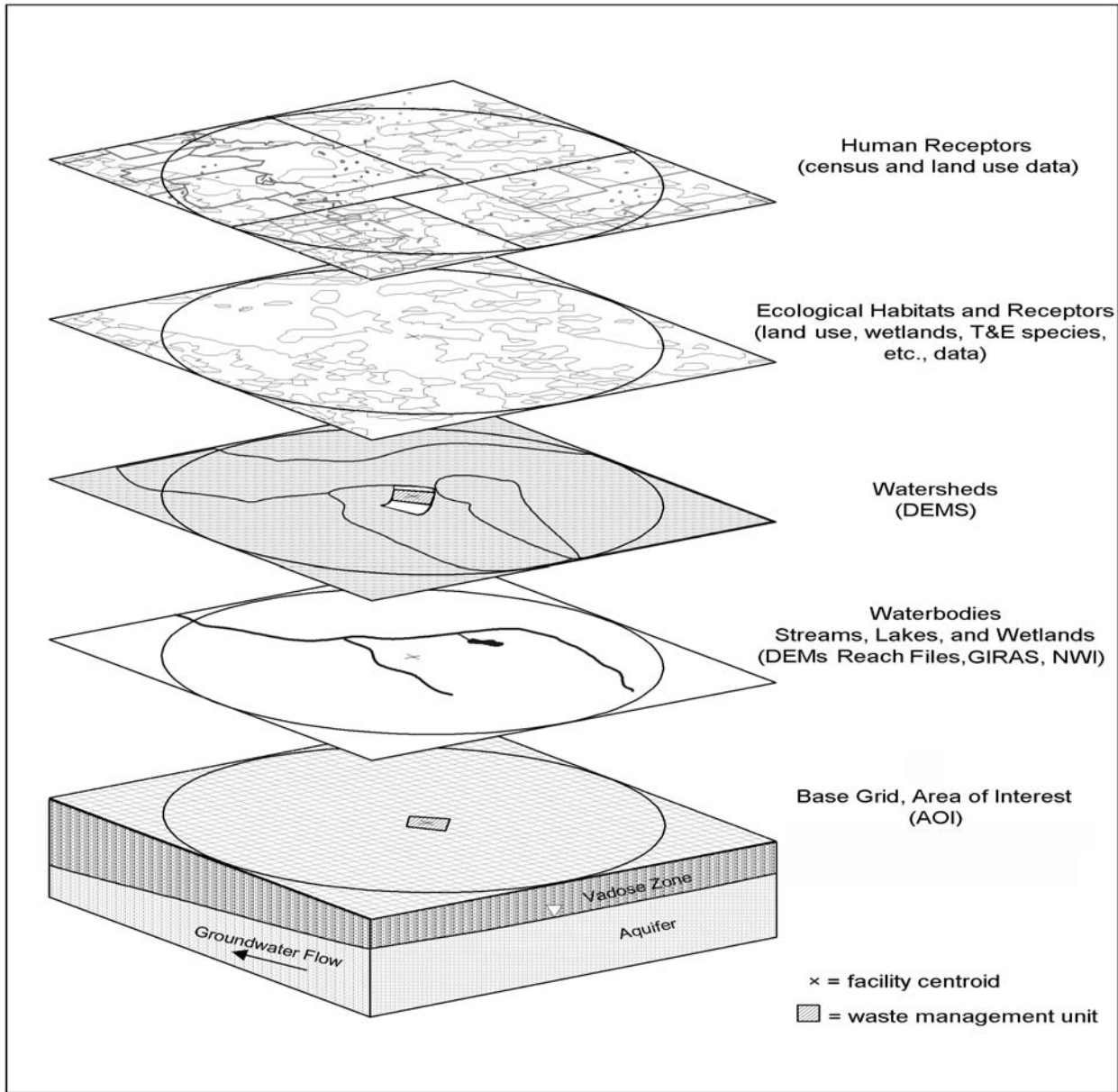
Approach to 3MRA Set-up for this Application

Set-up of the 3MRA model for conducting site assessments involves delineation of spatial features and specification of the modeling-based connectivity among them. Exhibit 6-8 displays the key spatial features that can be included in a 3MRA simulation. Also listed are GIS-based sources of information for describing the features. 3MRA allows delineation of physiographic features to conform to site-specific natural boundaries. Spatial features characterized for this model comparison application of 3MRA include specification of the area of interest (AOI), watersheds, a surface water network, and ecological habitats (including home ranges for resident species of interest). In addition, point locations where the atmospheric model reports mercury air concentrations and deposition fluxes were specified. The deposition fluxes are used to estimate location-specific soil concentrations.

The extent of the AOI to be modeled by 3MRA is generally constrained only by the availability of data and the spatial domain of the science modules. 3MRA applications to date have simulated AOIs extending to 15 kilometers from the source, with typical simulations extending a few kilometers. The AOI for this study (described in Chapter 2), however, was bounded, in terms of extent, primarily on the basis of specific water bodies that may be most affected by the mercury releases to the air from the source being modeled.

The approach taken for site set-up for this 3MRA application is characterized as a site-specific screening assessment. The physiographic layout is site-specific, with environmental data reflecting a combination of site-specific data, when readily available, and data representative of the region within which the site exists. The 3MRA modeling system includes

Exhibit 6-8
GIS View of Site-based Spatial Overlays for 3MRA Modeling System



regional data bases of model parameters. When site-specific information is not available for a model input, a random sample is taken from the regional data base and assigned to the site.

For this application, the following spatial features were delineated using GIS information sources:

- Watershed sub-basins;
- Surface water network (and associated reach definitions); and
- Ecological habitats (and associated species home ranges).

Watershed sub-basins for the AOI, along with the associated surface water network, are shown in Exhibit 6-9. Watersheds are modeled as a homogeneous land unit, each independent of others (i.e., there is no runoff or erosion of soils between watersheds). For this study 18 watershed sub-basins were delineated and modeled. With 3MRA, mercury concentrations in soil within the watershed can be estimated as a function of the atmospheric deposition reported at various locations within the watershed.⁷ For this application, however, a single point was assigned to the centroid of each watershed for estimating air deposition and soil concentration.

Watersheds deliver runoff, erosive fluxes of soil-based particles, and associated contaminant to surface waters. In 3MRA, surface water networks are constructed based on the connectivity among surface waters in the AOI. One or more surface water networks can be simulated within 3MRA. Each surface water network is segmented into “reaches,” reflecting individual ponds/lakes, wetlands, and segments of streams/rivers between tributaries. As shown in Exhibit 6-9, there is a single surface water network configured for this model application. The network consists of 15 reaches, three within the main river, which is the receiving water body for flow from all other reaches within the AOI. Other surface water reaches include four stream reaches, four wetland reaches, and four lake reaches. Surface water reaches receive contaminant loadings from the atmosphere and from watersheds. In this application of 3MRA, each water body receives runoff/erosion-based loadings from a single watershed and atmospheric loadings (i.e., deposition) based on a single air point (the centroid of the watershed). This connectivity can be inferred from Exhibit 6-9. However, 3MRA does have the flexibility to allow for surface water reaches to receive atmospheric contaminant loadings from multiple air points located within the area of specific reaches, and watershed loadings may be weighted (similar to the air points) to allow runoff and erosion to affect multiple water body reaches (these capabilities were not implemented in this assessment).

Ecological habitats are delineated for a 3MRA application based on simultaneous consideration of land use, surface water locations, watershed boundaries, and regional ecosystem classifications. For this application, as shown in Exhibit 6-6, 12 specific habitat areas were delineated: one residential, one lake, one stream, two forest wetlands, two crop, two forests, and three ponds. Each habitat area can be assigned a list of animal species whose home ranges are

⁷ If multiple deposition points in a watershed are used, the individual deposition fluxes are assigned weighting factors that determine their relative impact on the entire watershed. For example, 10 air points may be located within a single watershed, each with a weighting factor of 0.1. The single soil concentration estimated for this watershed, for purposes of estimating erosive fluxes, would be a function of the weighted average deposition flux.

**Exhibit 6-9
Watershed and Surface Water Reach Network Delineated for this Application**



—	Streams	Water Body Network Key		
■	Water Body Network	1. Stream/River	6. Wetland	11. Lake/Pond
- - -	Watershed Boundaries	2. Stream/River	7. Lake/Pond	12. Lake/Pond
X	Source	3. Stream/River	8. Stream	13. Wetland
		4. Stream	9. Lake/Pond	14. Wetland
		5. Stream	10. Wetland	15. Stream

contained within the habitat. Species can be assigned with the goal of representing a complete food web, thus enabling the estimation of chemical doses as a function of diet. For this application the species list for individual habitats was assigned based on regional ecosystem considerations, as opposed to a site-specific investigation (see Section 6.5 for a list of wildlife species included). Home ranges are typically assigned randomly within the habitat area with the condition that predator-prey relationships must be preserved (i.e., home ranges must overlap). For this application, however, home ranges were assigned such that overlap occurs for all species (thus all potential prey for a predator is available for dietary consumption).

6.2 Air and Leaves

This section provides a comparison of the modeling approaches affecting mercury concentrations in the air, deposition fluxes, and concentrations in the leaves, as well as a comparison of these modeling outputs. The comparison of outputs focuses primarily on TRIM.FaTE surface parcel SW2, TRIM.FaTE air parcels SSW2 and W2, 3MRA watershed 11, and 3MRA habitat 3 (Exhibit 6-6). These locations were selected because of the relatively good spatial match between 3MRA and TRIM.FaTE, and because habitat 3 and TRIM.FaTE surface parcel SW2 have similar vegetation types that can be compared. The spatial distribution of air concentrations and deposition fluxes is also discussed for the two models for the entire modeling region. In the two media being compared in this section, divalent mercury was the only mercury species modeled with 3MRA. Three mercury species were modeled with TRIM.FaTE (divalent, elemental, and methyl), but only divalent concentrations are presented because concentrations of the other two species are negligible in air and plant leaves.

6.2.1 Divalent Mercury Concentrations in Air

In this analysis, the initial input of chemical mass to all other media modeled with 3MRA and TRIM.FaTE comes from air. However, TRIM.FaTE and 3MRA use different methods for simulating chemical fate in the air (see Exhibit 6-10 for a comparison of air-related mass transfer and transformation processes used in the two models). 3MRA's air modeling is performed with EPA's Industrial Source Complex Short-Term Model, Version 3 (ISCST3). The fate and transport algorithms in ISCST3 are based on Gaussian dispersion equations that are solved for a given set of temporal and spatial circumstances. For this 3MRA application, the long-term average air concentration at ground level at each watershed centroid location was calculated using ISCST3 and 14 years of meteorological data, and each resulting value was applied to the entire corresponding 3MRA watershed as a constant throughout the duration of the simulation. ISCST3 formulates a steady-state representation of the contaminant plume each hour. The mass of contaminant in the ISCST3 plume is consistent with the mass emitted during that hour, but it is not a mass balance model because mass is not tracked hour-to-hour. TRIM.FaTE, which is a mass balance model, includes a grid-based air model in which chemical mass moves between air compartments via advection algorithms. Also, chemical mass is transferred by diffusion from multiple compartment types to the air in the TRIM.FaTE simulation. The chemical mass in a TRIM.FaTE air compartment is assumed to be distributed evenly throughout the compartment so that the concentration is constant (over space) for that compartment at a time-step. In this analysis, air concentrations calculated by TRIM.FaTE vary with time, while the air concentrations applied in 3MRA are constant values (i.e., each watershed centroid's long-term average derived by ISCST3). An additional study was performed by the 3MRA team to learn more about how the different methods used to model air concentrations (and deposition) affect the results. See the text box at the end of Section 6.2.2 for a summary of that study.

Exhibit 6-11 shows a comparison between the divalent mercury concentrations in TRIM.FaTE air compartments W2 and SSW2 and in 3MRA air over watershed 11 (based on the air concentration calculated at centroid 11). Two TRIM.FaTE locations are presented because 3MRA centroid 11 is near the border of TRIM.FaTE air parcels W2 and SSW2. Air concentrations modeled with 3MRA are higher than the comparable TRIM.FaTE air concentrations by five-fold (SSW2) to 11-fold (W2). In comparisons of air concentrations at

other locations, 3MRA results are higher than TRIM.FaTE by four- to nine-fold (Appendix E). The TRIM.FaTE results spike up and down through the five-year meteorological data period (and then repeat), and the 3MRA results are calculated as a long-term average and are thus constant over time.

Exhibit 6-10
Summary of Mass Transfer and Transformation Processes Modeled: Air ^a

TRIM.Fate (Hg ⁰ , Hg ²⁺ , MHg)	3MRA (Hg ²⁺ only)
Advection, air-to-air (horizontal), via compartment model [G or L] ^b	Advection, air-to-air, via Gaussian plume model [G or L]
Dry deposition of particles from air to surface soil, surface water, and particles-on-leaf [L]	Dry deposition of particles from air to surface soil, surface water, and leaf [L] ^c
Resuspension of particles from surface soil to air [G]	--
Blowoff of particles-on-leaf to air [G]	--
Diffusion (dry deposition) of vapors from air to surface soil, surface water, and leaf [L]	Dry deposition of vapors from air to surface soil, surface water, and leaf [L] ^c
Diffusion from surface soil, surface water, and leaf to air [Hg ⁰ and MHg only for surface soil and leaf] [G]	--
Wet deposition of particles from air to surface soil, surface water, and particles-on-leaf [L]	Wet deposition of particles from air to surface soil, surface water, and leaf [L] ^c
Wet deposition of vapors from air to surface soil, surface water, and leaf [Hg ⁰ and Hg ²⁺ only] [L]	Wet deposition of vapors from air to surface soil, surface water, and leaf [L]
Inhalation of air by wildlife [L]	--
Methylation of Hg ⁰ (0) ^d Demethylation of MHg (0)	Hg transformation in air not modeled
Reduction of Hg ²⁺ to Hg ⁰ (0)	
Oxidation of Hg ⁰ to Hg ²⁺ (0.00385/day)	

^a This and similar charts in this chapter include primarily descriptions of 3MRA as it is applied in this model comparison for the TRIM.FaTE mercury test case. 3MRA includes additional process-based fate and transport algorithms for other chemicals (organics and metals), plus several additional modules. For a description of the complete 3MRA multi-media modeling system, see the referenced 3MRA documentation.

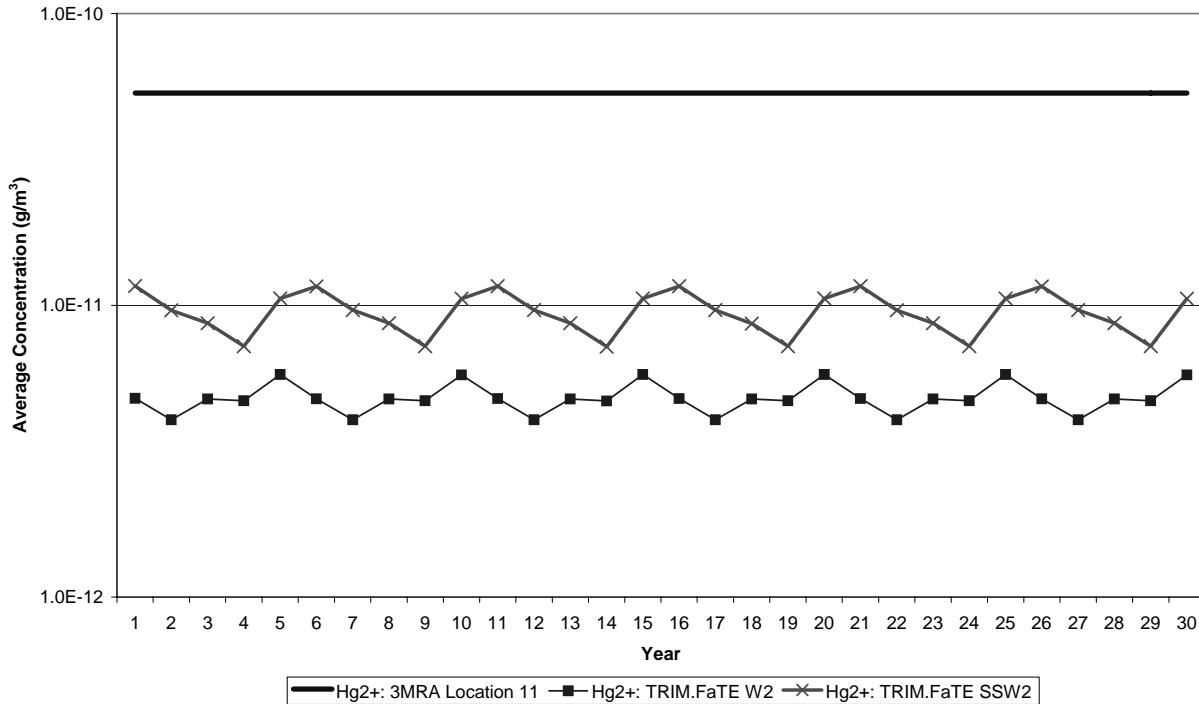
^b G = gain process, L = loss process, G or L indicates can be either.

^c Process not modeled in this application, although 3MRA/ISCST3 has this capability for some chemicals.

^d First-order rate constant shown in parentheses for all transformation reactions.

The differing long-term average air concentrations – generally within a half to full order of magnitude, depending on location – are probably a result of the different air modeling approaches and perhaps the different meteorological data used. A key modeling difference is that the TRIM.FaTE air concentration is an average in the full volume of the air compartment

Exhibit 6-11
Divalent Mercury Concentration in Air vs. Time: Near Source, Southwest^a



^a Annual average for TRIM.FaTE is based on instantaneous estimates every two hours throughout the year and represents an average concentration over a volume that extends from the ground to the mixing height. 14-year average for 3MRA (based on instantaneous estimates every hour throughout the period) is applied to entire period and is a point concentration at ground level.

(e.g., from ground level up to the mixing height), while the 3MRA value is the point concentration at ground level at the centroid of the watershed.⁸ In the comparison of the Gaussian plume model to the compartment model performed by the 3MRA team (see text box in Section 6.2.2), it was shown that the vertical average concentrations calculated from ISCST3 were lower than the ground-level concentrations at the same point, and closer to the compartment model results. Therefore, it is likely that vertical average results from 3MRA/ISCST3 for the full model application would be closer to the TRIM.FaTE results. An additional input identified as a possible reason for the different air concentrations simulated by the two models is the TRIM.FaTE air compartment size. The height of the compartments vary each hour based on the mixing height (ranges from 20 to 3,257 meters for this run; mean = 887 meters). In the Gaussian/plume model comparison, it was demonstrated that on average, these heights may be large compared to the height of the Gaussian plume at the same distances from the source. If that is the case, air concentrations modeled with TRIM.FaTE would consistently be smaller than even the vertically averaged ISCST3 results because they are being averaged over a larger height. Different modeled deposition fluxes may also be a factor contributing to the lower TRIM.FaTE air concentrations (see Section 6.2.2).

⁸ Note that the ground-level concentrations are expected to be higher than the volume-averaged concentrations because the source is emitting mercury at ground level.

6.2.2 Divalent Mercury Deposition

Exhibit 6-10 shows that mercury is transferred from the air to the surface soil, surface water, and leaves via deposition in both TRIM.FaTE⁹ and 3MRA. In this model comparison, four types of deposition were modeled with TRIM.FaTE (dry particle, dry vapor, wet particle, and wet vapor), and one type of deposition (wet vapor, which is expected to be the dominant process for divalent mercury) was modeled with 3MRA.¹⁰ Wet vapor deposition of divalent mercury is modeled with 3MRA (via ISCST3) by a scavenging ratio approach, so that the amount of chemical removed from the plume by wet deposition is a function of the scavenging rate coefficient and plume height (see Exhibit 6-12). TRIM.FaTE models wet vapor deposition of all forms of mercury using a washout ratio, which is based on Henry's Law. Both methods are a function of mercury concentration in air and rainfall rate.

In this model application, an attempt was made to ensure the consistency of values for the ISCST3 scavenging coefficient and the TRIM.FaTE washout ratio consistent. To do this, a plume height of 1,000 meters was assumed (similar to the average TRIM.FaTE mixing height), and a scavenging coefficient was calculated for use in the ISCST3 simulations based on this assumption (see Exhibit 6-12). However, because the deposition calculations done by ISCST3 are still dependent on plume height (which varies), and the TRIM.FaTE mixing height varies hourly, setting the scavenging coefficient and washout ratio equal at one plume depth will not result in equal deposition results at all times and locations.

**Exhibit 6-12
Comparison of Parameters and Inputs Used to Calculate Wet Vapor Deposition**

Scavenging Ratio Approach (3MRA/ISCST3)		Henry's Law Approach (TRIM.FaTE)	
Scavenging coefficient	0.00044 hr/mm-sec ^a	Washout Ratio	1.6E06 m ³ [air]/m ³ [rain] ^a
Plume height	Varies over space and time	Plume Height	Not applicable ^b
Air concentration of Hg ²⁺	Varies over space and time	Air Concentration of Hg ²⁺	Varies over space and time
Rainfall rate	Varies over time	Rainfall Rate	Varies over time

^a Constant values were used in both model application for the scavenging coefficient and the washout ratio.

^b TRIM.FaTE does not model a plume height, but the concentration of mercury in the air is a function of mixing height. Therefore, deposition is influenced somewhat by this height which varies by hour.

Exhibits 6-13 and 6-14 present the deposition flux comparison at the same location used for the air concentration comparisons. These are downward flux values which do not take into account resuspension or re-emission (i.e., they are not "net" deposition fluxes). Note that for

⁹ In TRIM.FaTE chemicals transferred to the leaf compartment via air deposition of particles go first to the particle-on-leaf compartment, which then exchanges chemical mass with the leaf compartment.

¹⁰ 3MRA/ISCST3 has the ability to model other types of deposition, but these processes were not implemented in this comparison model run.

deposition, TRIM.FaTE outputs are for the surface parcels, not for the air parcels (note also that only one TRIM.FaTE surface parcel is needed for a reasonable spatial match to the 3MRA location, compared to two TRIM.FaTE air parcels). On average, TRIM.FaTE total deposition flux of divalent mercury is three-fold higher than 3MRA divalent mercury wet vapor deposition flux at this location. TRIM.FaTE wet vapor deposition flux is 2.4-fold greater than the 3MRA wet vapor deposition flux and accounts for the majority (approximately 80 percent) of the TRIM.FaTE divalent mercury deposition. Other comparison locations are presented in Appendix E for which the TRIM.FaTE divalent mercury deposition fluxes are higher than the 3MRA wet vapor deposition fluxes by a greater amount (10-fold at 3MRA Swetts Pond location and 34-fold at 3MRA watershed 1). It appears from these three comparison locations that the difference in deposition fluxes between the two models increases with distance from the source (see Section 6.2.4). Exhibit 6-14 shows that the TRIM.FaTE deposition fluxes follow a five-year repeating pattern, which is related to the air concentrations and the five-year repeating set of meteorological data. 3MRA deposition fluxes are modeled as constant over time at a given location (long-term average based on the 14-year meteorological data set), just like the air concentrations.

Exhibit 6-13
Average Deposition Flux (g/m²-day) for Divalent Mercury: Near Source, Southwest ^a

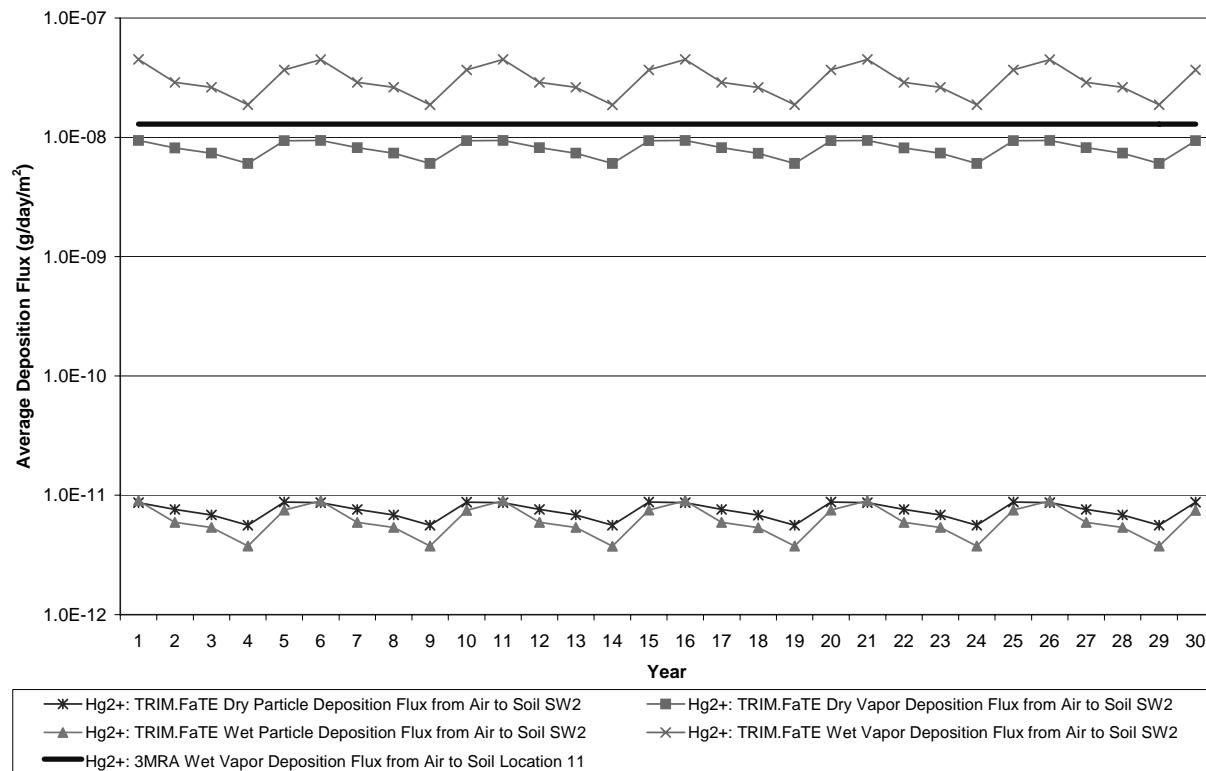
Process	TRIM.FaTE Surface Soil Compartment SW2	3MRA Watershed 11
Dry particle deposition	7.5E-12	--
Dry vapor deposition	8.1E-09	--
Wet particle deposition	6.3E-12	--
Wet vapor deposition	3.1E-08	1.3E-08
Total	3.9E-08	1.3E-08

^a For TRIM.FaTE, the average is derived as the arithmetic average of instantaneous estimates every two hours during the 30-year simulation period, while for 3MRA, it is an average from the results of the 14-year simulation of the air dispersion model ISCST3 (note that this average value was applied in 3MRA as a constant deposition flux).

The difference in deposition fluxes of divalent mercury between the models is probably a result of the different methods used to calculate deposition, with some contribution from different meteorology data. The additional types of deposition modeled with TRIM.FaTE also add to the difference, but not as much because wet vapor deposition is the predominant form of divalent mercury deposition in TRIM.FaTE for the test case scenario. As presented in Section 6.2.1, the TRIM.FaTE divalent mercury air concentrations are lower than the 3MRA air concentrations (which is the opposite pattern from the deposition results). Therefore, in an attempt to factor out differences in modeled air concentrations, a comparison was also made of the ratio of average deposition flux to average air concentration (i.e., to see how deposition fluxes would compare between the models if air concentrations were identical). For TRIM.FaTE surface parcel SW2 this ratio is between 4,100 and 6,980, and the 3MRA ratio for watershed 11 is 240. This higher ratio of deposition flux to air concentration for TRIM.FaTE indicates that for a given amount of divalent mercury in the air, more mercury is transferred to the surface than for

3MRA. This may help explain the lower TRIM.FaTE air concentrations described in Section 6.2.1. However, the 3MRA air concentration is a ground-level value, while the TRIM.FaTE concentration is a volume-averaged value, so the ratios are not directly comparable (i.e., if the TRIM.FaTE air concentration was a ground-level value as well, the corresponding ratio probably would be smaller and thus closer to the 3MRA ratio).

**Exhibit 6-14 - Log Scale
Divalent Mercury Deposition Flux from Air to Soil Surface vs. Time: Near Source,
Southwest ^a**



^aAnnual average for TRIM.FaTE based on instantaneous estimates every two hours throughout the year. 14-year average for 3MRA (based on instantaneous estimates every hour throughout the period) applied to entire period.

In addition to these observations, further research comparing the ISCST3 air and deposition modeling to the TRIM.FaTE compartment modeling approach for divalent mercury (see text box below) provides more insight into the differences between the deposition values. In the supplemental study, it was observed that because the ISCST3 scavenging coefficient input (which is treated as a constant) was set to the value for a plume height of 1,000 meters, not until the plume reaches that size would the deposition flux modeled with ISCST3 be expected to equal the TRIM.FaTE deposition flux. However, it was also observed in the supplemental study that by the time (i.e., distance from the source) the ISCST3 plume height reaches 1,000 meters, much of the divalent mercury mass in the TRIM.FaTE air compartments has already deposited, meaning that the deposition fluxes are still very different because they are proportional to the concentration (i.e., TRIM.FaTE is removing a greater portion of divalent mercury mass from the air near the source while 3MRA is removing a greater portion of the mercury mass from the air farther from the source).

Detailed Air Concentration and Deposition Study

A detailed follow-up study was performed by the 3MRA team to further compare the different approaches of TRIM.FaTE and 3MRA to atmospheric transport and wet deposition of vapor phase contaminant (Laniak and Schwede, in preparation). The objective of this study was to isolate the processes that are used to calculate air concentrations and deposition fluxes in the two models, and compare these approaches and resulting predictions independent of the many other processes that affect and complicate the full model comparison. A secondary goal was to see under what conditions a compartment model could be parameterized to produce air concentration and deposition predictions similar to a Gaussian plume model.

The two models use different conceptual approaches to air modeling, as discussed in Section 6.2.1. TRIM.FaTE is a compartment model which primarily uses advective transport for air modeling, while 3MRA uses ISCST3, which is a Gaussian plume model. Wet vapor deposition is also calculated differently by the two models (see Section 6.2.2). 3MRA uses an approach in which a scavenging coefficient is applied over the depth of a plume to remove contaminant via wet deposition. TRIM.FaTE uses a washout ratio which is independent of the actual plume depth and is a function only of contaminant concentration in air.

Differences in air concentrations and deposition results were compared for multiple simulations performed with a simplified compartment layout (similar to TRIM.FaTE compartment volumes in the east-southeast direction, but rotated so the downwind axis is directly west to east) and a single hour of meteorology. Consistent with results from the entire 3MRA/TRIM.FaTE comparison described in this document, the compartment model air concentrations were lower than the ground-level Gaussian plume air concentrations modeled with the simplified layout. After confirming this result, the 3MRA team performed several other simulations to test different hypotheses about the differences between the models. Some key topics analyzed are described below.

Averaging: The Gaussian results presented in the full comparison represent plume centerline, ground-level concentrations. In order to obtain concentrations more comparable to the volume-averaged results from the compartment model, the Gaussian results were vertically and laterally averaged across the plume. This reduced the differences, bringing the Gaussian results to within a factor of two of the compartment model results for some simulations, although in all cases, the compartment results were still lower (ranging from 0.05 to 0.7 times the overall average concentrations predicted by the Gaussian plume model).

Atmospheric Stability: When the Gaussian plume model was simulated with an unstable atmosphere, the Gaussian concentrations were closer to the compartment model predictions than when a stable atmosphere was modeled. The Gaussian plume spread is greater in an unstable atmosphere, so the concentrations were lower, leading to a closer match to the compartment model.

Matching Volumes: Since averaged Gaussian plume concentrations were still less than the concentrations simulated with the compartment model, and a less stable atmosphere (causing more plume spread) resulted in Gaussian concentrations slightly closer to the compartment model concentrations, an attempt was made to reduce the size of the compartment volumes so that they matched the volume of the Gaussian plume at the relevant distances from the source (using vertical and lateral spread parameters from the Gaussian plume model). This exercise showed that the compartment model could be parameterized to match the Gaussian plume model and that a major difference between the air concentration predictions stemmed from the compartment volumes being larger than the Gaussian plume volume.

When deposition was added to the simulation, more differences were identified due to the different methods used to calculate deposition. The method used by ISCST3 (scavenging coefficient) removes a greater portion of the contaminant mass farther from the source, and the method used by the compartment model (washout ratio) removes more contaminant near the source. In one set of analyses, the compartment model deposition was modified so that the washout ratio varied with distance, and the results were much more similar to ISCST3. This detailed study of the air and deposition methods provides valuable insight into the different methods used to model transport in the air and deposition for the two models. However, it is necessary to remember that in full 3MRA and TRIM.FaTE simulations, the layouts are more complex, there is variable meteorological data used, and there are many other processes affecting air concentrations.

6.2.3 Divalent Mercury Concentrations in Leaves

Exhibit 6-15 shows the mercury gain and loss processes associated with leaves for both TRIM.FaTE and 3MRA. In addition to receiving mercury by deposition processes, leaves in 3MRA also obtain mercury from the soil, and leaves in TRIM.FaTE obtain mercury by transfer from the stems (which get mercury from the soil). Mercury is lost from leaves in TRIM.FaTE by multiple processes. Some of these loss processes are also accounted for by the empirical loss rate constant used by 3MRA (but are not tracked in a mass-balance sense).

Exhibit 6-15
Summary of Mass Transfer and Transformation Processes Modeled: Leaf

TRIM.Fate (Hg ⁰ , Hg ²⁺ , MHg)	3MRA (Hg ²⁺ only)
Dry deposition of particles from air to particles-on-leaf (and subsequent exchange to leaf) [G] ^a	Dry deposition of particles from air to leaf [G] ^b
Diffusion (dry deposition) of vapors from air to leaf [G]	Dry deposition of vapors from air to leaf [G] ^b
Diffusion from leaf to air [Hg ⁰ and MHg only] [L]	Net loss of chemical from leaf surface [L]
Wet deposition of particles from air to particles-on-leaf (and subsequent exchange to leaf) [G]	Wet deposition of particles from air to leaf [G] ^b
Wet deposition of vapors from air to leaf [Hg ⁰ and Hg ²⁺ only] [G]	Wet deposition of vapors from air to leaf [G]
Exchange from leaf to particles-on-leaf [L]	--
Exchange from leaf to stem [L]	--
Exchange from stem to leaf (preceded by root zone soil-to-stem uptake) [G]	Soil-to-leaf uptake [G]
Deposition from leaf to surface soil during litter fall [L]	Litter fall deposition assumed to be included in empirical studies used to develop model [L]
Ingestion of leaf by certain wildlife [L]	--
Methylation of Hg ²⁺ (0) ^c Demethylation of MHg (0.03/day)	Hg transformation in leaf not modeled
Reduction of Hg ²⁺ to Hg ⁰ (0) Oxidation of Hg ⁰ to Hg ²⁺ (1,000,000/day)	

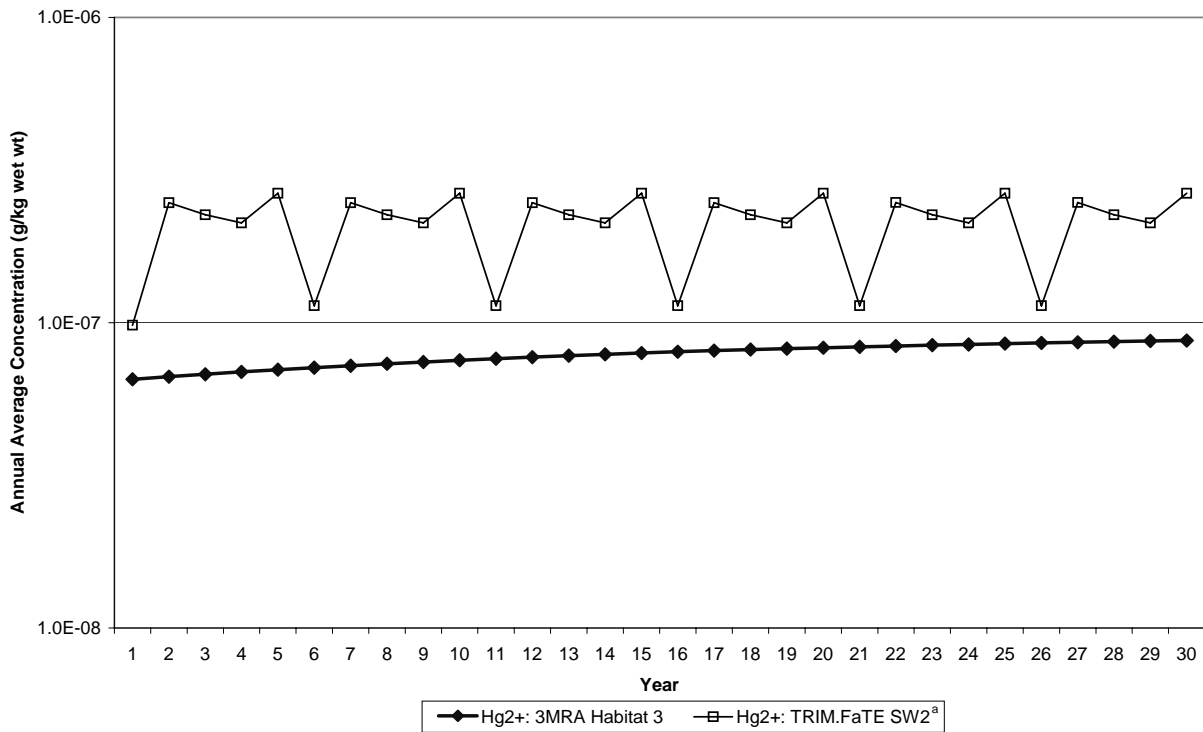
^a G = gain process, L = loss process.

^b Process not modeled in this application, although 3MRA/ISCST3 has this capability for some chemicals.

^c First-order rate constant shown in parentheses for all transformation reactions.

In Exhibit 6-16, divalent mercury concentrations in leaves from TRIM.FaTE surface parcel SW2 (grasses/herb) are compared with 3MRA leaf concentrations in habitat 3 (which is “matched to” air and soil from watershed 11). The divalent mercury concentrations in TRIM.FaTE leaf compartments at this location are on average three-fold greater than divalent mercury concentrations in the 3MRA leaves. This seems to follow directly from the similarly higher deposition fluxes for the TRIM.FaTE model at this location, illustrating the significant role of deposition on modeled leaf concentrations of divalent mercury. As shown in Exhibit 6-15, in both models deposition plays a part in the transfer of mercury from the air to the leaves. The TRIM.FaTE leaf concentrations follow a five-year repeating (and non-increasing) pattern based on the repeating meteorological data, and the 3MRA concentrations follow a fairly constant, but increasing, pattern over the 30-year modeling period. The concentration in TRIM.FaTE leaves in the first year of the five-year pattern is noticeably lower than the other values, presumably because of meteorology differences. This is not the same pattern seen in the annual average deposition fluxes to the parcel (Exhibit 6-14), but the TRIM.FaTE leaves for grasses/herbs vegetation type are modeled only for the growing season (annual average is calculated only based on the growing season period). Given that the meteorology (such as wind speed and direction and rainfall) is different in those growing season months from that in the rest of the year, it seems reasonable that the leaf concentrations follow a different pattern from the deposition flux.

Exhibit 6-16 - Log Scale
Divalent Mercury Concentration in Leaves (grasses/herbs) vs. Time:
Near Source, Southwest



^a Each TRIM.FaTE annual average data point shown is the average of values during the days (May 13 - September 29 each year) for which leaves were modeled as present during the entire day (i.e., represents a growing season average).

6.2.4 Spatial Patterns for Air Concentration and Deposition

The spatial variation in long-term average divalent mercury air concentrations and deposition fluxes for 3MRA and TRIM.FaTE is shown in Exhibits 6-17 and 6-18. Both maps are scaled to the same size, with the TRIM.FaTE concentrations and rates shown via background shading and the 3MRA results shown via dots of various sizes. On the air concentration map (Exhibit 6-17), the concentration ranges are the same for the two models, and the increment (in logarithmic units) for each concentration range is equal (i.e., a change in pattern or dot size reflects the same proportional increase for both models). On the deposition map (Exhibit 6-18), the concentration ranges differ for the two models because the model results span different numerical ranges, but the increment for each concentration range is equal (in logarithmic units) both within a model and across the two models.

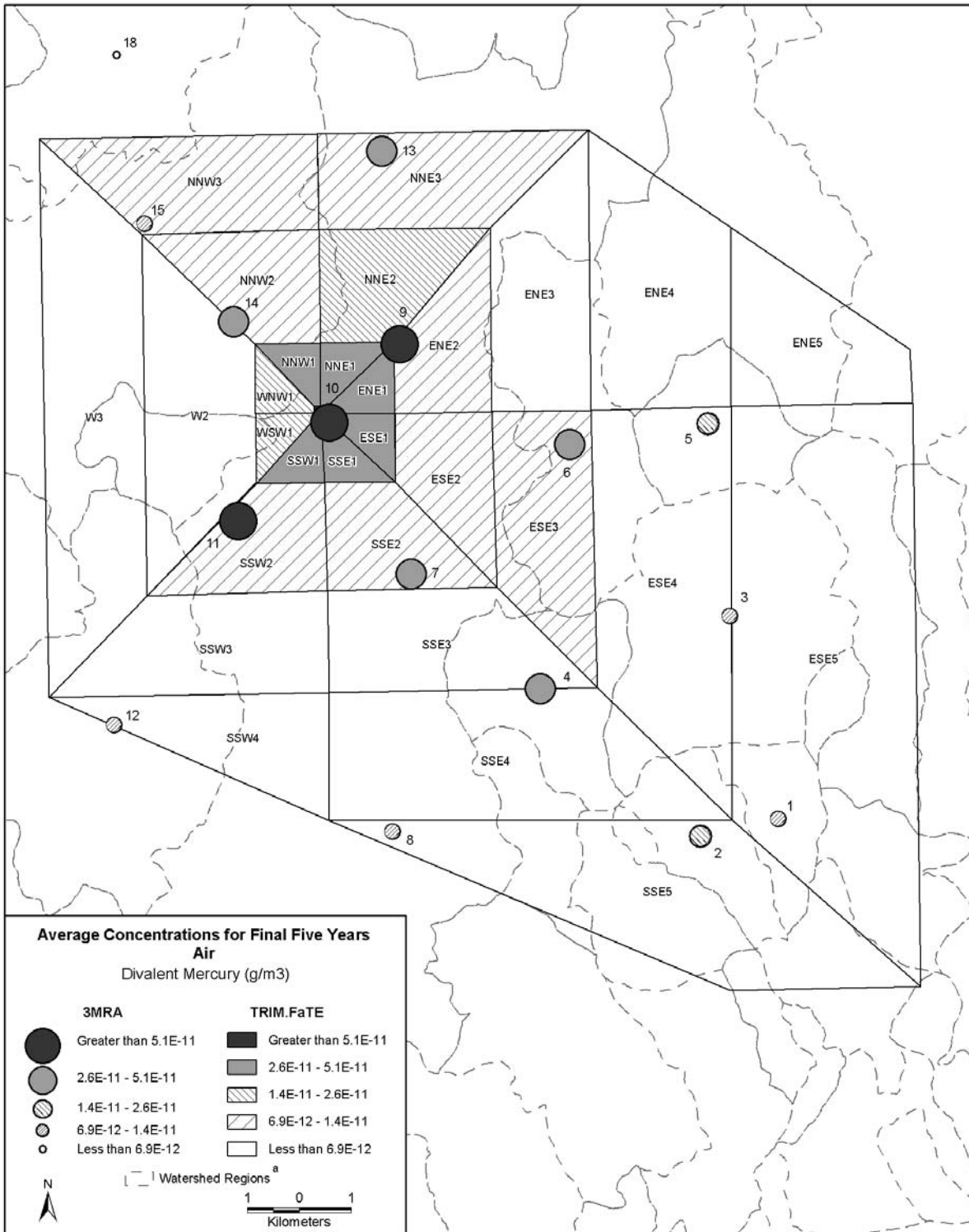
TRIM.FaTE air concentrations shown in Exhibit 6-17 are highest east and north of the source and lowest to the west. 3MRA concentrations are highest to the east, similar to TRIM.FaTE, and lowest to the northwest, then southwest, again similar to TRIM.FaTE. The directional differences in TRIM.FaTE annual average concentrations are fairly small, roughly three-fold between the highest and lowest air compartments at the same distance from the source (i.e., in the same “ring”). There are not enough data points to judge the relative magnitude of the directional differences for 3MRA. The ratio of the maximum to the minimum air concentration (excluding the source compartment) for the TRIM.FaTE layout is approximately 15. The maximum-to-minimum ratio for the 3MRA layout (excluding location 10, which is just adjacent to the source compartment, and all locations falling outside of the TRIM.FaTE layout) is approximately 24. Thus, there appears to be somewhat greater spatial variation in 3MRA air concentration results compared to TRIM.FaTE air results. A likely contributor to the observed difference in the spatial variation of the concentrations is the different types of spatial data being compared (i.e., point estimates at ground level for 3MRA versus volumetric averages for TRIM.FaTE) as well as the different size areas that these concentrations represent.

Because of the asymmetry of the TRIM.FaTE surface layout (for which deposition outputs are provided) and the small number of data points for both models, it is difficult to evaluate TRIM.FaTE and 3MRA deposition results by direction. Exhibit 6-18 indicates that the TRIM.FaTE deposition fluxes are very similar in the four parcels comprising the first “ring” around the source, and also in the five parcels comprising the second. (Note though that the surface parcel rings in TRIM.FaTE, unlike the inner air parcel rings, are not symmetrical.) The numerical results indicate that TRIM.FaTE deposition fluxes appear to be highest north and west of the source (different from air concentration patterns). 3MRA deposition fluxes appear highest to the west and lowest to the east, which is different from the 3MRA air concentration pattern. The directional differences between the deposition and air concentration patterns in both models probably can be explained by the weather patterns. For instance, the predominant wind direction when it is raining (which affects directional pattern of wet deposition) is not necessarily the same as the overall predominant wind direction (which is more closely linked to air concentration and dry deposition). A comparison of the wind roses in Exhibits 2-7 and 3-37 illustrates this difference for the TRIM.FaTE input data. The wind-rain relationship is important because the predominant type of deposition in TRIM.FaTE and the only type of mercury deposition in 3MRA occurs only when it is raining (i.e., wet vapor). When the TRIM.FaTE *dry* deposition

spatial pattern is examined separately, the spatial pattern is a closer match to the air concentration pattern, as expected, because precipitation does not affect modeled dry deposition.

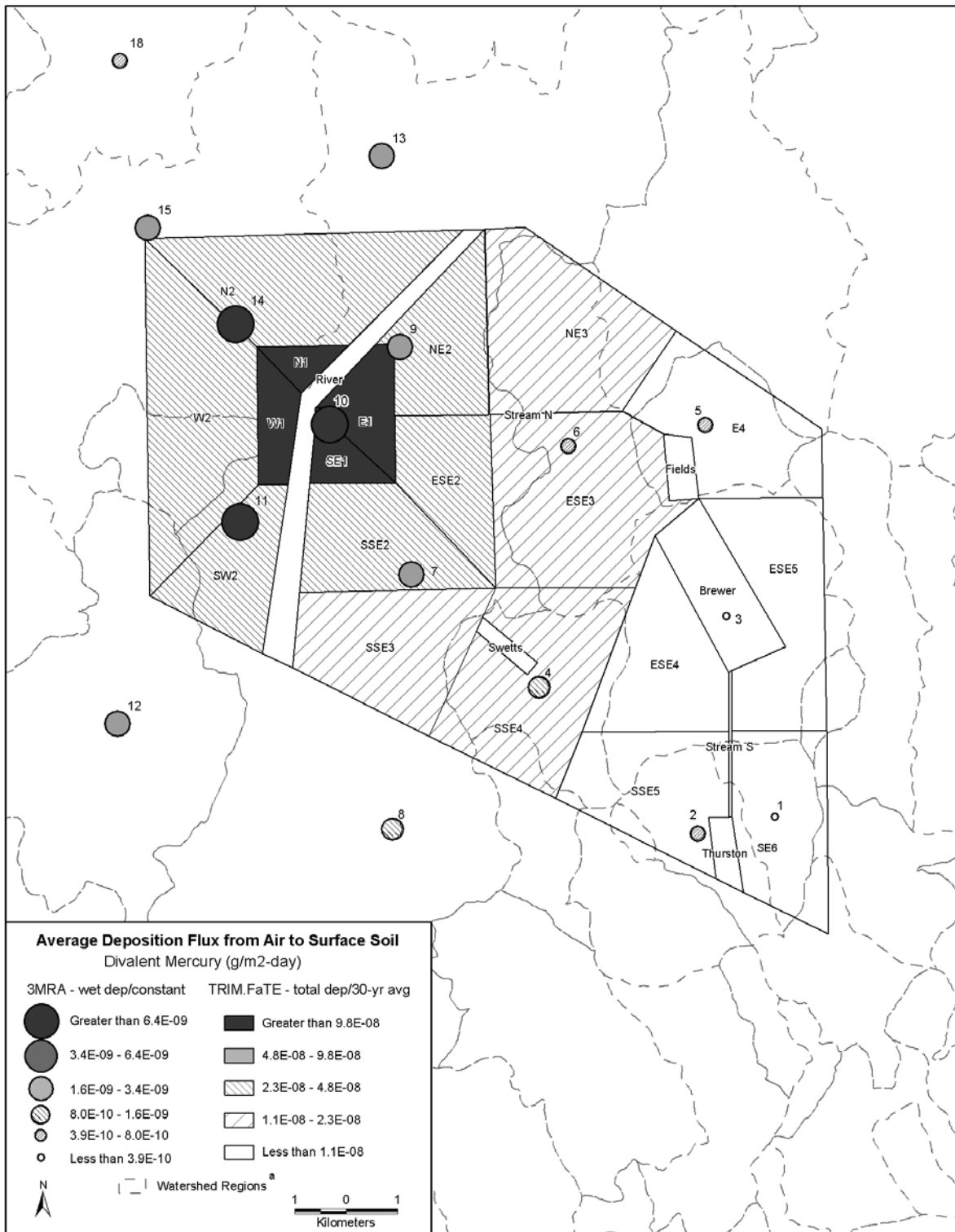
The ratio of the maximum-to-minimum total deposition flux (excluding the source compartment) for the TRIM.FaTE layout is approximately 18. The maximum-to-minimum ratio for the 3MRA layout (excluding location 10, which is just adjacent to the source compartment, and all locations falling outside of the TRIM.FaTE layout) is approximately 61. This illustrates the greater spatial variation in 3MRA deposition fluxes compared to TRIM.FaTE. As with the air concentrations, likely contributors to this difference are the comparison between 3MRA point estimates and TRIM.FaTE volumetric averages and the different size areas represented by the points or averages. Also, for both models there appears to be more spatial variation in deposition flux than in air concentration. These observations are related to the discussion in Section 6.2.2 that showed that the difference in deposition fluxes between the two models increases with distance (and that these differences are probably caused by the different methods used to calculate deposition fluxes).

Exhibit 6-17 Spatial Variation in Divalent Mercury Concentrations in Air



^a Not all watershed boundaries are shown. See Exhibit 6-9 for additional delineation of the watersheds.

Exhibit 6-18 Spatial Variation in Divalent Mercury Deposition Fluxes



^a Not all watershed boundaries are shown. See Exhibit 6-9 for additional delineation of the watersheds.

6.3 Soil and Soil Biota

This section provides a comparison between modeled mercury concentrations in 3MRA and TRIM.FaTE surface soil, plant roots, and earthworms and a discussion of the differences between the approaches to modeling mercury in soil and associated biota. The root zone, or “deeper” soil, is handled differently by the two models, contributing to some of the differences observed for associated biota (i.e., plant roots and earthworms). One major difference regarding the modeling of deeper soil is highlighted in a text box in Section 6.3.2. Surface soil and earthworm results are presented for TRIM.FaTE surface parcel SSE4 and 3MRA watershed 4 (habitat 11). The plant root comparison is made at TRIM.FaTE parcel SW2 and 3MRA habitat 3 (which corresponds to watershed 11), because the vegetation is similar at this location in the two models (same comparison location as for leaf).

Divalent mercury is the only species modeled with 3MRA in these media. Three species of mercury (divalent, elemental, and methyl) are modeled with TRIM.FaTE in these media, but results are presented only for divalent mercury when it is the predominant form. When other forms of mercury contribute significant percentages of the total mercury concentrations (>10%), then total and divalent mercury results are both shown for TRIM.FaTE.

6.3.1 Divalent Mercury Concentrations in Surface Soil

Exhibit 6-19 summarizes the TRIM.FaTE and 3MRA fate processes for mercury in the surface soil (i.e., top 1 cm of soil in both models). In both TRIM.FaTE and 3MRA, mercury is transferred to the surface soil from the air via deposition. TRIM.FaTE also simulates diffusion of mercury vapor from the air to the surface. Both models transfer mercury via erosion and runoff from the soil surface to water bodies; however, only TRIM.FaTE is set up to allow for runoff and erosion to transfer mercury from one surface soil location to another.

The divalent mercury concentrations in surface soil are compared in Exhibit 6-20 at 3MRA location 4 and TRIM.FaTE compartment SSE4. The divalent mercury concentrations in 3MRA soil at this and other locations (see Appendix E) are lower than the divalent mercury concentrations in the corresponding TRIM.FaTE surface soil compartments. The difference is less than a factor of six at most locations. This pattern is the opposite of the relative concentrations estimated for air by the two models, but follows from the higher TRIM.FaTE deposition fluxes (TRIM.FaTE deposition flux to parcel SSE4 is 11-fold higher than the 3MRA deposition flux at location 4). The shapes of the TRIM.FaTE and 3MRA surface soil concentration time series are similar with both curves showing smooth increases in concentration.

Exhibit 6-19
Summary of Mass Transfer and Transformation Processes Modeled: Surface Soil

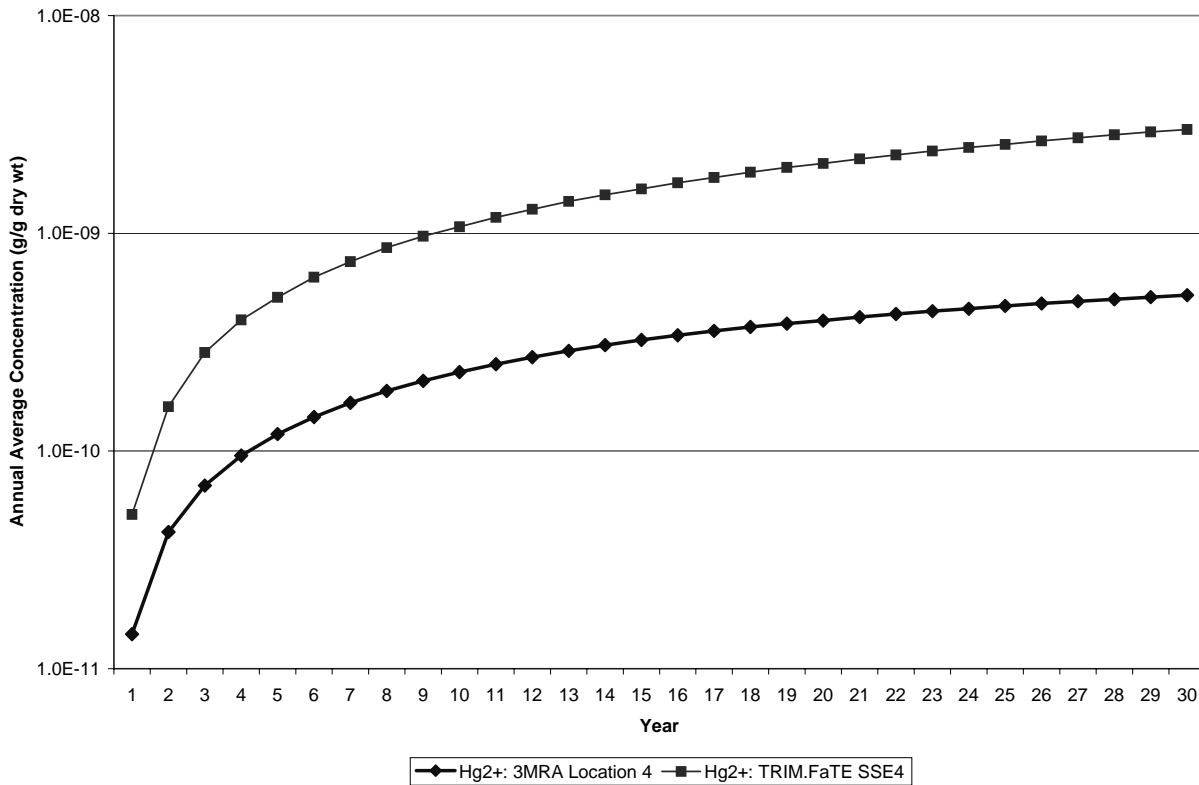
TRIM.Fate (Hg ⁰ , Hg ²⁺ , MHg)	3MRA (Hg ²⁺ only)
Dry deposition of particles from air to surface soil [G] ^a	Dry deposition of particles from air to surface soil [G] ^b
Resuspension of particles from surface soil to air [L]	--
Diffusion (dry deposition) of vapors from air to surface soil [G]	Dry deposition of vapor from air to surface soil [G] ^b
Diffusion (volatilization) from surface soil to air [Hg ⁰ and MHg only] [L]	--
Wet deposition of particles from air to surface soil [G]	Wet deposition of particles from air to surface soil [G] ^b
Wet deposition of vapors from air to surface soil [Hg ⁰ and Hg ²⁺ only] [G]	Wet deposition of vapors from air to surface soil [G]
Runoff (dissolved phase) from surface soil to surface soil and surface water [G or L]	Runoff (dissolved phase) from surface soil to surface water based on delineated watershed [L]
Erosion (solid phase) from surface soil to surface soil and surface water [G or L]	Erosion (solid phase) from surface soil to surface water based on delineated watershed [L]
Percolation from surface soil to root zone soil [L]	Percolation from surface soil to deeper soil [L]
Diffusion from surface soil to root zone soil [L]	Diffusion from surface soil to deeper soil [L]
Diffusion from root zone soil to surface soil [G]	--
Deposition from leaf and particles-on-leaf to surface soil during litterfall [G]	--
Washoff of particles-on-leaf to surface soil [G]	--
Ingestion of surface soil by wildlife [L]	--
Elimination to surface soil by wildlife [G]	--
Methylation of Hg ²⁺ (0.001/day) ^c Demethylation of MHg (0.06/day)	Hg transformation in soil not modeled
Reduction of Hg ²⁺ to Hg ⁰ (0.0000125/day)	
Oxidation of Hg ⁰ to Hg ²⁺ (0)	

^a G = gain process, L = loss process, G or L indicates can be either.

^b Process not modeled in this application, although 3MRA/ISCST3 has this capability for some chemicals.

^c First-order rate constant shown in parentheses for all transformation reactions.

**Exhibit 6-20 - Log Scale
Divalent Mercury Concentration in Surface Soil vs. Time: Swetts Pond Watershed**



6.3.2 Divalent Mercury Concentrations in Plant Roots

Plant roots in both models transfer mercury to and from the deeper soil as presented in Exhibit 6-21. Both models use empirical bioconcentration factors to model root mercury accumulation, but TRIM.FaTE uses a time-dependent approach¹¹ while 3MRA assumes equilibrium conditions. Transfer and transformation processes for the deeper (root zone) soil also are presented in Exhibit 6-21, given the prominent role of the deeper soil in accumulation of mercury mass by plant roots. The deeper soil layer is described in more detail in the accompanying text box.

Exhibit 6-22 compares the divalent mercury concentrations in TRIM.FaTE and 3MRA plant roots and deeper (root zone) soil at TRIM.FaTE parcel SW2 and 3MRA watershed 11 (which is matched to habitat 3). The divalent mercury concentrations in 3MRA roots are higher than the divalent and total mercury concentrations in the TRIM.FaTE roots (grasses/herbs); the difference is about an order of magnitude by the end of the 30-year modeling period. The greater difference earlier in the simulation is likely related to the more dynamic nature of the TRIM.FaTE approach to pollutant accumulation compared to the 3MRA equilibrium approach.

¹¹ As noted elsewhere, TRIM.FaTE can be run in steady-state or dynamic mode. Results for the latter are presented in this chapter.

Exhibit 6-21
Summary of Mass Transfer and Transformation Processes Modeled:
Root and “Deeper” Soil

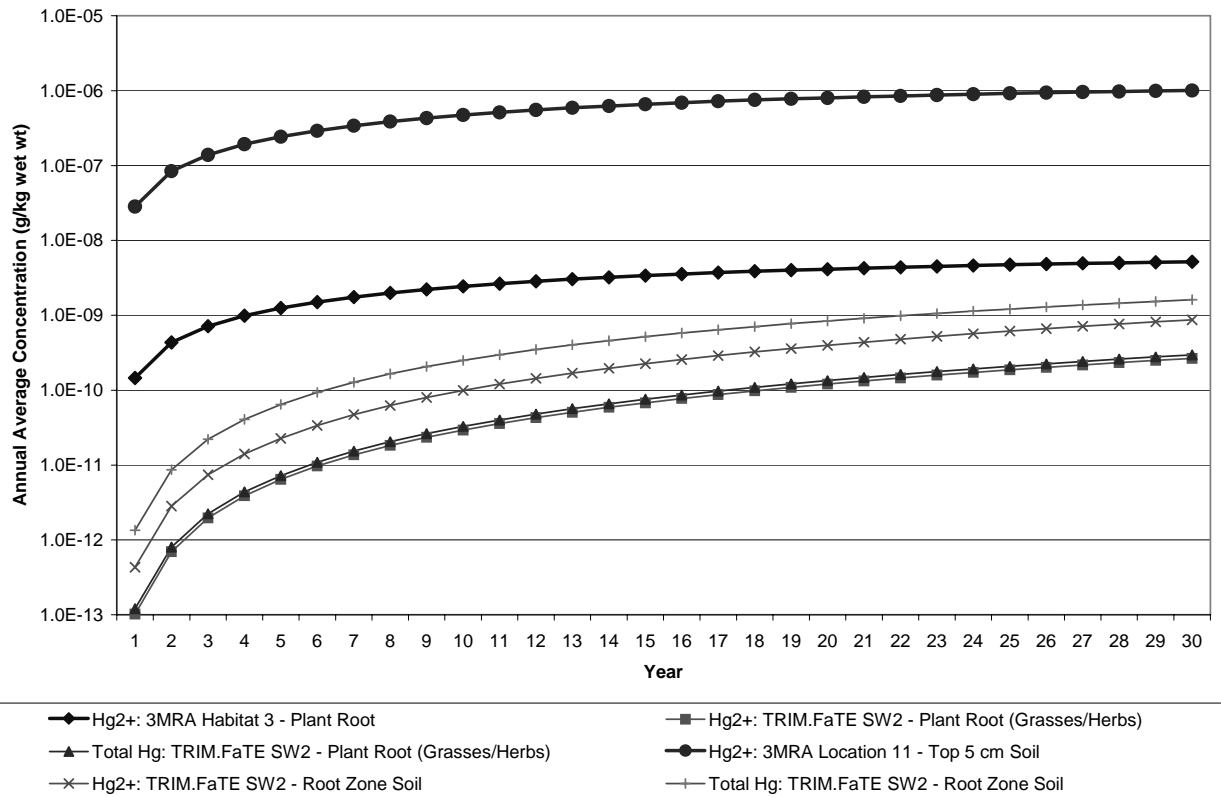
TRIM.Fate (Hg ⁰ , Hg ²⁺ , MHg)	3MRA (Hg ²⁺ only)
Root	
Partitioning from root zone (RZ) soil (1-56 cm) to root, based on a time-to-equilibrium model and empirical BCF [G] ^a	Partitioning from deeper soil (top 5 cm) to root at equilibrium, based on empirical BCF [G]
Partitioning from root to RZ soil, based on a time-to-equilibrium model and empirical BCF [L]	--
Methylation of Hg ²⁺ (0) ^b Demethylation of MHg (0)	Hg transformation in root not modeled (equivalent to TRIM.FaTE)
Reduction of Hg ²⁺ to Hg ⁰ (0)	
Oxidation of Hg ⁰ to Hg ²⁺ (0)	
Deeper Soil^c	
--	All surface soil processes (see Exhibit 6-19)
Percolation from surface soil to RZ soil [G]	Percolation from surface soil to deeper soil [G]
Diffusion from surface soil to RZ soil [G]	Diffusion from surface soil to deeper soil [G]
Diffusion from RZ soil to surface soil [L]	--
Percolation from RZ soil to vadose zone soil [L]	Percolation from deeper soil to vadose zone soil [L]
Diffusion from RZ soil to vadose zone soil [L]	--
Diffusion from vadose zone soil to RZ soil [G]	--
Partitioning from RZ soil to root, based on a time-to-equilibrium model and empirical BCF [L]	--
Partitioning from root to RZ soil, based on a time-to-equilibrium model and empirical BCF [G]	--
Partitioning from RZ soil to earthworm/arthropod, based on time-to-equilibrium model and empirical BCFs [L]	--
Partitioning from earthworm/arthropod to RZ soil, based on time-to-equilibrium model and empirical BCFs [G]	--
Methylation of Hg ²⁺ (0.001/day) ^b Demethylation of MHg (0.06/day)	Hg transformation in deeper soil not modeled
Reduction of Hg ²⁺ to Hg ⁰ (0.0000125/day)	
Oxidation of Hg ⁰ to Hg ²⁺ (0)	

^a G = gain process, L = loss process.

^b First-order rate constant shown in parentheses for all transformation reactions.

^c In this model comparison, the TRIM.FaTE root zone soil compartment (55 cm deep, directly under the 1 cm of surface soil) is defined differently from 3MRA deeper soil (top 5 cm, including 1 cm of surface soil).

Exhibit 6-22 - Log Scale
Divalent and Total Mercury Concentration in Roots (grasses/herbs) and Associated Soil vs.
Time: Near Source, Southwest



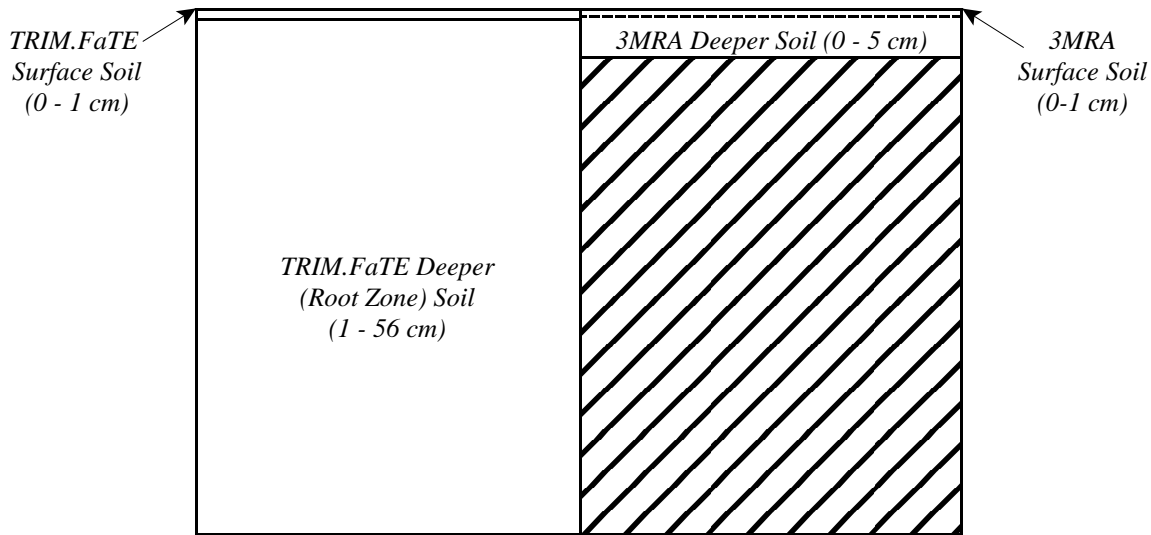
As described in the accompanying text box, the lesser depth for the deeper soil layer in the 3MRA simulation than the TRIM.FaTE simulation contributes to the higher mercury concentrations predicted by 3MRA for this soil layer. Because the plant roots (and earthworms) in both models obtain all of their mercury from this soil layer (see Exhibits 6-21 and 6-23), it follows that the mercury concentrations predicted by 3MRA for these biota are also higher. Note that in both models, the depth of this soil layer can be specified by the user.

A way to compare the impact of the different approaches to modeling mercury accumulation in roots, which is independent from differing soil concentrations, is to compare the factor by which divalent mercury is concentrated in roots from the associated soil. Given the equilibrium aspect of the 3MRA approach, this value is 0.005 throughout the simulation for every habitat. The dynamic nature of TRIM.FaTE, however, means that this value varies until the system reaches equilibrium. The TRIM.FaTE value for this factor is 0.31 for the near source, southwest parcel (SW2) at the end of the simulation, while it is 0.24 for year 1. All four TRIM.FaTE parcels with the grasses/herbs vegetation type (i.e., N1, NE2, W1 and SW2) have a ratio of approximately 0.31 at the end of the simulation. The overall higher factor associated with the TRIM.FaTE approach contributes to the finding that the two models' root concentrations are less different than their associated deeper soil concentrations.

Data on uptake of divalent mercury by plant roots in the open literature are sparse; we identified a single experimental study that was not used to derive the uptake ratio used in TRIM.FaTE. Chunilall et al. (2004) examined divalent mercury uptake by roots and stems/leaves of spinach plants grown in soil to which mercuric sulfate was added at levels ranging from 10 to 50 ppm mercury. Assuming that the roots in this study were 75 percent water and assuming that the soil moisture content was low, after 10 weeks of growth, the wet-weight divalent mercury accumulation factors for roots in this study ranged from 0.2 to 1.6. This range is similar to the wet-weight divalent mercury accumulation factors of 0.24 to 0.31 that resulted in the TRIM.FaTE simulation and higher than the accumulation factor of 0.005 used in the 3MRA simulation.

Deeper (Root Zone) Soil

Both 3MRA and TRIM.FaTE allow for modeling of soil layers deeper than the surface layer. The deeper soil modeled with 3MRA in this simulation is the soil from the surface to 5 cm deep (see diagram below). Therefore, the 3MRA deeper soil is inclusive of the surface soil layer (0 to 1 cm). In this model simulation, the TRIM.FaTE deeper soil (i.e., root zone soil compartment) is the soil from a depth of 1 cm to 56 cm. Unlike the 3MRA deeper soil, the TRIM.FaTE deeper soil does not include the top 1 cm surface layer. The mercury concentrations calculated for the deeper soil in both models are representative of the average over the entire depth. Therefore, this difference in deeper soil definition means that deeper, lower concentration soil is essentially “averaged in” to calculate the TRIM.FaTE deeper soil concentration value. Moreover, the higher concentration of the top 1 cm of soil is averaged into the 3MRA deeper soil concentration. The result of these differences in definition is that the 3MRA deeper soil has a much higher divalent mercury concentration than the TRIM.FaTE deeper soil (see Exhibit 6-22).



The table below provides an example of divalent mercury concentration averages for the surface and deeper soil layers from both models. Additionally, ranges were estimated for TRIM.FaTE soil concentration between 0-5 cm and 3MRA soil concentrations for the depth of 1-56 cm. The concentration modeled in the surface soil with 3MRA is lower than the concentration modeled with TRIM.FaTE. Additionally, the concentration directly modeled with 3MRA in the deeper soil (0 - 5 cm) is lower than the range estimated for TRIM.FaTE at that same depth. The upper end of the concentration range estimated for 3MRA in the 1 - 56 cm deeper soil is higher than the TRIM.FaTE modeled value for that depth.

Divalent Mercury Concentration in Soil Layers, Year 30 Average – Swetts Pond Watershed

Soil Layer	Soil Depth	Soil Concentration (g/g dry wt)	
		TRIM.FaTE – SSE4	3MRA – Location 4
Surface soil	0 - 1 cm	3.0E-9	5.2 E-10
Deeper soil (per 3MRA)	0 - 5 cm	$[6.0E-10 < x < 3.0E-9]^a$	1.2E-10
Deeper soil (TRIM.FaTE root zone)	1 - 56 cm	5.1E-13	$[< 2.0E-11]^b$

^a The deeper soil concentration from 0 - 5 cm for TRIM.FaTE presented here is estimated via manipulation of model outputs (although TRIM.FaTE could have been set up to output a soil concentration representing 0 - 5 cm in depth). The upper end of the estimated range is the modeled concentration at 0 - 1 cm. The lower end was calculated using the following formula:

$$\text{concentration}_{0-5\text{cm}} = [(1 \text{ cm} * \text{concentration}_{0-1\text{cm}}) + (4 \text{ cm} * \text{concentration}_{1-56\text{cm}})] / 5 \text{ cm}.$$

^b The deeper soil concentration from 1 - 56 cm for 3MRA presented here is an estimate based on manipulation of model outputs. It is an upper end of the possible range, calculated from the following formula:

$$\text{concentration}_{1-56\text{cm}} = (5 \text{ cm} * \text{concentration}_{0-5\text{cm}} - 1 \text{ cm} * \text{concentration}_{0-1\text{cm}}) / 4 \text{ cm}.$$

6.3.3 Divalent Mercury Concentrations in Earthworms

As shown in Exhibit 6-23, earthworms in both models accumulate mercury from contact with the deeper soil. Similar to the plant roots, both models use empirical bioconcentration factors to estimate earthworm mercury accumulation, but TRIM.FaTE uses a time-dependent approach while 3MRA assumes equilibrium conditions.

**Exhibit 6-23
Summary of Mass Transfer and Transformation Processes Modeled: Earthworm**

TRIM.Fate (Hg ⁰ , Hg ²⁺ , MHg)	3MRA (Hg ²⁺ only)
Partitioning from root zone soil (1-56 cm) to earthworm, based on a time-to-equilibrium model and empirical BCF [G] ^a	Partitioning from deeper soil (top 5 cm) to earthworm at equilibrium, based on empirical BCF [G]
Partitioning from earthworm to root zone soil, based on a time-to-equilibrium model and empirical BCF [L] ^a	--
Ingestion of earthworm by wildlife [L]	--
Methylation of Hg ²⁺ (0) ^b Demethylation of MHg (0)	Hg transformation in earthworm not modeled (equivalent to TRIM.FaTE)
Reduction of Hg ²⁺ to Hg ⁰ (0)	
Oxidation of Hg ⁰ to Hg ²⁺ (0)	

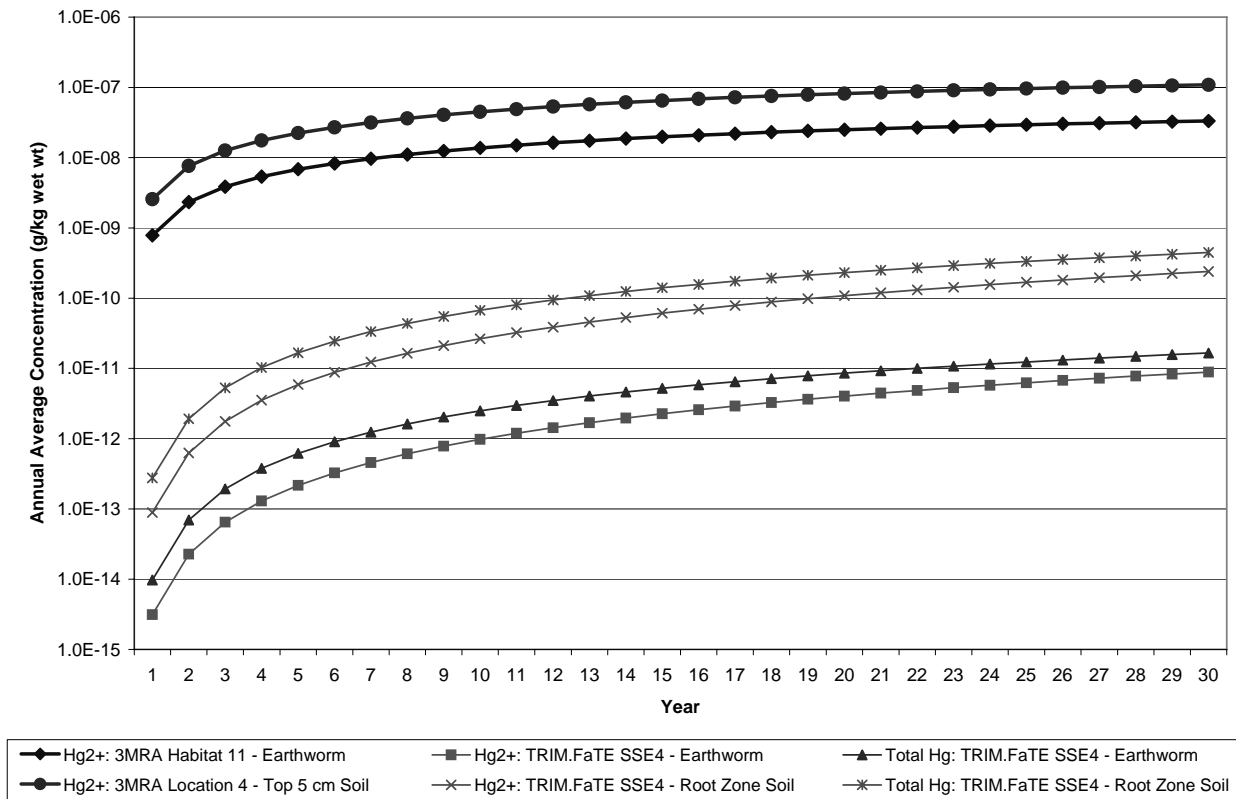
^a G = gain process, L = loss process.

^b First-order rate constant shown in parentheses for all transformation reactions.

Given the much higher concentrations in deeper soil for 3MRA, it would be expected that the 3MRA earthworm mercury concentrations would be higher than the TRIM.FaTE concentrations (see deeper soil discussion in Section 6.3.2). Exhibit 6-24 shows that divalent mercury concentrations in 3MRA earthworms in habitat 11 are about three orders of magnitude higher than total and divalent mercury concentrations in the TRIM.FaTE SSE4 earthworm compartment. More locations are compared in Appendix E, and 3MRA concentrations are consistently three to four orders of magnitude higher than TRIM.FaTE concentrations.

As was done in Section 6.3.2 for the plant root results, the ratios of earthworm to deeper soil divalent mercury concentrations (wet-weight) can be compared between the two models. The value is 0.31 for 3MRA and 0.037 for TRIM.FaTE in the near source parcel (SW2) at the end of the simulation (it varies very little across all TRIM.FaTE parcels). The higher value for 3MRA is opposite the situation for roots, where the ratios indicate that 3MRA accumulates less mercury mass in the roots per deeper soil mercury mass than TRIM.FaTE. These differences explain why even though both earthworms and roots obtain mercury from the deeper soil in both models, the root concentrations from 3MRA and TRIM.FaTE are only one order of magnitude different while the earthworm concentrations are three to four orders of magnitude different. Ultimately, the model-to-model differences in these ratios result from the different bioaccumulation factors used by the two models for this application.

**Exhibit 6-24 - Log Scale
Divalent and Total Mercury Concentration in Earthworms and Associated Soil vs. Time:
Swetts Pond Watershed**



With respect to typical literature values for earthworm accumulation of mercury (see Sample et al. 1998), the calculated ratios (i.e., bioaccumulation factors, or BAFs) for earthworms for both models appear to be low. Data in the literature indicate that earthworm BAFs change with soil concentration, and they tend to be higher with lower soil mercury concentrations. Using the 30 observations in Appendix A of Sample et al. (1998) from five separate studies, it appears that the concentration of total mercury in earthworms is higher than the soil concentration only for soil concentrations less than approximately 1 mg/kg dry weight. At higher soil mercury concentrations, the earthworm tissue concentrations tend to be lower than the soil concentrations (see text box).

The soil mercury concentrations for both 3MRA and TRIM.FaTE are well below 1 mg/kg dry or wet weight, hence one would expect bioaccumulation at such low soil concentrations. Even though earthworms are approximately 80 percent water, and a wet-weight BAF would be somewhat lower than a dry-weight BAF depending on the soil water content, one would still expect bioaccumulation of mercury in earthworms at the low soil concentrations predicted in both 3MRA and TRIM.FaTE. Although the 3MRA and TRIM.FaTE deeper soil concentrations predicted in this test case are much lower than any found in the literature studies reviewed, it appears that higher BAF values may be more appropriate than the ones calculated

from both the TRIM.FaTE and 3MRA results. These results indicate a possible area for further research and refinement of model input values affecting earthworm bioaccumulation.

The shapes of the TRIM.FaTE and 3MRA earthworm time series are similar at all locations. Total and divalent mercury concentrations in earthworms in the same TRIM.FaTE parcel are not identical, reflecting the same proportional representation of elemental mercury in the TRIM.FaTE earthworm compartments as predicted for the associated root zone soil compartment. For simplicity of presentation, only total and divalent concentrations are shown in Exhibit 6-24.

Earthworm Dry-weight Bioaccumulation Factors (BAFs) for Total Mercury (mg[Hg]/kg[earthworm dry wt]/mg[Hg]/kg[soil dry wt])^a			
Soil Hg Concentration Interval (mg[Hg]/kg[soil dry wt])	Number of Observations	Average Soil [Hg] (mg[Hg]/kg[soil dry wt])	Average Earth- worm BAF
0.010 - 0.050	3	0.020	29
0.051 - 0.100	5	0.80	8
0.101 - 0.250	9	0.19	2.5
0.251 - 1.00	5	0.52	0.94
1.01 - 5.00	6	2.8	0.15
9.9, 269 (actual values)	2	139	0.044

^a Data from Sample et al. (1998).

6.3.4 Spatial Pattern for Surface Soil

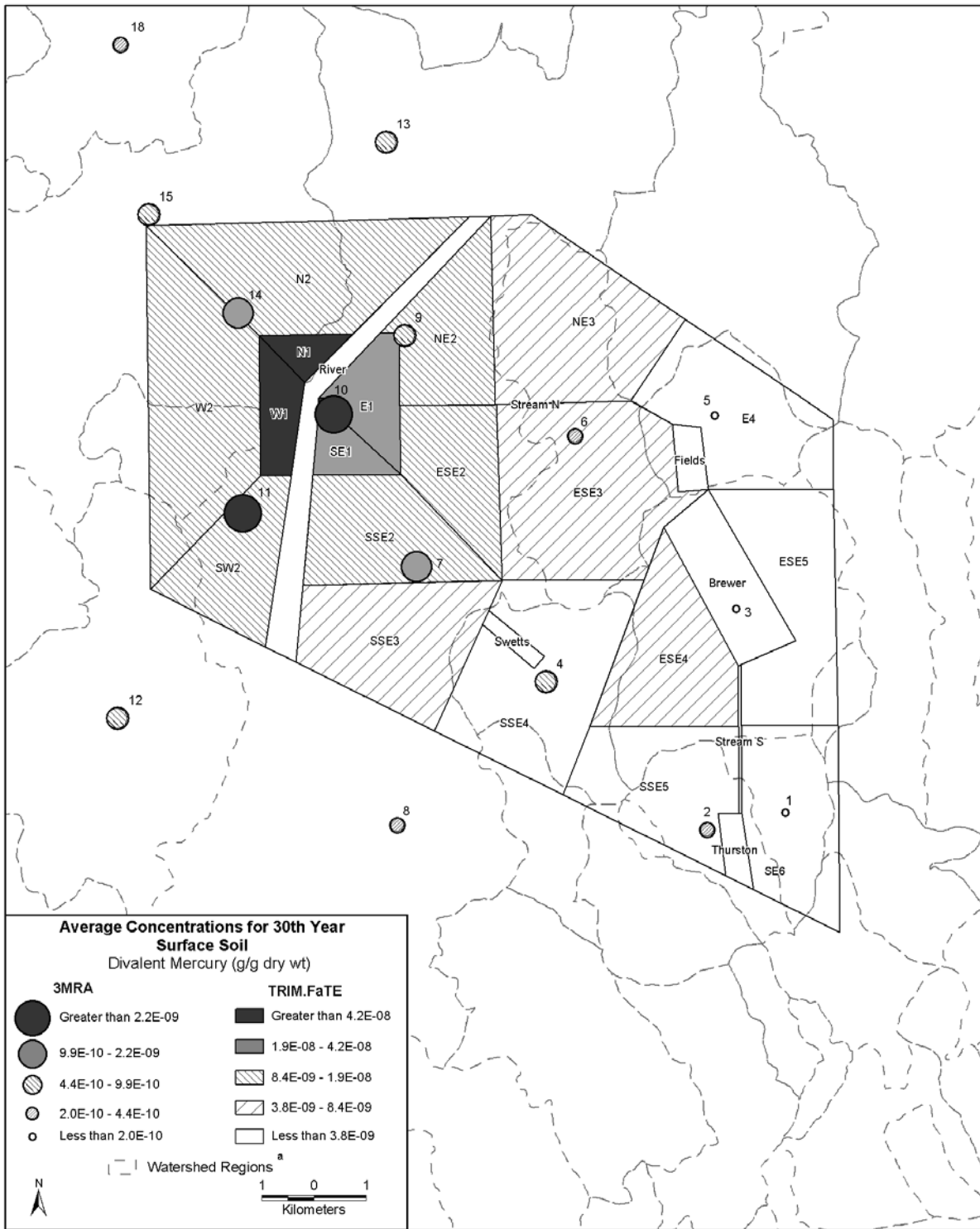
Exhibit 6-25 shows the spatial variation in divalent mercury concentration results for surface soil from 3MRA and TRIM.FaTE. The map is scaled to the same size as Exhibits 6-17 and 6-18. As with the previous maps, the TRIM.FaTE concentrations are shown via background shading and the 3MRA concentrations are shown via dots of various sizes. The increment for each range category is equal (in logarithmic units) both within a model and across the two models (i.e., a change in pattern or dot size reflects the same proportional increase for both models). However, the concentration range categories differ for the models because of the limited overlap of the modeled concentration ranges.

Because of the asymmetry in the locations of results and the few data points for both models, it is difficult to evaluate TRIM.FaTE and 3MRA surface soil results by direction. Like the deposition patterns, TRIM.FaTE soil concentrations appear to be highest north of the source, but concentrations to the west and east are fairly close (and much closer than for air concentrations). Overall, the soil directional pattern generally corresponds to the air concentration pattern, with some differences (such as higher concentrations to the west close to the source) that appear to reflect the deposition patterns. 3MRA surface soil concentrations appear highest to the southwest and lowest to the north and east, which is somewhat different

from the 3MRA air concentration pattern (highest to the northeast) but appears to be similar to the deposition pattern (highest to the southwest).

The TRIM.FaTE maximum-to-minimum ratio for divalent mercury soil concentration for the entire layout (excluding the source compartment) is approximately 26. The 3MRA maximum-to-minimum ratio for the entire layout (excluding location 10, which is just adjacent to the source compartment, and all locations falling outside of the TRIM.FaTE layout) is approximately 48. The slightly higher ratio for 3MRA soil results (less than a factor of two), which is consistent with the findings for air concentrations and deposition fluxes, may be attributable to the point estimate outputs of 3MRA versus the homogenous compartments of TRIM.FaTE. Both TRIM.FaTE and 3MRA results show a greater maximum-to-minimum ratio for the soil concentrations than the air concentrations, indicating a similarity in the importance of deposition in divalent mercury transport near the source.

Exhibit 6-25 Spatial Variation in Divalent Mercury Concentrations in Surface Soil



^a Not all watershed boundaries are shown. See Exhibit 6-9 for additional delineation of the watersheds.

6.4 Surface Water, Sediment, and Fish

This section presents a comparison of the modeling approaches affecting mercury concentration and speciation in surface water, sediment, and fish, as well as a comparison of the outputs for these media from TRIM.FaTE and 3MRA simulations. For all output comparisons in this section, mercury concentration results for Swetts Pond are used because it is the primary surface water body discussed in other chapters of this report. This location corresponds to the TRIM.FaTE parcel labeled as Swetts Pond and the 3MRA location (1,7) for surface water, sediment, and fish. For mercury speciation comparisons, results are also presented for Brewer Lake to show the variation across water bodies. Additional comparisons of results for these media are presented in Appendix E.

6.4.1 Mercury Concentrations and Speciation in Surface Water

As shown in Exhibit 6-26, TRIM.FaTE and 3MRA use different methods for simulating chemical transport and transformation processes in surface water. Key differences in the two simulations being compared are listed below.

- In TRIM.FaTE, chemical exchanges between macrophytes and surface water are modeled explicitly, which may contribute to observed differences in concentration and speciation of mercury in surface water as compared to 3MRA surface water.
- In TRIM.FaTE, algae are modeled explicitly in surface water and participate in partitioning of the various mercury species from surface water, which may contribute to different concentrations and speciation profiles than 3MRA surface water.

As shown in Exhibit 6-27 for Swetts Pond, the TRIM.FaTE total and divalent mercury concentrations in surface water are similar, with TRIM.FaTE total mercury being less than two-fold different from 3MRA total mercury (all comparisons in this section based on total water-column concentrations, not dissolved concentrations). In Brewer Lake (see Appendix E, Chart E7-b), the difference is greater, with TRIM.FaTE total mercury less than five-fold higher than 3MRA total mercury. The higher TRIM.FaTE surface water concentrations for the two water bodies are consistent with the higher atmospheric deposition fluxes modeled by TRIM.FaTE. The larger difference between total mercury concentrations in Brewer Lake compared to Swetts Pond may partially result from the larger difference in deposition fluxes between the two models with increasing distance from the source (see Section 6.2.2). In general, both the TRIM.FaTE and 3MRA mercury concentrations (total, divalent, and methyl) are higher in the surface water of Swetts Pond than of Brewer Lake because Swetts Pond is a smaller (shallower) water body and is closer to the emission source.

Exhibit 6-26
Summary of Mass Transfer and Transformation Processes Modeled:
Surface Water and Macrophyte

TRIM.FaTE (Hg ⁰ , Hg ²⁺ , MHg) ^a	3MRA (Hg ⁰ , Hg ²⁺ , MHg)
Surface Water	
Advective (bulk) flow from surface water to surface water (downstream only) [G or L] ^b	Advective (bulk) flow along reaches within water body network (downstream only) [G or L]
Dispersive flow from surface water to surface water (both directions) [G or L]	Dispersive flow along reaches within water body network (both directions) [G or L]
Advective flow from ground water to surface water [G]	Advective flow between ground water and surface water (both directions) [G or L]
Runoff (dissolved phase) from surface soil to surface water (downgradient only) [G]	Runoff (dissolved phase) from surface soil to surface water (downgradient only) [G]
Erosion (solid phase) from surface soil to surface water (downgradient only) [G]	Erosion (solid phase) from surface soil to surface water (downgradient only) [G]
Dry deposition of particles from air to surface water [G]	Dry deposition of particles from air to surface water [G] ^c
Diffusion (dry deposition) of vapors from air to surface water [G]	Dry deposition of vapors from air to surface water [G] ^c
Diffusion (volatilization) from surface water to air [L]	Diffusion (volatilization) from surface water to air [L]
Wet deposition of particles from air to surface water [G]	Wet deposition of particles from air to surface water [G] ^c
Wet deposition of vapors from air to surface water [Hg ⁰ and Hg ²⁺ only] [G]	Wet deposition of vapors from air to surface water [G]
Particle deposition (including algae phase) from surface water to sediment [L]	
Particle resuspension from sediment to surface water [G]	Effects of particle settling and resuspension and diffusive exchanges on contaminant fate are modeled using a bulk sediment-water exchange term [G or L]
Diffusion from surface water to sediment [L]	
Diffusion from sediment to surface water [G]	
Partitioning from surface water to macrophyte, based on a time-to-equilibrium model and empirical BCF [L]	--
Partitioning from macrophyte to surface water, based on a time-to-equilibrium model and empirical BCF [G]	--
Elimination to surface water by fish [G]	--

TRIM.FaTE (Hg ⁰ , Hg ²⁺ , MHg) ^a	3MRA (Hg ⁰ , Hg ²⁺ , MHg)
Ingestion of surface water algae phase by fish [L]	--
Ingestion of surface water by wildlife [L]	--
Elimination to surface water by wildlife [G]	--
Methylation of Hg ²⁺ (0.001/day) ^d Demethylation of MHg (0.013/day)	Methylation of Hg ²⁺ (9.9E-6/day) Demethylation of MHg (0.024/day)
Reduction of Hg ²⁺ to Hg ⁰ (0.0075/day) Oxidation of Hg ⁰ to Hg ²⁺ (0)	Reduction of Hg ²⁺ to Hg ⁰ (0.04/day) Oxidation of Hg ⁰ to Hg ²⁺ (0.0024/day)
Reduction of MHg to Hg ⁰ (0)	Reduction of MHg to Hg ⁰ (0.0026/day)
Macrophyte	
Partitioning from surface water to macrophyte, based on a time-to-equilibrium model and empirical BCF [G]	Macrophytes not included in this model application
Partitioning from macrophyte to surface water, based on a time-to-equilibrium model and empirical BCF [L]	
Methylation of Hg ²⁺ (0) ^d Demethylation of MHg (0)	Macrophytes not included in this model application
Reduction of Hg ²⁺ to Hg ⁰ (0) Oxidation of Hg ⁰ to Hg ²⁺ (1.0E+9/day)	

^a Algae are modeled explicitly as a phase of surface water in TRIM.FaTE, which affects the phase distribution of mercury species in surface water, and thereby affects the concentration and speciation of mercury in surface water and related compartment types.

^b G = gain process, L = loss process, G or L indicates can be either.

^c Process not modeled in this application, although 3MRA/ISCST3 has this capability for some chemicals.

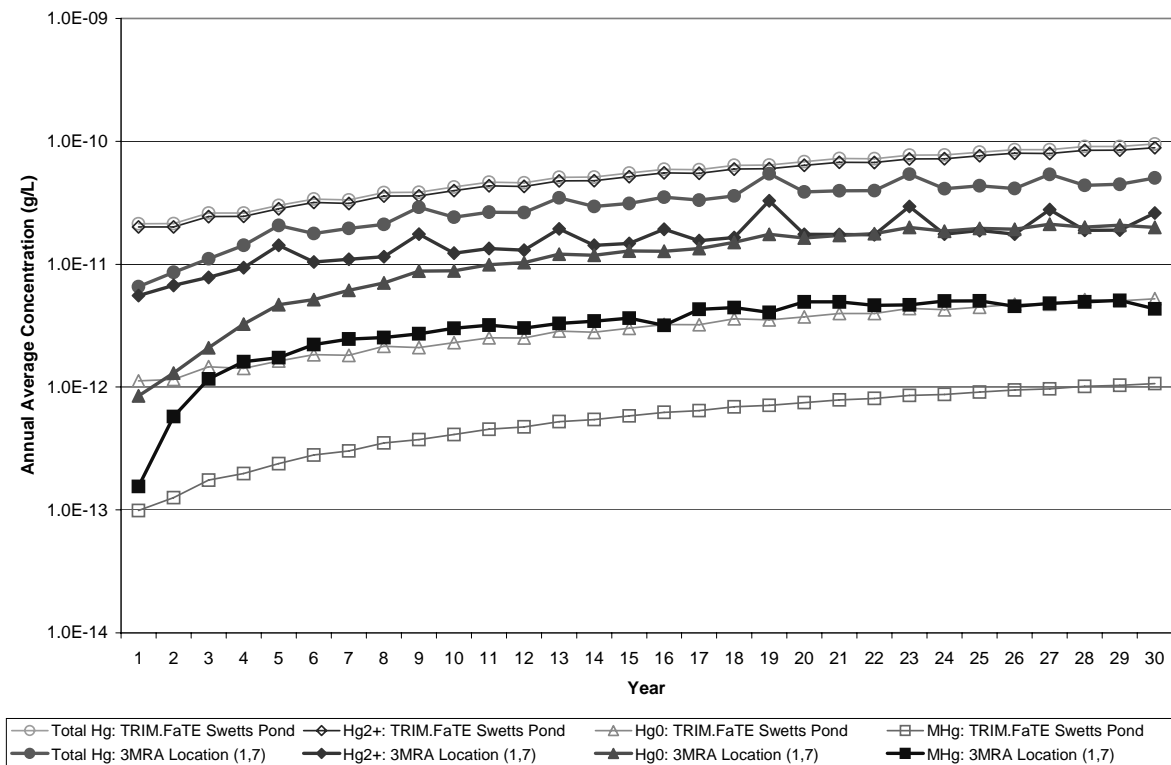
^d First-order rate constant shown in parentheses for all transformation reactions.

In both models, the mercury concentrations increase over time. In both Swetts Pond and Brewer Lake, the TRIM.FaTE total and divalent mercury concentrations increase with a slight five-year repeating pattern corresponding to the five years of meteorological data that were used as inputs to the TRIM.FaTE model. The 3MRA total and divalent mercury concentrations in both surface water bodies spike every few years (with less pronounced spikes in Brewer Lake), corresponding to the 14 years of meteorological data that were used as inputs to the 3MRA model. Even though the mercury deposition and air concentration are input as constants in this 3MRA simulation, these spikes are related to the repeating meteorological data set because the 3MRA watershed module inputs and uses the hourly meteorological data for processes such as runoff and erosion.

While the total mercury concentration predicted by the two models for each water body is not that different, representation of the three mercury species and their temporal pattern varies. Exhibit 6-28 displays the mercury speciation profile in surface water at year 30 of the modeling period. The exhibit shows the majority of mercury predicted in Swetts Pond and Brewer Lake by TRIM.FaTE is in the divalent form at year 30 (i.e., 93 and 85 percent of total mercury as divalent mercury in Swetts Pond and Brewer Lake, respectively), with lesser amounts of

elemental (six and 14 percent) and methyl (one and one percent) mercury. 3MRA predicts noticeably greater representation by elemental and methyl mercury (i.e., 40 and eight percent in Swetts Pond, 63 and six percent in Brewer Lake). The methyl mercury percentages for both models are within the ranges reported in EPA's *Mercury Study Report to Congress* (EPA 1997), which cites percent methyl mercury ranges in fresh surface waters of 1 to 12 percent in Swedish lakes, 2 to 14 percent in Swedish mires, 1 to 6 percent in Swedish runoff, and less than 2.5 percent in Lake Crescent, WA. In a study of 92 lakes in New Hampshire and Vermont, Kamman et al. (2004) measured percent methyl mercury in the hypolimnion (1 meter above sediment-water interface) to be 9.19 percent, with a median value of 6.68 percent, and in the epilimnion (subsurface at approximately 0.2 meters) the percent methyl mercury to be 2.17 with median value 18.28 percent.

**Exhibit 6-27 - Log Scale
Mercury Concentration in Surface Water vs. Time: Swetts Pond**

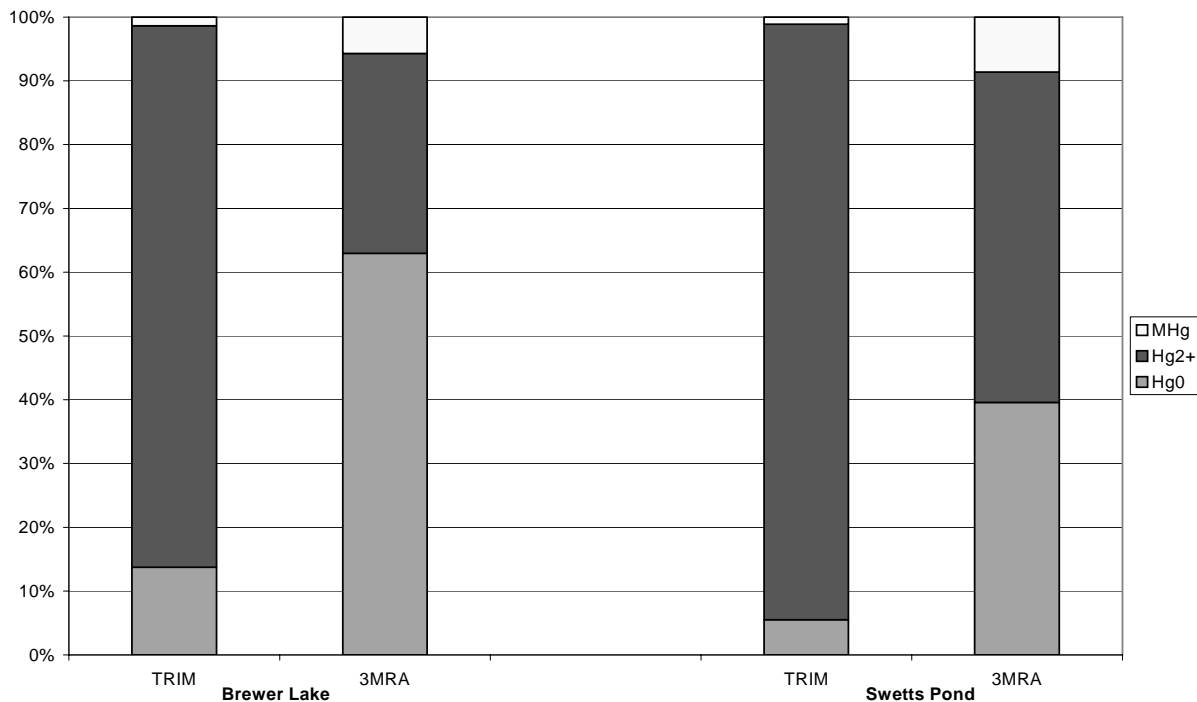


Throughout the simulation time period, the relationship between the three mercury species predicted by TRIM.FaTE does not vary substantially, but the relationship predicted by 3MRA does. This is shown in Exhibit 6-27, particularly with regard to the relationship between divalent and elemental mercury. Initially in 3MRA, the divalent mercury concentration is almost an order of magnitude greater than that for elemental mercury, but they are quite similar by 30 years. In Brewer Lake, the 3MRA concentrations of elemental mercury surpass those of divalent mercury by year 9 of the simulation (see Appendix Chart E-7b).

The mercury speciation differences in surface water between the two models' outputs are likely due to differences in input values and in the simulation of some mass transfer processes,

including (1) different rate constants for the conversion of mercury from one species to another (see Exhibit 6-26), (2) differences in the magnitude of atmospheric deposition at these distances from the source (see Section 6.2.2), (3) partitioning of the various forms of mercury to algae in TRIM.FaTE surface water but not in 3MRA surface water, (4) uptake of the various forms of mercury from surface water by macrophytes (and subsequent rapid conversion of elemental to divalent mercury within macrophytes) that are included in TRIM.FaTE but not in 3MRA, and (5) substantially different input values for suspended solids concentration (4.3 mg/L in the TRIM.FaTE scenario, total of suspended sediment and algae, versus roughly 150 mg/L for 3MRA), which can affect phase distribution and thus the fate of the various mercury species.

Exhibit 6-28
Mercury Speciation Profile in Surface Water at Year 30



6.4.2 Mercury Concentrations and Speciation in Sediment

TRIM.FaTE and 3MRA use different methods for simulating chemical transport and transformation processes in sediment (see Exhibit 6-29). One key process difference between the two simulations is that in TRIM.FaTE, particle deposition from surface water to sediment includes deposition from the algae phase, which is not modeled explicitly in 3MRA.

As shown in Exhibit 6-30 for Swetts Pond, the TRIM.FaTE predictions for total and divalent mercury concentrations in sediment are higher than the corresponding 3MRA predictions by one to two orders of magnitude. The same relationship is observed in the sediment of Brewer Lake (see Appendix Chart E-8b), with slightly larger differences. Methyl

mercury concentrations are higher in TRIM.FaTE sediments than 3MRA sediments to varying degrees, and 3MRA elemental mercury concentrations are consistently greater than TRIM.FaTE elemental mercury concentrations in sediments. This pattern is generally similar (except for methyl mercury) to that observed in surface water, as would be expected; however, the magnitude of the concentration difference is greater in sediment than in surface water. This is at least partly a result of the larger percentage of total mercury as divalent mercury in surface water in TRIM.FaTE, which deposits more rapidly to the sediment than elemental mercury (which is at a much higher percentage in surface water in 3MRA). In general, TRIM.FaTE and 3MRA mercury concentrations (total, divalent, and methyl) are higher in the sediment of Swetts Pond than of Brewer Lake, which also follows the pattern seen for concentrations in surface water.

Exhibit 6-29
Summary of Mass Transfer and Transformation Processes Modeled: Sediment

TRIM.FaTE (Hg ⁰ , Hg ²⁺ , MHg)	3MRA (Hg ⁰ , Hg ²⁺ , MHg)
Particle deposition (including algae phase) from surface water to sediment [G] ^a	
Particle resuspension from sediment to surface water [L]	Effects of particle settling and resuspension and diffusive exchanges on contaminant fate are modeled using a bulk sediment-water exchange term [G or L]
Diffusion from surface water to sediment [G]	
Diffusion from sediment to surface water [L]	
Partitioning from sediment to benthic invertebrate, based on time-to-equilibrium model and empirical BCF [L]	
Partitioning from benthic invertebrate to sediment, based on time-to-equilibrium model and empirical BCF [G]	
Methylation of Hg ²⁺ (0.0001/day) ^b Demethylation of MHg (0.0501/day)	Methylation of Hg ²⁺ (0.00037/day, upper sed) Demethylation of MHg (0.0015/day, upper sed)
Reduction of Hg ²⁺ to Hg ⁰ (1.0E-6/day) Oxidation of Hg ⁰ to Hg ²⁺ (0)	Reduction of Hg ²⁺ to Hg ⁰ (0) Oxidation of Hg ⁰ to Hg ²⁺ (0)

^a G = gain process, L = loss process.

^b First-order rate constant shown in parentheses for all transformation reactions.

For both models, the mercury concentrations increase over time with relatively smooth patterns. In contrast to the surface water concentrations, the TRIM.FaTE concentrations in sediment do not show the five-year repeating pattern corresponding to the meteorological data; however, the 3MRA concentrations of divalent and methyl mercury in sediment do show slight fluctuations, similar to the spikes observed in the surface water concentrations (see Exhibit 6-27). This difference is possibly due to the spikes in surface water concentrations being greater for 3MRA than TRIM.FaTE, and therefore not being damped out completely in the sediment by the mass transfer processes as they are for TRIM.FaTE.

**Exhibit 6-30 - Log Scale
Mercury Concentration in Sediment vs. Time: Swetts Pond**

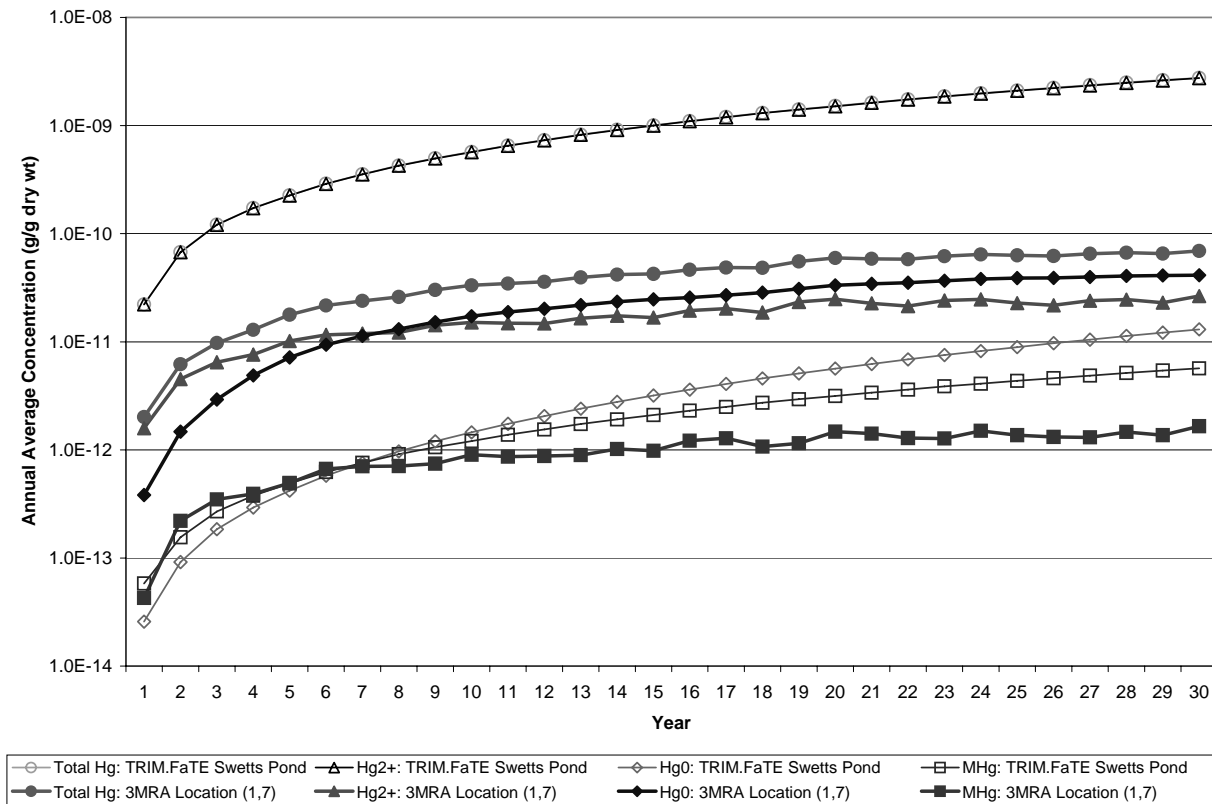
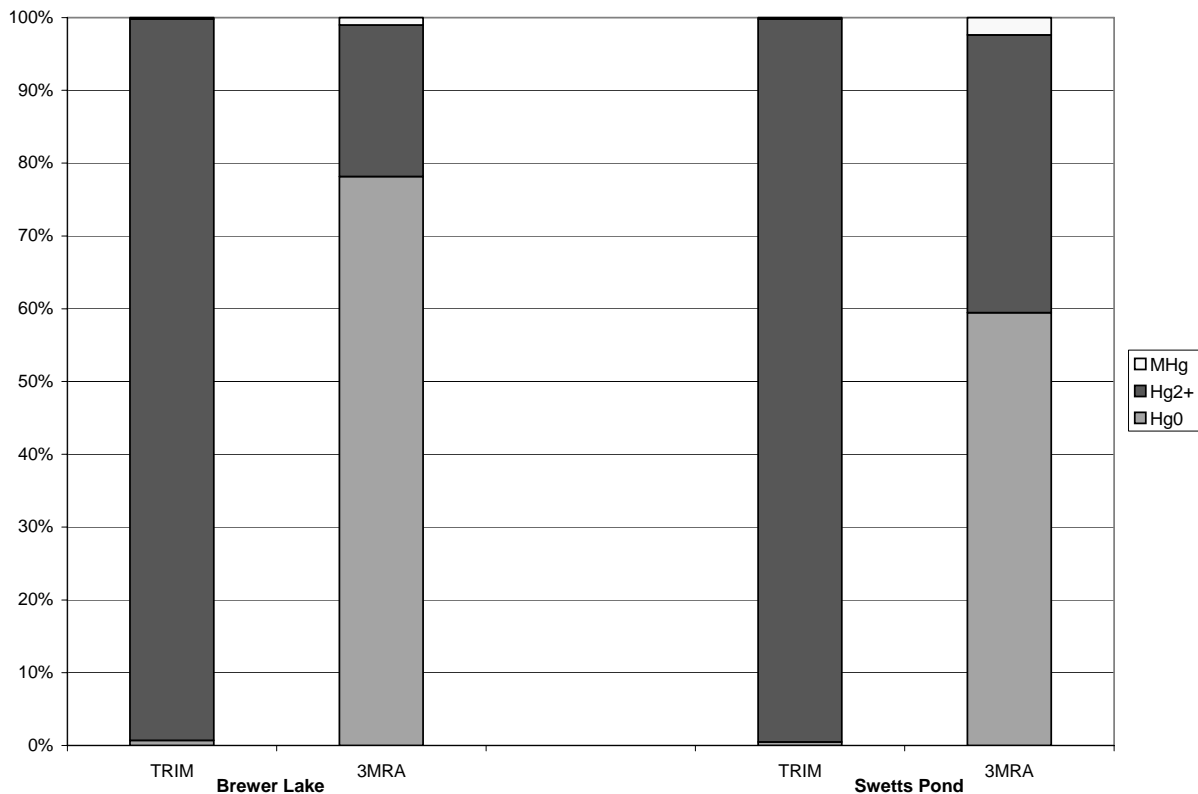


Exhibit 6-31 displays the mercury speciation profile in sediment at year 30 of the modeling period. The percent of mercury in each form in sediment differs between the two models. Nearly all of the mercury modeled by TRIM.FaTE in the sediment is divalent mercury at year 30 (i.e., 99 percent of total mercury as divalent mercury in Swetts Pond and Brewer Lake). In contrast, at year 30 the majority of mercury modeled by 3MRA in the sediment is elemental mercury (i.e., 59 percent and 78 percent of total mercury as elemental mercury in Swetts Pond and Brewer Lake, respectively). The percent of mercury that is methyl mercury in the sediment is small for both models (i.e., 0.2 percent in both water bodies for TRIM.FaTE; 1.0 percent in Brewer Lake for 3MRA; and 2.4 percent for Swetts Pond for 3MRA). The observed speciation differences are likely a result of many contributing factors, including to at least some degree all the possible factors mentioned for surface water and also including the different mercury transformation rate constants used by the two models for sediment.

A few sources were identified in the literature in which authors reported the percent of mercury measured as methyl mercury in sediment. In 92 New Hampshire and Vermont lakes, percent measured methyl mercury in surficial sediment (0 to 5 cm) ranged from 0.24 to 7.84 percent (mean 1.84, median 1.46 percent; Kamman et al. 2004). The authors note that these results are similar to measurements made at six locations in the Quabbin Reservoir in Massachusetts (Gilmour et al. 1992) that ranged from 0.1 to 3.1 percent (at a seventh location, the methyl mercury was measured at 16.3 percent). In the *Mercury Study Report to Congress*

(EPA 1997), the percent methyl mercury measured in four lakes in Finland was reported to be between 0.03 and 6 percent (Verta and Matilainen 1995). No sources were identified that reported the percent of elemental mercury in lake sediment. Thus, it is difficult to determine whether the speciation calculated for TRIM.FaTE or for 3MRA is more representative of sediment; however, methyl mercury speciation from both models falls within the range of values reported in the literature.

**Exhibit 6-31
Mercury Speciation Profile in Sediment at Year 30**



From a mass balance perspective, one would expect the TRIM.FaTE results to show more mercury mass in the Swetts Pond system than the 3MRA results, given that the TRIM.FaTE deposition flux of mercury from air is approximately an order of magnitude higher (air deposition is a primary source of modeled mercury inputs to Swetts Pond, along with soil erosion and runoff; see Exhibits 6-26 and 6-29 for all sources of mercury to the surface water and sediment). Unlike TRIM.FaTE, 3MRA cannot provide mass results for individual compartments/media, but the concentration results for the two models imply that there is more mercury mass in the Swetts Pond system in the TRIM.FaTE simulation. TRIM.FaTE predicts higher mercury concentrations (and thus mass, given similar media volumes modeled) in the key mass-accumulating media in Swetts Pond, including sediment (one and a half orders of magnitude), surface water (slightly higher), and macrophytes (not modeled in 3MRA). 3MRA predicts slightly higher mercury concentrations in fish, but the fish biomass is relatively very small (compared to the volume of the water bodies), and thus the amount of mercury in fish is negligible in a mass balance context.

6.4.3 Methyl Mercury Concentrations in Fish

As shown in Exhibit 6-32, TRIM.FaTE and 3MRA use different methods for simulating chemical transport and transformation processes in fish. Key differences in the two simulations are presented below.

- TRIM.FaTE uses a bioenergetics¹² approach for accumulation of methyl mercury in fish, whereas 3MRA uses a bioaccumulation factor (BAF) approach based on the dissolved water concentration.
- For purposes of this model comparison, both 3MRA and TRIM.FaTE expressed chemical concentrations in aquatic organisms at integer trophic levels. 3MRA evaluated two trophic levels: T4 fish (i.e., secondary carnivores that are the apex predator species in the system) and T3 fish (i.e., primary carnivores that may be both predator and prey).¹³ TRIM.FaTE also evaluated T2 (i.e., benthic invertebrates that consume detritus (largely decaying plant material) and herbivorous fish).¹⁴
- TRIM.FaTE modeled two distinct aquatic food chains, a benthic and a water-column food chain, whereas 3MRA did not in this application. 3MRA assumed that methyl mercury concentrations in fish are directly related to methyl mercury concentrations in surface water regardless of the amount of benthic prey consumed by the fish. Bioaccumulation factors based on mercury concentrations in sediment were not used in 3MRA for this model comparison.
- Because TRIM.FaTE is a chemical mass-balanced model, estimates of total fish biomass at T2, T3, and T4 are needed to run the model, whereas they are not needed for 3MRA. The estimates of fish biomass at each integer trophic level in TRIM.FaTE represented all populations and portions of populations of fish at that trophic level in the modeled surface water body.
- In both 3MRA and TRIM.FaTE, the modeled chemical concentration at an integer trophic level was intended to be close to what would be found in a fish of average size and age at that trophic level, rather than in fish of a particular species (which may feed on prey from multiple trophic levels). With TRIM.FaTE, chemical concentrations in fish of a particular species (e.g., largemouth bass, which feed on smaller fish and invertebrates at smaller adult sizes and feed more exclusively on fish at larger adult sizes, consuming prey from both the water-column and the benthic environment) were estimated from the

¹² The bioenergetics approach used by TRIM.FaTE allows the user to explicitly incorporate multiple exposure pathways for fish. The user can assign more than one diet item to each type of fish, creating a web-like set of trophic relationships. However in this application, each TRIM.FaTE fish compartment was set to have a diet that is only the fish in the trophic level below it.

¹³ T1 and T2 type aquatic organisms can be modeled with 3MRA, but were not in this application.

¹⁴ Odum (1971) defines four basic trophic levels: T1 = primary producers (plants); T2 = primary consumers (herbivores); T3 = secondary consumers (primary carnivores that consume herbivores); and T4 = tertiary consumers (secondary carnivores that consume primary carnivores).

modeled concentrations for appropriate TRIM.FaTE trophic levels and estimates of the relative biomass for the species in the different trophic levels.¹⁵

Exhibit 6-32
Summary of Mass Transfer and Transformation Processes Modeled: Fish

TRIM.FaTE (Hg ²⁺ , Hg ²⁺ , MHg)	3MRA (MHg only)
Ingestion of surface water algae phase by fish (water-column herbivores only) [G] ^a	Empirical bioaccumulation factor (BAF) relates dissolved water-column concentration and whole body and filet concentration of MHg in T3 and T4 fish (this factor is intended to represent all relevant gains and losses under equilibrium conditions) [G or L]
Ingestion of benthic invertebrates by fish (benthic omnivores only) [G]	
Ingestion of fish by fish (benthic carnivore and water-column omnivore and carnivore) [G or L]	
Elimination to surface water by fish [L]	
Ingestion of fish by semi-aquatic wildlife [L]	
Methylation of Hg ²⁺ (0) ^b Demethylation of MHg (0)	Hg transformation in fish not modeled explicitly; however, MHg concentrations predicted for fish use MHg-specific BAFs from empirical studies and should reflect methylation <i>in vivo</i>
Reduction of Hg ²⁺ to Hg ⁰ (0)	
Oxidation of Hg ⁰ to Hg ²⁺ (1.0E+6/day)	

^a G = gain process, L = loss process, G or L indicates can be either.

^b First-order rate constant shown in parentheses for all transformation reactions.

For purposes of this model comparison, the methyl mercury concentration time series for the 3MRA T4 fish, the two TRIM.FaTE top trophic level fish compartments modeled (i.e., benthic carnivore, water-column carnivore), and three top predator fish species developed from TRIM.FaTE fish compartment data were evaluated (Exhibit 6-33). The top predator fish species were developed as an additional comparison with 3MRA fish (which are modeled using empirical BAFs) and as a demonstration of how the concentration calculated in a fish species based on diet would differ from the TRIM.FaTE T3 and T4 fish. See the accompanying text box for discussion of how TRIM.FaTE fish compartment outputs were used to develop mercury concentration predictions for the top predator fish species.

As shown in Exhibit 6-33 for Swetts Pond, the shapes of the time series for the TRIM.FaTE and 3MRA fish are similar, showing increased concentrations with time. In general, the methyl mercury concentrations for top predator fish in 3MRA and TRIM.FaTE are similar despite the different methods used to model methyl mercury uptake and accumulation in fish. Specifically, the methyl mercury concentrations are all within approximately one order of magnitude by year 30, with the TRIM.FaTE water-column carnivore compartment within a factor of three of the 3MRA T4 fish. The Brewer Lake results are even closer, with the 3MRA

¹⁵ The fish bioenergetic model in TRIM.FaTE also can be used to directly simulate individual fish species that feed at multiple trophic levels in one or more environments. In that case, estimates of total fish biomass are calculated for species instead of for integer trophic levels.

T4 fish falling within the span of the various TRIM.FaTE results (see Appendix Chart E-9b). The 3MRA T4 fish concentrations are likely greater than the TRIM.FaTE largemouth bass/smallmouth bass/northern pike concentrations because the consumption behavior of these fish species is a hybrid of 70 percent mid-trophic level fish (i.e., omnivores) and 30 percent top trophic level fish (i.e., carnivores). Of the two top predator fish compartments modeled in TRIM.FaTE, the methyl mercury concentrations are greater for the one associated with the water-column food chain than the one associated with the benthic food chain. The same pattern is observed in Brewer Lake.

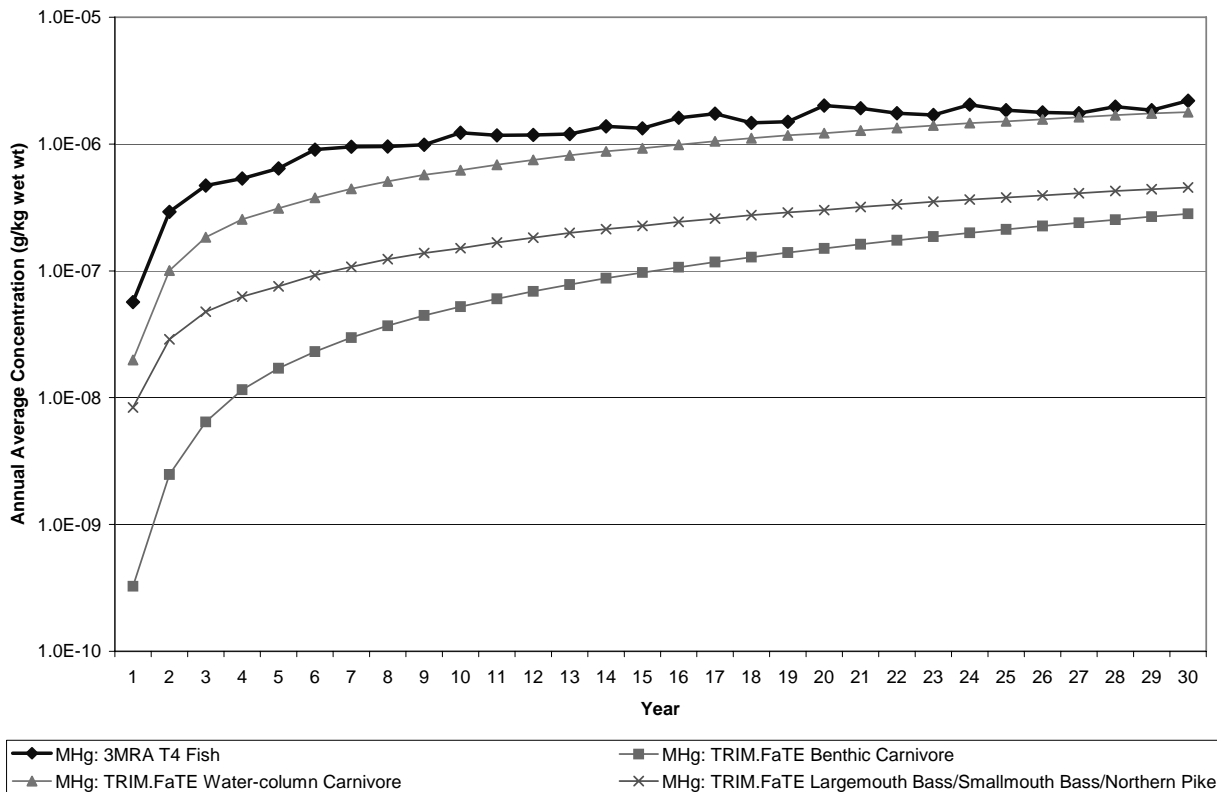
Using TRIM.FaTE Outputs to Calculate Concentrations in Specific Fish Types

TRIM.FaTE pollutant concentration predictions in fish compartments can be used – along with information on the diets of specific fish species (as used in setting up the TRIM.FaTE scenario) – to calculate pollutant concentration estimates for specific fish types. Such a calculation was done in this model comparison to develop methyl mercury concentration estimates for some top predator species (i.e., largemouth bass/smallmouth bass/northern pike). These estimates are derived using the relevant model outputs (i.e., the compartments exhibiting feeding behavior of the species of interest) and fractional values representing the relative prevalence of those feeding behaviors by the species of interest. For example, data consulted in setting up the simulation indicated that 35 percent of the largemouth bass diet in lakes in the region consists of benthic invertebrates (which is the diet of the TRIM.FaTE benthic omnivore compartment in this simulation), 35 percent consists of water-column herbivores (same diet as water-column omnivore compartment), 15 percent consists of benthic omnivores (same diet as benthic carnivore compartment), and 15 percent consists of water-column omnivores (same diet as water-column carnivore compartment).^a Therefore, the estimated methyl mercury (MHg) concentration for largemouth bass would be:

$$(0.35 * [\text{MHg}_{\text{benthic omnivore}}]) + (0.35 * [\text{MHg}_{\text{water-column omnivore}}]) + (0.15 * [\text{MHg}_{\text{benthic carnivore}}]) + (0.15 * [\text{MHg}_{\text{water-column carnivore}}]).$$

^a Dietary fractions from Kelso and Johnson (1991).

**Exhibit 6-33 - Log Scale
Methyl Mercury Concentration in Fish vs. Time: Swetts Pond**



In both modeling approaches, the fish methyl mercury concentrations in the highest accumulating fish are dependent on the concentrations of dissolved methyl mercury in the surface water. This relationship is explicit and direct in 3MRA, where mercury accumulation in fish is derived from the dissolved water concentration of methyl mercury and an empirical BAF. In TRIM.FaTE, the same relationship is true, but a bioenergetics approach is used in which the methyl mercury is transferred among media and biota based on food chain relationships (i.e., ingestion of food contaminated with mercury), beginning with methyl mercury in the surface water. For example, the methyl mercury concentration in surface water affects the concentration of methyl mercury in the algae phase, which is consumed by the water-column herbivorous fish, which are consumed by the next trophic level water-column fish and then by the T4 water-column fish according to the defined ingestion rates and modeled contamination levels. Lower methyl mercury concentrations are predicted in the TRIM.FaTE benthic carnivore compartment than in the water-column carnivore compartment, indicating lower mercury accumulation in the TRIM.FaTE benthic food chain.

Because the two models use different methods to predict mercury accumulation in fish and because the two models predict somewhat different surface water concentrations of the various forms of mercury, it is informative to evaluate the ratios between dissolved surface water concentrations and fish tissue concentrations of methyl mercury (i.e., BAFs calculated from the model estimates of surface water-dissolved methyl mercury concentrations and fish tissue methyl mercury concentrations) in addition to the fish tissue methyl mercury concentration time series.

The dissolved methyl mercury concentrations in surface water, the methyl mercury concentrations in fish, and the ratios between the surface water and fish concentrations (i.e., calculated BAFs) for TRIM.FaTE and 3MRA for Swetts Pond at year 30 are presented in Exhibit 6-34. These BAFs are within the range of methyl mercury BAFs identified in the literature for upper trophic level fish that are typically consumed by humans. The range of BAF values presented in EPA's *Water Quality Criterion for the Protection of Human Health: Methylmercury* is 500,000 to 10,000,000 (Glass et al. 1999, Loes et al. 1998, Miles and Fink 1998, Watras et al. 1998, Mason and Sullivan 1997, as cited in EPA 2001). EPA's *Mercury Study Report to Congress* provides a range of BAFs for methyl mercury in T4 fish from 4,000,000 to 11,400,000 (EPA 1997). The methyl mercury water quality criterion document also notes that within any single trophic level, empirically derived BAFs for methyl mercury from studies nationwide vary by up to two orders of magnitude. Therefore, the BAFs derived from this TRIM.FaTE simulation and used in the 3MRA simulation fall within the ranges reported in the current scientific literature.

Exhibit 6-34
TRIM.FaTE and 3MRA Methyl Mercury Concentrations in Surface Water and Fish
and Calculated BAFs in Swetts Pond at Year 30

	Surface Water dissolved MHg concentration (g/L)	Fish MHg concentration (g/kg, ww)	Calculated BAF fish:dissolved water (L/kg)
3MRA	3.2E-13	--	--
T4 fish	--	2.2E-6	6.8E6
TRIM.FaTE	7.4E-13	--	--
Water-column carnivore	--	1.8E-6	2.4E6
Benthic carnivore	--	2.8E-7	3.8E5
Largemouth bass/smallmouth bass/northern pike	--	4.5E-7	6.2E5

As might be expected based on the water-column mercury concentrations for Swetts Pond that are presented in Exhibit 6-27, the dissolved water concentrations of methyl mercury in TRIM.FaTE and 3MRA are similar, with the 3MRA concentration being less than three-fold lower than the TRIM.FaTE concentration.¹⁶ The slightly higher 3MRA fish results may be explained by the slightly higher BAFs observed for 3MRA (calculated value shown in Exhibit 6-34 matches the 3MRA input BAF used, as expected) versus TRIM.FaTE at year 30 in the simulations. Note that the fish tissue methyl mercury concentrations appear to be continuing on an upward trend (see Exhibit 6-33) at year 30 and also that the BAF for the TRIM.FaTE water-column carnivore compartment is still increasing somewhat with time (see accompanying text box). Thus, the 3MRA and TRIM.FaTE calculated BAFs will be slightly closer as TRIM.FaTE approaches steady-state.

TRIM.FaTE BAFs Increase Over Time

In this 3MRA simulation, a constant BAF value for T4 fish is used (i.e., 6.8E6), assuming equilibrium conditions. Because TRIM.FaTE uses a different approach to predict methyl mercury accumulation in fish, its calculated BAF values for top predator fish increase over time until an equilibrium condition is achieved. Using the TRIM.FaTE water-column carnivore in Swetts Pond for example, the calculated BAF increases with time as shown below:

Year 10 BAF = 2.19E6

Year 20 BAF = 2.37E6

Year 30 BAF = 2.43E6

The calculated BAF increases rather dramatically at the very early stages of the modeling period (first couple years, not shown) and then the rate of increase tapers off, as shown above. The steady-state BAF value for the TRIM.FaTE water-column carnivore in Swetts Pond, calculated from the steady-state modeling results (see Chapter 4), is 2.6E6, which is consistent with the dynamic modeling results shown above.

¹⁶ The relationship for dissolved water concentration of methyl mercury (TRIM.FaTE higher than 3MRA) is opposite that for whole water concentration of methyl mercury (3MRA higher) because the two models predicted different phase distributions of methyl mercury. Based on the inputs used, TRIM.FaTE estimated 69 percent of methyl mercury in surface water in the dissolved phase, and 3MRA estimated 5 to 7 percent (varies by year in 3MRA). This difference is thought to be largely due to the very different values used for total suspended solids, 4.3 mg/L for TRIM.FaTE versus an average of roughly 150 mg/L for 3MRA (varies by year in 3MRA). The methyl mercury water quality criterion document (EPA 2001) cites 61 percent as a default value for dissolved fraction of methyl mercury in lakes (geometric mean of literature values), corresponding to a total suspended solids value in the range of 1 to 2 mg/L (higher suspended solids = lower dissolved fraction). Pankow and McKenzie (1991) found typical total suspended solids values for lakes in eastern Washington state range from 0.5 to 5 mg/L and for rivers range from 5 to 50 mg/L.

6.5 Wildlife

This section compares the modeling approaches used by 3MRA and TRIM.FaTE for simulation of mercury accumulation in selected terrestrial wildlife and the results obtained by those approaches. It is important to note that, as mentioned in Section 6.1.1 and discussed below, some aspects of the 3MRA approach were specific to this application and do not necessarily reflect the way that 3MRA is usually employed.

For all of the comparisons presented in this section, the mercury concentration results are for TRIM.FaTE parcel SSE4 comprising the Swetts Pond watershed and 3MRA habitat 11 and watershed location 4, representing the Swetts Pond watershed. This location was selected because the Swetts Pond area is a focus of the overall mercury test case (see Section 3.2) and because adequate comparison data are available. Comparison results for additional locations are presented in Appendix E. The 3MRA body burden results for wildlife are for total mercury (unspeciated), and even though TRIM.FaTE provides speciated mercury results, the TRIM.FaTE total mercury results (sum of elemental, divalent, and methyl) are presented here to facilitate comparisons. Furthermore, as noted previously in this report, there is a relatively high level of uncertainty about the rate of transformation of mercury in terrestrial animals. Since the mercury speciation in wildlife is based on these transformation rate constants, there is also a high level of uncertainty about the TRIM.FaTE results for individual mercury species in wildlife.

As shown in Exhibit 6-35, TRIM.FaTE simulates different chemical uptake, elimination, and transformation processes in wildlife from those represented in 3MRA. The 3MRA wildlife species that are the focus of this comparison, listed in Exhibit 6-36, are limited to those for which the 3MRA framework derives contaminant concentrations (EPA 1999c).¹⁷ The TRIM.FaTE wildlife species are compared to each 3MRA wildlife category in Exhibit 6-36.

For the wildlife compared, the largest difference in estimating chemical concentrations (i.e., body burden) between the two models is that TRIM.FaTE uses bioenergetics to simulate food web transfers of mercury, whereas for the prey species modeled in this application, 3MRA uses soil-based empirical BAFs. Specifically, chemical uptake by wildlife in TRIM.FaTE is predicted through the simulation of wildlife exposures via dietary and inhalation pathways, as well as elimination losses for each animal modeled. Therefore, the wildlife in TRIM.FaTE are obtaining mercury from the air, surface soil, surface water, plants, terrestrial and semi-aquatic animals, fish, and benthic invertebrates that are contaminated with mercury, as appropriate for each species modeled. It is important to note that several TRIM.FaTE wildlife compartment types – including those represented by mink, raccoon, and tree swallow – obtain a significant portion of their diets from surface water sources (e.g., fish and benthic invertebrates). As noted previously (see Section 6.4.3), fish and benthic invertebrate accumulation patterns in TRIM.FaTE differ from those for biota that are more directly influenced by air and soil concentrations, such as terrestrial plants and earthworms. For the 3MRA prey species modeled

¹⁷ 3MRA categorizes wildlife as either prey or predator. For prey, it predicts body burdens (i.e., biota concentrations) and for the predators it predicts pollutant intake (e.g., mg/kg/day) based on the simulated diet for each predator. The prey species (for which biota concentrations are predicted) are the focus of these comparisons. TRIM.FaTE can also predict pollutant intake for wildlife, but that option was not employed for this application.

in this application, chemical uptake was simulated by 3MRA's Terrestrial Food Web Module using mercury concentrations in deeper soil (i.e., top 5 cm of soil), rather than surface soil (i.e., top 1 cm of soil), and empirical BAFs for each wildlife category (e.g., small birds, small mammals). These different approaches are important because the TRIM.FaTE results are highly influenced by diet, as discussed further in each section below.

Exhibit 6-35
Summary of Mass Transfer and Transformation Processes Modeled: Wildlife

TRIM.FaTE (Hg ⁰ , Hg ²⁺ , MHg)	3MRA (Total Hg)
Inhalation of air by wildlife [G] ^a Ingestion of surface soil by wildlife [G] Elimination to surface soil by wildlife [L] Ingestion of surface water by wildlife [G] Elimination to surface water by wildlife [L] Ingestion of leaf and particles-on-leaf by certain wildlife [G] Ingestion of terrestrial/semi-aquatic animals (including earthworm) by certain wildlife [G or L] Ingestion of fish/benthic invertebrates by certain semi-aquatic wildlife [G]	Chemical body burden (mg/kg) for prey species (i.e., excluding top predators) included in this application estimated using empirical BAFs that express the relationship between chemical concentrations in upper soil horizons (top 5 cm of soil used here) and chemical residue concentrations in animals; the empirical BAFs are intended to represent all relevant pathways of exposure such as the ingestion of contaminated biota and media ^b
Methylation of Hg ²⁺ to Hg ⁰ (0) ^c Demethylation of MHg (0.09/day)	Transformation of Hg in wildlife not modeled
Reduction of Hg ²⁺ to Hg ⁰ (0) Oxidation of Hg ⁰ to Hg ²⁺ (1.0/day)	

^a G = gain process, L = loss process, G or L indicates can be either.

^b 3MRA also has a separate module, *not* used in this model comparison, that calculates applied doses (in mg/kg-day) for all species based on: ingestion of surface soil, ingestion of surface water, ingestion of leaf and particles-on-leaf, ingestion of terrestrial/semi-aquatic animals (including earthworm) at lower trophic levels, and ingestion of fish/benthic invertebrates by semi-aquatic animals.

^c First-order rate constant shown in parentheses for all transformation reactions.

Another important difference is that TRIM.FaTE results are developed for wildlife populations representing trophic/functional groups (see Exhibit 2-4). The results for each wildlife compartment, therefore, represent an average concentration for that population, which is assigned to a particular volume element but may have associations (e.g., via predators and/or diet components) with other volume elements. For this model comparison, the 3MRA results are the maximum pollutant concentration among all species modeled for a wildlife category (see Exhibit 6-36) in a habitat associated with a particular 3MRA watershed.¹⁸

¹⁸ 3MRA has been developed to report the minimum and/or maximum values among all the species in each wildlife category. For this application, however, only the maximum values were reported.

Exhibit 6-36
Wildlife Species Modeled by TRIM.FaTE and 3MRA in Comparison Categories

3MRA Wildlife for Which Concentrations Are Derived ^a		TRIM.FaTE Representative Species/Subgroups Identified for Comparison	
<i>Category</i>	<i>Representative Species</i>	<i>Subgroup</i>	<i>Representative Species</i>
Small birds	Marsh wren Spotted sandpiper Tree swallow	Terrestrial insectivore Semi-aquatic aerial insectivore	Black-capped chickadee Tree swallow
Omniverts ^b	American kestrel American robin American woodcock Belted kingfisher Great blue heron Green heron Herring gull Long-tailed weasel Mallard duck Mink Raccoon River otter Short-tailed weasel	Terrestrial carnivore Semi-aquatic omnivore Semi-aquatic carnivore	Long-tailed weasel Mallard duck Raccoon Mink
Small mammals	Deer mouse Least weasel Little brown rat Meadow vole	Terrestrial ground-invertebrate feeder Terrestrial herbivore Terrestrial omnivore	Short-tailed shrew Meadow vole Mouse

^a 3MRA has been developed to report the maximum and/or minimum modeled concentration values among all the species in each wildlife group. For this application, however, only the maximum concentrations were reported.

^b Omnivert is a term used in 3MRA for omnivorous vertebrates.

6.5.1 Total Mercury Concentrations in Small Birds

The 3MRA total mercury concentration in the small bird wildlife group was compared to two small bird compartments (insectivores) in TRIM.FaTE: the tree swallow and the black-capped chickadee. As noted previously, the 3MRA value is derived directly from the concentration of mercury in the deeper soil (top 5 cm) at a specific point, while the two TRIM.FaTE small bird compartments receive mercury from their diet and through the inhalation pathway. In the case of the tree swallow, its diet is comprised wholly of insects who spend a stage of their life as benthic invertebrates in the neighboring water body. The chickadee was assigned a diet of 70 percent soil arthropods and 30 percent leaf material.

In general, the total mercury concentration in 3MRA small birds and the total mercury concentration in TRIM.FaTE tree swallow are within one to two orders of magnitude, depending on the comparison location, even though the modeling approach is quite different. As shown in

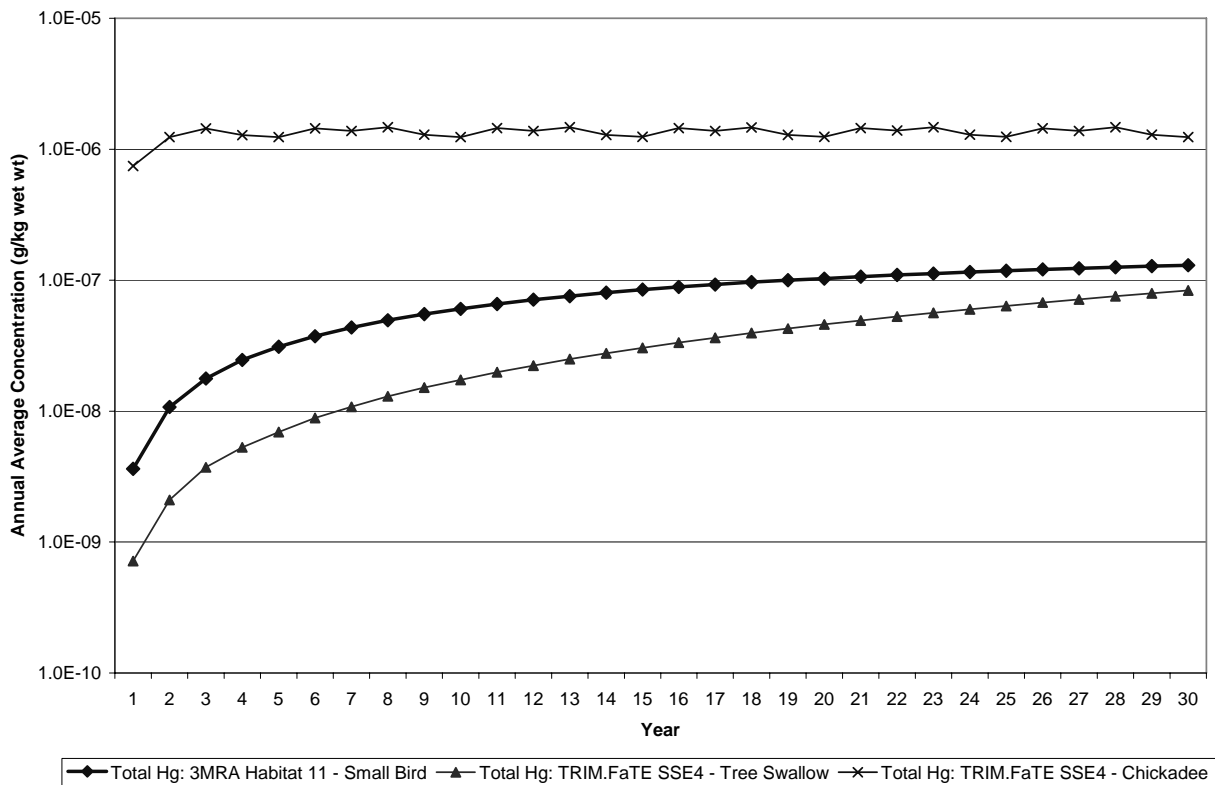
Exhibit 6-37 for the Swetts Pond watershed, the total mercury concentrations in the 3MRA small birds are higher than, but similar to, the total mercury concentrations in the TRIM.FaTE tree swallow compartment. Although the direction of this relationship remains the same in the TRIM.FaTE near source, southwest location, which is compared to 3MRA habitat 3 (see Appendix Chart E-10b), the total mercury concentrations in 3MRA small birds are much higher than in the TRIM.FaTE tree swallow compartment at this location. These differences can be attributed to differences in the TRIM.FaTE food sources at these two locations. Specifically, the TRIM.FaTE tree swallow consumes flying aquatic insects that spend a life stage as benthic invertebrates in the adjacent surface water body. In the TRIM.FaTE results, Swetts Pond is more contaminated with mercury than the modeled river compartment, resulting in higher total mercury concentrations in the tree swallow in the Swetts Pond watershed location than in the near source, southwest location. Furthermore, in 3MRA, the concentration of mercury in the small birds is calculated directly from the deeper soil (0-5 cm depth) concentration, which yields much higher values in habitat 3 than habitat 11 because the former is closer to the emission source.

Exhibit 6-37 also shows that the 3MRA small bird and TRIM.FaTE tree swallow time series curves for total mercury are similar in shape. This is expected because the 3MRA small bird time series curve is similar to the 3MRA deeper soil (0-5 cm depth) curve (from which the small bird concentrations are calculated directly), and the TRIM.FaTE tree swallow curve is similar to the TRIM.FaTE sediment curve (from which the mercury in the diet of the tree swallow compartment is derived).

The TRIM.FaTE chickadee is not as good of a match to the 3MRA small bird because, as mentioned earlier, the chickadees' diet includes both soil arthropods and leaf material, the latter of which contains higher concentrations of mercury.¹⁹ In addition, the inclusion of plants in the chickadees' diet results in a time series pattern that is highly influenced by the varying concentration of mercury in terrestrial plants (related to the varying concentration in air) instead of the mercury accumulation in the soil which influences the 3MRA small bird. Regardless, the results for the two models are within an order of magnitude at both locations.

¹⁹ Seeds and berries, which are a component of the diet of chickadees, were not modeled explicitly (i.e., as separate compartments) in this TRIM.FaTE application. Rather, leaves and particles on leaves were used to represent plant material in the chickadee diet. It is recognized, however, that mercury accumulation and the adherence of dust particles may differ among various types of plant material.

**Exhibit 6-37 - Log Scale
Total Mercury Concentration in Small Birds vs. Time: Swetts Pond Watershed**



6.5.2 Total Mercury Concentrations in Omniverts

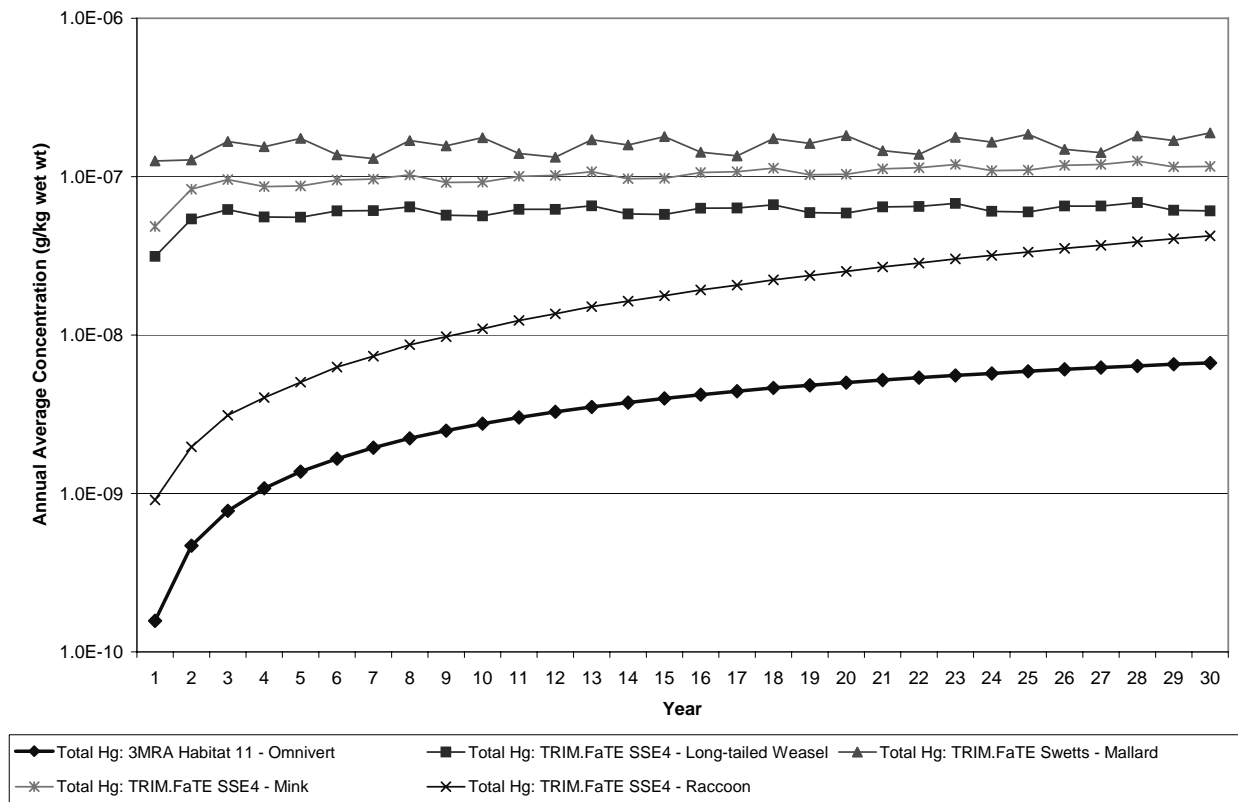
The 3MRA maximum total mercury concentration in the omnivert (omnivorous vertebrate) category was compared to four wildlife compartments in three representative subgroups in TRIM.FaTE: a terrestrial carnivore (long-tailed weasel), two semi-aquatic omnivores (mallard duck and raccoon), and a semi-aquatic carnivore (mink). As noted previously, the 3MRA total mercury concentration is derived directly from the concentration of mercury in the deeper soil (0-5 cm depth) at a specific point, while the four TRIM.FaTE wildlife compartments receive mercury from their diets and through the inhalation pathway. In the case of the long-tailed weasel, its diet is comprised of terrestrial animals. The mallard consumes terrestrial leaf material and benthic invertebrates, and the raccoon consumes benthic invertebrates and fish plus earthworms. The mink consumes fish and benthic invertebrates along with terrestrial animals.

In general, the maximum total mercury concentrations for the 3MRA omnivert category are within approximately one order of magnitude of the TRIM.FaTE compartments identified for comparison. At most of the locations, the TRIM.FaTE compartments have higher total mercury concentrations. Exhibit 6-38 displays the total mercury concentration time series for the Swetts Pond watershed, where the maximum total mercury concentrations for the 3MRA omniverts are lower than the total mercury concentrations in all the TRIM.FaTE compartments. The differences in total mercury concentrations between the models are partially due to the inclusion

of food items from surface water sources in the diets of some TRIM.FaTE wildlife compartments, as well as to the differences in modeled soil and leaf concentrations. The differences among the various TRIM.FaTE compartment types are due to dietary differences, as listed above.

The total mercury concentration in 3MRA omniverts is derived directly from the mercury concentration in deeper soil (0-5 cm depth); therefore, that time series curve is similar in shape to the 3MRA soil time series curve. Interestingly, the shape of the TRIM.FaTE raccoon time series curve is similar to that of the 3MRA omnivert. However, this is largely a reflection of the similar shapes of the TRIM.FaTE sediment curve and the 3MRA deeper soil curve, because the TRIM.FaTE raccoon obtains mercury primarily from benthic invertebrates (69 percent of diet), which derive their mercury directly from sediments.

**Exhibit 6-38 - Log Scale
Total Mercury Concentration in Omniverts vs. Time: Swetts Pond Watershed**

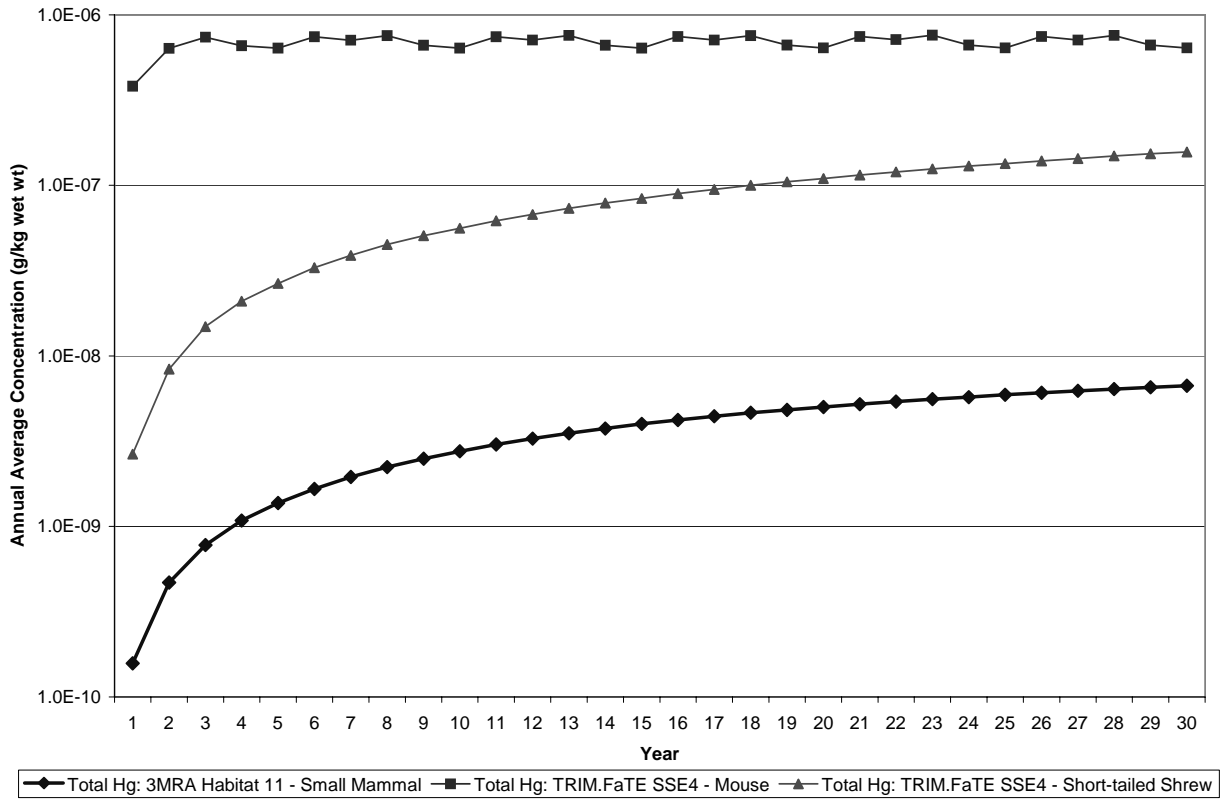


6.5.3 Total Mercury Concentrations in Small Mammals

The 3MRA maximum total mercury concentration in the small mammal category was compared to concentrations in three wildlife compartments in three representative subgroups in TRIM.FaTE: a terrestrial ground-invertebrate feeder (short-tailed shrew), a terrestrial herbivore (meadow vole), and a terrestrial omnivore (mouse). As noted previously, the 3MRA total mercury concentration is derived directly from the concentration of mercury in the deeper soil (0-5cm depth) at a specific point, while the three TRIM.FaTE wildlife compartments receive mercury from their diet and through the inhalation pathway. In the case of the TRIM.FaTE short-tailed shrew compartment, the diet consists of earthworms and soil arthropods, which are exposed to mercury in root zone soil. The short-tailed shrew also consumes relatively large amounts of contaminated surface soil in TRIM.FaTE. The meadow vole's diet consists solely of leaf material, and the mouse's diet is divided evenly between leaf material and soil arthropods.

In general, as shown in Exhibit 6-39 for the Swetts Pond watershed, the maximum total mercury concentrations for 3MRA small mammals are lower than the total mercury concentrations in the TRIM.FaTE mouse, short-tailed shrew, and meadow vole, with the concentrations falling within approximately two orders of magnitude by year 30. These concentration differences result because the two models use different approaches to predict mercury concentrations in wildlife. Specifically, 3MRA uses the deeper soil (0-5 cm depth) concentration and an empirical BAF to estimate total mercury concentrations in small mammals. TRIM.FaTE uses a bioenergetics/food chain approach based on the animal's diet and mercury contamination levels. The use of a bioenergetics approach in TRIM.FaTE also results in the differences in total mercury concentrations observed among the TRIM.FaTE small mammal compartment types at different locations. As shown in Exhibit 6-39, the shapes of the TRIM.FaTE short-tailed shrew and 3MRA small mammal time series curves are similar, reflecting the consumption of contaminated surface soil by the shrew as well as the source of the short-tailed shrews' diet (i.e., earthworms and soil arthropods, which accumulate mercury from the root zone soil compartment in TRIM.FaTE). Because the surface soil mercury concentrations in TRIM.FaTE are higher than the deeper soil (0-5 cm depth) mercury concentrations in 3MRA and because the short-tailed shrew consumes relatively large amounts of contaminated surface soil, it appears reasonable that the total mercury concentrations in the TRIM.FaTE short-tailed shrew compartment would be higher than in the analogous 3MRA small mammal. The TRIM.FaTE mouse consumes terrestrial plants and soil arthropods. Its time series curve reflects the cyclical pattern of mercury accumulation in terrestrial plants, as well as the higher mercury concentrations in leaf material than in soil arthropods. The shape of the time series curve for the TRIM.FaTE meadow vole compartment (see Appendix Chart E-12c) is similar to the mouse compartment curve, reflecting the meadow voles' terrestrial plant diet.

**Exhibit 6-39 - Log Scale
Total Mercury Concentration in Small Mammals vs. Time: Swetts Pond Watershed**



6.6 Summary of 3MRA-TRIM.FaTE Comparison

In a comparison between two complex multimedia models such as this, it is not expected that results will match exactly, given the different methods, algorithms, and inputs used by the two models. However, for most media, the results of this comparison of 3MRA and TRIM.FaTE applications are fairly close (within an order of magnitude), especially considering the differences in inputs and model processes. The ultimate objective of this work is to enhance the level of confidence in both models, and this comparison met that objective since differences in results were in most cases explainable and additional information was gained to help both teams in future applications (e.g., which input properties are highly sensitive to change, what properties or algorithms may need to be adjusted or investigated further).

6.6.1 Overview of Results and Model Differences

Some of the specific differences between the applications of the two models that clearly influence the results are the different:

- Methods of estimating chemical concentrations over space (volume average versus point concentrations);
- Methods for simulating chemical fate in the air;
- Meteorological input data;
- Soil depths and soil layers modeled;
- Mercury transformation rates (e.g., in water and sediment);
- Values used for suspended solids fraction in surface water;
- Processes modeled in surface water (e.g., algae, macrophytes); and
- Methods used to simulate chemical uptake by wildlife.

Many of the variations between results can be explained by these modeling differences. For instance, the differences between the mercury concentrations in air (where the 3MRA mercury concentrations are higher than TRIM.FaTE concentrations) can be explained by the different air modeling methods (Gaussian plume versus advective transport between compartments), the comparison of point versus volume average, and the meteorological data. However, the air concentrations have similar general directional patterns for the two models (highest in the same direction).

Unlike the air concentrations, the TRIM.FaTE deposition fluxes are higher than 3MRA deposition fluxes, and the difference between the fluxes increases with distance from the source. The methods used to calculate deposition are not the same for the two models, which helps to explain why the relative difference between the models is not the same as in the air. The spatial deposition patterns for the two models vary from the patterns observed for air concentrations because of weather patterns (the predominant wind direction when it is raining is not the same as the overall predominant wind direction). As expected based on the deposition fluxes, the mercury concentrations in TRIM.FaTE leaves and surface soil compartments are greater than the corresponding concentrations in these 3MRA media.

In the deeper soil (i.e., root zone soil), plant roots, and earthworms, the 3MRA mercury concentrations are greater than the TRIM.FaTE mercury concentrations. This is due primarily to

the different depths of the deeper soil used in the two model applications. The TRIM.FaTE application deeper soil (root zone compartment) is much deeper, and does not include the top 1 cm of soil, while the 3MRA deeper soil is shallower and includes the top 1 cm of soil. Therefore, it is not surprising that the 3MRA deeper soil mercury concentrations are greater than the corresponding TRIM.FaTE concentrations. Also, because in both models roots and earthworms both obtain their mercury directly from the deeper soil, it is reasonable that the concentrations modeled with 3MRA would be higher. However, the ratio of mercury in the roots to the soil is greater for TRIM.FaTE than 3MRA, and the ratio of mercury in earthworms to the soil is greater for 3MRA than TRIM.FaTE, identifying an area where further investigation would be useful.

The total mercury concentrations in the surface water bodies are very similar for the two model applications with TRIM.FaTE values slightly higher, which is once again consistent with the deposition fluxes. However, the speciation of mercury in the water bodies is very different, due to different processes, mercury transformation rates, and suspended sediment concentrations modeled in the water bodies, with the 3MRA surface water bodies having much larger percentages of elemental and methyl mercury than the TRIM.FaTE water bodies have. As for the surface water, the mercury concentrations in the fish are very similar for the two models. It appears that the slight differences in mercury concentrations in fish are a result of the different uptake factors used by the models and that the concentrations in the fish for TRIM.FaTE have not yet reached an equilibrium level. In the sediment, TRIM.FaTE total mercury concentrations are also higher than 3MRA concentrations (like the surface water), but by a greater magnitude than in the surface water. The mercury speciation is very different for the two models in the sediment – divalent mercury is predominant for TRIM.FaTE, but elemental mercury is predominant for 3MRA.

In the applications presented here, the two models estimate chemical concentrations in wildlife differently – TRIM.FaTE uses bioenergetics to simulate food web transfers of mercury, whereas for the prey species modeled in this application, 3MRA uses soil-based empirical BAFs. The comparisons between the mercury concentrations in animals vary depending on (among other factors) the diets of the animals and the comparison locations. In some cases, TRIM.FaTE concentrations are higher (most omniverts and small mammals), and in some cases 3MRA concentrations are higher (some small birds).

Overall, the largest differences between model results were seen in earthworms, deeper soil, and sediment. The difference in the deeper soil results is largely due to the large difference in soil depth (a user-specified parameter). This depth difference also explains the mercury concentrations in earthworms (along with different factors used for earthworm mercury accumulation). The sediment differences can be explained mostly by the different processes that were modeled in the surface water and sediment by the two models.

The comparison helped to identify some of the strengths and limitations of the TRIM.FaTE and 3MRA modeling approaches and individual process models, thus informing scientists with regard to future applications pertinent to these models. Both models are flexible in terms of adjusting inputs, layouts, and outputs, which may – depending on the level of complexity desired – have corresponding cost in terms of effort required for their use. The overall difference in their design is 3MRA's use of multiple models (including several EPA

legacy models, such as ISCST3 and EXAMS) to simulate the transport of pollutant from source to receptor of interest, and TRIM.FaTE's use of a fully coupled, compartmentalized environment in which bi-directional pollutant transfers between compartments are tracked, with complete accounting for mass. Within those differing designs, a better understanding of the similarities and differences in individual process modeling has been achieved, with some implications for future uses.

6.6.2 Possible Future Areas for Model Comparison

As mentioned at the beginning of this chapter, the focus of this analysis was primarily on conducting an initial comparison for TRIM.FaTE and 3MRA focusing on outputs from various model compartments and was not intended to be a comprehensive comparison of modeling concepts, structures, algorithms, and data inputs of the two models. Where possible, explanations for the differences between TRIM.FaTE and 3MRA results are suggested in this chapter, and in a few cases model processes and parameters are examined in detail to explain different results. Findings were specifically informative with regard to several aspects of TRIM.FaTE model set-up (e.g., layering of soil depending on the specific application site; earthworm partition coefficient values; methods and inputs used for sediment modeling; and the calculations used for deposition).

Additional investigation in several areas may be useful to further the understanding of and confidence in both models. A few areas where model results differ, and more in-depth evaluations might be informative, are listed below.

- Deposition is the major means by which mercury mass is transferred from the air to the surface in both model applications. The detailed examination of air and deposition modeling processes that was performed by the 3MRA team helps to explain some of the reasons for the differences observed in results of the two model applications. However, further investigation could provide a deeper user understanding of the two modeling approaches in similar multimedia applications. Such investigation might consider dry deposition, chemical reactions, building effects, and complex terrain.
- The difference in the deeper soil definition employed in the applications of the two models helps to explain much of the discrepancy between the 3MRA and TRIM.FaTE root and earthworm concentrations, as shown in Exhibits 6-20 and 6-22. However, further investigation relating the TRIM.FaTE processes and input parameters and the 3MRA BAF values might also be informative to future applications.
- Multiple hypotheses for differences observed in mercury speciation in surface water and sediment, as well as in total mercury concentrations in sediment are presented in Sections 6.4.1 and 6.4.2, including different mercury conversion rate constants, different atmospheric deposition fluxes, partitioning to algae with TRIM.FaTE but not 3MRA, uptake and conversion by macrophytes with TRIM.FaTE but not 3MRA, and different suspended solids values. A more in-depth and comprehensive consideration of the current literature and scientific knowledge regarding the salient processes would further inform this assessment.

- While comparisons of the wildlife results highlighted differences in modeling approaches employed by the two models, investigation and review of the literature would improve understanding of strengths and limitations of the two approaches and of the input values employed.
- Valuable insight might be gained by re-running one or both of the models with various inputs and options matched more closely including possibly the site-layouts and comparison points, meteorological data, inclusion of dry deposition, and certain salient input parameters.

7. COMPARISONS WITH MEASUREMENT DATA

Comparing multimedia model outputs with chemical monitoring data is challenging because a comprehensive and accurate history of a site is rarely available, making it extremely difficult – if not impossible – to accurately match modeling conditions to actual site conditions. This is particularly true when attempting to characterize the sources of chemicals for a modeling exercise. In addition, the available measurement data may not be geographically and temporally representative of the natural system being modeled, and accurate multimedia modeling is a challenging exercise due to the complexity of natural systems. Nevertheless, even a limited measurement data set can provide an opportunity for informative model-to-data comparison. In the early stages of model evaluation, these analyses can serve as a helpful diagnostic tool and lead to discoveries of potentially important processes or inter- and intramedia relationships.

The purpose of the comparisons discussed in this chapter is to contribute to the overall model evaluation of TRIM.FaTE through an analysis of model results in the context of relatively recent measurement data for the modeled site. This exercise provides another frame of reference for evaluation and interpretation of TRIM.FaTE modeling results. It is important to note that this comparative analysis is *not* meant to be a validation of the performance of the model, and model results should not be interpreted as more or less “correct” based on their value relative to the available measurement data presented here. The modeling for this application was not designed to account for all sources that may have contributed to mercury levels in near-site environmental media. The TRIM.FaTE results compared to measurement data in this section represent predicted media and biota concentrations of mercury resulting from facility emissions case C (i.e., source emissions plus air boundary contributions and initial concentrations in media and biota). However, there may have been significant and direct mercury releases to soil or water from the modeled facility and other sources in the modeling region that were not included in the TRIM.FaTE modeling scenario. Sources outside the modeling region that contributed to mercury contamination within the modeling region via transport across the boundary in media other than air also were not considered (e.g., contamination entering the region via surface water inflows). It is important to keep these considerations in mind when interpreting the comparisons presented in this chapter.

7.1 Description of Measurement Data and Relationship to TRIM.FaTE Model Results

Appendix F provides details on the off-site monitoring data sets identified for the area in the vicinity of the test case site. For each data set, the following information is provided:

- Environmental medium;
- Number of data points (including, where relevant, the number of duplicates and measurements below the detection limit);
- Measurement endpoint(s) and units;
- Sampling date(s) and location(s);
- Purpose of monitoring;
- Range, mean, and standard deviation of the data set;

- Raw data (i.e., actual measurement data values), or a summary of the data set where presentation of all data values is not feasible; and
- Other relevant information.

Off-site measurement data for comparison were identified for air, soil, lake/pond surface water and sediment, and various biota. Some measurement data were also identified for the river, including concentrations in surface water, sediment, and biota (eel and minnow). However, the river is tidal at this site but was modeled for test case and general model evaluation purposes as a simple river, and the modeling does not account for tidal influence on river flow. Therefore, the river data are excluded from the measurement to model comparison and are not presented in Appendix F.

Measurement data discussed in this evaluation were collected between 1995 and 2000 through different sampling events and over a range of time scales. As a result, the monitoring data do not exactly match the temporal representation of the long-term (30-year) source used in the model run. However, because the test case facility began operating in the late 1960s, the modeled concentrations at the end of the 30-year model run are expected to represent a temporal scale similar to the actual source contributions. For this analysis, point measurements of the monitoring data (or, where many data points were available, statistical summaries of the measurement data) are presented for comparison with temporally averaged modeling results (i.e., concentrations in environmental media and biota) from TRIM.FaTE. In spatial terms, the TRIM.FaTE results in general represent a defined volume (i.e., a volume element) for abiotic media, and a population associated with a defined area (i.e., a parcel) for biota.

At the end of the 30-year emissions simulation, most of the modeled concentrations for the non-air compartments included in this comparison are still increasing. Therefore, with the exception of concentrations in air, the TRIM.FaTE results compared to measurement data in this chapter are the average concentration of the 30th year of the model run. An annual average was selected for comparison in order to account for fluctuations that occur over the course of a year due to variations in meteorological and other data inputs. For air compartments, the long-term average concentration does not appear to be increasing over the course of the 30-year modeling time scale (i.e., there appears to be no significant accumulation of mass in the air compartments after the very beginning of the modeling period), but concentrations do vary significantly from hour to hour on a five-year basis due to the five-year meteorological data set used. Therefore, statistics calculated from the last five years of modeled air results (i.e., years 26 through 30) are used for the comparison with measurement data. More details regarding temporal variation in TRIM.FaTE results are presented in Chapter 3 of this report.

The parcel layout for the test site was constructed, in part, based on the available monitoring data so that data comparisons would be relevant and meaningful (e.g., a surface parcel was defined in the vicinity of a park where several samples were taken; some measurement data were available for each of the four lakes included in the test case). Sampling locations for which measurements are available are presented in Exhibits 7-1 and 7-2 for air and non-air media. TRIM.FaTE air and surface parcels for the test case are overlaid on these maps for reference. Descriptions of the sampling locations corresponding to the codes on the maps are presented in Exhibit 7-3.

**Exhibit 7-1
Locations of Air Monitoring Stations (with TRIM.FaTE Air Parcel Layout)**

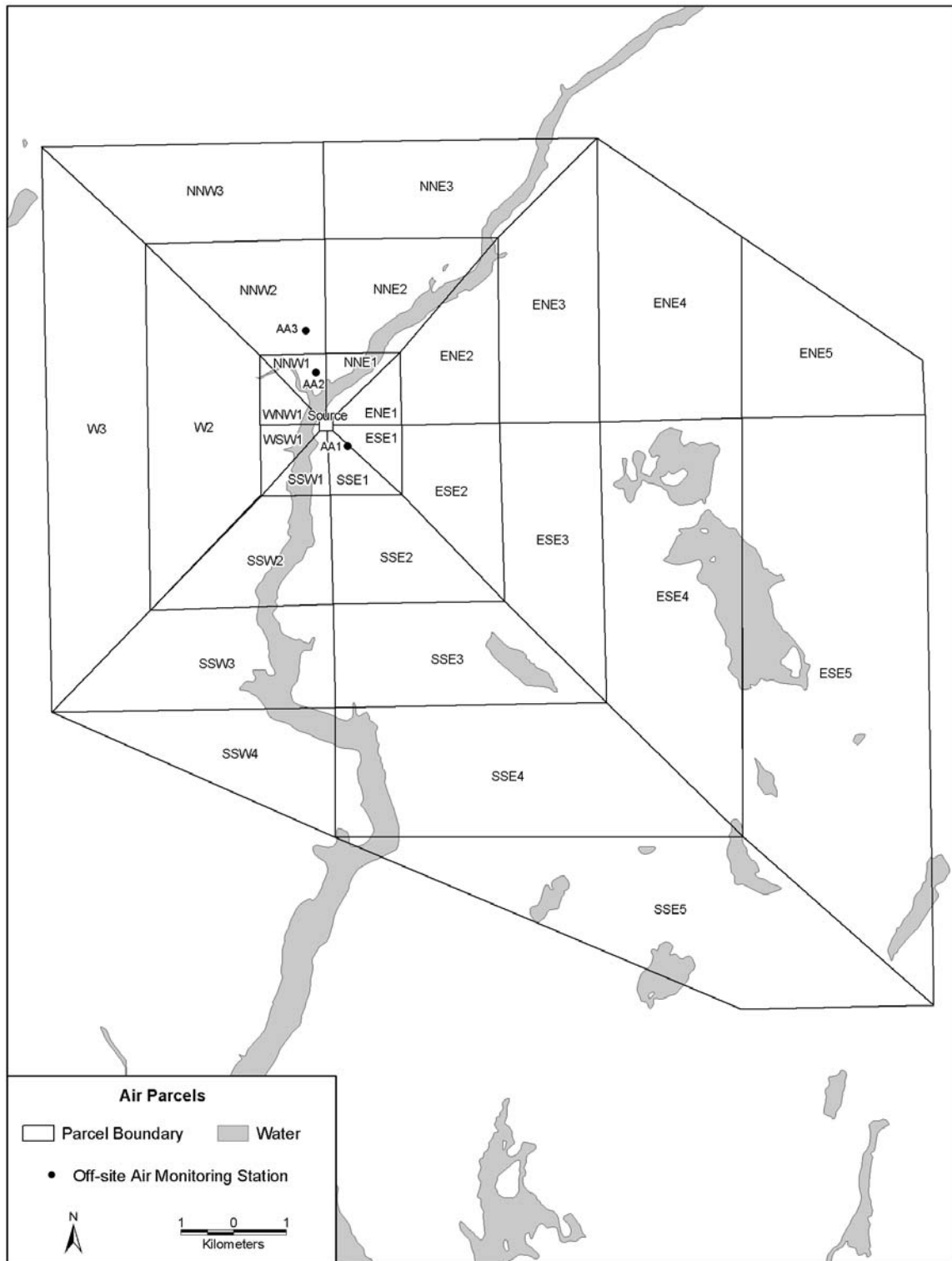


Exhibit 7-2
Sampling Locations for Non-Air Measurement Data
(with TRIM.FaTE Surface Parcel Layout)

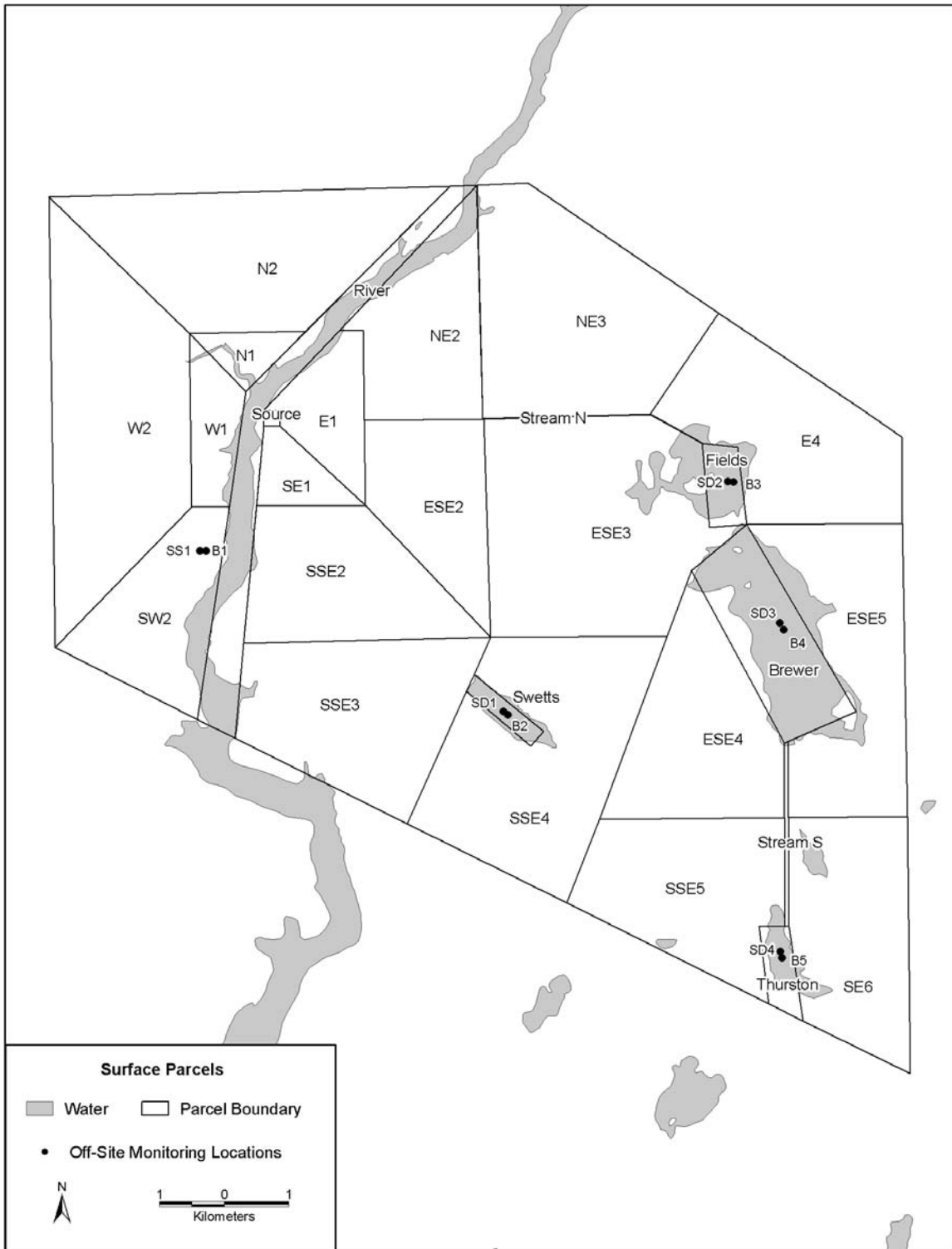


Exhibit 7-3
Key for Off-site Monitoring Location Maps^a

Map Code	Location	Monitoring Data
AA1	Near facility (450 m to SE)	Ambient air: 1 sample location (Sept 1998 - Nov 1999)
AA2	Near facility (1300 m to NNW)	Ambient air: 1 sample location (Sept 1998 - Sept 1999)
AA3	Near facility (1950 m to NNW)	Ambient air: 1 sample location (Sept 1998 - Sept 1999)
SS1	Park (2200 m to SSW)	Surface soil: 1 sample location (1995) Surface soil: 3 sample locations (1997)
SD1	Swetts Pond	Sediment (deepest part of water body) (1996)
SD2	Fields Pond	Sediment (deepest part of water body) (1996)
SD3	Brewer Lake	Sediment (deepest part of water body) (1996)
SD4	Thurston Pond	Sediment (deepest part of water body) (1996)
B1	Park (2200 m to SSW)	Deer mouse: 1 sample location (1995) Earthworm: 1 sample location (1995) Short-tailed shrew: 1 sample location (1995)
B2	Swetts Pond	White perch: 1 sample location (1996)
B3	Fields Pond	White perch: 1 sample location (1996)
B4	Brewer Lake	White perch: 1 sample location (1996)
B5	Thurston Pond	White perch: 1 sample location (1996)

^a Measurement data were also identified for abiotic and biotic media in the river; however, these data were excluded from the measurement to model comparison.

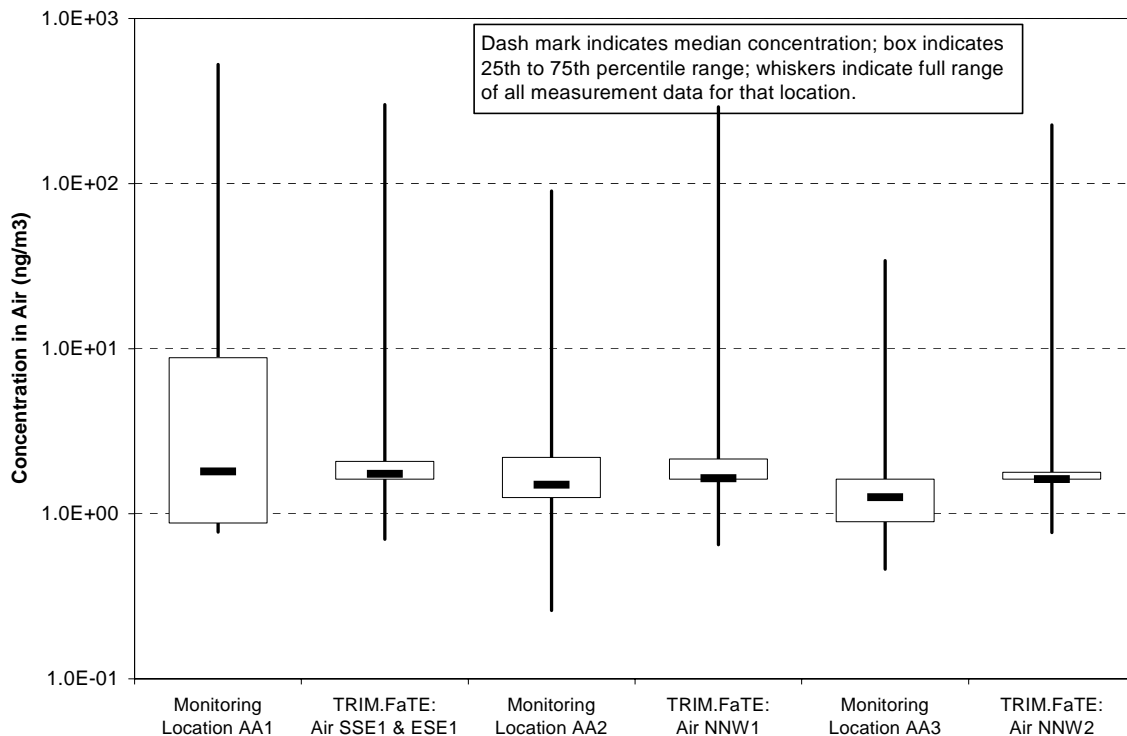
The measurement data presented in this section are compared with model results obtained for emission case C, as noted earlier. This scenario, which includes at least some “background” mercury contamination, is assumed to be the closest approximation of the actual conditions at the site of the three dynamic modeling emission cases that were modeled. However, as noted previously, it is likely that this modeling scenario does not account for all sources of mercury affecting environmental media at the site (and in particular does not cover releases directly to soil or water). In addition, it is important to note that the background air concentration used to define the boundary contributions for this scenario is based on previous analysis by EPA for the *Mercury Study Report to Congress* (EPA 1997) and is assumed to be generally representative of mercury concentrations in air across the U.S. for the industrial (present-day) time period. Specific local or regional sources in the vicinity of the test case facility were not accounted for in this analysis. Thus, mercury contamination from “background” (i.e., other than the modeled source) is likely to be underestimated. Moreover, there is substantial uncertainty about the emission rates and mercury speciation assumed for the modeled source, and the emitted amounts of various forms of mercury may be over- or underestimated.

The model setup and emission scenario for the TRIM.FaTE runs used to generate the modeling data are described in more detail in Chapter 2.

7.2 Comparison with Air Measurement Data

A large number (thousands) of measurements of total gaseous mercury (TGM) were collected from three stationary monitoring locations near the facility between August 1998 and September 1999. The facility was in operation during this period and was emitting mercury. According to information in the report summarizing air monitoring results, the instrumentation used to measure TGM at these sites poorly detects non-elemental mercury (Earth Tech 1999); therefore, the measurements may under-report the actual amount of divalent mercury. However, given that TRIM.FaTE predicts airborne mercury in the test case emission scenario C to be predominantly (>98 percent) elemental mercury in the vapor phase, it seems reasonable to compare the measurement data for TGM with TRIM.FaTE results for total concentrations of mercury in air. In Exhibit 7-4, air measurements are compared with ambient concentrations of total mercury estimated by TRIM.FaTE for several corresponding air compartments. Measurement location AA1 falls on the boundary between two TRIM.FaTE air parcels; therefore, TGM measurements for this location are compared with estimated total mercury concentrations for the two corresponding TRIM.FaTE air compartments (ESE1 and SSE1). The other two measurement locations, AA2 and AA3, are situated within TRIM.FaTE air parcels NNW1 and NNW2, respectively.

Exhibit 7-4
Comparison of Monitoring Data for Total Gaseous Mercury with TRIM.FaTE
Modeled Concentrations of Total Mercury in Air



Given the large number of measurements, the air monitoring data for each site are presented in box and whisker format (representing variability over time) in Exhibit 7-4. TRIM.FaTE two-hour results for the last five years of the model run for the corresponding air compartments are also plotted in box and whisker format (also primarily representing variability over time) to show the range of measured and modeled data.

Overall, the model output is in relatively close agreement with the measured values. Median measured and modeled concentrations are nearly identical for these comparisons. The distributions of the TRIM.FaTE air results for these compartments are tighter than the spread of measurement data between the 25th and 75th percentiles. For both sets of air comparisons, the total spread between the minimum and maximum values spans a similar range (i.e., two to three orders of magnitude).

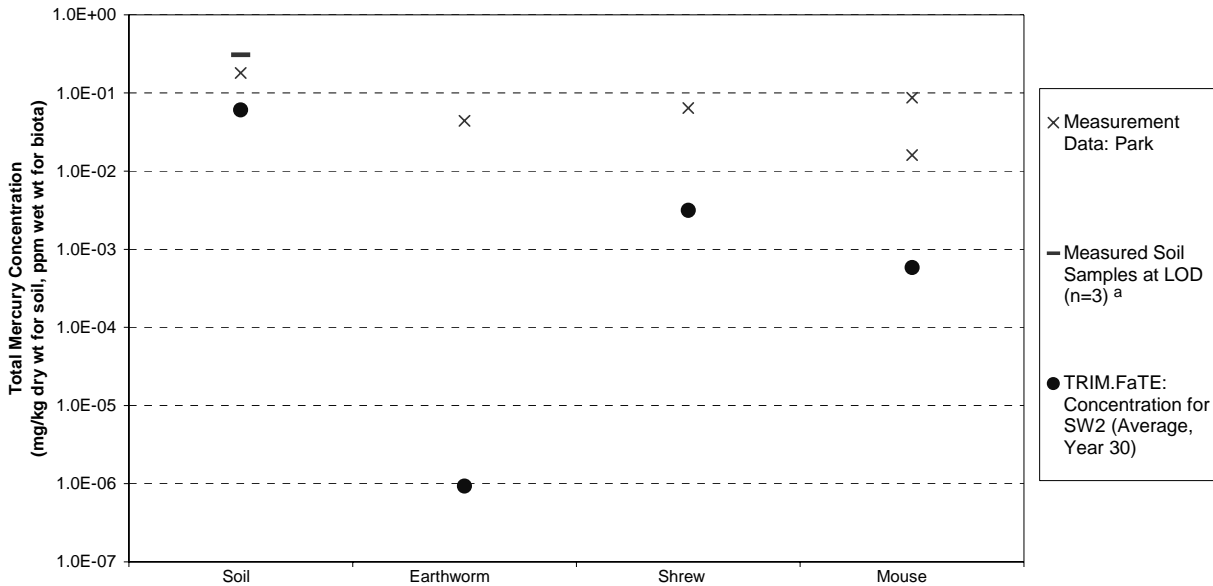
It is important to note that the meteorological data used as inputs for TRIM.FaTE modeling correspond to measurement stations near the modeling region but not actually at the site, and are not for the exact time period represented by the monitoring data. As noted earlier, lack of knowledge about the historical source emissions may also contribute to the observed differences. Therefore, the actual conditions at the site would not be expected to exactly match the data used as TRIM.FaTE inputs. Because air concentrations depend heavily on meteorological conditions, some of the difference between measured and modeled air concentrations may be a result of the difference between site-specific conditions and the meteorological data used for TRIM.FaTE. It is noted, however, that the input meteorology data for wind speed and direction used for TRIM.FaTE are generally similar to the limited on-site data that are available. Hourly measurements of wind speed and direction were recorded at the facility between November 1998 through October 1999 as a component of the TGM monitoring program carried out during that time and were reported in the air monitoring report. Data recovery for wind direction and wind speed measurements for this time period was 96.7 percent and 93.5 percent, respectively. Overall, the wind direction was reported to be predominantly from the south and the northwest, and very rarely from the east (see Appendix F for the wind rose based on measurement data that was included with the monitoring report). This is very similar to the prevailing wind directions for the meteorological data used as TRIM.FaTE inputs (see Figure 2-7 for a wind rose based on TRIM.FaTE modeling data). Average wind speed of the measurement data was reported to be 6.99 miles per hour, which is converted to 3.21 m/sec; this value is similar to the mean of the TRIM.FaTE modeling data of 3.64 m/sec.

7.3 Comparison with Soil and Soil Biota Measurement Data

Measurements of mercury in soil and terrestrial organisms were collected as part of a site investigation conducted in 1995 and 1997 at a park located southwest of the facility, which roughly corresponds to surface parcel SW2. Measurement data are plotted along with predicted TRIM.FaTE concentrations for corresponding surface soil and biotic compartments located at SW2 in Exhibit 7-5. Measured mercury concentrations are plotted as x's, and TRIM.FaTE annual average concentrations for the 30th year of the model run plotted as dots.

Four soil measurements were collected at this location, with only one measurement reported above the level of detection (LOD). The three soil values below the LOD are

Exhibit 7-5 Comparison of Measurement Data for Soil and Terrestrial Organisms with TRIM.FaTE Modeled Concentrations



^aNote that the LOD reported for these three samples is *higher* than the actual measurement reported for the fourth sample. These three samples were taken during a different year from the fourth (presumably under different analytical conditions).

represented in Exhibit 7-5 with a single dash mark at the LOD (see exhibit footnote). Soil samples were described as surface soil but the sampling depth was not specified; for this comparison, it is assumed that the measurement data correspond to the surface soil compartment in TRIM.FaTE (i.e., depth of 1 cm). TRIM.FaTE model results indicate that soil concentrations are still increasing at 30 years, so the last year of modeling data were used to estimate average concentrations in the surface soil. The TRIM.FaTE average concentration of total mercury for surface soil in parcel SW2 is lower than the measurement data but within a factor of three of the detected value (within a factor of five of the LOD for the other three samples).

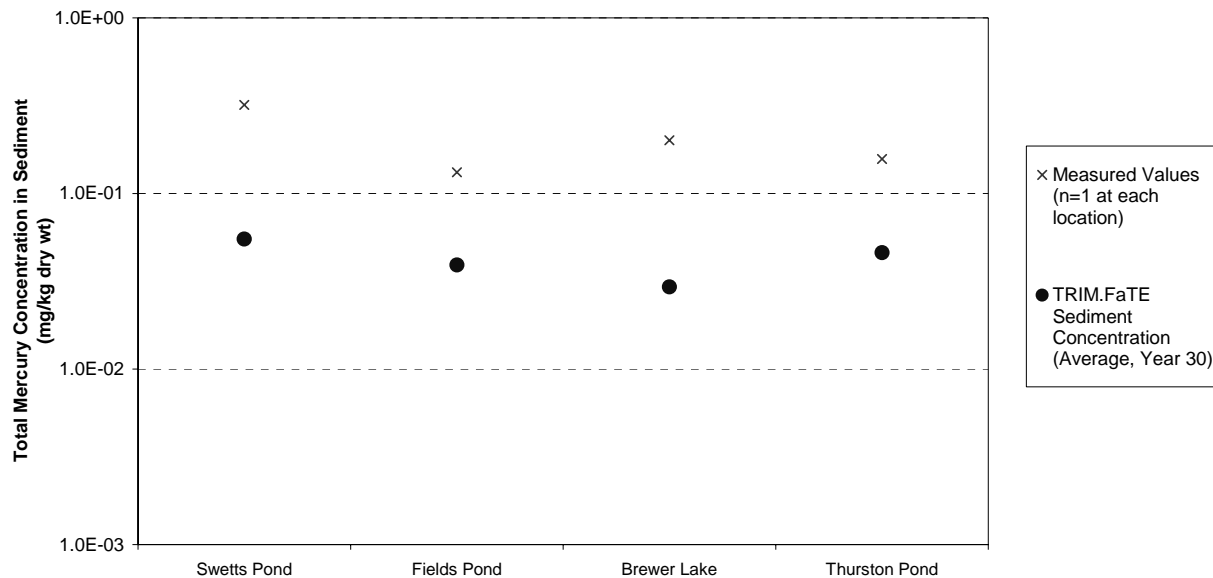
For terrestrial organisms, one measurement each for earthworm and short-tailed shrew and two measurements for deer mouse were collected in 1995 or 1997 at the park. Measured data represent whole-body, wet weight total mercury concentrations. TRIM.FaTE total mercury concentrations for biotic compartments (and therefore representative of whole-body, wet weight) are presented for the corresponding compartments located at SW2 and are presented in Exhibit 7-5 with the measurement data. TRIM.FaTE concentrations represent the average for the last year of the model run. For all three organisms, the model predictions for mercury are less than the measured values, with differences of nearly five orders of magnitude for the earthworm and one to two orders of magnitude for the shrew and mouse. Due to the limited number of measurement data points, it is not possible to judge the representativeness of the measurement data. For the available data, however, it is apparent that measured and modeled results are more similar for the shrew and mouse than for the earthworm. One possible explanation for the greater difference observed for the earthworm could be that the earthworm compartment in this TRIM.FaTE application is associated with relatively deep root zone soil, not surface soil, and for

simplicity no direct contact with surface soil (e.g., during rain events, when earthworms might be expected to move to the surface) is modeled for the earthworm in the test case. Modeled concentrations in root zone soil are approximately three to four orders of magnitude lower than concentrations in surface soil. Similarly, off-line calculations indicate that if total mercury concentration in the earthworm compartment is estimated using TRIM.FaTE *surface soil* concentration for SW2, the result is also about three to four orders of magnitude higher (i.e., on the order of 10^{-3} ppm) and consequently within two orders of magnitude of the measurement data. This relationship would also affect other terrestrial organisms that ingest earthworms.

7.4 Comparison with Sediment and Aquatic Biota Measurement Data

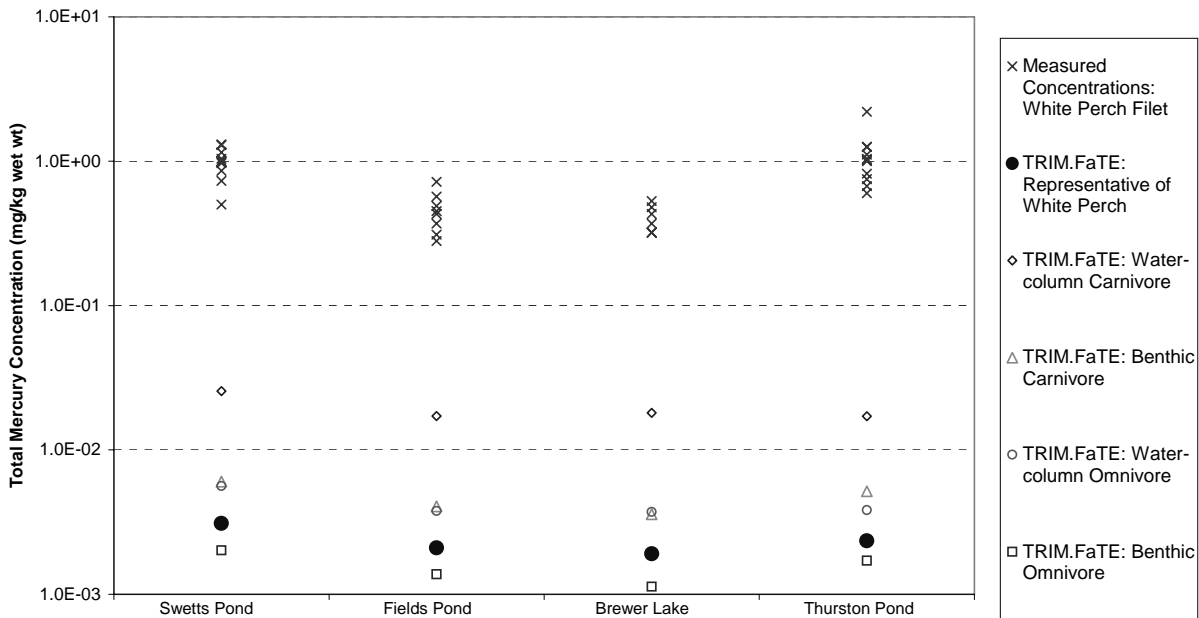
Lake sediment samples were collected and analyzed for total mercury in 1996 as part of a study to evaluate the impact of local air emission sources. One sample was obtained for each of the four lakes/ponds included in the test case, with samples taken from sediment at the deepest part of the water body and reported as total mercury concentration (dry weight). These data are compared to TRIM.FaTE sediment compartment concentrations in Exhibit 7-6 (note that the samples may not be representative of the entire sediment in each lake). TRIM.FaTE concentrations presented here are the average for year 30 and represent a volume-average for the entire sediment compartment (with one sediment compartment representative of a single lake). Model results for all four sediment compartments are about an order of magnitude lower than the corresponding measured value.

Exhibit 7-6
Comparison of Measurement Data for Lake Sediment with TRIM.FaTE
Modeled Concentrations



White perch also were collected from each of these four lakes during the same 1996 study and analyzed for total mercury, with measured concentrations reported for skinless fillets. These results are presented in Exhibit 7-7 along with TRIM.FaTE modeled values for total mercury representing whole-body concentrations (year 30 annual average).¹ For this comparison, a representative concentration for white perch was estimated by combining results for two TRIM.FaTE omnivore compartments based on white perch dietary habits (see Section 6.4.3 for more discussion of estimating fish species concentrations based on TRIM.FaTE fish compartment results). The unadjusted concentrations for four TRIM.FaTE fish compartments (i.e., water-column and benthic omnivores and carnivores) in each water body are also presented in Exhibit 7-7 for comparison. The representative modeled values are approximately two orders of magnitude below the measured white perch fillet values. In general, the TRIM.FaTE concentrations for water-column fish compartments are generally higher than the representative modeled values for white perch (and therefore closer to the measured data for white perch). Unfortunately, no information is available on the measured concentration of total mercury in the water column from this study; therefore, it is not possible to calculate water-to-fish concentration ratios for measurement data that might be useful in interpreting differences between the predicted and measured values.

Exhibit 7-7
Comparison of Measurement Data for Fish with TRIM.FaTE Modeled Concentrations



^a All TRIM.FaTE values are annual average for year 30.

¹ Whole fish concentrations of methyl mercury are usually lower than fillet concentrations, but quantitative data on the relationship between methyl mercury concentrations in whole fish versus fillets were not identified for the current analysis.

7.5 Summary of Measurement Data Comparisons

As noted in the introduction to this chapter, the relatively limited measurement data set identified for the test case site can be useful as an additional analytical tool for model evaluation.² Based on the results of this comparison, additional consideration of the configuration of TRIM.FaTE earthworm and fish compartments may be appropriate. For earthworms, it may be reasonable to establish a link between the surface soil and earthworm compartments in order to account for exposure of earthworms as a result of bioturbation (i.e., mixing of soil by organisms). For fish compartments, it would be helpful to derive appropriate conversion factors to facilitate a better comparison of whole body fish concentrations to skinless fillet concentrations. In addition, the availability of additional measurement data would help to clarify the relationship between lake water-column concentrations and mercury levels of fish residing in those lakes.

As stated previously, emission case C results are expected to provide the most appropriate modeling results for comparison with measurement data because this case accounts for at least some of the background contributions of mercury. However, to provide additional context for the analysis presented in this chapter, it may be useful to consider the contribution of the modeled background to the TRIM.FaTE results compared here with measurement data. The incremental effects of background can be assessed by considering the corresponding compartment concentrations for emission case B (i.e., same emissions but no boundary contributions/initial concentrations). A more complete discussion of case B and case C results is presented in Section 3.5.2. In addition, the relative impact of modeled background is summarized in Exhibit 7-8 for compartments included in the comparison with measurement data.

It is unlikely that the major sources of mercury within the modeling region over the 30-year operation of the facility are fully accounted for by the case C boundary contributions and initial concentrations used in this analysis. As a result, it seems reasonable that the modeled TRIM.FaTE values are generally lower than the concentrations included in the limited monitoring data that were identified. In addition, the analysis of time patterns of TRIM.FaTE test case concentrations suggests that concentrations in most non-air compartments are still increasing at the end of the 30-year emission period (see Chapter 3 for details). It is possible that the predicted rates of some fate and transport processes in TRIM.FaTE are defined such that mercury mass is modeled to accumulate in abiotic and biotic media slower than it actually does. Alternatively, there may be processes that are not accounted for by TRIM.FaTE algorithms that would contribute to higher media concentrations, thereby contributing to the difference between modeled and measured data. It also is possible, as noted earlier, that historical mercury emissions from the modeled source are underestimated or that the limited observational data are not representative of the overall natural system being modeled.

² In addition to the measurements described here, measured values were also identified for mercury concentrations in sediment and organisms in the river, and blood collected from loons that were associated with water bodies in the area and the state in general. However, as described above, the river compartment was not modeled at the level of detail necessary to capture the tidal influence on river flows present at the site. In addition, blood levels in loons were not estimated from the whole body concentrations modeled for loon compartments. As a result, these additional measurements are not included in the current comparison.

Exhibit 7-8
**Effect of Modeled Background Concentrations on TRIM.FaTE Results Included
in Comparison with Measurement Data**

TRIM.FaTE Compartment	Case C Results vs. Case B Results
Air – SSE1, ESE1, NNW1, and NNW2	3 to 4 times higher for closer air parcels (SSE1, ESE1, NNW1); 9 times higher for NNW2
Surface soil – SW2	6 times higher
Earthworm – SW2	9 times higher
Short-tailed shrew – SW2	6 times higher
Mouse – SW2	4 times higher
Sediment in four ponds/lakes	13 to 20 times higher
Water-column fish and benthic fish in four ponds/lakes	13 to 30 times higher

8. REFERENCES

- Beck, M. B., Ravetz, J. R., Mulkey, L. A., and T. O. Barnwell. 1997. On the problem of model validation for predictive exposure assessments. *Stochastic Hydrology and Hydraulics*. 11: 229-254.
- Becker, D. S. and G. N. Bigham. 1995. Distribution of mercury in the aquatic food web of Onondaga Lake, New York. *Water Air and Soil Pollution* 80: 563-571.
- Bloom, N. S. 1992. On the chemical form of mercury in edible fish and marine invertebrate tissue. *Canadian Journal of Fisheries and Aquatic Sciences* 49:1010-1017.
- Brandes, L. J., den Hollander, H., and D. van de Meent. 1997. SimpleBOX v. 2.0. Netherlands: National Institute of Public Health and the Environment (RIVM).
- Chunilall, V., Kindness, A., and S.B. Jonnalagadda. 2004. Heavy metal uptake by spinach leaves grown on contaminated soils with lead, mercury, cadmium, and nickel. *J. Environ. Sci. Health, Part B - Pesticides, Food Contaminants, and Agricultural Wastes*, B39(3): 473-481.
- Cowan, C.E., Mackay, D., Feihtel, T. C. J., van de Meent, D., DiGuardo, A., Davies, J., and N. Mackay. 1995. The multi-media fate model: A vital tool for predicting the fate of chemicals. Pensacola, FL: SETAC Press.
- Earth Tech, Inc. 1999. Ambient Total Gaseous Mercury and Meteorological Monitoring Results. Prepared for [company name and location withheld]. December.
- Gilmour, C.C., Henry, E.A., and R. Mitchell. 1992. Sulfate stimulation of mercury methylation in freshwater sediments. *Environmental Science and Technology* 26(11):2281-2287.
- Glass, G., Sorenson, J.A., and G.R. Rapp, Jr. 1999. Mercury deposition and lake quality trends. Final report Project: I-11/I-15, Legislative Commission on Minnesota Resources, St Paul, MN.
- Habicht, F.H. 1992. Memorandum from the Deputy Administrator of the U.S. EPA. U.S. EPA, Office of the Administrator, Task Force on Environmental Regulatory Modeling: Washington, DC. March 7.
- Hill, W. R., Stewart, A. J., and G. E. Napolitano. 1996. Mercury speciation and bioaccumulation in lotic primary producers and primary consumers. *Canadian Journal of Fisheries and Aquatic Sciences* 53:812-819.
- Kamman, N.C., Lorey, P.M., Driscoll, C.T., Estabrook, R., Major, A., Pientka, B., and E. Glassford. 2004. Assessment of mercury in waters, sediments, and biota of New Hampshire and Vermont lakes, USA, sampled using a geographically randomized design. *Environmental Toxicology and Chemistry* 23:1172-1186.

- Kelso, J.R.M., and M.G. Johnson. 1991. Factors related to the biomass and production of fish communities in small, oligotrophic lakes vulnerable to acidification. *Canadian Journal of Fisheries and Aquatic Sciences* 48:2523-2532.
- Kinsey, J.S., Swift, J., and Bursey, J. 2004. Characterization of fugitive mercury emissions from the cell building at a US chlor-alkali plant. *Atmospheric Environment* 38:623-631.
- Landis, M.S., Keeler, G.J., Al-Wali, K.I., and R.K. Stevens. 2004. Divalent inorganic reactive gaseous mercury emissions from a mercury cell chlor-alkali plant and its impact on near-field atmospheric dry deposition. *Atmospheric Environment* 38:613-622.
- Laniak, G. and D. Schwede. In preparation. Application-based Comparison of the 3MRA Gaussian Plume Model and the TRIM.FaTE Compartmental Model for Atmospheric Fate and Transport. U.S. Environmental Protection Agency, Office of Research and Development: Athens, GA and Research Triangle Park, NC.
- Lores, E.M., J. Macauley, L.R. Goodman, R.G. Smith, and D.M. Wells. 1998. Factors affecting bioavailability of methylmercury in Florida Bay. *Soc. Environ. Toxicol. Chem.* 19th Annual Meeting. Charlotte, NC. Abstr. No. 468. p. 101.
- Mason, R. P., Laporte, J. M., and S. Andres. 2000. Factors controlling the bioaccumulation of mercury, methyl mercury, arsenic, selenium, and cadmium by freshwater invertebrates and fish. *Archives of Environmental Contamination and Toxicology* 38:283-297.
- Mason, R.P., and K.A. Sullivan. 1997. Mercury in Lake Michigan. *Environmental Science and Technology* 31:942-947.
- McKone, T. E. 1993a. CalTOX, A Multimedia Total-Exposure Model for Hazardous Wastes Sites Part I: Executive Summary, Lawrence Livermore National Laboratory, Livermore, CA, URL-CR-11456, Pt. I.
- McKone, T. E. 1993b. CalTOX, A Multimedia Total-Exposure Model for Hazardous Wastes Sites Part II: The Dynamic Multimedia Transport and Transformation Model, Lawrence Livermore National Laboratory, Livermore, CA, UCRL-CR-111456, Pt. II.
- McKone, T. E. 1993c. CalTOX, A Multimedia Total-Exposure Model for Hazardous Wastes Sites Part III: The Multiple-Pathway Exposure Model, Lawrence Livermore National Laboratory, Livermore, CA, UCRL-CR-111456, Pt. III.
- Miles, C.J., and L.E. Fink. 1998. Monitoring and mass budget for mercury in the Everglades nutrient removal project. *Archives of Environmental Contamination and Toxicology* 35:549-557.
- Odum, E.P. 1971. *Fundamentals of Ecology*. Philadelphia, PA: W.B. Saunders Company; p 63.

Pankow, J.F., and S.W. McKenzie. 1991. Parameterizing the equilibrium distribution of chemicals between the dissolved, solid particulate matter, and colloidal matter compartments in aqueous systems. *Environmental Science and Technology* 25:2046-2053.

Sample, B.E., Beauchamp, J.J., Efroymson, R.A., Suter, II, G.W., and Ashwood, T.L. 1998. Development and Validation of Bioaccumulation Models for Earthworms. Prepared by Lockheed Martin Energy Systems, Inc., at Oak Ridge National Laboratory for the US Department of Energy, Office of Environmental Management.

Scheuhammer, A. M., A. H. K. Wong, and D. Bond. 1998. Mercury and selenium accumulation in common loons (*Gavia immer*) and common mergansers (*Mergus merganser*) from eastern Canada. *Environmental Toxicology and Chemistry* 17:197-201.

Southworth, G.R., Lindberg, S.E., Zhang, H., and Anscombe, F.R. 2004. Fugitive mercury emissions from a chlor-alkali factory: sources and fluxes to the atmosphere. *Atmospheric Environment* 38:597-611.

Tremblay, A., M. Lucotte, and I. Rheault. 1996. Methylmercury in a benthic food web of two hydroelectric reservoirs and a natural lake of Northern Quebec (Canada). *Water Air and Soil Pollution* 91: 255-269.

U.S. EPA (Environmental Protection Agency). 2005a. Agency Guidance for Conducting External Peer Review of Environmental Regulatory Modeling. Science Policy Council, Office of Research and Development: Washington, DC. February (last updated). <http://epa.gov/osa/spc/htm/modelpr.htm>

U.S. EPA (Environmental Protection Agency). 2005b. Evaluation of TRIM.FaTE, Volume IV: Model Performance Focusing on Dioxin Test Case. Office of Air Quality and Planning Standards: Research Triangle Park, NC. In preparation.

U.S. EPA (Environmental Protection Agency). 2004. Evaluation of TRIM.FaTE, Volume III: Model Comparison Focusing on Dioxin Test Case. EPA-453/R-04-002. Office of Air Quality and Planning Standards: Research Triangle Park, NC. December.

U.S. EPA (Environmental Protection Agency). 2003a. Draft Guidance on the Development, Evaluation, and Application of Regulatory Environmental Models. Council for Regulatory Environmental Modeling (CREM), Office of Research and Development: Washington, DC. November.

U.S. EPA (Environmental Protection Agency). 2003b. Total Risk Integrated Methodology: TRIM.FaTE User's Guide. Office of Air Quality Planning and Standards: Research Triangle Park, NC. March.

U.S. EPA (Environmental Protection Agency). 2002a. Evaluation of TRIM.FaTE, Volume I: Approach and Initial Findings. EPA-453/R-02-0012. Office of Air Quality and Planning Standards: Research Triangle Park, NC. September.

U.S. EPA (Environmental Protection Agency). 2002b. Total Risk Integrated Methodology: TRIM.FaTE Technical Support Document. Volume I: Description of Module. EPA-453/R-02-011a. Office of Air Quality Planning and Standards: Research Triangle Park, NC. September.

U.S. EPA (Environmental Protection Agency). 2002c. Total Risk Integrated Methodology: TRIM.FaTE Technical Support Document. Volume II: Description of Chemical Transport and Transformation Algorithms. EPA-453/R-02-011b. Office of Air Quality Planning and Standards: Research Triangle Park, NC. September.

U.S. EPA (Environmental Protection Agency). 2001. Water Quality Criterion for the Protection of Human Health: Methylmercury, Final. EPA-823-R-01-001. Office of Water, Office of Science and Technology: Washington, DC. January.

U.S. EPA (Environmental Protection Agency). 2000a. An SAB Advisory on the Agency's Total Risk Integrated Methodology (TRIM). EPA-SAB-EC-ADV-00-004. Science Advisory Board: Washington, DC. May.

U.S. EPA (Environmental Protection Agency). 2000b. Deposition of Air Pollutants to the Great Waters: Third Report to Congress. EPA-453/R-00-005. Office of Air Quality Planning and Standards: Research Triangle Park, NC. June.

U.S. EPA (Environmental Protection Agency). 1999a. Total Risk Integrated Methodology: Status Report. EPA-453/R-99-010. Office of Air Quality Planning and Standards: Research Triangle Park, NC. November.

U.S. EPA (Environmental Protection Agency). 1999b. National Air Toxics Program: The Integrated Urban Strategy. Federal Register 64: 38705-38740. July 19.

U.S. EPA (Environmental Protection Agency). 1999c. Terrestrial Food Web Module: Background and Implementation for the Multimedia, Multipathway, and Multireceptor Risk Assessment (3MRA) for HWIR99. Office of Solid Waste: Washington, DC. October.

U.S. EPA (Environmental Protection Agency). 1999d. Advisory on the White Paper on the Nature and Scope of Issues on Adoption of Model Use and Acceptability Guidance. EPA-SAB-EC-ADV-99-011. Science Advisory Board: Washington, DC. July.

U.S. EPA (Environmental Protection Agency). 1998a. The Total Risk Integrated Methodology: Technical Support Document for the TRIM.FaTE Module. Draft. EPA-452/D-98-001. Office of Air Quality Planning and Standards: Research Triangle Park, NC. March.

U.S. EPA (Environmental Protection Agency). 1998b. Advisory on the Total Risk Integrated Methodology (TRIM). EPA-SAB-EC-ADV-99-003. Science Advisory Board: Washington, DC. December.

U.S. EPA (Environmental Protection Agency). 1998c. White Paper on the Nature and Scope of Issues on Adoption of Model Use and Acceptability Guidance, External Review Draft. Science Policy Council: Washington, DC.

U.S. EPA (Environmental Protection Agency). 1997. Mercury Study Report to Congress. Volume III: Fate and Transport of Mercury in the Environment. EPA-452/R-97-005. Office of Air Quality Planning and Standards: Research Triangle Park, NC and Office of Research and Development: Cincinnati, OH.

U.S. EPA (Environmental Protection Agency). 1994. Report of the Agency Task Force on Environmental Regulatory Modeling: Guidance, Support Needs, Draft Criteria, and Charter. EPA 500-R-94-001. Office of Solid Waste and Emergency Response: Washington, DC.

van de Meent, D. 1993. SIMPLEBOX: A generic multimedia fate evaluation model. Report No. 672720 001. National Institute of Public Health and Environmental Protection (RIVM). Bilthoven, Netherlands.

Verta, M. and T. Matilainen. 1995. Methylmercury distribution and partitioning in stratified Finnish forest lakes. *Water, Air, and Soil Pollution* 80:585-588.

Watras, C.J., Back, R.C., Halvorsen, S., Hudson, R.J.M., Morrison, K.A., and S.P. Wentz. 1998. Bioaccumulation of mercury in pelagic freshwater food webs. *Science of the Total Environment* 219:183-208.

